RADIATIVE TRANSFER WITH STOKES VECTORS

A Thesis
Submitted For The Degree of
Doctor of Philosophy In The Faculty of Science
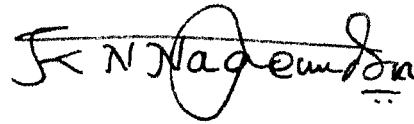
BANGALORE UNIVERSITY

By
K. N. NAGENDRA

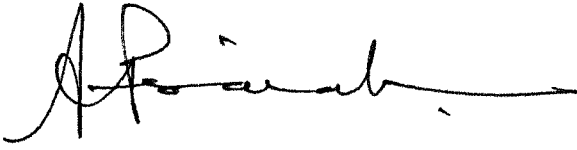INDIAN INSTITUTE OF ASTROPHYSICS
BANGALORE 560034
INDIA

March 1986

DECLARATION

I hereby declare that the matter embodied in this thesis is the result of the investigations carried out by me in the Indian Institute of Astrophysics, Bangalore and the Department of Physics, Central College, Bangalore, under the supervision of Dr.A.Peraiah and Dr.B.C.Chandrasekhara and has not been submitted for the award of any degree, diploma, associateship, fellowship, etc.of any university or Institute.

(K.N.Nagendra)
Candidate

A.Peraiah

B.C.Chandrasekhara

Supervisors

Bangalore
Dt.3.4.1986

DEDICATION

This thesis is dedicated to the memory

of my father Sri K.N.Nanjunda Rao

who constantly encouraged me to

continue my studies even in

the most difficult times

ACKNOWLEDGEMENTS

cooperation, but also for the time and the work she expended in neatly writing up the entire set of equations appearing in the thesis. I respectfully thank my mother for her everlasting affection and encouragement. Sincere thanks are also due to my family members for their continued support. I cheerfully acknowledge the love and understanding of my daughter Ms.N.Sumana.

(K.N.Nagendra)

Bangalore
dt. 3·4·1986

CONTENTS

ABSTRACT

The solution of the radiative transfer equation taking account of the polarization state of the radiation field is an important problem. The light emitted by any physical system is polarized only if there exists an intrinsic anisotropy in the medium, in which the radiation interacts with matter. The anisotropy in both microscopic as well as macroscopic scales produces a net polarization of the diffuse radiation field in the medium. The equation of radiative transfer establishes a natural link between the microphysical quantities like absorption and scattering coefficients, refractive indices etc.and thermodynamic quantities such as temperature and radiative flux gradients as well as the geometric structure of the medium. Hence a correct theoretical interpretation of the observed polarization data using the theory of polarization radiative transfer offers a better chance to determine the physical state of the matter in the emitting regions and the spatial, temporal and geometrical parameters of these regions. These parameters are the basic data needed in further studies of any astrophysical problem. In this thesis we have made an attempt to develop general solutions of the problem of radiative transfer for

polarized radiation field. We mainly use the Stokes vector representation in the polarization transfer equations.

In the first chapter we describe the need for the solutions to polarization radiative transfer problems. In the second chapter we have studied the pure absorption continuum polarization transfer problems in some detail. Here we bring out the relation between the Stokes vector and normal wave representations. We apply the solution method to the problem of continuum polarization in magnetic white dwarfs. In the third chapter we describe a general numerical method of solution which can be used in both pure absorption and scattering problems. After a discussion of the calculation of anisotropic transfer coefficients, we use the method of solution in the computation of polarized radiation in the atmospheres of magnetic white dwarfs and neutron stars. In the fourth chapter we concentrate on the Zeeman line transfer problems. We also suggest here an approximate method of solution of the transfer problem. The chapter five is devoted to some new physical processes which are of importance in various astrophysical situations. We incorporate these effects - individually into the polarization radiative transfer equation and solve it. In the sixth chapter we have attempted

to compute the linear polarization in resonance lines
when the scattering and the frequency redistribution
effects are taken into account. The line transfer
problem is solved in both the plane parallel and spheri-
cally symmetric media. The effects of sphericity on
the lines formed under the mechanisms of coherent scatter-
ing, complete redistribution and partial frequency re-
distribution is indicated.

CHAPTER 1

INTRODUCTION

1.1 The generation of polarized radiation in astronomical objects and the importance of its measurement

The observations of electromagnetic radiation received from astronomical objects is the major source of information regarding these objects. Hence our emphasis should be on finding the connection between the microscopic phenomena, like the interaction of radiation with matter (with and without external fields) and the macroscopic phenomena like the transfer of radiation, the conduction, convection or mass motions, in order to understand the physical nature of these astronomical objects. Unless such a link is established, a correct theoretical modelling of the regions emitting the radiation becomes difficult and ambiguous. We shall now describe some astronomical objects where significant amount of polarization of light is observed, and mention the theoretical efforts made to explain the observations.

(i) The environment: Light which we are exposed to in the environment is in general partially linearly polarized, the degree of linear polarization being as much as 70% or more in a cloudless sunlit sky. It may reach very small values for a thick overcast sky. The circular polari-

zation is very small (a fraction of a percent). The polarization of our environment is explained in terms of multiple scattering of sunlight in an atmosphere composed of molecules, dust, aerosols etc., along with a reflecting ground.

(ii) Planetary atmospheres: The sunlight reflected by planetary atmospheres is observed to be polarized (5-10%) linear polarization). The theoretical calculations of this so called planetary problem is quite complicated. A surface with a given law of ground reflection is assumed here a priori. The radiation transfer equation for the polarized radiation is solved in a molecular atmosphere where dust particles and aerosols are suspended. A combination of Rayleigh-Chandrasekhar theory and Mie theory of scattering has to be used. A good level of understanding has been achieved in general, in this area.

(iii) Stellar intrinsic polarization: This term refers to the polarization due to scattering in the atmospheres of stars. Practically all stars that show emission lines in their spectrum, including those of early type stars have some intrinsic (5-10% linear) polarization. Even in the sun, this has been observed near the limb ($p \sim 10^{-3}$–$10^{-2}\%$), with the electric vector nearly tangential to the limb.

The circular polarization is zero in principle, because
of the spherical symmetry of the stars. These stellar
and solar observations are interpreted in terms of
scattering by electrons,atoms and molecules as well as
the scattering involving the bound levels of resonance
lines, as the case may be. We deal with such problems in
our present studies. Another class of important observa-
tions is the polarimetry of magnetic stars like Ap and
Am stars, white dwarfs etc. The theory of Zeeman and
Stark effects in the line are important for the former,
whereas both continuum and line polarization are important
for magnetic white dwarfs. The modelling has been attempted
only in recent years. The difficulty is with magnetic
field strengths and geometries. We shall discuss these
type of problems in this thesis.

(iv) Circumstellar and interstellar polarization: The
polarization of light is produced in the circumstellar
dust envelope around a star. The red variables, cool
giants and shell stars show this type of polarization.
The polarization ($\sim$ 5-15%) is wavelength dependent and
show time variability. The interstellar polarization
is produced by scattering of star light in the inter-
stellar medium, and is also wavelength dependent. The
observations are interpreted in terms of Mie scattering
on dust grains of various shapes, sizes and composition.

The grain alignment by the interstellar magnetic field ($\sim 10^{-5}$ G) happens to be crucial. The circular polarization is also observed.

(v) Polarization of light in the nebulae: The scattering of starlight by the dust grains in reflection nebulae produces a strong polarization (1-30%). These objects offer a chance of studying the scattering and optical properties of grains in relatively small volume of space. In the calculations, the major difficulty arises from the irregular geometry of any such nebula.

(vi) Miscellaneous objects: It has been recently discovered that the pulsed emission from any pulsar is highly polarized (1-15%). The time variation of the degree of linear polarization and the position angle of polarization gives an idea of the magnetic field strength and inclination, for an assumed model of the emitting region. The results on the beaming of polarized radiation in strong field emitting regions presented in the thesis fall in this class of theoretical modelling. The light received by extragalactic objects, external galaxies, magellanic clouds etc., is also polarized. A combination of high energy (Compton scattering) or low energy (Thomson scattering) processes with the thermal and non-thermal synchrotron radiation is used for the interpretation of the observations. The quasars, BL

Lac objects and Seyfert galaxies also emit highly
polarized radiation, and the radio observations
offer a useful tool in understanding the structure
of these objects. In one of our examples studied,
we have pointed out a more complete and correct way
of treating the radiative transfer of radio waves in
a magnetized medium.

Almost all aspects of polarization, with parti-
cular reference to astronomy, namely the instrumenta-
tion, observation and theory can be found in a great
collection of papers presented in the book "Planets,
Stars and Nebulae" studied with photopolarimetry,
edited by Tom Gehrels (1974).

1.2 <u>The representation of polarized radiation and the
Stokes vector of an arbitrarily polarized beam of
light</u>

It is well known that, on scattering, light in
general gets polarized. The scattering being a natural
way of radiation-matter interaction, it is understood
that the radiation, in general is always polarized
to a smaller or larger extent in most of the physical
situations. The diffuse radiation field in a scattering
medium, for example is always partially polarized. Also,
it is well known that to describe a general radiation

field, four parameters should be specified which will give the intensity, the degree of polarization, the plane of polarization and the ellipticity of the radiation, at each point in the medium and in any given direction. Before discussing the problems of radiative transfer for the polarized radiation, it is useful to understand how a beam of arbitrarily polarized light is represented. This fixes our idea, about what are going to be repeatedly used in the forthcoming chapters the Stokes vector and the polarization normal waves - and helps to avoid the confusion with notations. It has been shown by Chandrasekhar (1950) that the formulations of the equations of radiative transfer can be most conveniently effected if a parametric representation of the polarized light in terms of four parameters, originally introduced by Stokes are employed. We give below certain basic definitions, which are useful in future discussion. A clear mathematical description of all aspects of polarized radiation is given in Chandrasekhar (1950), from which we have selected the required equations.

(i) Stokes parameters: An arbitrarily polarized beam of light can be completely analyzed by the following procedure. Introduce a known amount of phase retardation in one direction relative to the direction at right angles

to it, and then measure the intensity in all directions
in the transverse plane. Let

$$\xi_l = \xi_l^{(o)} \sin(\omega t - \epsilon_l) \quad \text{and} \quad \xi_r = \xi_r^{(o)} \sin(\omega t - \epsilon_r) \quad , \tag{1-1}$$

represent instantaneous
vibrations of the elec-
tric vector in a beam of
light. The amplitudes
and phases undergo irre-
gular variations in a
partially polarized beam
– but the ratio of ampli-
tudes and the difference
in phases 'remain con-
stant'. At present we
are interested in phase differences only. Hence equation
(1-1) can be written as
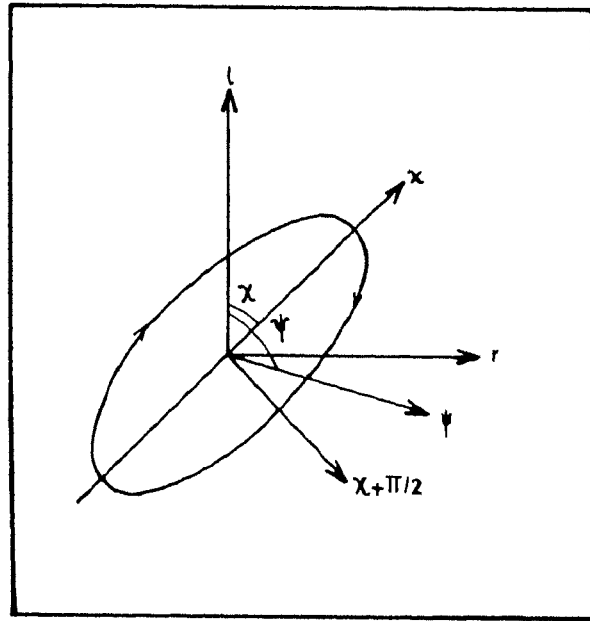
$$\xi_l = \xi_l^{(o)} \sin \omega t \quad \text{and} \quad \xi_r = \xi_r^{(o)} \sin(\omega t - \delta) \tag{1-2}$$

subjecting the second component to a phase retardation

ϵ , we get

$$\xi_l = \xi_l^{(o)} \sin \omega t \quad \text{and} \quad \xi_r = \xi_r^{(o)} \sin(\omega t - \delta - \epsilon) \tag{1-3}$$

Resolve the vibration (1-3) in a direction making an angle ψ with respect to the l direction, i.e.

$$\xi_l^{(o)} \sin \omega t \; \cos \psi + \xi_r^{(o)} \sin(\omega t - \delta - t) \sin \psi$$

$$= \left[\xi_l^{(o)} \cos \psi + \xi_r^{(o)} \cos(\delta + \epsilon) \sin \psi \right] \sin \omega t -$$

$$- \xi_r^{(o)} \sin(\delta + \epsilon) \sin \psi \cos \omega t \tag{1-4}$$

The momentary intensity is therefore given as the sum of the squares of the amplitudes,

$$\xi^2(\psi, \epsilon) = \left[\xi_l^{(o)} \right]^2 \cos^2 \psi + \left[\xi_r^{(o)} \right]^2 \sin^2 \psi +$$

$$+ 2 \xi_l^{(o)} \xi_r^{(o)} (\cos \delta . \cos \epsilon - \sin \delta . \sin \epsilon) \sin \psi \cos \psi . \tag{1-5}$$

To get the apparent intensity in the direction ψ, we must take the mean of this expression keeping ψ and ϵ constant. Thus

$$I(\psi, \epsilon) = \overline{\left[\xi_l^{(o)} \right]^2} . \cos^2 \psi + \overline{\left[\xi_r^{(o)} \right]^2} . \sin^2 \psi$$

$$+ \left\{ 2 \overline{\left[\xi_l^{(o)} \xi_r^{(o)} \cos \delta \right]} \cos \epsilon - 2 \overline{\left[\xi_l^{(o)} \xi_r^{(o)} \sin \delta \right]} \sin \epsilon \right\} \sin \psi \cos \psi \tag{1-6}$$

From this equation it is clear that the intensities in the l and γ directions are independent of ϵ and are given by

$$I_l = \overline{\left[\xi_l^{(o)} \right]^2} \qquad ; \qquad I_\gamma = \overline{\left[\xi_r^{(o)} \right]^2} \tag{1-7}$$

Now, let

$$U = 2\overline{\left[\, \xi_l^{(o)}\, \xi_r^{(o)}\, \cos\delta\,\right]} \quad \text{and} \quad V = 2\overline{\left[\, \xi_l^{(o)}\, \xi_r^{(o)}\, \sin\delta\,\right]}\;.$$

(1-8)

These definitions of the Stokes parameters are consistent with the usual definition for an elliptically polarized beam of light given by

$$I_l = \overline{\left[\, \xi_l^{(o)}\,\right]^2}\;; \quad I_r = \overline{\left[\, \xi_r^{(o)}\,\right]^2}\;; \quad Q = I_l - I_r\;,$$

(1-9)

$$U = 2\overline{\left[\, \xi_l^{(o)}\, \xi_r^{(o)}\,\right]}\cos\delta\;; \quad V = 2\overline{\left[\, \xi_l^{(o)}\, \xi_r^{(o)}\,\right]}\sin\delta\;.$$

(1-10)

since in the latter case, the phase difference remains constant. From the equations (1-7),(1-8) and (1-6), we can write

$$I(\psi,\epsilon) = I_l\cos^2\psi + I_r\sin^2\psi + (U\cos\epsilon - V\sin\epsilon)\,\frac{\sin 2\psi}{2}$$

(1-11)

or, defining

$$\left.\begin{array}{l} I = I_l + I_r = \overline{\left[\, \xi_l^{(o)}\,\right]^2} + \overline{\left[\, \xi_r^{(o)}\,\right]^2} \\[2mm] Q = I_l - I_r = \overline{\left[\, \xi_l^{(o)}\,\right]^2} - \overline{\left[\, \xi_r^{(o)}\,\right]^2} \end{array}\right\}\;,$$

(1-12)

we can also write

$$I(\psi, \epsilon) = \frac{I+Q}{2}\cos^2\psi + \frac{I-Q}{2}\sin^2\psi + (U\cos\epsilon - V\sin\epsilon)\frac{\sin 2\psi}{2}$$

$$= \frac{1}{2}[I + Q\cos 2\psi + (U\cos\epsilon - V\sin\epsilon)\sin 2\psi] \ . \qquad (1\text{-}13)$$

From the equation (1-13) we can see that an arbitrarily polarized light is characterized by the set of four Stokes parameters I, Q, U and V. The vector $(I \ Q \ U \ V)^T$ is called the Stokes vector of the polarized radiation field.

(ii) Equivalence: Two beams characterized by the same set of Stokes parameters are equivalent.

(iii) Additivity: The Stokes parameters of a mixture of several 'independent streams' of elliptically polarized light is given by an algebraic sum of the Stokes parameters of the separate streams. Thus

$$\left.\begin{array}{l} I = \sum I^{(n)} \quad ; \quad I_\ell = \sum I_\ell^{(n)} \quad ; \quad I_r = \sum I_r^{(n)} \\[2mm] Q = \sum Q^{(n)} = \sum I^{(n)}\cos 2\beta_n \ \cos 2\psi_n \\[2mm] U = \sum U^{(n)} = \sum I^{(n)}\cos 2\beta_n \ \sin 2\psi_n \\[2mm] V = \sum V^{(n)} = \sum I^{(n)}\sin 2\beta_n \end{array}\right\} \qquad (1\text{-}14)$$

$I^{(n)}$, χ_n and β_n are the intensity, the plane of polarization, and the ellipticity of the component streams. This

property holds as long as the component streams
forming the mixture have no permanent phase rela-
tions between themselves.

(iv) Natural light: It is represented by

$$I(\psi, \epsilon) = \frac{1}{2} I \quad ; \quad Q = U = V = 0 \tag{1-15}$$

(v) Elliptically polarized light: If the orientation of
the ellipse is χ, then

$$\tan \beta = \pm \frac{\text{minor axis}}{\text{major axis}} \quad , \quad [0, \pi/2] \tag{1-16}$$

The $\pm$ signs of β correspond respectively to right and
left handed polarizations. Also

$$I^2 = Q^2 + U^2 + V^2 \tag{1-17}$$

(vi) Oppositely polarized streams: Two streams related
in the manner (β , χ) and ($-\beta$, $\chi + \pi/2$) are said
to be oppositely polarized. It can be shown that the
natural light is equivalent to any two independent
'oppositely polarized' streams of half the intensity.
This concept of opposite polarization is useful in
understanding the polarization normal waves introduced
in section (2.1).

Notice that, for partially polarized radiation,
$I^2 > Q^2 + U^2 + V^2$ The degree of linear polari-
zation (p), circular polarization (q) and the polari-
zation position angle (ϕ) are defined as

$$p = \sqrt{Q^2+U^2}/I \quad ; \quad q = V/I \quad ; \quad \phi = \tfrac{1}{2} \tan^{-1}(U/Q) \qquad (1\text{-}18)$$

We use this notation throughout our discussion in the
thesis.

1.3 A preview of the results presented in the thesis

We review the existing literature and recent
developments in each individual chapter. Here we indi-
cate only the topics discussed in the chapters to follow
and try to make a common link between them. In Chapter 2
we first describe the simple case of radiative transfer
equation for the continuum polarization in two alternative
but equivalent representations. We then calculate the
strong field continuous dichroism for various absorption
coefficients relevant to a realistic stellar atmosphere.
We also give a second order accurate formula for cal-
culating the magnetic dichroism of a general power-law
type opacity. This may be useful in rapid computations
of magnetic dichroism in a practical model construction,

where the transfer equation has also to be integrated over a visible disk of the star. Then we compare the solutions obtained on some test cases with standard methods used by other authors. Lastly we present the results on continuum polarization in magnetic white dwarfs, and discuss the interesting behaviour of linear (p) and circular (q) polarizations near the absorption edges of the bound-free absorption coefficient.

In chapter 3 we treat the more complicated problem of magneto-scattering plus magneto-absroption, in the continuum. Here we describe in detail the numerical method of solution of the radiative transfer equation, for true absorption and coherent scattering taken together. Next, we calculate the magnetic dichorism of the continuum absorption and scattering coefficients exactly, using recent developments in the calculation of these cross sections. Since the theory of these cross sections was originally given for the polarization normal modes of a plasma, we have preferred to solve the transfer equation in the normal mode representation itself, though a transformation to the Stokes representation is straight forward. Then we describe the polarization of radiation in the realistic atmosphere of a hot magnetic white dwarf. The strong field magneto-scattering and absorption are included in the computation of the

emergent intensities. A similar calculation has also been done for the conditions typical of polar cap regions of the accreting magnetized neutron stars. We discuss the interesting behaviour of the polarization and spectra when both these types of atmospheres are externally irradiated. The role of change in the source function gradients caused by such an irradiation and heating, is also shown. It should be noted that the computation of magnetic dichroism is more exact here than the second chapter and the scattering has also been included.

In Chapter 4 we compute the Zeeman line profiles formed in strong magnetic fields of white dwarfs. First we describe the line transfer equation in both the Stokes vector as well as normal wave representations. Then we study the line formation under general physical conditions. The magnetic field whose magnitude and direction changes with depth, the velocity fields in the atmosphere or the combination of those factors taken together are included in studying the Zeeman line formation. We also indicate a simplification of our earlier method of solution described in chapter 3, in treating the true absorption problems. We show the practical utility of this simplification by applying it to some computationally time consuming problems, like disk integrated continuum polari-

zation and cyclotron resonance absorption problems.
The pure Zeeman line transfer equations described
in this section are useful for our future discussion
in chapter 5, where we solve the line transfer equation
including many new physical effects.

The chapter 5 mainly deals with the Zeeman line
formation in much more realistic conditions than
considered earlier. First we briefly discuss the
very recent development of combined Stark-Zeeman effect.
Stark effect has not been consistently included in any
of the Zeeman line formation problems till now, to
our knowledge. We present this somewhat difficult but
essential computation briefly. We show the impact of
combined Stark-Zeeman effect on the hydrogen line forma-
tion in a main sequence star model atmosphere, represen-
tative of a magnetic Ap star. The plasma polarization
shift of hydrogen-like ionic lines has been studied in
laboratory plasmas for quite some time. Here we have
discussed the impact of this effect on some Zeeman sub-
components of Hc II lines as a function of magnetic
field and the temperature. This mechanism, is shown
to affect the line formation strongly. The influence
of the orientation of atomic magnetic moment in a strong
magnetic field is found to contribute to the broadband
polarization, in strong field white dwarfs. The effect
of organized velocity fields or the atmospheric structure

are shown to affect the Zeeman lines strongly. Lastly
in this chapter we write the normal wave transfer
equation for correctly treating the transfer of long
wavelength radiation in a magnetoplasma. We demonstrate
that one has to include the ray refraction effects in
treating the transfer of microwaves and radiowaves etc.,
to get reliable flux and polarization spectra of the
extended radio-emitting regions.

In chapter 6 we develop a solution of the equation
of transfer for the resonance line polarization. First
we describe the relevant general equations of the problem.
Then we describe a general numerical method of solution
of the problem, including the frequency redistribution
in the line source function, and the sphericity of the
atmosphere. After making a comparitive study of the
solutions, using some standard results available in the
literature, we proceed to calculate the line profiles
and polarizations in a spherically symmetric medium taking
account of various line scattering mechanisms such as
coherent scattering, complete frequency redistribution
and partial frequency redistribution.

CHAPTER 2

THE SOLUTION OF THE EQUATIONS OF CONTINUUM RADIATIVE
TRANSFER IN ANISOTROPIC ABSORBING MEDIA

The equation of transfer for Zeeman split lines
was formulated by Unno (1956) in the Stokes vector
formalism. Those general equations can be used for
the polarization transfer in the continuum also as we
do now in this chapter. Unno equations hold in
general to any anisotropic media under pure absorption
approximation. Kemp (1970a) showed that the light
emitted from any thermal source in a magnetic field
is characterized by diffuse circular polarization in
the continuum. He has proven his prediction in the
laboratory,and has found the effect in a white dwarf
Kemp (1970b). This was the starting point of really
serious attempts to detect and then interpret conti-
nuum circular polarization in stellar objects, which,
for obvious reasons was believed to be extremely small
as to go undetected. After unsuccessful attempts to
explain the 'wavelength dependent' continuum polari-
zation of magnetic white dwarfs,using the 'magneto-
emission' theory it was realised that a radiative
transfer calculation is essential to get the correct
wavelength dependence (see Shipman,1971). Later
Angel and Landstreet (1974) extended his approach.
Lamb and Sutherland (1974) gave a general treatment

of the magnetic dichroism of bound-free and free-
free absorption coefficients and gave analytical
solution to the transfer equation, written as a density
matrix equation. The same problem was approached in
the so called 'normal wave representation', by Gnedin
and Pavlov (1974). After wards many refinements have
been made, in terms of using realistic atmospheres,
including new dichroic opacities and using various
field geometries (see Martin and Wickramasinghe,1984
and references there in). In this section we shall
present a numerical solution for this problem of conti-
nuum radiative transfer in a magnetoactive medium. We
shall use LTE (local thermodynamic equilibrium) model
atmospheres in plane parallel approximation in all our
studies. We shall use both uniform and dipole field con-
figurations and compute the emergent spectrum and pola-
rization.

2.1   The continuum transfer equation in Stokes vector
      formalism and its relation to the polarization
      normal wave transfer equations

(i) Stokes vector transfer equation: Unno derived the
Stokes vector transfer equation for magneto-absroption
only. Beckers (1969) introduced the magneto-optical
effects (also called magnetic birefringence) into the

Unno equation. Further on we shall always use the Unno-Beckers equation when we work in Stokes vector formalism. The equation is written as

$$\mu \frac{dI}{\rho dz} = - (K_I I + K_Q Q + K_V V) + K_I B_\gamma \quad , \qquad (2\text{-}1)$$

$$\mu \frac{dQ}{\rho dz} = - (K_Q I + K_I Q - \rho_R' U) + K_Q B_\gamma \quad , \qquad (2\text{-}2)$$

$$\mu \frac{dU}{\rho dz} = - (\rho_R' Q + K_I U - \rho_W' V) \quad , \qquad (2\text{-}3)$$

$$\mu \frac{dV}{\rho dz} = - (K_V I + \rho_W' U + K_I V) + K_V B_\gamma \qquad (2\text{-}4)$$

where $I = (I \ Q \ U \ V)^T$ is the Stokes vector with the four Stokes parameters as components. $\mu = \cos\theta$, θ = angle between the ray direction and the axis along which the optical depth is measured (Z-axis). B_γ is the local source function which is just the Planck function in LTE approximation. The absorption coefficients for the Stokes parameters are given by

$$K_I = \frac{1}{2} K_p' \sin^2\psi + \frac{1}{4} (K_\ell' + K_r') (1 + \cos^2\psi) \quad , \qquad (2\text{-}5)$$

$$K_Q = \frac{1}{2} K_p' \sin^2 \psi - \frac{1}{4} (K_l' + K_r') \sin^2 \psi$$

$$(2-6)$$

$$K_V = \frac{1}{2} (K_r' - K_l') \cos \psi \quad ;$$

$$(2-7)$$

where ψ is the angle between the direction of the ray
and the direction of the magnetic field. k_p' , k_1' and k_r'
are the Zeeman-shifted continuous absorption coefficients.
The solution $(I \; Q \; U \; V)^T$ to Equations (2-1) to (2-4)
is to be multiplied by

$$
\begin{bmatrix}
1 & 0 & 0 & 0 \\
0 & \cos 2\varphi & -\sin 2\varphi & 0 \\
0 & \sin 2\varphi & \cos 2\varphi & 0 \\
0 & 0 & 0 & 1
\end{bmatrix}
$$

$$(2-8)$$

to obtain the actual solution for an arbitrary orienta-
tion of the magnetic field in a coordinate system in
which φ is the field azimuth with respect to an arbi-
trary x-axis at right angles to the line of sight.
The parameters ρ_R' and ρ_W' represent the magneto-optical
effects due to free electrons. ρ_R' produces a rotation
of the electric vector of linearly polarized light. ρ_W'
leads to a phase retardation between the linear polari-

zations parallel and perpendicular to the field direction. These parameters, for $\omega \gg \omega_c$ are given by

$$\rho'_R = -\frac{\omega_p^2 \, \omega_c \cos\psi}{c(\omega^2 - \omega_c^2)} \quad , \tag{2-9}$$

$$\rho'_W = -\frac{\omega_p^2 \, \omega_c^2 \sin^2\psi}{2c\omega(\omega^2 - \omega_c^2)} \quad ; \tag{2-10}$$

where $\omega_p^2 = (4\pi N e^2 / m_e)$ is the plasma frequency and $\omega_c = eB/m_e c$ is the cyclotron frequency. k'_p , k'_l and k'_r are the continuous absorption coefficients at the Zeeman shifted frequencies when it is assumed that all the sources of opacities are dichroic $(k'_p = k_o , k'_l = k_- , k'_r = k_+)$. We can also select only those opacities as dichroic for which Lamb-Sutherland shifts are known to be applicable (Landstreet and Angel, 1975). With this choice equations (2-5) to (2-7) become

$$K_I = \beta + \tfrac{1}{2} k_p \sin^2\psi + \tfrac{1}{4} (k_l + k_r)(1 + \cos^2\psi) \quad , \tag{2-11}$$

$$K_Q = \tfrac{1}{2} k_p \sin^2\psi - \tfrac{1}{4} (k_l + k_r) \sin^2\psi \quad , \tag{2-12}$$

$$K_V = \tfrac{1}{2} (k_r - k_l) \cos\psi \quad ; \tag{2-13}$$

where $\beta = (k^c - k_p)$ is the 'residual opactity'. $k_p = k_o(\text{H-bf, H-ff, He-bf, He-ff, } \bar{\text{H}}\text{-bf, } \bar{\text{H}}\text{-ff, } \bar{\text{He}}\text{-ff})$ is

the 'selective' continuous opacity for p electrons in our choice (see Unno,1956; p.113). Defining an optical depth scale $d\tau = -k^c\rho\, dZ$ using the non-magnetic opacity k^c , we can write equations (2-1) to (2-4) as

$$\mu \frac{dI}{d\tau} = \eta_I (I - B_\nu) + \eta_Q Q + \eta_V V \; , \tag{2-14}$$

$$\mu \frac{dQ}{d\tau} = \eta_Q (I - B_\nu) + \eta_I Q - \rho_R U \; , \tag{2-15}$$

$$\mu \frac{dU}{d\tau} = \rho_R Q + \eta_I U - \rho_W V \tag{2-16}$$

$$\mu \frac{dV}{d\tau} = \eta_V (I - B_\nu) + \rho_W U + \eta_I V \; ; \tag{2-17}$$

with

$$\eta_I = \left(\frac{k_I}{k^c}\right) = \epsilon + \frac{\eta_p}{2} \sin^2\psi + \frac{\eta_l + \eta_r}{4} \left(1 + \cos^2\psi\right) \tag{2-18}$$

and

$$\left.\begin{aligned} \eta_Q = (K_Q / k^c) \; , \quad \eta_V = (K_V / k^c) \; , \quad \eta_{p,l,r} = (k_{p,l,r} / \rho\, k^c) \\ \rho_{R,W} = (\rho'_{R,W} / \rho\, k^c) \quad \text{and} \quad \epsilon = (\beta / \rho\, k^c) \end{aligned}\right\} \tag{2-19}$$

Note that $\epsilon << 1$. Equations (2-14) to (2-17) represent outgoing rays ($0 < \mu \le 1$). The same set of equations represents the inward going rays by replacing μ by ($-\mu$),

$(0 < \mu \le 1)$. The method of solution which is based
on the 'discrete space theory of radiative transfer',
Grant and Hunt (1968a,1969a,b) and Peraiah and Grant
(1973), suitably modified for the case of magnetized
media will be presented in section 3.3 along with a
detailed comparison with some standard methods of
solution. The Unno solution for equations (2-14) to
(2-17) at $\tau = \tau_{max}$ can be employed as a suitable
boundary condition for the problem (see section 4.1).

(ii) Normal wave transfer equations: The formalism
described above is very general. There is a formalism
which is considerably simpler, and faster on a computer.
However, it is far from being always applicable. This
is called the 'normal wave representation' of the pola-
rization transfer equations. This is based on the concept
of two normal (natural) waves - the ordinary and extra-
ordinary which propagate in an anisotropic medium inde-
pendently of each other. See also the definition of
'oppositely polarized streams' given in section 1.1. It
consists of a system of two 'uncoupled' transfer equations
for the intensities of the normal waves. This formalism
of the polarization radiative transfer equation is appli-
cable in an optically thick medium if at distances corres-
ponding to unit optical thickness the phase shift of one
normal wave compared to the other is large, that is
$\omega \, |n_1 - n_2| \, / c \, >> (k_1 + k_2) / 2$ where ω is the angular fre-

quency of the radiation, η_1 and η_2 are the refractive indices of the normal waves, and k_1 and k_2 their absorption coefficients. The reduction from the general density matrix equations (which are fully equivalent to the Stokes vector formalism), to the normal wave transfer equations is explained in Gnedin and Pavlov (1974). We shall simply write down the equations which we have used in our computations. We shall also discuss briefly the conditions of their validity. The transfer equation for the intensities of elliptically polarized normal waves is given by

$$\mu \frac{d I_j}{\rho\,dz} = - k_j I_j + k_j \frac{B_{\eta}}{2} \quad ; \quad j = 1, 2., \qquad (2\text{-}20)$$

under the usual LTE approximation. $k_j B_{\eta} / 2$ is the thermal emission coefficient with B_{η} the Planck function. The absorption coefficients of the normal waves are given by

$$k_j = k_j^{bf} + k_j^{ff} + \cdots \cdots \cdots \qquad (2\text{-}21)$$

where bf = bound-free and ff = free-free, representing the type of absorption. The relation with Stokes parameters is represented by

$$I = \sum_j I_j \quad ; \quad Q = \sum_j P_Q^j I_j \quad ; \quad U = \sum_j P_U^j I_j \quad ; \quad V = \sum_j P_V^j I_j \quad , \qquad (2\text{-}22)$$

$j = 1, 2$. For the transfer equation in the restricted coordinate system (χ = the azimuth of the magnetic field $\equiv 0$), $P_U^j \equiv 0$ and $U \equiv 0$. The coefficients P_Q^j and P_V^j are given by

$$P_Q^j = (-1)^j \frac{|q|}{\sqrt{1+q^2}} \quad ; \quad P_V^j = (-1)^j \frac{sgn(q)}{\sqrt{1+q^2}} \quad ; \quad q = \frac{1-\xi^2}{2\xi} \cdot \frac{\omega_c}{\omega} \tag{2-23}$$

It is important to note that, we can also write

$$P_Q^j = \frac{1-K_j^2}{1+K_j^2} \cos 2\chi_j \quad ; \quad P_V^j = \pm \frac{2K_j}{1+K_j^2} \quad , \tag{2-24}$$

where $K_j = a_j / b_j$ is the ratio of the major to the minor axes of the polarization ellipses of the normal waves and χ_j the orientation of their major axes with respect to a fixed axis in space, in the plane transverse to the direction of propagation. It is also important to remember that the equation (2-20) can be used when the normal waves are orthogonal to each other that is, when the major axes of their polarization ellipses are perpendicular to each other $(|\chi_1 - \chi_2| = \pi/2)$ and the ellipses themselves are similar. In a magneto-active plasma, the requirement of orthogonality is satisfied for 'any angle of propagation' and for 'any magnitude' of the magnetic field if the radiation frequency

$\omega \gg \nu_e$, the electron ion collision frequency. Thus
we can define a non-orthogonality parameter $|x|, 0 \le |x| \le 1$
as a measure of applicability of the normal wave transfer
equations. This parameter is defined as

$$|x|^2 = \frac{1 - \sqrt{1-y^2}}{1 + \sqrt{1-y^2}} \;\; ; \;\; y = \frac{2b}{(a^2 + b^2 + 1)} \;\; ; \quad \begin{array}{l} a = \mathcal{R}e\,(\gamma) \\ b = \mathcal{I}m\,(\gamma) \end{array} \qquad (2\text{-}25)$$

where γ is a dimensionless complex parameter whose
value depends on the particular situation under consider-
ation. For example, for a cold tenuous ($\omega \gg \omega_p$, $\omega_p = \sqrt{\frac{4\pi N_e e^2}{m_e}}$
being the plasma frequency) magnetoactive plasma, for
which $|n_j - 1| \ll 1$, the γ and y parameters
are given by

$$\gamma = \frac{1}{2}\frac{\omega_c}{\omega + i\nu_e}\,\sin\psi\,\tan\psi \;\; ; \;\; y = \frac{\omega_c\,\nu_e\,\sin\psi\,\tan\psi}{\omega^2 + \nu_e^2 + (\omega_c^2\,\sin^2\psi\,\tan^2\psi)/4} \;\; , \qquad (2\text{-}26)$$

where $\omega_c = eB/m_e c$ is the cyclotron frequency. From
this equation, we see that total orthogonality occurs
in a cold magnetoactive plasma only for longitudinal
and transverse propagations of waves ($\psi = 0$, $\psi = \pi/2$)
or under conditions that $\nu_e = 0$. When $\omega \gg \nu_e$, $|x| \ll 1$,
so that the normal waves are almost orthogonal. If the
two conditions $\omega_c\,|\sin\psi\,\tan\psi\,| = 2\,\nu_e$ and
$\omega \to 0$ (or actually $\omega \to \omega_p$) are fulfilled at the
same time, then we have total non-orthogonality ($\gamma = \pm\,i$;
$\chi_{1,2} = \pi + \pi/4$ for $\psi > \pi/2$ and $\chi_{1,2} = \pi - \frac{\pi}{4}$ for $\psi < \frac{\pi}{2}$)

that is, instead of two normal waves, we obtain one
linearly polarized in a direction inclined at an angle
of $\pi/4$ to the direction of the magnetic field.

The absorption coefficients have been derived in
the cold plasma approximation by many authors (see eg.
Gnedin and Sunyaev,1974a and Meszaros,1982 for details
of earlier work). We employ the expressions in the form
given by Kaminker et al.(1982). These coefficients
will be described in section 2.2. Our discussion till
now shows that the two formalisms are closely related
and the transformation is simple, though quite often
it is not necessary to do so. The real connection
is needed mainly because we can utilize the important
work in plasma physics literature where the transfer
coefficients (absorption coefficients, refractive indices,
anomalous dispersion coefficients etc) are derived usually
for the normal waves. We can easily transform them to
the absorption coefficients for p,l and r electrons etc.
such explicit connections are made again in section 4.1
where the line formation problem is treated in both
these representations.

2.2 The calculation of anisotropic continuum transfer coefficients in a magnetic field

(i) Anisotropic transfer coefficients for the Stokes

parameters (η_{I} , η_{Q} , η_{V} , ρ_{R} and ρ_{W}): we have already given expressions for $\eta_{\text{I,Q,V}}$ and $\rho_{\text{R,W}}$ in section 2.1. Notice that $\eta_{\text{I,Q,V}}$ are functions of $\eta_{\text{p,l,r}}$ which have to be primarily calculated for any given set of physical parameters, like magnetic field (B), temperature (T) electron density (N_e) and the particular atomic species involved. We shall apply these calculations in a cool magnetic white dwarf atmosphere, where almost all important sources of continuous opacities are operative. Initially all these non-magnetic opacities are calculated using the polynomial approximations given in Kurucz (1970). The corresponding magnetic dichroism is calculated as described below.

Bound-free dichroism: Following Lamb and Sutherland (1974), we write the field free opacity of hydrogen like atoms in a general form

$$ k(\nu) = const. \, \nu \, f(\nu) , $$

<div align="right">(2-27)</div>

where f(ν) is a continuous function of frequency ν . Further, under the rigid wave function approximation introduced by the same authors, the opacities in the presence of a strong magnetic field for the right circularly polarized light (corresponding to a $\Delta M = +1$ transition) and left circularly polarized light (corres-

ponding to a $\Delta M = -1$ transition) are given by

$$k_{\Delta M}(\nu) = const. \; \nu \, f(\nu - \Delta M \, \nu_L) \quad , \qquad (2-28)$$

$$\Delta M = M_f - M_i = 0, \pm 1 \; , \; \nu_L = eB/4\pi m_e c \; , \qquad (2-29)$$

where M_f and M_i are the final and initial state magnetic quantum numbers respectively, and ν_L is the Larmor frequency. Equations (2-28) are accurate to first order in ($\nu_L \,/\, \nu$). From Equation (2-27) and (2-28) the magnetic dichroism is calculated by

$$\left(\frac{\Delta k}{k}\right)_\nu = \frac{k_+(\nu) - k_-(\nu)}{k_o(\nu)} = \frac{f(\nu - \nu_L) - f(\nu + \nu_L)}{f(\nu)} \qquad (2-30)$$

Expanding the functions $f(\nu - \nu_L)$ and $f(\nu + \nu_L)$ in a Taylor series about ν , one obtains correctly to $O(\nu_L / \nu)$

$$\left(\frac{\Delta k}{k}\right)_\nu = -2 \, \nu_L \, \frac{df(\nu)}{d\nu} \, \frac{1}{f(\nu)} \qquad (2-31)$$

If the unshifted compoment $k_o(\nu)$ can be expressed as a power law, say

$$k_o(\nu) = const. \; \nu^{-\alpha} \qquad (2-32)$$

where α = spectral index of opacity, then from equations (2-27) and (2-31) we get

$$\left(\frac{\Delta k}{k}\right)_{\nu} = 2\,(\alpha + 1)\,\frac{\nu_L}{\nu} \quad . \tag{2-33}$$

Equation (2-32) is very useful for an approximate calculation of circular dichroism. The coefficients $k_+(\nu)$ and $k_-(\nu)$ can be calculated separately in the following manner. From equation (2-27) we get under the rigid wave function approximation of Lamb and Sutherland

$$f\,(\nu - \nu_L) = \frac{k_0\,(\nu - \nu_L)}{Const.\,(\nu - \nu_L)} \quad , \tag{2-34}$$

$$f\,(\nu + \nu_L) = \frac{k_0\,(\nu + \nu_L)}{Const.\,(\nu + \nu_L)} \quad , \tag{2-35}$$

$$f\,(\nu) \;=\; \frac{k_0(\nu)}{Const.\,\nu} \quad ; \tag{2-36}$$

and substituting equations (2-34) and (2-35) in equation (2-28), we find that

$$k_+(\nu) \;=\; \frac{\nu}{(\nu - \nu_L)}\; k_0\,(\nu - \nu_L) \quad , \tag{2-37}$$

$$k_-(\nu) \;=\; \frac{\nu}{(\nu + \nu_L)}\; k_0\,(\nu + \nu_L) \tag{2-38}$$

It can be verified that this approximation gives the same result as expressed in equation (2-31). Sub-

-stituting equations (2-34) to (2-36) into equation (2-30)

and after simple algebra one gets for an opacity varying

like (2-32), the general expression

$$\left(\frac{\Delta k}{k}\right)_\nu = \nu \left[\frac{2(\alpha+1)\nu^\alpha \nu_L + 2(\alpha-1)\nu\nu_L^\alpha}{\nu^{-\alpha}(\nu+\nu_L)^{\alpha+1}(\nu-\nu_L)^{\alpha+1}} \right] \qquad (2\text{-}39)$$

For $\nu_L \ll \nu$ which is satisfied for weaker fields, equation

(2-39) reduces to equation (2-31) as

$$\left(\frac{\Delta k}{k}\right)_\nu = \nu \left[\frac{2(\alpha+1)\nu^\alpha \nu_L}{\nu^{-\alpha}\nu^{2(\alpha+1)}} \right] = 2(\alpha+1)\frac{\nu_L}{\nu} \quad . \qquad (2\text{-}40)$$

Notice however that equation (2-39) is more accurate

formula than equation (2-33). But in the actual compu-

tations of dichroism we have used the exact formulae

(2-37) and (2-38).

Free-free dichroism: Free-free dichroism for H and He

were predicted by Kemp (1977a,b). The coefficient $\alpha \simeq 3.0$

for both these atoms. As a first approximation, we have

used the Lamb-Sutherland frequency shifts for the cal-

culation of free-free dichroism also, though they were

originally derived only for bound-free mechanism. We

make this identification because both the grey body

emission formula of Kemp and the rigid wave function

approximation, give same values for the bound-free

dichroism. In fact we have calculated the dichroism

of all the opacity sources using the equations (2-37)

and (2-38).

(ii) Anisotropic transfer coefficients for the normal

waves (k_1 and k_2): we give below some accurate

formulae derived in recent years.

Bound-free absorption coefficients:- For weaker magnetic

fields ($\omega_c << \omega$) an expression given by Pavlov

(1973) in the hydrogenic approximation, can be used

$$k_j^{bf}(\xi) = \left(\frac{k}{\rho}\right)^{obf} \left[1 + \frac{3}{4}\left(\frac{\omega_c}{\Delta\omega}\right)^{3/2} f(x,a) \, A_j(\xi)\right] \tag{2-41}$$

where k^{obf} is the zero field linear absorption coeffi_

cient.

$$x = \frac{\delta\omega}{\omega_c} = \frac{\Delta\omega - N\omega_c}{\omega_c} = \left[\frac{\hbar\omega - E_n}{\hbar\omega_c} - \frac{1}{2}\right] - N = D - N \, , \tag{2-42}$$

where N = Integer (D). Therefore $0 \leqslant x \leqslant 1$.

$$a = \Gamma_D / \omega_c = \frac{\omega}{\omega_c}\sqrt{\frac{kT}{Mc^2}} \, , \tag{2-43}$$

M = mass of the emitting atom. The profile function

f(x,a) which is a periodic function with period unity,

is given by

$$f(x,a) = \frac{1}{a\sqrt{\pi}} \sum_{k=-\infty}^{+\infty} \int_0^{+1} y^{-1/2} \exp\left[-(x-y-k)^2/a^2\right] dy \qquad (2\text{-}44)$$

In the dipole approximation, the absorption amplitudes are given by

$$A_1(\xi) = \xi^2 \quad ; \quad A_2(\xi) = 1 \qquad (2\text{-}45)$$

The energy of the nth level $E_n = I_H(1-1/n^2)$, where $I_H \simeq 21.36 \ 10^{-12}$ ergs. n is the principal quantum number of the bound state. In the optical range (the Paschen continuum), the value of n is 3. Pavlov has calculated the normal wave absorption coefficients for the H^- opacities also. It is interesting to note that k_j of both these opacities undergo resonances at $s\,\omega_c$ (s=1,2,3........) which is the general characteristic expected of a free-free absorption coefficient.

Free-free absorption coefficients:- The free-free absorption coefficient for an ion of charge (Ze) is given by

$$k_j^{ff}(\xi) = \frac{1}{P} \sum_{\alpha=-1}^{+1} t_\alpha^2 \zeta^{(\alpha)} a_\alpha^j(\xi) \qquad , \qquad (2\text{-}46)$$

where $\sigma_T \, N_e \, \zeta^{(\alpha)}$ is the true linear absorption coeffi-

cient for the αth component, of the cyclic projection of (of the medium polarizability tensor) $e_\alpha^j (\zeta)$ see Kaminker et al.(1982)

$$\zeta^{(+1)} = \zeta^{(-1)} \equiv \zeta_\perp = \nu_\perp / \nu \qquad (2\text{-}47)$$

$$\zeta^{(0)} = \zeta_{||} \equiv \nu_{||} / \nu \qquad (2\text{-}48)$$

where the longitudinal and transverse effective colli-sion frequencies are given by (see Pavlov and Panov, 1976; Ventura,1973; Nagel and Ventura,1983)

$$\nu_{||,\perp} = \left(\frac{2\pi}{m_e}\right)^{1/2} \frac{N_i Z^2 e^4}{(kT)^{3/2}} \frac{kT}{\hbar\omega} (1 - \exp[-(\hbar\omega / kT)]) \, g_{||,\perp} \qquad (2\text{-}49)$$

The radiative width is

$$\nu_\gamma = 2 e^2 \omega^2 / 3 m_e c^3 \qquad (2\text{-}50)$$

The magnetic Gaunt factors $g_{||,\perp}$ exhibit resonances at $s\omega_c$ (s=1,2,3,.....). In the present computations we have employed $g_{||,\perp} = g$, the non-magnetic Gaunt factor, which is a good approximation for $\omega_c << \omega$. In the equation (2-46) the quantities t_α which are the dimensionless components of the polarizability tensor of an electron in cyclic coordinates, are given by

$$t_\alpha = \left(1 + \alpha \sqrt{u}\right)^{-1} \quad ; \quad \sqrt{u} = \frac{\omega_c}{\omega} = \frac{eB}{m_e c \omega} \tag{2-51}$$

The amplitudes $a_\alpha^j(\xi)$ are given by

$$a_0^j(\xi) = \frac{1-\xi^2}{2}\left(1 + P_a^j\right) \quad ; \quad a_{\pm 1}^j(\xi) = $$

$$= \frac{1}{4}\left[1 + \xi^2 \pm 2 P_v^j \xi - P_a^j(1-\xi^2)\right] \tag{2-52}$$

satisfying the completeness and transversality conditions (Ventura, 1979)

$$\sum_{j=1,2} a_\pm^j(\xi) = \frac{1+\xi^2}{2} \quad ; \quad \sum_{j=1,2} a_0^j(\xi) = 1 - \xi^2 \quad ; \quad \sum_{\alpha=-1}^{+1} a_\alpha^j(\xi) = 1 \quad , \tag{2-53}$$

The factors P_a^j and P_v^j are defined in equation (2-23). After having given the formulae required for calculating the magnetic dichroism we shall study the wavelength dependence of these dichroisms. The reason for this particular interest is that the main application of the theory has been in the calculation of the wavelength dependent polarization of the magnetic white dwarfs. The wavelength dependence of the dichroic opacities of H bound-free transitions is shown in Figure 1a. The opacities are calculated for the physical conditions at an optical depth $\tau_{5000} \sim 0.75$ of the model atmosphere of a white dwarf. The local temperature is $T \sim 9050°K$. The dichroism at the absorption edges predicted by Lamb and Sutherland (1974) for optically thin conditions, is found to be
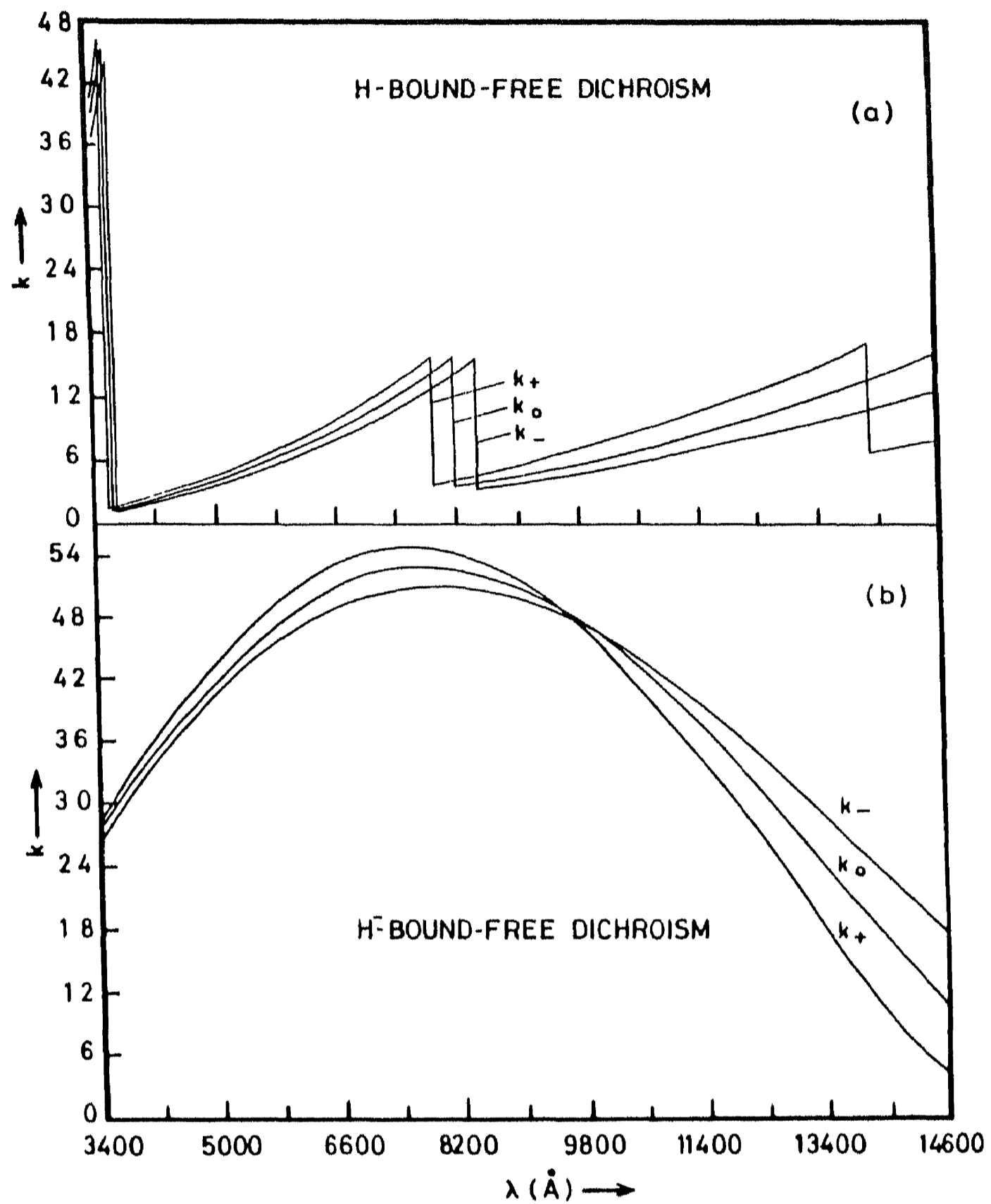
Fig.1. Wavelength dependence of the dichroic opac-ities k_o, k_+, and k_- for $B = 10^7 G$. The symbol k represents the mass absorption coefficient (in the units $g^{-1}cm^2$). The values correspond to an optical depth τ ($\lambda = 5000 \overset{o}{A}$)$\sim 0.75$, where $T = 9040^o K$. (a) Hydrogen bound-free dichroism. (b) Negative hydrogen ion (H^-) bound-free dichroism.

present even for a realistic model also. The strong
polarization changes that occur at these edges can
manifest themselves in the continuous spectrum even
after integrating over the stellar disk. The H^- bound-
free opacity is shown in Figure 1b. This opacity dominates
in the optical wavelengths and reaches its maxima in
the infrared. This source of opacity and dichroism plays
a key role in producing the continuum polarization and
the spectra in the present model. We note that we have
included the He bound-free dichroism also in the cal-
culation using the same hydrogenic prescription of
Lamb-Sutherland shifts. Its spectral index α is nearly
equal to 3. Its wavelength dependence is also almost
similar to that of hydrogen.

In the Figure 2a we have shown the H free-free
dichroism. It can be seen from the figure that the
contribution to dichroism is significant in the far
infrared ($\lambda >$ 13000 Å) though the opacity is still small,
in comparison with the H and H^- bound-free opacities.
This opacity is important mainly in deeper layers of the
stellar atmosphere. The contribution to total dichroism
from He free-free-transitions is again very small for
the temperatures that we have considered. In the model
employed by us, H^- free-free ($\alpha \geq$ 1) is an important
source of dichroism and opacity particularly in the
infrared, see Figure 2b. This was first introduced into
magnetic white dwarf continuum polarization modelling by
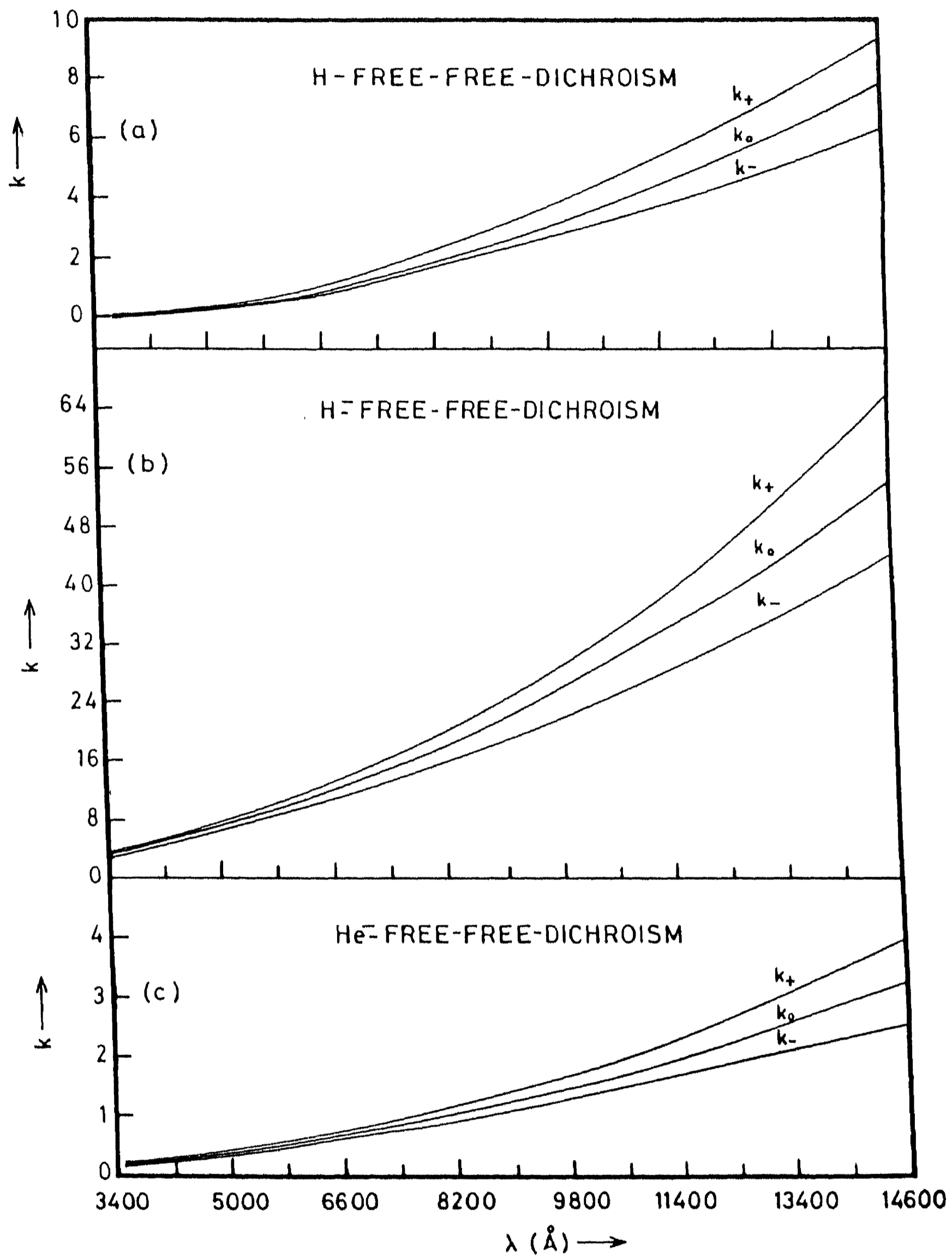
Fig.2. Same as Figure 1 but for free-free dichroic opa-
cities. (a) Hydrogen free-free dichroism. (b) Negative
hydrogen ion dichroism. (c) Negative helium ion (He⁻)
dichroism.

Liebert et al.(1975). The He free-free dichroism ($\alpha \simeq 1.85$) is shown in Figure 2c. An extension of the rigid wavefunction approximation to this important source of opacity in cooler He-rich stars was made by Landstreet and Angel (1975). Figures 1 and 2 also show explicitly the relative contribution to total opacity and dichroism, by different absorbers, in a cool hydrogen-rich white dwarf atmosphere. The main emphasis is to approximately indicate the regions of the spectrum where flux and polarization can be expected to undergo noticeable changes.

We like to point out that the dichroism calculated using the more exact formulae (that of normal waves) also give a similar wavelength dependence except for the fact they undergo resonances at the cyclotron hormonics, with a strong resonance near the fundamental. The Lamb-Sutherland formulae, on the other hand are basically suitable only for $\gamma_L << \gamma$ where γ_L is the Larmour frequency. The cold plasma normal wave absorption coefficients also have a rather similar restriction. They can be generalized by relaxing the 'cold-plasma' and 'collisionless' plasma approximations. Such calculations have been recently attempted by many authors. See Pavlov et al.(1980) for detailed calculations and references to earlier work. The review article by

Meszaros (1982) is also useful in this regard.

2.3 <u>The solution of the transfer problem and its compari-</u>
<u>son with some existing methods</u>

The solution of the polarization radiative transfer
equation (for continuum or the lines), in the true absor-
ption limit is relatively simple compared to the solution
of the general true absorption plus scattering problem,
which is explained in full detail in the next chapter
(chapter 3). The true absorption problem is a special
case of that more general treatment, and all those
equations of the solution method go over to the true ab-
sorption problem by simply substituting $\overline{\omega} \equiv 0$, where $\overline{\omega}$
is the 'albedo' for single scattering (=probability of
scattering). The method of solution is based on 'the
discrete space theory of radiative transfer' developed
by Grant and Hunt (1968a,1969a,b), suitably extended
here for the case of magnetized media. We just mention
here, for the sake of clarity, that the same algorithm
of continuum transfer can be used even for true absor-
ption lines, the difference being only in the construction
of the transfer matrix $\underline{\eta}$. Since for true absorption
mechanism there is no coupling of any two frequency points
in a line or continuum, the transfer problem can be
solved for individual frequency points separately. Because
of the absence of coupling between any two angles, the

the true absorption problem can be solved ray by ray,
in otherwords, for individual values of μ, instead of
simultaneously solving the transfer equation for a
grid of μ'_s . Thus the dimensions of the matrices
appearing in the algorithm is now just (4 x 4) or (2 x 2),
depending on whether one is working in Stokes vector
representation or normal wave representation. The normal
wave transfer equation further can be decoupled from the
matrix form of transfer equation to a set of scalar
transfer equations for ordinary and extraordinary waves,
because the transfer matrix is diagonal. It is not
possible on the other hand to 'diagonalize' the transfer
matrix η of the Stokes vector representation for any
given set of angles ψ and χ , though it can be done
under restrictive conditions on η and χ (see Stenflo,1971
for details). The asymptotic boundary conditions (using
the Unno solution at τ_{max}) in both representations are
given in section 4.1.

With these comments, we shall proceed further to study
the usefulness of the method of solution, in some detail.
This we do, by comparing the solutions obtained by three
methods viz. Runge-Kutta method (RK) Martin-Wickramasinghe
method (MW) and our method of solution, which we call
discrete-space method (DSM). The tables (1) to (5) are

Table 1. Unno atmosphere with a linear source function B_ν = $1+0.2\,\tau$ for the given values of constant opacities η_r and $\eta_p = \eta_l = 1$.

		Runge-Kutta	Martin & Wickramasinghe	Stokes vector representation	Normal wave representation
$\rho_R = 0$; $\rho_W = 0$; $U \equiv 0$					
$\eta_r = 1$	I	1.16000	1.16000	1.16000	1.16000
$\eta_r = 1.1$	I	1.15427	1.15445	1.15445	1.15434
	Q	.00190	.00190	.00190	.00190
	V	-.00521	-.00521	-.00521	-.00521
$\eta_r = 2$	I	1.12566	1.12585	1.12585	1.12585
	Q	.01169	.01169	.01169	.01169
	V	-.03209	-.03209	-.03209	-.03209
$\eta_r = 100001$	I	–	1.08000	1.08000	1.08251
	Q	–	.02738	.02738	.02825
	V	–	-.07517	-.07517	-.07757
$\rho_R = 1.5$; $\rho_W = 0.75$					
$\eta_r = 2$	I	1.12256	1.12276	1.12276	–
	Q	.00855	..00855	.00855	–
	U	-.00836	-.00836	-.00836	–
	V	-.02482	-.02482	-.02482	–

Table 2. A gray atmosphere temperature structure $T = T_e\,(0.75\tau+0.5)^{\frac{1}{4}}$ for different constant opacities η_r and $\eta_p = \eta_l = 1$.

		Runge-Kutta	Martin & Wickramasinghe	Stokes vector representation	Normal wave representation
$\rho_R = 0$; $\rho_W = 0$; $U \equiv 0$					
$\eta_r = 1$	I	1.66270	1.66320	1.66378	1.66328
$\eta_r = 1.1$	I	1.64428	1.64481	1.64535	1.64487
	Q	.00630	.00629	.00631	.00630
	V	-.01730	-.01728	-.01732	-.01730
$\eta_r = 2$	I	1.54135	1.54196	1.54228	1.54189
	Q	.04153	.04150	.04158	.04150
	V	-.11401	-.11391	-.11415	-.11406
$\eta_r = 100001$	I	–	1.33161	1.33160	1.33668
	Q	–	.11350	.11359	.11499
	V	–	-.31157	-.31160	-.31714
$\rho_R = 1.5$; $\rho_W = 0.75$					
$\eta_r = 2$	I	1.53306	1.53375	1.53405	–
	Q	.03466	.03464	.03468	–
	U	-.02477	-.02476	-.02480	–
	V	-.09218	-.09212	-.09226	–

Table 3. A realistic model atmosphere from Wickramasinghe (1972), T_e = 12,000 K for constant opacities η_r and η_p = η_l = 1.

		Runge-Kutta	Martin & Wickramasinghe	Stokes vector representation	Normal wave representation
ρ_R = 0; ρ_W = 0; U≡0					
η_r = 1	I	2.64584	2.64677	2.65103	2.64975
η_r = 1.1	I	2.61067	2.61165	2.61400	2.61457
	Q	.01204	.01202	.01205	.01206
	V	-.03305	-.03299	-.03309	-.03300
η_r = 2	I	2.40256	2.40377	2.40658	2.40629
	Q	.08327	.08317	.08317	.08340
	V	-.22859	-.22832	-.22900	-.22875
η_r = 10000	I	-	1.82349	1.82571	1.82352
	Q	-	.28179	.28238	.28187
	V	-	-.77354	-.77527	-.77377
ρ_R = 1.5; ρ_W = 0.75					
η_r = 2	I	2.38942	2.39083	2.39460	-
	Q	.07454	.07448	.07468	-
	U	-.04114	-.04111	-.04129	-
	V	-.19063	-.19042	-.19090	-

Table 4. A realistic model atmosphere from Wickramasinghe (1972), T_e = 12000 K for τ-dependent opacities η_p = η_l = η with η = 0.2 + τ

		Runge-Kutta	Martin & Wickramasinghe	Stokes vector representation	Normal wave representation
ρ_R = 0; ρ_W = 0; U≡0					
η_r = 1η	I	2.98068	2.97477	2.98229	2.97047
η_r = 1.1η	I	2.95500	2.94920	2.95658	2.94474
	Q	.00879	.00875	.00880	.00870
	V	-.02412	-.02403	-.02415	-.02417
η_r = 2η	I	2.79155	2.78625	2.79293	2.78140
	Q	.06473	.06453	.06481	.06471
	V	-.17770	-.17713	-.17792	-.17764
η_r = 10000η	I	-	1.98794	1.99154	1.99295
	Q	-	.33778	.33911	.34051
	V	-	-.92722	-.93090	-.93460
ρ_R = 1.5; ρ_W = 0.75					
η_r = 2η	I	2.78459	2.77945	2.78606	-
	Q	.05787	.05809	.05828	-
	U	-.06609	-.06537	-.06598	-
	V	-.13551	-.13541	-.13586	-

arranged in the order of increasing complexity; for
example table 1 represents the case of a depth independent
transfer matrix, called the Unno atmosphere, which is
actually a Milne-Eddington mode with a source function,
linear in optical depth. The values given for the
coefficients $\eta_{p,l,r}$ nearly represent various postions
in a hypothetical p,l,r Zeeman triplet, say far in the
continuum or almost near one of the σ - components of
the triplet,etc.(see the first column in the tables).
The tables are self explanatory. The column with the
title Runge-Kutta represents the solutions obtained in
one of the most accurate methods of solving the linear
differential equations. Beckers (1969) used a fourth
order RK for solving the transfer problem (which is
currently a matrix differential equation), and since
then many authors have been using this method. We have
programmed one such RK scheme for computing the results
presented in the column Runge-Kutta. Just as in Beckers
method it is a constant step size matrix RK method, the
step size h being fixed arbitrarily (RK fourth order
schemes are $\sim h^5$ accurate). It turns out that a con-
stant and small step size h is not really needed at all
positions in a line. This is dictated by the magnitudes
of the numbers occuring in the transfer matrix $\underset{\sim}{\eta}$.
But there is no consistent way of exploiting this advantage,

Table 5. A realistic model atmosphere from Wickramasinghe (1972), $T_e = 12000$ K for τ - dependent opacities $\eta_l = 1$, $\eta_p = 1 + \tau$.

		Runge-Kutta	Martin & Wickramasinghe	Stokes vector representation	Normal wave representation
$\rho_R = 0; \rho_W = 0; U \equiv 0$					
$\eta_r = 1$	I	2.55208	2.55216	2.55378	2.55819
	Q	-.09376	-.09461	-.09452	-.09156
	V	0	0	0	0
$\eta_r = 1.1$	I	2.52056	2.52072	2.52123	2.52605
	Q	-.07783	-.07868	-.07856	-.07568
	V	-.02692	-.02684	-.02694	-.02784
$\eta_r = 2$	I	2.32724	2.32773	2.33065	2.31166
	Q	.01778	.01701	.01734	.01892
	V	-.19306	-.19254	-.19324	-.17455
$\eta_r = 100001$	I	–	1.75273	1.75506	1.74403
	Q	–	.25757	.25840	.25736
	V	–	-.70706	-.70934	-.70650
$\rho_R = 1.5; \rho_W = 0.75$					
$\eta_r = 2$	I	2.32646	2.32713	2.33013	–
	Q	.03671	.03618	.03644	–
	U	-.02388	-.02393	-.02392	–
	V	-.18553	-.18522	-.18583	–

Table 6. Accuracy and specific times t (in Secs) on IBM 370/155, required for obtaining a solution $(IQUV)^T$. For all the cases $\mu = 0.8$, $\xi = 0.7$, $Cos\ 2\chi = 0.6$.

Positions		Unno/ exact	Beckers/ RK	Variable step RK	DSM- Strokes
Inside the line: Unno atmosphere B=1+0.2 τ, $\eta_p=\eta_1=1$, $\eta_r=2$, $\rho_R=1.5$, $\rho_W=.75$	I	1.12276	1.12276	1.12268	1.12276
	Q	.00855	.00855	.00852	.00855
	U	-.00836	-.00836	-.00837	-.00836
	V	-.02482	-.02482	-.02476	-.02482
	t	0.05	40	10	0.9
Inside the line: Real atmosphere. $\eta_p=\eta_1=\eta$, $\eta_r=2\eta$, $\eta=0.2+\tau$, $\rho_R=1.5$, $\rho_W=.75$	I	-	2.78459	2.78657	2.78606
	Q	-	.05787	.05768	.05828
	U	-	-.06609	-.06585	-.06598
	V	-	-.13551	-.13535	-.13586
	t	-	40	10	0.9
Continuum: Unno atmosphere B=1+0.2τ, $\eta_p=1$, $\eta_1=.95$, $\eta_r=1.04$, $\rho_R=-.75$, $\rho_W=-.01$	I	1.16076	1.16076	1.16041	1.16076
	Q	-.00004	-.00004	-.00004	-.00004
	U	-.00016	-.00016	-.00016	-.00016
	V	-.00508	-.00508	-.00505	-.00507
	t	0.05	40	7	0.7
Continuum: Real atmosphere $\eta_p=1+.1\tau$, $\eta_1=.95+.106\tau$, $\eta_r=1.04+.0952\tau$, $\rho_R=-.75$, $\rho_W=-.01$	I	-	2.60191	2.60171	2.60125
	Q	-	-.00036	-.00036	-.00036
	U	-	-.00092	-.00091	-.00091
	V	-	-.02641	-.02634	-.02630
	t	-	40	7	0.7

in constant step RK methods. Exactly this inability
makes the constant step RK a slower method. Landi
Degl'Innocenti (1976) improved the RK solutions by
deriving a step size criterion. This criterion is
based on the properties of the eigenvalues of the
transfer matrix η . So this criterion consitently
and automatically fixes the step sizes for different
positions in the line. By using the variable h, we
find that RK scheme becomes nearly 4 to 5 times faster
than the constant step size RK method (see table 6),
retaining almost same accuracy. The third column in
the tables (1-6) represents the MW solutions. Since
we have repeated the test case of Martin and Wickra-
masinghe (1979b), we have simply taken these numbers
from their work. The fourth column 'Stokes vector re-
presentation' are the solutions obtained by our method.
Here, also, the step size is automatically determined by
certain criterion called the positivity of the trans-
mission matrix. It is straight forward to see that this
criterion leads to a step size, calculated using $\tau \leq \tau_{crit} =$
$Min\ (2\ \underline{M}\ \underline{A}^{-1}\ )$. We discuss more about this τ_{crit} in
section 4.2. But we mention here that, this so called
critical optical depth τ_{crit} criterion ($\tau \leq \tau_{crit}$)
is not a strict requirement for the 'true absorption
problems' at least in the stellar atmospheres where the

source function is nearly linear function of τ and, its gradient is smoothly varying. The last column 'normal wave representation' are the solutions obtained in the discrete space method itself, but employing the normal wave transfer equation. The transfer coefficients k_j can be obtained by algebraic transformations, using the parametric values of $\eta_{p,L,r}$ given in the first column, and the analytic expressions for k_j.

The method of solution is second order accurate because of the half-implicit differencing (diamond scheme). It can be used in arbitrary situations, with ease and no extra precaution is needed. From the tables it can be noticed that the solutions obtained using normal wave representation are quite accurate when compared to the Stokes vector formalism, keeping in view of the approximations involved in the normal wave representation at the formulation stage itself, the correctness of which depends also on the 'wavelength position in the line'. The accuracy of the later depends on the position in the line. Actually, near the line centre, the normal waves are non-orthogonal and the basic treatment itself becomes inapplicable. Excepting such situations, it can be used as a convenient alternative to Stokes vector formalism for rapid computations, in realistic situations. The Stokes vector representation however, is the most general,

accurate and complete. The average times in seconds, on IBM 370/155 computer, required to obtain a solution $(I \ Q \ U \ V \ )^T$ in the tables 1 through 5 are: Beckers/RK (36), variable step RK (9), MW(0.35), DSM-Stokes (0.8) DSM-normal wave (0.5). A further comparison of accuracy and computing time is made in the table 6 for both the continuum and line problems in ideal or realistic atmospheres. We conclude that DSM solutions are sufficiently accurate, economical and the method is easily generalizable to true absorption plus scattering problems.

2.4 An astrophysical application: the continuum polarization in magnetic white dwarfs

As already described in section 2.2, it turns out that one has to solve the vector transfer equation for polarized radiation taking into account properly of the magnetically anisotropic absorption coefficients (or magnetic dichroism) in order to get the correct wavelength dependent polarization observed in the magnetic white dwarfs. The review article by Angel (1977) gives an account of various aspects, observational and theoretical, of the problem of polarization in magnetic white dwarfs. It is now possible to make good modelling of these interesting class of objects, by including various dichroisms, strong field Zeeman effect, realistic atmos-

pheric structure and magnetic field distributions on the surface etc., in the radiative transfer equation, and then by surface integrating the specific intensities obtained for a two dimensional grid of latitudes and longitudes over the stellar disk. See Wickramasinghe and Martin (1979), Martin and Wickramasinghe (1984) and Angel et al.(1981) for the develop ments and a detailed list of investigations carried out by many authors. Still, some problems are left open, namely the correct wavelength dependence of flux and polarization in strong field ($B > 5 \cdot 10^{7}$ G) white dwarfs, and the wavelength dependence of all the polarization parameters ($p(\lambda)$, $q(\lambda)$ and $\phi(\lambda)$) in the entire range of wavelengths $\lambda \lambda$ 3000 Å to 14,000 Å. The large degrees of circular and linear polarization and, in particular an increase in these polarizations in infrared wavelengths (contrary to what one expects in a thermal model),in some of the suspected strong field white dwarfs are still not fully understood. However, the inclusion of non-thermal sources of opacities such as cyclotron resonance absorption etc., and a carefully chosen field strength and its distribution over the disk are found to explain the observations fairly well (see Martin and Wickramasinghe, 1984).

We shall now see some details of the radiative trans-

fer solution in a magnetized media. We have used the Stokes vector representation throughout. The model atmosphere employed was provided by Dr.Wehrse (private communication). A grid of atmospheric models for DA (H-rich) and DB (He-rich) white dwarfs have been published by Wehrse (1976) and Wickramasinghe (1972). The model parameters now used are $T_{eff} = 9000$ K, log $g = 8.0$, log A (He,C,N,O) = solar value and log A (metals) = solar value -2.0 (A = elemental (abundance). This model has also been published in Wehrse (1976). We have computed all the non-magnetic opacities using the polynomial approximations of Kurucz (1970). We have compared total opacities calculated in this manner with the opacity data which was also provided by Dr.Wehrse for this particular model, and found the calculation to be accurate. While calculating the magnetic dichroism, one needs the opacity values at two shifted wavelengths also, along with the original wavelength. If one is working in the continuum wavelengths away from the absorption edges, these opacities at the shifted wavelength can be obtained by an accurate interpolation in the non-magnetic opacity table. But such a procedure is not possible when we are close to the edges. Hence we have directly computed the dichroic opacities for all the required wavelength points. First

we have compared the non-magnetic flux F_λ computed by us with the published flux values in Wehrse (1976). This is to check the accurate integration of the transfer equation so that the calculated results genuinely represent the model. The fluxes can be calculated using the definition $F_\lambda = F_I$ ($\tau = 0$) $= 2\pi \int_{-1}^{+1} I(o,\mu) \mu \, d\mu$. From the Figure 3 it can be seen that our calculation of continuum non-magnetic fluxes is accurate and coincides with the original model (the comparison of numbers also is made actually). For the convenience of the flux calculation we have solved the transfer equation for the roots (μ_j, j=1,4) of a Gaussian quadrature.

For the calculation of results presented in Figures (4) to (6) a uniform magnetic field directed along the Z-axis (the symmetry axis of the plane parallel atmosphere) is employed. In Figure 4a, the optical depth dependence of the net flux $F(\tau) = F_I(\tau) = 2\pi \int_{-1}^{+1} I(\tau,\mu) \mu \, d\mu$ is shown, for $\lambda = 5000 \, \overset{o}{A}$. The net flux increases sharply from $\tau = 8$ to $\tau = 0.1$ and then remains almost constant. The magnetic fluxes are slightly smaller than the non-magnetic fluxes. The degree of circular polarization assuming the entire opacity as dichroic ($\epsilon \equiv 0$) is shown in Figure 4b. The polarization of light behaves in an
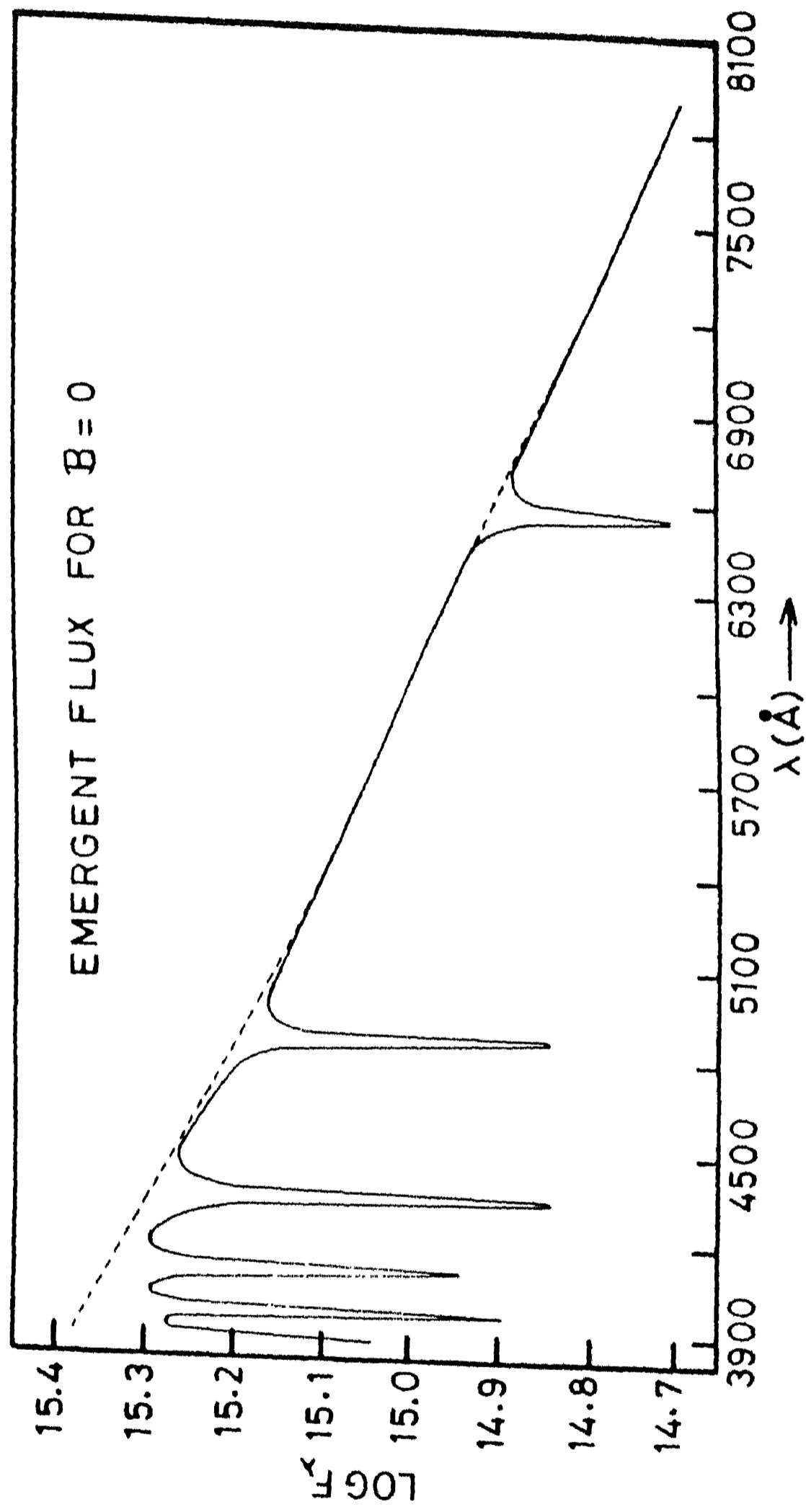
Fig.3. Comparison of our zero-field ($B = 0$) emergent flux (dashed line) with line-blanketed flux taken from Wehrse (solid line). The flux units are erg $cm^{-2} s^{-1}$ per unit wavelength interval $\Delta\lambda = 1$ cm.
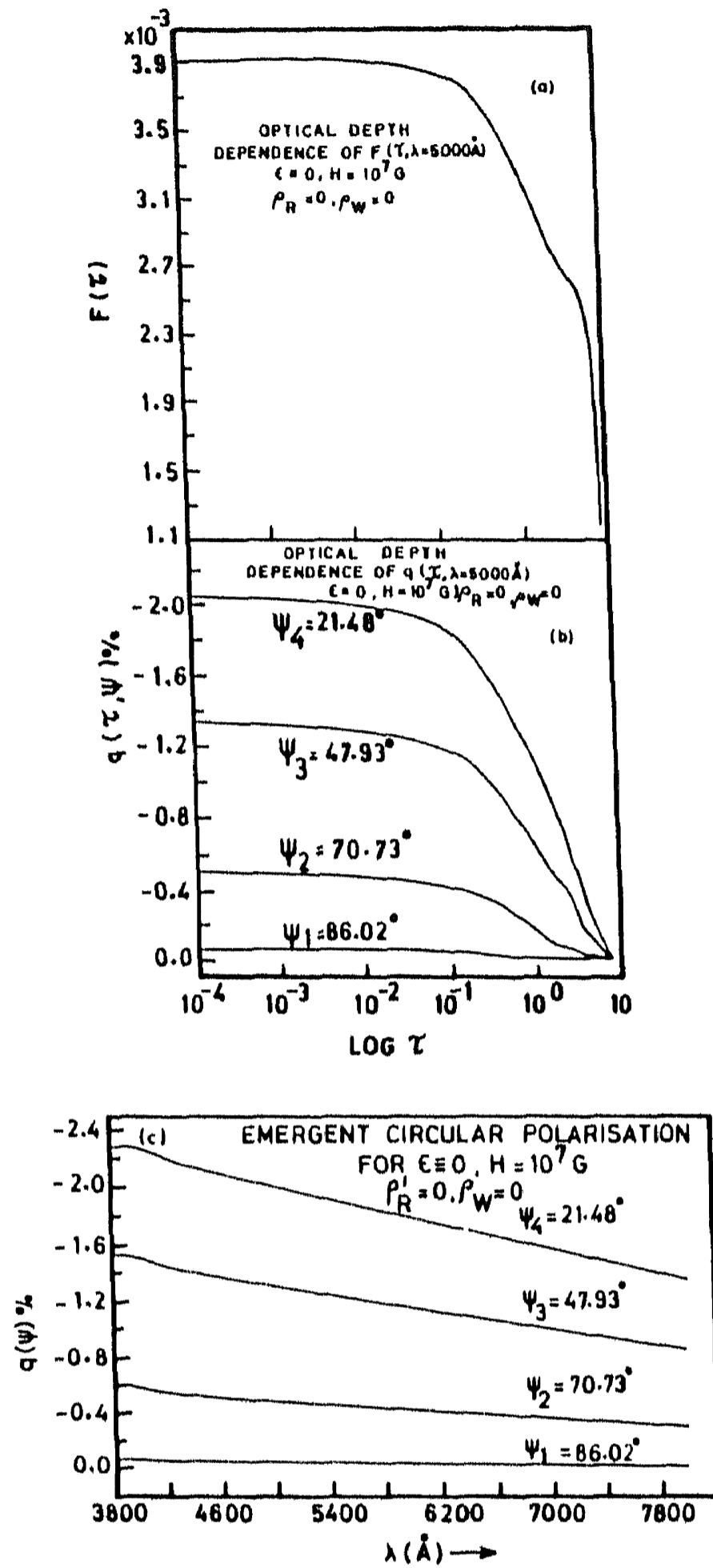
Fig.4. Optical depth dependence of flux and circular polarization. (a) Net flux as a function of optical depth τ (λ = 5000 Å), in units of erg $cm^{-2}s^{-1}Hz^{-1}$. (b) Circular polarization (percentage) as a function of optical depth for $B = 10^7 G$. ψ is the angle between line-of-sight and magnetic field. (c) Wavelength dependence of circular polarization for different values of ψ.

analogous manner to the net flux F (τ). q(τ , ψ)
is larger for smaller v lues of ψ . This behaviour is
as expected of an absorbing layer ot Zeeman active gas.
The wavelength dependence of q(ψ) shown in Figure 4c
reflects the wavelength dependence of the flux unless
there is a source function gradient reversal which
for instance can arise as a result of discontinuity in
the opacity. Notice that the wavelength dependence is
angle dependent. The wavelength dependence is very
weak for ψ = 86.02^o. This is because of the increased
coupling to linear polarization which has a weak wave-
length dependence, unlike circular polarization. The
effect of an absorption 'edge' on the linear polarization
p and circular polarization q is shown in Figure 5a,b
for $\epsilon \neq 0$. The hydrogen bound-free absorption co-
efficient which undergoes drastic changes at the absor-
ption edges (see Figure 1a) gives rise to a large change
in the magnitudes of p and q as well as their signs, the
effect which was predicted by Lamb and Sutherland, for the
optically thin case. The Figures 6 and 7 show the same
quantities for other two intermediate values of angles ψ
where, both p and q are quite large. In all these compu-
tations (Figures 4 to 7), we have neglected magnetic
birefingence ($\rho_R = \rho_W = 0$). In Figure 8 we have
plotted the circular polarization spectrum $\bar{q}(\lambda) = F_V(\lambda) \big/ F_I(\lambda)$
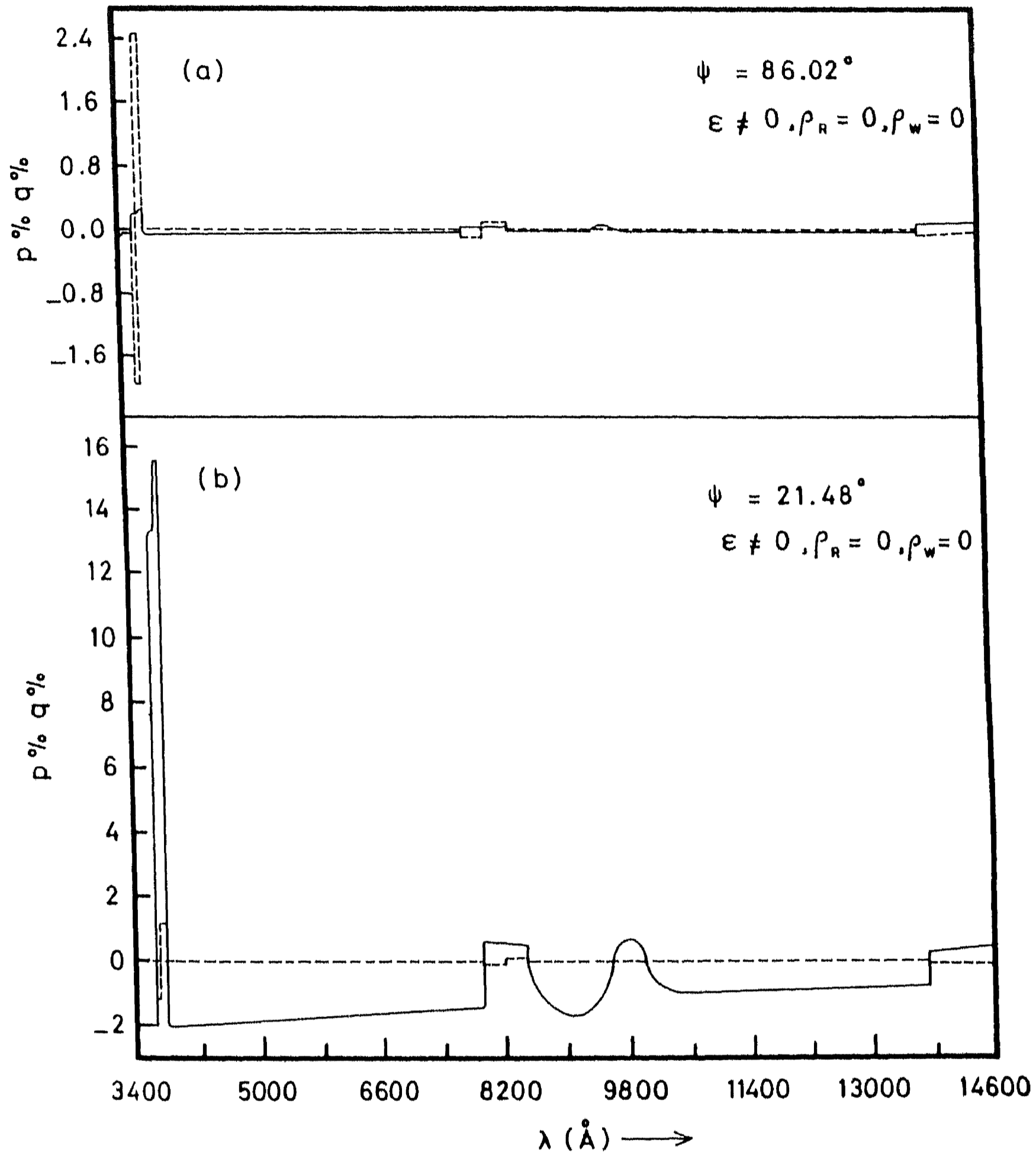
Fig.5. Wavelength dependence of linear polarization p
(dashed line) and circular polarization q (full line)
for $\mathbf{B} = 10^7 G$, and a selective absorption ($\varepsilon \neq 0$).
(a) $\psi = 86.02°$.   (b) $\psi = 21.48°$.
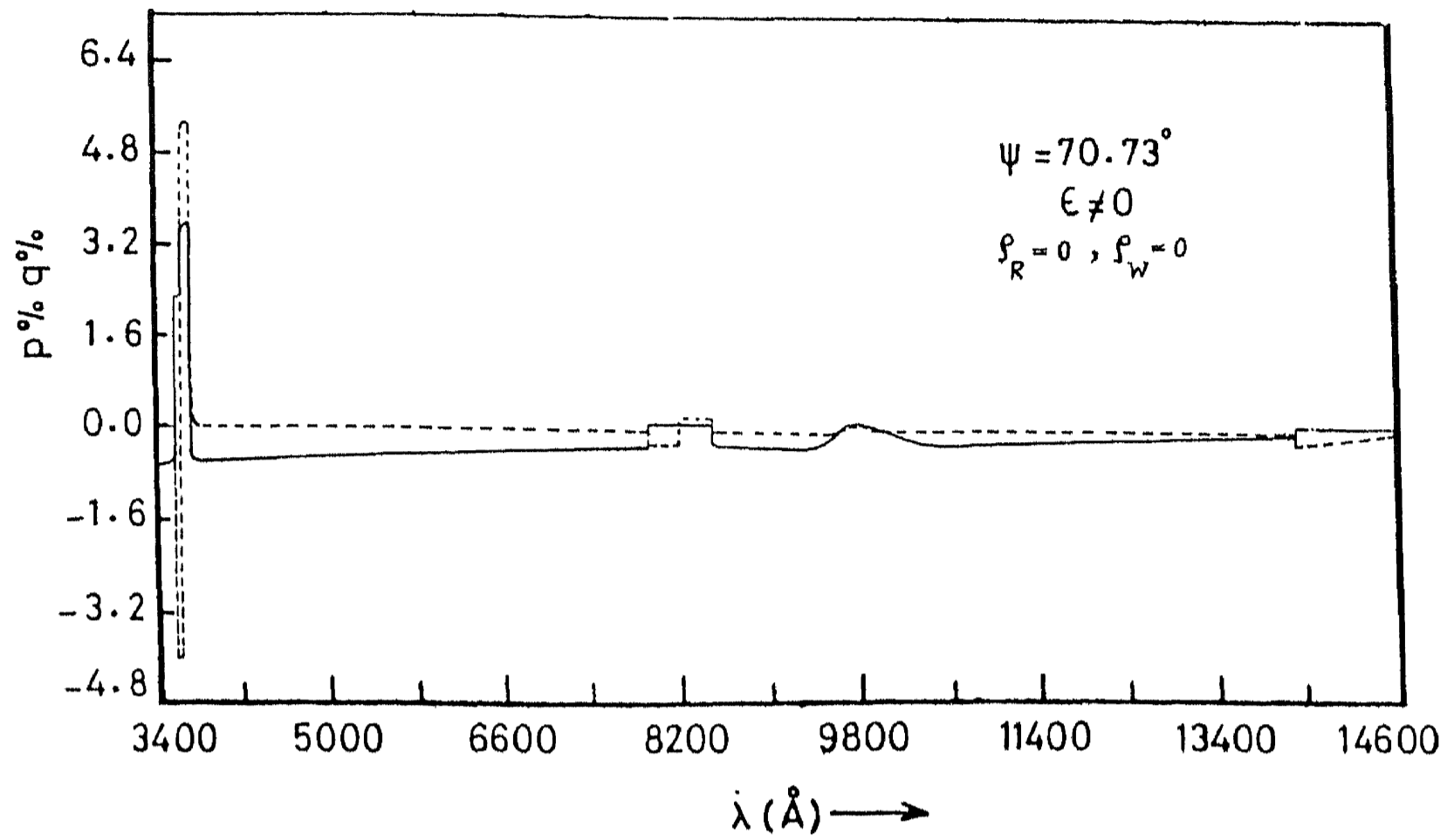
Fig.6. Same as Fig.5 but for ψ = 70.73°

Fig.7. Same as Fig.5 but for ψ = 47.93°

DISK INTEGRATED CIRCULAR POLARISATION

$\epsilon \neq 0 ; H_P = 10^7 G ; i = 0^\circ ; \rho_R \neq 0 ; \rho_W \neq 0$
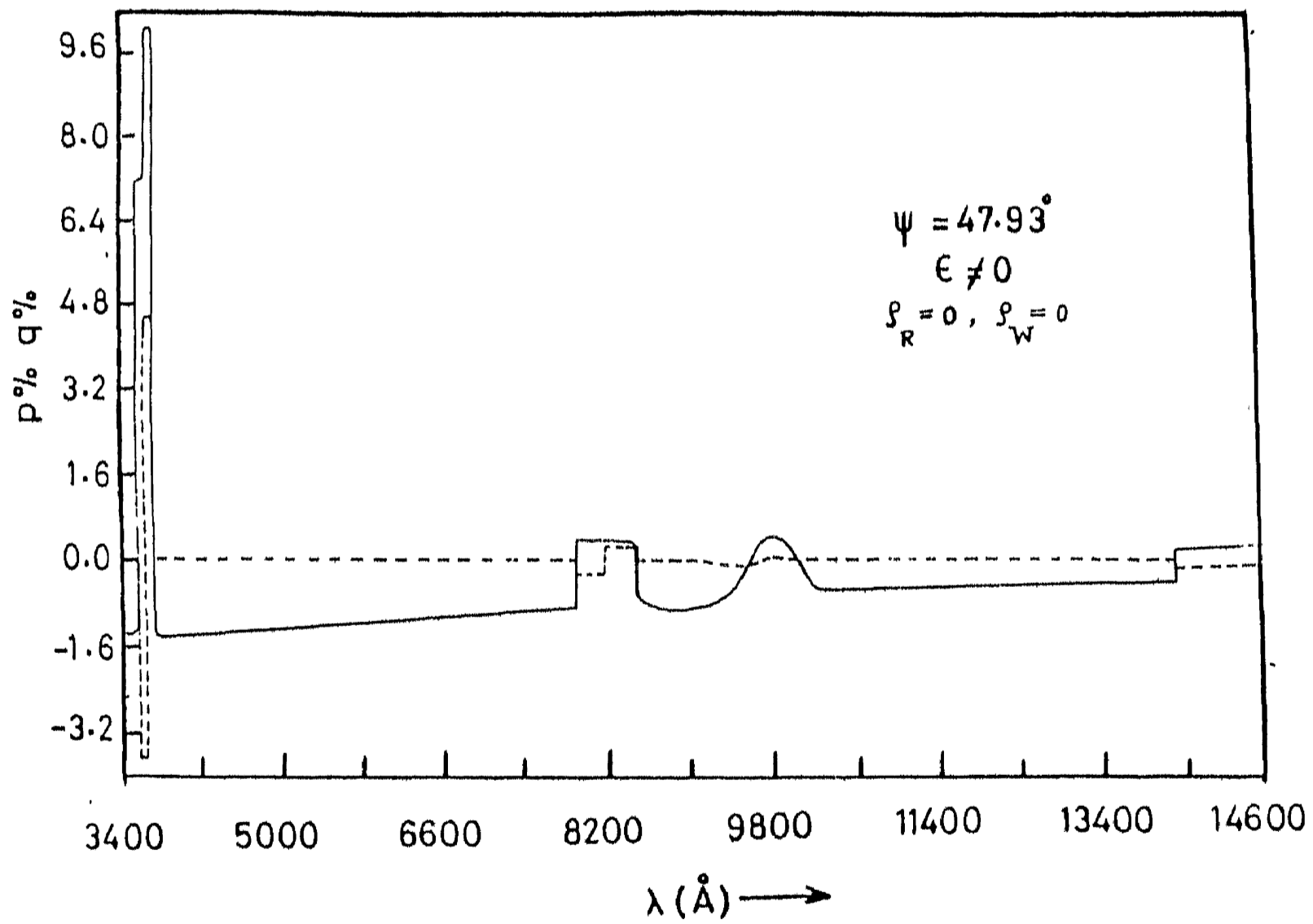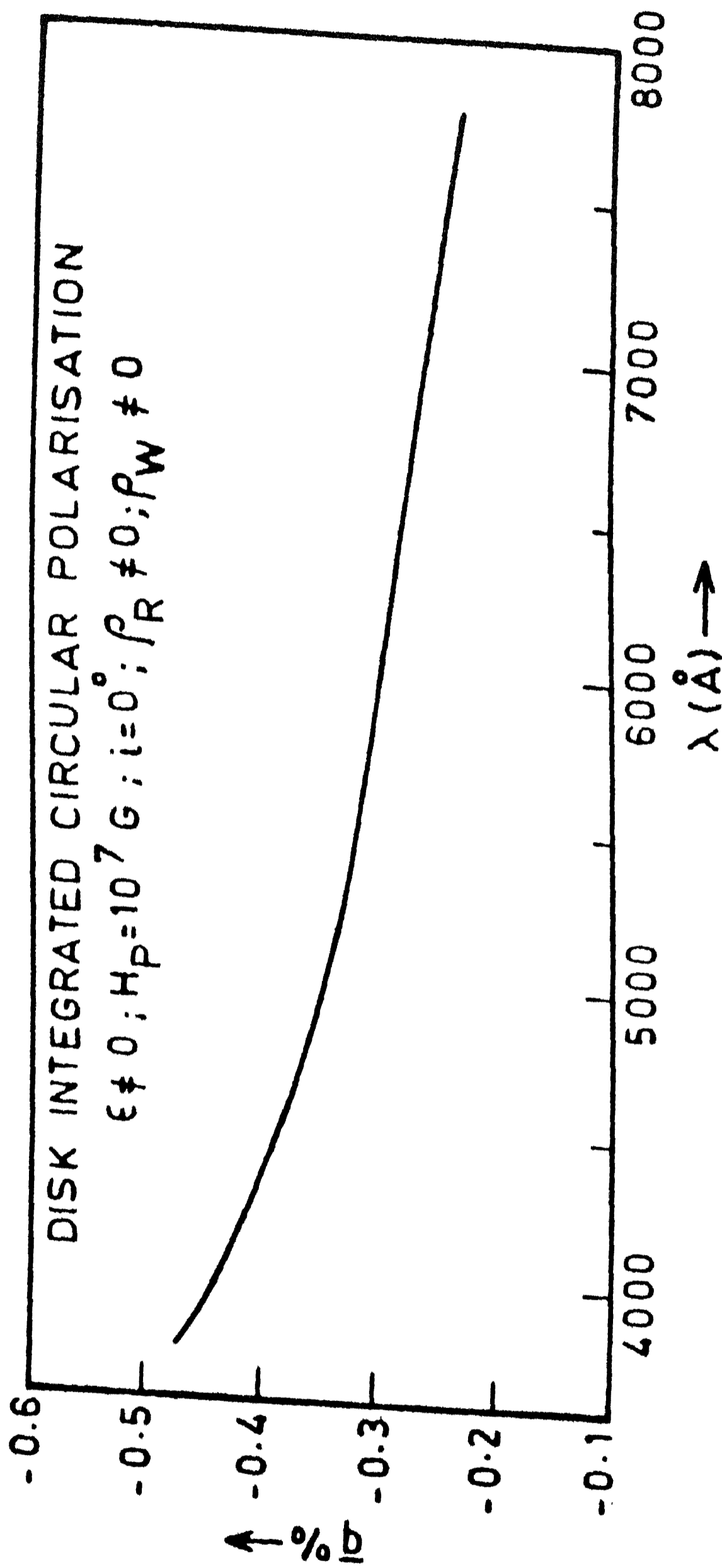
Fig.8 Wavelength dependent circular polarization $\bar{q}$ for a dipole field geometry.

58

computed assuming a centred dipole of field strength $H_p = 10^7 G$. The angle i between the dipole axis and the line of sight is taken as zero. We have used 8 latitudes and 8 longitudes. The field strengths and orientations are calculated at all the grid points. The polarization radiative transfer equations are solved at all these grid points, and then rotated properly using the rotation matrix to refer the solution to a fixed frame of reference. The solution is then integrated over the disk. The disk integrated linear polrization $\overline{P} \equiv 0$ because of the symmetry (i=0). The magneto-optical effects are included ($\rho_R \neq 0$; $\rho_W \neq 0$), but they do not have significant effect on the values of $\overline{q}$ because, in the cold atmospheric model we have employed, the electron densities are quite small. We feel that $\overline{q}$ is probably overestimated because of the lower order angular quadrature used for averaging over the disk. It can be clearly seen from Figure 8 that the thermal magneto-absorption model gives the expected wavelength dependence of $\overline{q}$ in the atmosphere of a magnetic white dwarf, though the treatment of magnetic dichroism is quite approximate. Useful solutions can be obtained only by an accurate disk integration of the transfer equation, assuming a realistic field distribution. Such calculations are necessary for any realistic modelling of the continuum polarization and the spectrum of magnetic white dwarfs.

THE SOLUTION OF THE EQUATIONS OF CONTINUUM RADIATIVE

TRANSFER IN ANISOTROPIC ABSORBING-SCATTERING

MEDIA

In the previous section, we confined ourselves to
the true absorption approximation in treating the polari-
zation radiative transfer. For the transfer of radiation
in the atmospheres of cold magnetic white dwarfs, where it
is a reasonably good approximation. Often in astrophysi-
cal applications we come across situations, when scatter-
ing of radiation is extremely important. Whenever the
albedo $\overline{\omega}$ defined as the ratio of the scattering coeffi-
cient to the extinction (scattering + absorption) coeffi-
cient, $(0 \leq \overline{\omega} \leq 1)$ is large, the correct and the
natural way of obtaining the radiation field in a medium,
is to solve the transfer equation where scattering is in-
cluded. The transfer equation for the polarized radi-
ation, taking scattering into account was formulated by
Chandrasekhar (1950), in the Stokes vector representa-
tion. He used this equation to solve the problem of
polarization of the sunlit sky. These equations being
very general in nature can be extended to treat the
transfer problem whenever the scattering mechanism can
be approximated as dipole scattering. For this reason,
the scattering by molecules or electrons can be treated

using the same Rayleigh scattering equations, with the
only difference that the 'scattering phase matrix' and
the scattering cross section are different in each context.
Chandrasekhar's equations have also been generalized to
treat more difficult problems such as polarization by
the Hanle effect or the resonance line polarization with
frequency redistribution. We shall, in this chapter
address ourselves to solving the polarization (absorption
+ scattering) transfer equations in a different context,
different in the sense that the absorption process is also
anisotropic, along with scattering. This situation arises
when there is a strong magnetic field in the medium. The
calculation of absorption and scattering coefficients in
a strong magnetic field by itself is a difficult problem,
and the cross sections have been calculated only recently.
In this section, we use the Stokes vector as well as normal
wave representation depending on the convenience.

3.1 The continuum radiative transfer equation in anisotropic absorbing - scattering media

The radiation polarization density matrix transfer
equation have been discussed in Dolginov et al.(1970) for
an arbitrary anisotropic medium. For the general arguments leading from these equations to the normal wave
equations see Gnedin and Pavlov (1974) and section 2.1.

At present we shall confine ourselves to coherent
scattering in the continuum. The transfer equation
for the intensities of elliptically polarized normal
waves ($j = 1$ extraordinary and $j = 2$ ordinary wave) is
given by

$$(\vec{\Omega} \cdot \nabla) I_j (z,\Omega) = - \alpha_j (z,\Omega) I_j (z,\Omega) +$$

$$+ \sum_k \int_{\Omega'} \frac{d\sigma_{jk}(z,\Omega,\Omega')}{d\Omega} I_k (z,\Omega') + k_j (z,\Omega) \frac{B_j(z)}{2} \qquad (3\text{-}1)$$

The following approximations are made in deriving the
equation (3-1) from the general density matrix equation
(which is fully equivalent to Chandrasekhar equation):

(i) The plasma is tenuous and cold that is, thermal and
recoil effects are negligible, with the refractive
indices η_j ($j=1,2$) not differing much from unity.
(ii) The polarization ellipses of the intensity components
I_1 and I_2 are similar and orthogonal. (iii) The relative
phase shift $\omega |\eta_1 - \eta_2| >> (k_1 + k_2) / 2$ where k_1 and
k_2 are the absorption coefficients. It is this last
assumption (that of strong Faraday depolarization),
which diagonalizes the density matrix and allows to define
the normal wave 'intensities'. In a magnetized plasma
the approximations made above are justified if (ν_{coll}/γ)
$<< 1$, (ω_c / ω) $<< 1$ and the medium is optically thick.

ν_{coll} is the electron ion collision frequency.

The equation (3-1) is a full range ($-1 \leq \mu = \cos \Theta \leq +1$) equation for the azimuthally symmetric radiation field in plane parallel geometry. Θ is the angle between the ray and the Z-axis along which the optical depth τ is measured. Since all the quantities are dependent on Z and n, we do not write them explicitly in what follows, except where informative. $\alpha_j = (\sigma_j + k_j)$ is the mass extinction coefficient which is the sum of the integral scattering coefficient σ_j and the total absorption co-efficient k_j of the mode j. $k_j B_\nu / 2$ is the thermal emission coefficient with B_ν the Planck function. In a more explicit and simplified form we can write equation (3-1) as

$$\mu \frac{dI_j}{\rho dz} = -\alpha_j I_j + \sum_k \int_{-1}^{+1} \frac{d\sigma_{jk} (\xi, \xi')}{d\xi} I_k (\xi') d\xi' + k_j \frac{B_\nu}{2} \qquad (3-2)$$

$\xi = \cos \psi$ where ψ is the angle between the ray and the magnetic field and χ is the field azimuth in an ortho-gonal system, with the ray going along the z-axix. ρ is the mass density. $d\sigma_{jk} (\xi, \xi') / d\xi$ is now, the azi-muthally symmetric differential mode conversion scattering coefficient.

For a detailed discussion and references to works based
on the multiple scattering 'Stokes vector transfer
equations' and various methods of solution, see van de
Hulst (1980) and, for applications, Gehrels (1974).
The other approach, which is useful for most of the
astrophysical plasmas but less general, is the 'polari-
zation normal wave representation' transfer equation
which is a special case of the general density matrix
formulation of the transfer equation (see Ginzburg,
1964;Dolginov,Gnedin and Silant'ev,1970; Zheleznyakov,
1970; Lamb and ter Haar,1971). A slightly different
approach is taken in Pacholczyk (1977) and Melrose (1980).
For recent literature on the applications of this method
see Meszaros (1984).

3.2 Calculation of the continuum scattering and absorption coefficients in strong magnetic fields

The cross sections for the normal waves in the 'cold
plasma' limit have been calculated by a number of authors
(see e.g.Canuto et al.,1971; Gnedin and Sunyaev,1974a;
Ventura,1979 etc). We employ the expression in the form
given by Kaminker et al. (1982)

$$\frac{d\sigma_{jk}(\vec{\Omega},\vec{\Omega}')}{d\Omega} = \frac{3}{8\pi}\left(\frac{N_e\sigma_T}{\rho}\right)\left|\sum_{\alpha=-1}^{+1} t_\alpha\, e_\alpha^j(\vec{\Omega})\, e_\alpha^{*k}(\vec{\Omega}')\right|^2 =$$

$$= \frac{3}{8\pi}\left(\frac{N_e\sigma_T}{\rho}\right)\sum_{\alpha,\beta=-1}^{+1} t_\alpha\, t_\beta\, a_{\alpha\beta}^{*j}(\vec{\Omega})\, a_{\alpha\beta}^k(\vec{\Omega}') \;, \qquad (3-3)$$

$j, k = 1, 2,$ $\alpha, \beta = 0, \pm 1.$ The cyclic projections of
the cold plasma 'medium polarizability tensor'

$$\Pi = \frac{1}{1-u} \begin{bmatrix} 1 & -i\sqrt{u} & 0 \\ i\sqrt{u} & 1 & 0 \\ 0 & 0 & 1-\sqrt{u} \end{bmatrix} ; \quad \sqrt{u} = \frac{\omega_c}{\omega}, \quad \omega_c = \frac{eB}{m_e c}, \tag{3-4}$$

onto the orthogonal coordinate system (x_0, y_0, z_0),
with z_0 axis along B and the (z_0 x_0) plane being
parallel to ($\mathbb{Z} X$) plane, are given by

$$e_0^j(n) = e_z = (-1)^{j+1} \frac{(1 + P_v^j + P_a^j)}{2\sqrt{1 + P_v^j}} \left(1 - \xi^2\right)^{1/2} \tag{3-5}$$

$$e_{\pm 1}^j(n) = \mp \frac{e_x \pm i e_y}{\sqrt{2}} = (-1)^{j+1} \frac{(1 \pm \xi)(1 + P_v^j) - (1 \mp \xi) P_a^j}{2\sqrt{2(1 + P_v^j)}} e^{\mp i\varphi} \tag{3-6}$$

which form circular polarization basis vectors. $(e_x e_y e_z)$
are the electric field components in the (x y z) ortho-
gonal system, with the ray going along the z-direction.
They form a linear polarization basis system. The Stokes
parameters are actually defined in this frame. The major
axes of the extraordinary and ordinary wave are per-

pendicular and parallel respectively to the (zx) plane. $\xi = \cos \psi$ where ψ is the angle between the ray and the magnetic field. φ is the azimuthal angle measured anticlockwise from the ($B x_o$) plane. The scattering amplitudes are given by

$$a^j_{\alpha \beta} (\Omega) = e^{*j}_{\alpha} (\Omega) \cdot e^j_{\beta} (\Omega) \tag{3-7}$$

The dimensionless constants $t_\alpha = (1 + \alpha \sqrt{u})^{-1}$ are the eigenvalues of the complex polarizability tensor (3-4) in cyclic coordinates. P^j_Q, $P^j_U = \tan 2\beta_j$ together represent the degree of linear polarization. $P^j_U \equiv 0$ because, for the normal waves $| \beta_2 - \beta_1 | = \pi/2$, β_j being the inclination of the major axes of the normal waves in the (xy) plane with respect to x. In other words, normal waves are ortho-gonal. P^j_V is the degree of circular polarization. With-out any loss of generality, we can take $\varphi \equiv 0$.which means that the radiation field is azimuthally symmetric. This choice makes the opacity calculations simple and leads to $(z X) \parallel (z_o x_o) \parallel (z x)$. The corresponding azimuth angle averaged form of the equation (3-3) can be obtained by equating $\varphi = 0$ and then integrating the resulting expression over φ' . Thus, the azimuthally symmetric (azimuth angle independent) form of the transfer

equation is given by equation (3-2). The differential
scattering cross sections are given by

$$\frac{d\,\sigma_{jk}\,(\xi,\xi')}{d\xi} = \frac{3}{4}\left(\frac{N_e\sigma_T}{\rho}\right)\sum_{\alpha=-1}^{+1} t_\alpha^2\, a_\alpha^j(\xi)\, a_\alpha^k(\xi') \ , \tag{3-8}$$

since

$$a_\alpha^j(\xi) = a_{\alpha\alpha}^j(\xi) \equiv \left|\,e_\alpha^j(\xi)\right|^2 \ ; \int_0^{2\pi} a_{\alpha\beta}^k(\xi',\varphi')d\varphi' \equiv 2\pi\,\delta_{\alpha\beta}\,a_{\alpha\beta}^k(\xi') \tag{3-9}$$

The scattering amplitudes are now given by

$$a_o^j(\xi) = \frac{1-\xi^2}{2}\left(1 + P_a^j\right) \quad , \tag{3-10}$$

$$a_{\pm 1}^j(\xi) = \frac{1}{4}\left(1 + \xi^2 \pm 2\,P_v^j\,\xi - P_a^j(1-\xi^2)\right) \ , \tag{3-11}$$

satisfying the completeness and transversality conditions (Ventura, 1979)

$$\sum_{j=1,2} a_{\pm 1}^j(\xi) = \frac{1+\xi^2}{2} \ ; \ \sum_{j=1,2} a_o^j(\xi) = (1-\xi^2) \ ; \ \sum_{\alpha=-1}^{+1} a_\alpha^j(\xi) = 1 \tag{3-12}$$

which assert that the normal modes span the two dimensional
plane transverse to the direction of propagation.

$$P_a^j = (-1)^j \frac{|q|}{\sqrt{1+q^2}} \quad ; \quad P_v^j = (-1)^j \frac{sgn(q)}{\sqrt{1+q^2}} \quad ; \quad q = \frac{1-\xi^2}{2\xi} \cdot \frac{\omega_c}{\omega} \quad , \tag{3-13}$$

$$\left. \begin{aligned} \xi &= \cos\psi = \mu \cdot \cos\Theta_B + (1-\mu^2)^{1/2} \sin\Theta_B \\ \xi' &= \cos\psi' = \mu' \cos\Theta_B + (1-\mu'^2)^{1/2} \sin\Theta_B \end{aligned} \right\} \tag{3-14}$$

where Θ is the angle between the Z-axis and the field direction measured in the (XZ) plane. The integrated 'partial' scattering coefficients are given by integrating over the outgoing angles,

$$\sigma_{jk}(\xi) = \int_{-1}^{+1} \left[\frac{d\sigma_{jk}(\xi,\xi')}{d\xi} \right] d\xi' = \left(\frac{N_e \sigma_T}{\rho} \right) \sum_{\alpha=-1}^{+1} t_\alpha^2 \, a_\alpha^j(\xi) \, A_\alpha^k \quad , \tag{3-15}$$

satisfying the 'normalization conditions'

$$A_\alpha^k = \frac{3}{4} \int_{-1}^{+1} a_\alpha^k(\xi) \, d\xi \quad ; \quad \sum_{k=1,2} A_\alpha^k = 1 \quad ; \quad \sum_{\alpha=-1}^{+1} A_\alpha^k = \frac{3}{2} \tag{3-16}$$

With the help of equations (3-15), we can obtain the 'full' integrated scattering coefficients by summing over the final polarization states,

$$\sigma_j(\xi) = \sum_{k=1,2} \sigma_{jk}(\xi) = \sigma_{j1}(\xi) + \sigma_{j2}(\xi) = \left(\frac{N_e \sigma_T}{\rho} \right) \sum_{\alpha=-1}^{+1} t_\alpha^2 \, a_\alpha^j(\xi) \quad . \tag{3-17}$$

The absorption coefficients $k_j = k_j^{bf} + k_j^{ff} + \cdots\cdots$ for the normal waves can be calculated as the sum of contributions from individual atomic processes. We have described the calculation of important absorption coefficients in the previous chapter (see equations (2-41) to (2-50)).

3.3 A general numerical solution of the anisotropic transfer equation in an absorbing-scattering medium

Now we present the method of solution. Since the basic theoretical development of the discrete space theory of radiative transfer and its methodology are well described in detail in the early pioneering papers by Grant and Hunt (1968a, and 1969a,b), Peraiah and Grant (1973) and recently reviewed by Peraiah (1984), we do not go into the details of the discrete space theory. Instead we present the extensions to be made, to calculate the radiation field in an anisotropically absorbing and scattering medium. The problem of non-magnetic, pure anisotropic scattering (the standard Rayleigh scattering polarization transfer problem) has been solved by Grant and Hunt (1968b). Basically, in discrete space theory, the 'finite difference equations' are derived by a discrete ordinate approximation to the equations of radiative transfer. The discrete ordinate form of equation (3-2) can be written in a matrix form as

$$\mu \frac{d\underline{I}(\mu)}{d\tau} = \underline{\underline{A}}(\mu)\underline{I}(\mu) - \left\{ \bar{\omega} \int_{-1}^{+1} \underline{\underline{P}}(\mu,\mu')\,\underline{I}(\mu')d\mu' + (1-\bar{\omega})\,\underline{\underline{A}}_a(\mu)\,\underline{B}(\mu) \right\}$$

$$- \bar{\omega}\,\underline{\underline{P}}_*(\mu,\mu_0)\,\underline{I}_*(\mu_0)\,e^{-\tau/\mu_0} \quad , \tag{3-18}$$

$$-\mu \frac{d\underline{I}(-\mu)}{d\tau} = \underline{\underline{A}}(-\mu)\,\underline{I}(-\mu) - \left\{ \bar{\omega} \int_{-1}^{+1} \underline{\underline{P}}(-\mu,\mu')\,\underline{I}(\mu')d\mu' + (1-\bar{\omega})\,\underline{\underline{A}}_a(-\mu)\,\underline{B}(-\mu) \right\}$$

$$- \bar{\omega}\,\underline{\underline{P}}_*(-\mu,\mu_0)\,\underline{I}_*(\mu_0)\,e^{-\tau/\mu_0} \quad , \tag{3-19}$$

where $\mu \in (0,1)$ and $\underline{B}(\mu)$ is taken as generally anisotropic.
The last terms on the right hand side in equations (3-18)
and (3-19) represent the contribution to the source function
due to the directly transmitted beam $\underline{I}_*(\mu_0)$ in the
direction μ_0 incident on the free surface ($\tau=0$) of the
medium. Equations (3-18) and (3-19) represent the rays
in the upper and lower half space of angles respectively,
with respect to optical depth scale, increasing into the
atmosphere. In the continuous analytic form each one
of the equations above is a matrix equation with $\underline{\underline{A}}$ and $\underline{\underline{P}}$
being (2x2) matrices and $\underline{I}$ and $\underline{B}$ the (2x1) vectors. The
optical depth scale $d\tau = -(k^c + \sigma_T)\rho\,dz$ is defined with
respect to the zero field extinction coefficient. The
$\underline{\underline{A}}$ matrices are defined as

$$\underline{\underline{A}}^{\pm} = \bar{\omega}\,\underline{\underline{A}}_s^{\pm} + (1-\bar{\omega})\,\underline{\underline{A}}_a^{\pm} \;;\; \bar{\omega} = \frac{\sigma_T}{\sigma_T + k^c} \;,\; \underline{\underline{A}}^{\pm} = \underline{\underline{A}}(\pm\mu) \;, \tag{3-20}$$

$$\underset{\sim}{A}{}^{\pm}_{s} = \frac{1}{\sigma_{T}} \begin{bmatrix} \sigma_{1}^{\pm} & 0 \\ 0 & \sigma_{2}^{\pm} \end{bmatrix} \; ; \; \underset{\sim}{A}{}^{\pm}_{a} = \begin{bmatrix} k_{1}^{\pm} & 0 \\ 0 & k_{2}^{\pm} \end{bmatrix} \; , \; \left. \begin{array}{l} \underset{\sim}{A}_{a} = \underset{\sim}{A}_{a} \, (\pm \mu) \\ \underset{\sim}{A}{}^{\pm}_{s} = \underset{\sim}{A}_{s} \, (\pm \mu) \end{array} \right\}$$ (3-21)

's' and 'a' denote the scattering and true absorption.
$\overline{\omega}$ is the albedo for single scattering ($0 \leq \overline{\omega} \leq 1$).
The scattering phase matrix defined as

$$\underset{\sim}{P} (\mu, \mu') = \frac{1}{\sigma_{T}} \frac{d \, \overline{\sigma_{jk}} \, (\xi, \xi')}{d \xi} = \frac{1}{\sigma_{T}} \frac{d}{d \xi} \begin{bmatrix} \overline{\sigma_{11}} \, (\xi, \xi') & \overline{\sigma_{12}} \, (\xi, \xi') \\ \overline{\sigma_{21}} \, (\xi, \xi') & \overline{\sigma_{22}} \, (\xi, \xi') \end{bmatrix}$$ (3-22)

satisfies the normalization

$$\frac{1}{2} \int_{-1}^{+1} \underset{\sim}{P} (\mu, \mu') \, d\mu' = 1 \; ; \; -1 \leq \mu \, , \; \mu' \leq +1 \; .$$ (3-23)

The scattering integral source term gives rise to a
diffuse radiation field. The second term in the
flower brackets is the 'internal thermal emission'
source term. The intensity and the anisotropic thermal
source vector are written respectively as

$$\underset{\sim}{I} (\pm \mu) = \begin{bmatrix} I_{1} \, (\pm \mu) \\ I_{2} \, (\pm \mu) \end{bmatrix} \; ; \; \underset{\sim}{B} (\pm \mu) = \begin{bmatrix} B \, (\pm \mu) \, / 2 \\ B \, (\pm \mu) \, / 2 \end{bmatrix}$$ (3-24)

Now, the 'discrete ordinate' forms of equations (3-18) and (3-19) are written, in matrix form, as

$$\underset{\sim}{M}\frac{d\underset{\sim}{I}^+}{d\tau}=\underset{\sim}{A}\,\underset{\sim}{I}^+-\left\{\bar{\omega}\left[\underset{\sim}{P}^{++}\underset{\sim}{C}\,\underset{\sim}{I}^++\underset{\sim}{P}^{+-}\underset{\sim}{C}\,\underset{\sim}{I}^-\right]+(1-\bar{\omega})\,\underset{\sim}{A}_a\,\underset{\sim}{B}^+\right\}-\bar{\omega}\,\underset{\sim}{P}^{++}_*\,\underset{\sim}{I}^+_*\,e^{-\tau/\mu_o}\quad,\qquad (3\text{-}25)$$

$$-\underset{\sim}{M}\frac{d\underset{\sim}{I}^-}{d\tau}=\underset{\sim}{A}\,\underset{\sim}{I}^--\left\{\bar{\omega}\left[\underset{\sim}{P}^{-+}\underset{\sim}{C}\,\underset{\sim}{I}^++\underset{\sim}{P}^{--}\underset{\sim}{C}\,\underset{\sim}{I}^-\right]+(1-\bar{\omega})\,\underset{\sim}{A}_a\,\underset{\sim}{B}^-\right\}-\bar{\omega}\,\underset{\sim}{P}^{-+}_*\,\underset{\sim}{I}^+_*\,e^{-\tau/\mu_o}\quad,\qquad (3\text{-}26)$$

where the signs in the superscript indicate the signs attached to $|\mu|$ in the respective physical quantities.

$$\underset{\sim}{M}=\begin{bmatrix} M' & 0 \\ 0 & M' \end{bmatrix}\;;\quad \underset{\sim}{C}=\begin{bmatrix} c' & 0 \\ 0 & c' \end{bmatrix}\;;\quad \left.\begin{array}{l} M'=[M_{jk}]=\mu_j\,\delta_{jk} \\[4pt] c'=[c_{jk}]=c_j\,\delta_{jk} \end{array}\right\}\;j,k=1,2,\cdots J,\qquad (3\text{-}27)$$

and

$$\underset{\sim}{P}^{++}=\begin{bmatrix} P^{++}_{11} & P^{++}_{12} \\ P^{++}_{21} & P^{++}_{22} \end{bmatrix}\;;\quad \left.\begin{array}{l} P^{++}_{\alpha\beta}=P_{\alpha\beta}(\mu_j,\mu_k)=P^{--}_{\alpha\beta} \\[4pt] P^{+-}_{\alpha\beta}=P_{\alpha\beta}(\mu_j,-\mu_k)=P^{-+}_{\alpha\beta} \end{array}\right\}\;\begin{array}{l}\alpha,\beta=1,2 \\[4pt] \mu_j,\mu_k>0\end{array}\quad,\qquad (3\text{-}28)$$

with similar expressions for $\underset{\sim}{P}^{--}$, $\underset{\sim}{P}^{+-}$ and $\underset{\sim}{P}^{-+}$. J is the order of the quadrature formula which is used for angular discretization. Hence all the matrices are now of dimension (2J x 2J) and the vectors are of dimension (2J x 1). The matrices $\underset{\sim}{P}^{+-}_*$ and $\underset{\sim}{P}^{--}_*$ and $\underset{\sim}{I}^+_*$ are

given by

$$P_*^{++} = \begin{bmatrix} P_{11*}^{++} & P_{12*}^{++} \\ P_{21*}^{++} & P_{22*}^{++} \end{bmatrix} \; ; \quad \left. \begin{array}{l} P_{\alpha\beta*}^{++} = P_{\alpha\beta*}(\mu_j, \mu_0\delta_{k1}) = P_{\alpha\beta*}^{--} \\ P_{\alpha\beta*}^{-+} = P_{\alpha\beta*}(-\mu_j, \mu_0\delta_{k1}) = P_{\alpha\beta*}^{+-} \end{array} \right\} \quad \begin{array}{l} \alpha, \beta = 1, 2 \\[4pt] \mu_j > 0 \end{array} \qquad (3\text{--}29)$$

$$\underline{I}_*^+ \quad \begin{bmatrix} I_*(\mu_0)\,\delta_{k1} & I_*(\mu_0)\,\delta_{k1} \end{bmatrix}^T \qquad (3\text{--}30)$$

Integrating the matrix equations (3-29) and (3-30) over a 'cell' bounded by the planes τ_n and τ_{n+1} we get

$$\underline{M}[\underline{I}_{n+1}^+ - \underline{I}_n^+] = \Delta\tau \underline{A}_{n+\frac{1}{2}}^+ \underline{I}_{n+\frac{1}{2}}^+ - \Delta\tau \left\{ \bar{\omega}_{n+\frac{1}{2}} [P_{n+\frac{1}{2}}^{++} \underline{C} \underline{I}_{n+\frac{1}{2}}^+ + P_{n+\frac{1}{2}}^{+-} \underline{C} \underline{I}_{n+\frac{1}{2}}^-] + \right.$$

$$\left. + \bar{\omega}_{n+\frac{1}{2}} P_{*,n+\frac{1}{2}}^{++} \underline{I}_*^+ \frac{e^{-\tau_n/\mu_0}}{2} (e^{-\Delta\tau/\mu_0} + 1) + (1 - \bar{\omega}_{n+\frac{1}{2}}) \underline{A}_{a,n+\frac{1}{2}}^+ \underline{B}_{n+\frac{1}{2}}^+ \right\}, \qquad (3\text{--}31)$$

$$-\underline{M}[\underline{I}_{n+1}^-\ \underline{I}_n^-] = \Delta\tau \underline{A}_{n+\frac{1}{2}}^- \underline{I}_{n+\frac{1}{2}}^- - \Delta\tau \left\{ \bar{\omega}_{n+\frac{1}{2}} [P_{n+\frac{1}{2}}^{-+} \underline{C} \underline{I}_{n+\frac{1}{2}}^+ + P_{n+\frac{1}{2}}^{--} \underline{C} \underline{I}_{n+\frac{1}{2}}^-] + \right.$$

$$\left. + \bar{\omega}_{n+\frac{1}{2}} P_{*,n+\frac{1}{2}}^{-+} \underline{I}_*^+ \frac{e^{-\tau_n/\mu_0}}{2} (e^{-\Delta\tau/\mu_0} + 1) + (1 - \bar{\omega}_{n+\frac{1}{2}}) \underline{A}_{a,n+\frac{1}{2}}^- \underline{B}_{n+\frac{1}{2}}^- \right\}, \qquad (3\text{--}32)$$

with $\underline{I}_n^+ = \underline{I}^+(\tau_n)$; $\underline{I}_{n+1}^+ = \underline{I}^+(\tau_{n+1})$, $n = 1, 2, \cdots N,$ where N = number of shells into which the atmosphere is divided. The suitable cell averages based on the diamond scheme (see Grant and Hunt 1968a) are expli-

citely used in writing equations (3-31) and (3-32).

The subscript $n+\frac{1}{2}$ denotes such averages, for example

$\overline{w}_{n+\frac{1}{2}} = \left(\overline{w}_{n+1} + \overline{w}_n\right)/2$ and so on. The last term is written

by cell averaging the dilution coefficient $\exp(-\tau/\mu_0)$

of the direct beam $\underline{I}^{+}_{n+\frac{1}{2}}$ over the given cell. We

take $\Delta\tau = \left(k^{c} + \sigma_T\right)_{n+\frac{1}{2}} \cdot \rho_{n+\frac{1}{2}} \left(z_n - z_{n+1}\right) = \tau_{n+1} - \tau_n$.

Making use of the expressions

$$\underline{I}^{\pm}_{n+\frac{1}{2}} = \frac{1}{2}\left(\underline{I}^{\pm}_{n+1} + \underline{I}^{\pm}_n\right) \quad , \tag{3-33}$$

we can re-arrange equations (3-31) and (3-32) in a

canonical form as

$$\begin{bmatrix} \underline{I}^{+}_{n+1} \\ \underline{I}^{-}_n \end{bmatrix} = \begin{bmatrix} \underline{t}(n+1, n) & \underline{r}(n, n+1) \\ \underline{r}(n+1, n) & \underline{t}(n, n+1) \end{bmatrix} \begin{bmatrix} \underline{I}^{+}_n \\ \underline{I}^{-}_{n+1} \end{bmatrix} + \begin{bmatrix} \underline{\Sigma}^{+}_{n+\frac{1}{2}} \\ \underline{\Sigma}^{-}_{n+\frac{1}{2}} \end{bmatrix} \tag{3-34}$$

This straightforward, but tedious elimination can be

cast in the form of a computing algorithm which we have

given below. The operators $\underline{r}$ and $\underline{t}$ appearing in the

canonical form (3-34) have the physical interpretation

as matrix operators for diffuse reflection and trans-

mission respectively, of the radiation incident on the

shell between the planes τ_n and τ_{n+1}. Similarly the

vector operators $\underline{\Sigma}_{n+\frac{1}{2}}$ represent the radiation which

emerges from the surfaces of the shell due to internal
emission sources plus the contribution from directly
transmitted beam.

A computational note: The procedure is based on the com-
putation of $\underset{\sim}{r}, \underset{\sim}{t}$ and $\underset{\sim}{\Sigma}$ operators of all the N shells, into
which we have divided the medium. We have explicitely
assumed in deriving the equations (3-31) and (3-32) that
the stability and non-negativity of the cell operators,
and hence of the specific intensity vectors is assured,
for the value of the shell thickness $\Delta\tau \leq \tau_{crit}$. τ_{crit} is
the 'local critical optical depth' which is actually cal-
culated by requiring that $\underset{\sim}{S}^{+-} \geqslant 0, \underset{\sim}{S}^{-+} \geqslant 0$ and $\underset{\sim}{\Delta}^{\pm} \geqslant 0$. For
a large class of scattering problems one can use the ex-
pression

$$\left(\tau_{crit}\right)_n = \underset{j}{Min}\left[\frac{2\mu_j}{\left(1-\varpi_{n+\frac{1}{2}} \, \underset{\sim}{p}^{++}_{n+\frac{1}{2}} \, (\mu_j, \mu_j) \, c_j\right)}\right] , \qquad (3\text{-}35)$$

to compute this value. If $\Delta\tau > \tau_{crit}$ .the shell is fur-
ther sub-divided, and the $\underset{\sim}{r}, \underset{\sim}{t}$ and $\underset{\sim}{\Sigma}$ operators of the
composite thick shell can be generated by a fast doubling
algorithm (Grant and Hunt 1969b). A convenient test of
the accuracy of the solution is offered by the requirement
of 'global flux conservation'- the outgoing flux should
equal the incident flux for a 'conservative' scattering
atmosphere ($\varpi \equiv 1$). It is shown in Grant and Hunt
(1969b) and Peraiah and Grant (1973) that this criterion

is always satisfied provided care is taken to ensure
that the scattering phase matrix is normalized to a
high degree of accuracy. Consequently, it is pre-
ferable that a finer angular discretization is employed,
particularly for the strong field scattering phase
matrices which are highly anisotropic. A complete
discussion of these aspects viz. the spatial and
angular discretization and flux conservation in the
finite difference schemes, can be found in Wiscombe
(1976a,b). Since the recursive algorithm used for
computing the internal and emergent radiation fields
is the same as that given in Grant and Hunt (1968b)
and Peraiah (1984); we do not discuss them here. But,
the $\underset{\sim}{r}, \underset{\sim}{t}$ and $\underset{\sim}{\Sigma}$ operators should now be computed from the
algorithm given below along with the relevant boundary
conditions which are specified based on the problem.
Algorithm: Computation of transmission and reflection
matrices and source vectors.

Define that

$$\underset{\sim}{Q}_{n+\frac{1}{2}}^{++} = \overline{\omega}_{n+\frac{1}{2}} \, \underset{\sim}{P}_{n+\frac{1}{2}}^{++} \, \underset{\sim}{c} \; ; \qquad \underset{\sim}{Q}_{n+\frac{1}{2}}^{+-} = \overline{\omega}_{n+\frac{1}{2}} \, \underset{\sim}{P}_{n+\frac{1}{2}}^{+-} \, \underset{\sim}{c} \; ;$$

$$\tag{A1}$$

$$\underset{\sim}{Q}_{n+\frac{1}{2}}^{--} = \overline{\omega}_{n+\frac{1}{2}} \, \underset{\sim}{P}_{n+\frac{1}{2}}^{--} \, \underset{\sim}{c} \; ; \qquad \underset{\sim}{Q}_{n+\frac{1}{2}}^{-+} = \overline{\omega}_{n+\frac{1}{2}} \, \underset{\sim}{P}_{n+\frac{1}{2}}^{-+} \, \underset{\sim}{c} \; ,$$

and then

$$\underset{\sim}{S}^{++} = \underset{\sim}{M} - \frac{1}{2} \tau_{n+\frac{1}{2}} \left(\underset{\sim}{A}_{n+\frac{1}{2}}^{+} - \underset{\sim}{Q}_{n+\frac{1}{2}}^{++} \right) \; ; \quad \underset{\sim}{S}^{+-} = \frac{1}{2} \tau_{n+\frac{1}{2}} \, \underset{\sim}{Q}_{n+\frac{1}{2}}^{+-} \; ;$$

$$\tag{A2}$$

$$\underset{\sim}{S}^{--} = \underset{\sim}{M} - \frac{1}{2} \tau_{n+\frac{1}{2}} \left(\underset{\sim}{A}_{n+\frac{1}{2}}^{-} - \underset{\sim}{Q}_{n+\frac{1}{2}}^{--} \right) \; ; \quad \underset{\sim}{S}^{-+} = \frac{1}{2} \tau_{n+\frac{1}{2}} \, \underset{\sim}{Q}_{n+\frac{1}{2}}^{-+} \; ,$$

and

$$\underset{\sim}{\Delta}^{+} = \left[\underset{\sim}{M} + \tfrac{1}{2}\,\mathcal{C}_{n+\frac{1}{2}}\left(\underset{\sim}{A}^{+}_{n+\frac{1}{2}} - \underset{\sim}{Q}^{++}_{n+\frac{1}{2}}\right)\right]^{-1} \;;\; \underset{\sim}{\Delta}^{-} = \left[\underset{\sim}{M} + \tfrac{1}{2}\,\mathcal{C}_{n+\frac{1}{2}}\left(\underset{\sim}{A}^{-}_{n+\frac{1}{2}} - \underset{\sim}{Q}^{-}_{n+\frac{1}{2}}\right)\right]^{-1} . \quad \text{(A3)}$$

Write

$$\underset{\sim}{\Upsilon}^{+-} = \underset{\sim}{\Delta}^{+}\,\underset{\sim}{S}^{+-} \;;\; \underset{\sim}{\Upsilon}^{-+} = \underset{\sim}{\Delta}^{-}\,\underset{\sim}{S}^{-+} , \quad \text{(A4)}$$

and

$$\underset{\sim}{t}^{+} = \left[\underset{\sim}{I} - \underset{\sim}{\Upsilon}^{+-}\,\underset{\sim}{\Upsilon}^{-+}\right]^{-1} \;;\; \underset{\sim}{t}^{-} = \left[\underset{\sim}{I} - \underset{\sim}{\Upsilon}^{-+}\,\underset{\sim}{\Upsilon}^{+-}\right]^{-1} \quad \text{(A5)}$$

Then, the transmission and reflection matrices are given by

$$\underset{\sim}{t}\,(n+1, n) = \underset{\sim}{t}^{+}\left[\underset{\sim}{\Delta}^{+}\underset{\sim}{S}^{++} + \underset{\sim}{\Upsilon}^{+-}\underset{\sim}{\Upsilon}^{-+}\right] \;;\; \underset{\sim}{\Upsilon}\,(n+1, n) = 2\underset{\sim}{t}^{-}\underset{\sim}{\Upsilon}^{-+}\underset{\sim}{\Delta}^{+}\underset{\sim}{M} \;;$$

$$\text{(A6)}$$

$$\underset{\sim}{t}\,(n, n+1) = \underset{\sim}{t}^{-}\left[\underset{\sim}{\Delta}^{-}\underset{\sim}{S}^{--} + \underset{\sim}{\Upsilon}^{-+}\underset{\sim}{\Upsilon}^{+-}\right] \;;\; \underset{\sim}{\Upsilon}\,(n, n+1) = 2\underset{\sim}{t}^{+}\underset{\sim}{\Upsilon}^{+-}\underset{\sim}{\Delta}^{-}\underset{\sim}{M} ,$$

and, the source vectors have the form

$$\underset{\sim}{\Sigma}^{+}(n+1, n) = \left(1 - \bar{\omega}_{n+\frac{1}{2}}\right)\mathcal{C}_{n+\frac{1}{2}}\,\underset{\sim}{t}^{+}\left[\underset{\sim}{\Delta}^{+}\underset{\sim}{\Sigma}^{+}_{n+\frac{1}{2}} + \underset{\sim}{\Upsilon}^{+-}\underset{\sim}{\Delta}^{-}\underset{\sim}{\Sigma}^{-}_{n+\frac{1}{2}}\right] ,$$

$$\text{(A7)}$$

$$\underset{\sim}{\Sigma}^{-}(n, n+1) = \left(1 - \bar{\omega}_{n+\frac{1}{2}}\right)\mathcal{C}_{n+\frac{1}{2}}\,\underset{\sim}{t}^{-}\left[\underset{\sim}{\Delta}^{-}\underset{\sim}{\Sigma}^{-}_{n+\frac{1}{2}} + \underset{\sim}{\Upsilon}^{-+}\underset{\sim}{\Delta}^{+}\underset{\sim}{\Sigma}^{+}_{n+\frac{1}{2}}\right] ,$$

where

$$\underset{\sim}{\Sigma}^{+}_{n+\frac{1}{2}} = \bar{\omega}_{n+\frac{1}{2}}\,\mathcal{C}_{n+\frac{1}{2}}\,\underset{\sim}{P}^{++}_{*\,n+\frac{1}{2}}\,\underset{\sim}{I}^{+}_{*} \cdot \frac{e^{-\mathcal{C}_{n}/\mu_{0}}}{2}\cdot\left(e^{-\mathcal{C}_{n+\frac{1}{2}}/\mu_{0}} + 1\right) + \underset{\sim}{A}^{+}_{a,n+\frac{1}{2}}\,\underset{\sim}{B}^{+}_{n+\frac{1}{2}}$$

$$\text{(A8)}$$

$$\underset{\sim}{\Sigma}^{-}_{n+\frac{1}{2}} = \bar{\omega}_{n+\frac{1}{2}}\,\mathcal{C}_{n+\frac{1}{2}}\,\underset{\sim}{P}^{-+}_{*\,n+\frac{1}{2}}\,\underset{\sim}{I}^{+}_{*} \cdot \frac{e^{-\mathcal{C}_{n}/\mu_{0}}}{2}\cdot\left(e^{-\mathcal{C}_{n+\frac{1}{2}}/\mu_{0}} + 1\right) + \underset{\sim}{A}^{-}_{a,n+\frac{1}{2}}\,\underset{\sim}{B}^{-}_{n+\frac{1}{2}}$$

We shall now give some simple forms of the normal wave transfer equation which provide a simple way to understand the propagation of normal waves in an optically thick magnetoplasma. Further, we can use the limiting case $(B \equiv 0)$ of the normal waves to check the correctness of the program. It is also useful in understanding the degree of excess anisotropy caused by the magnetic field. We give the required equations below.

Zero feild limit of the cold plasma normal wave transfer equations: The governing equation can be obtained by substituting the magnetic field strength $B=0(u=0; q=0; P_{\alpha}^{j}=0; P_{\nu}^{j} = \mp 1; t_{\alpha}=1, \alpha = 0, \pm 1; j = 1,2)$. Since there is no preferred direction in the medium which is isotropic, we can take $\xi \equiv \mu$. The normal waves $I_{1,2} = (I \mp V)/2$ are now circularly polarized with the Z-axis, the normal to the atmosphere, being the physically distinguished direction.

From the normal wave equation (3-2) we finally get

$$\mu \frac{d}{d\tau}\begin{bmatrix} I(\mu) \\ V(\mu) \end{bmatrix} = \begin{bmatrix} I(\mu) \\ V(\mu) \end{bmatrix} - \frac{3}{16}\,\tilde{\omega}\int_{-1}^{+1}\begin{bmatrix} 3-\mu^2+(3\mu^2-1)\mu'^2 & 0 \\ 0 & 4\mu\mu' \end{bmatrix}\begin{bmatrix} I(\mu') \\ V(\mu') \end{bmatrix}\cdot d\mu' - (1-\tilde{\omega})\begin{bmatrix} B_\nu \\ 0 \end{bmatrix} \quad (3\text{-}36)$$

Notice that these equations can also be obtained from the Stokes vector equations of Chandrasekhar by taking $I_{l,r}=I/2$ in the azimuth-independent part of the phase matrix. The

first equation is simply the transfer for Rayleigh

phase function (see Chandrasekhar, 1960 p.17). So,

this case can be used as a check on the correct pro-

gramming of the algorithm, since the tabulated solutions

for this standard problem are available, e.g. van de

Hulst (1980). There is one more interesting case of the

normal wave transfer equations; that of superstrong mag-

netic fields, found near magnetized neutron stars. This

helps in calculating the so called directional diagrams,

or the angular dependence of polarized radiation in a

strongly magnetized plasma.

Limiting case of superstrong magnetic fields: If we have

a situation where $\omega \ll \omega_c$ for example the optical range

and the magnetic field $B \gg 10^9 G$ the normal waves are cha-

racterized by a large linear polarization over a wide

range of angles ξ . For this case $(u \gg 1; q \gg 1; P_a^j \simeq \mp 1;$

$P_v^j \simeq 0; t_{\pm 1} = 0, t_0 = 1; j = 1, 2)$ we get the following transfer equations

$$\mu \frac{dI_1(\mu)}{d\tau} \simeq 0 \qquad \text{or} \qquad I_1 \simeq \text{constant}, \qquad (3\text{-}37)$$

$$\mu \frac{dI_2(\mu)}{d\tau} \simeq 2(1-\xi^2) I_2(\mu) - \bar\omega \frac{3}{4} \int_{-1}^{+1} (1-\xi^2)(1-\xi'^2) I_2(\xi') d\mu'$$
$$\rightarrow (1-\bar\omega)(1-\xi^2) \frac{B_\nu}{2}, \qquad (3\text{-}38)$$

$\xi = \xi(\mu), \xi' = \xi'(\mu')$. It is intersting to note that the

ordinary wave equation (3-38) is independent of the

field strength but becomes highly angle dependent.
Particularly, for quasi-transverse propagation, the
electric vector vibrates in the directions almost parallel
to the field lines, which is responsible for the little
influence of the field on the electron oscillations.
The absorption and scattering coefficients are nearly
equal to their field free values. As far as the extra-
ordinary wave is concerned, these coefficients become
extremely small compared to the ordinary wave. There-
fore the radiative transfer hardly alters the value of
$I_\perp$, which remains constant according to equation (3-37).

3.4 Two astrophysical applications: transfer of polari-
zed radiation in the atmospheres of magnetic white
dwarfs and neutron stars

The method of solution given here can be used for
computing polarization of radiation under true absorp-
tion mechanism, by setting the albedo $\bar{\omega} \equiv 0$. We apply
the theory presented in the previous sections to cal-
culate angle dependence of the polarization in the at-
mospheres of hot magnetized white dwarfs and a plasma
slab immersed in a superstrong magnetic field. This kind
of plasma emission regions are found to be responsible
for the polarized pulse emission from the pulsars. We
show the changes in the polarization and spectrum caused

by external illumination and heating of the outer
layers of a white dwarf atmosphere. In the strong field
case we have clearly demonstrated the large changes
(such as the beaming of the radiation) caused by the
magnetic field. A comparison is made with the non-
magnetic Thomson scattering model. The optical depth
effects are also discussed.

Recently two hot magnetic white dwarfs have been
discovered by Liebert et al.(1983). In the atmospheres
of such stars, scattering plays a significant role at
lower optical depths. In weaker magnetic fields $(\omega_c << \omega;$
$B \sim 10^7 q$ and optical wavelengths), the transfer co-
efficients do not differ much from the non-magnetic
values. So the polarization is in general very small,
and $p \sim q^2$ as in the case of magneto absorption models
of chapter 2.

In Figure 1 the angular distribution of the emergent
$\bar{I}, p$ and q are shown when isotropic radiation is incident
at τ_{max} given by $\bar{I}_j (\tau_{max}) = \frac{B(\tau_{max})}{2}$ and no radiation
is incident on the top of the atmosphere; these are
the conventional boundary conditions. The computations
have been carried out for a model of white dwarf with
T_{eff} =50,000 K, log g = 8, taken from Wesemael et al.
(1980). The field strength is set at $B = 5 \ 10^6 G$. An
eight point Gauss quadrature is used in the angular dis-
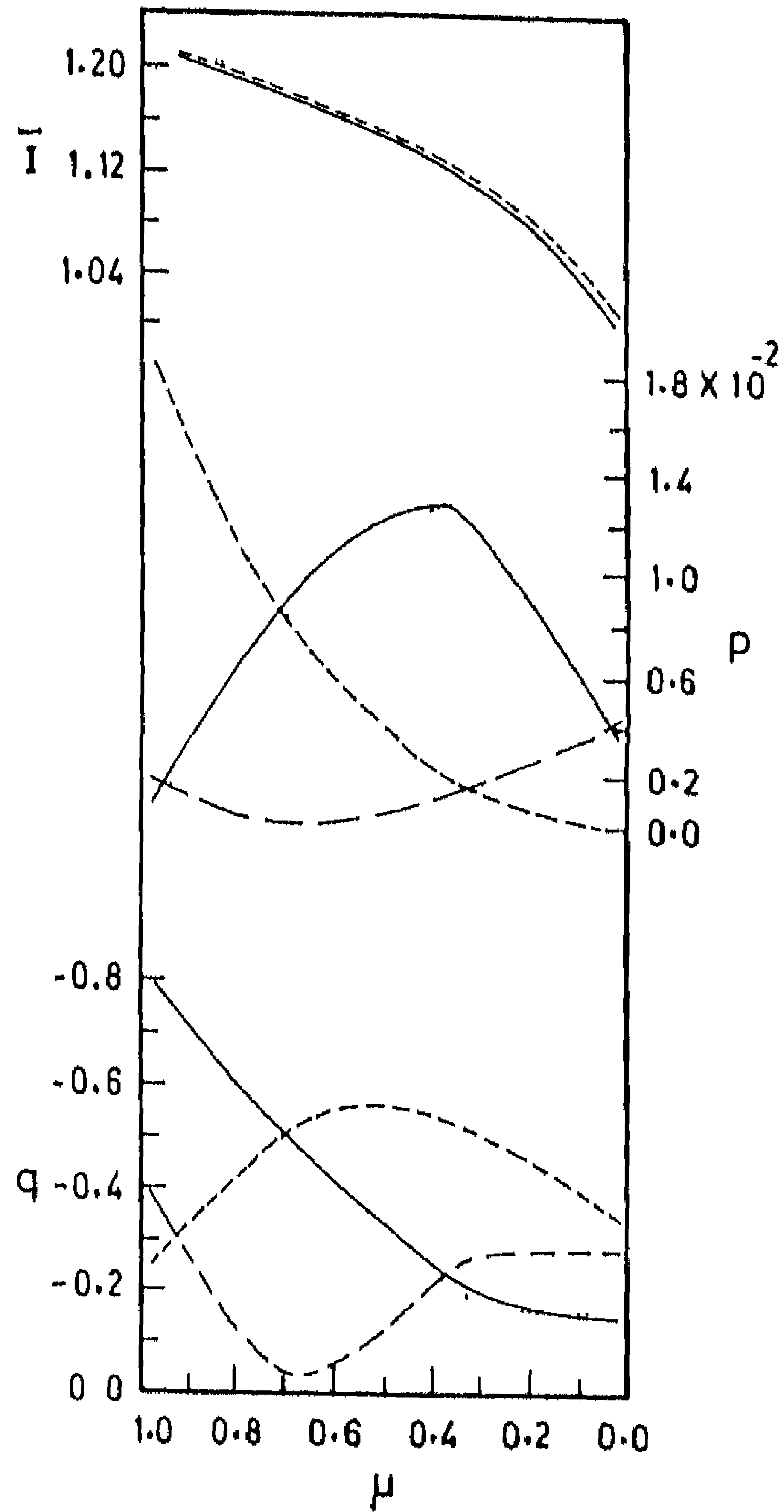
Fig.1. Angular distribution of emergent intensity
Ī(in the units of $B_\nu(r_0)$, T_0 being the temperature
at $\tau = 0$), percentage linear polarization p =
Q/I and circular polarization q = V/I computed for
a model atmosphere of pure hydrogen white dwarf.

cretization. The transfer equations are integrated
up to $\tau \sim 22$. Full lines correspond to $\Phi_B = 0$
where Φ_B is the angle between the field direction
B and the normal Z to the plane parallel atmospheric
layers. Dot-dash lines and dashed lines correspond to
$\Phi_B = \pi/4$ and $\pi/2$ respectively. The dotted lines
represent the special case of the magneto-absroption
($\omega = 0$). The intensity distributions for $\Phi_B = 0$
and $\Phi_B = \pi/4$ are not resolved in the adopted scale.
The angular distributions of $\overline{I}$ are almost similar for all
the cases, namely $\Phi_B = 0$, $\pi/4$, $\pi/2$, with the emergent
intensity in general increasing by a very small amount
(~ 1 per cent) with the increasing values of Φ_B .
But p and q are more sensitive with respect to the angle
Φ_B . The angular distributions for $\overline{\omega} = 0$ and $\overline{\omega}$
$= \omega\, (\tau)$ do not differ very much because the 'partial'
angular dependence has already entered through k_j in the
former case (true absorption) also. Notice that the
angular dependence is not only determined by the magnetic
field effects, but also by the limb darkeing phenomena
which has modified the former effect. The effect of
external illumination ($I_j^+ (\tau=0) \neq 0$) on the free
surface, along with the inner boundary condition is shown
in the Figure 2. For all the cases shown, $\Phi_B = 0$.
Full lines: an isotropic low-temperature irradiance given
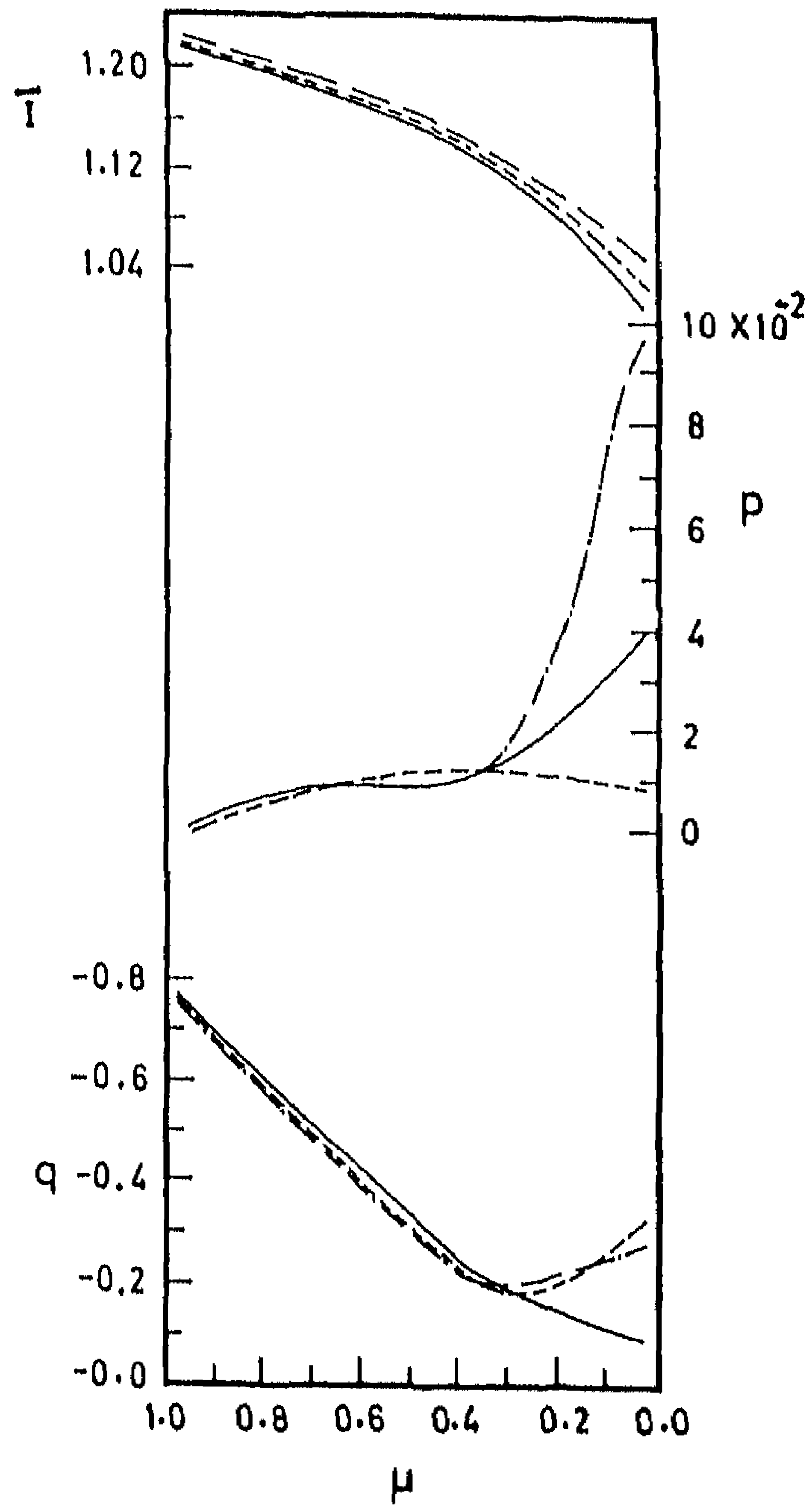
Fig.2. As Figure 1, but showing the effect on
$\bar{I}$,p and q, of an external illumination on the
top surface τ = 0, along with an input at
τ = τ max.

by $I_j(\mu) = B_\gamma(T_0)/2$, $j=1,2$. Dashed lines: an external illumination distributed as $\cos\theta$, i.e.

$I_j(\mu) = [B_\gamma(T_0)/2]\mu$, $\mu = \cos\theta$. Dot-dashed lines: a high-temperature external irradiance $I_j(\mu) = [B_\gamma(T=75,000\ K)/2]\mu$, an arbitrary change in the temperature gradient obtained by enhancing the local temperature continuously, from 1% at $\tau = 10^{-4}$ to 11% at $\tau \simeq 0$, thus changing the source function gradient. For isotropic illumination, p is enhanced by a large amount, particularly for transverse directions $(\phi_B=0 ; \theta = \pi/2)$, while q is only slightly reduced. Notice that the original angular dependence of p itself is changed. Thus, the isotropically illuminated stellar atmospheres are better suited for polarization observations near the limb. For an anisotropic unpolarized diffuse external irradiance (not the direct beam), the value of p increases, but its relative importance near the limb is suppressed because of the angular dependence of the incident radiation, which dominates that of the emergent radiation field. q increases near the limb for the same reason. The effect of altering the normal 'source function gradient', by irradiating a high temperature ambient radiation at $\tau=0$, is again larger on the p values than on q, particularly in transverse directions. In general, the circular polarization q is proportional to the 'temperature gradient' in a high

temperature atmosphere, unlike the case of a cooler medium where it is proportional to the radiative flux gradient (see Gnedin and Sunyaev 1974b; Kaminker et al. 1982). Notice also that an increase in p is always associated with a decrease in the values of q.

In Figure 3(a) we have shown the realtive intensities of the extraordinary (ext) and ordinary (ord) modes, for a 'self emitting' plasma slab whose parameters are representative of a polar cap emitting region of a magnetized neutron star: $T = 10^8 K$, $\left(\frac{\hbar\omega}{kT}\right) = 1$; $\left(\frac{\hbar\omega}{\hbar\omega_c}\right) = 0.2$; $N_e = 10^{23}$ cm^{-3}; the total optical depth of the slab $= 10^3$. The ext-mode dominates because of its larger mean free path (smaller α) over the ord-mode. But more important is the effect of 'mode conversion scattering' by which the ordinary photons enter the ext-channel and escape easily. This process is effective because the medium is optically very thick resulting in large mean number of scatterings. For this reason, p and q (Figure 3(b)) depend strongly on the thermal structure of the medium and the details of transfer, than on the cross-sections of the normal waves themselves (see Meszaros and Bonazzola, 1981). Figure 4(a) corresponds to a physically identical but relatively thin slab, and hence $I_j(\mu) \propto (\alpha_j(\mu) / \mu)$ contrary to the optically thick case. The scale on the left refers to normal waves. The dotted and dot-dashed curves, which correspond to an identical non-magnetic slab are refered

(b)

-56

-48

-40

-32

-24

p&q

-16

-8

0

8

P

q

1.0   0.8   0.6   0.4   0.2   0.0

μ

(a)

1.6

1.4

1.2

1.0

$\dfrac{I(\mu)}{I(\mu\sim.87)}$ 0.8

0.6

0.4

0.2

0.0

EXT

ORD

1.0   0.8   0.6   0.4   0.2   0.0

μ
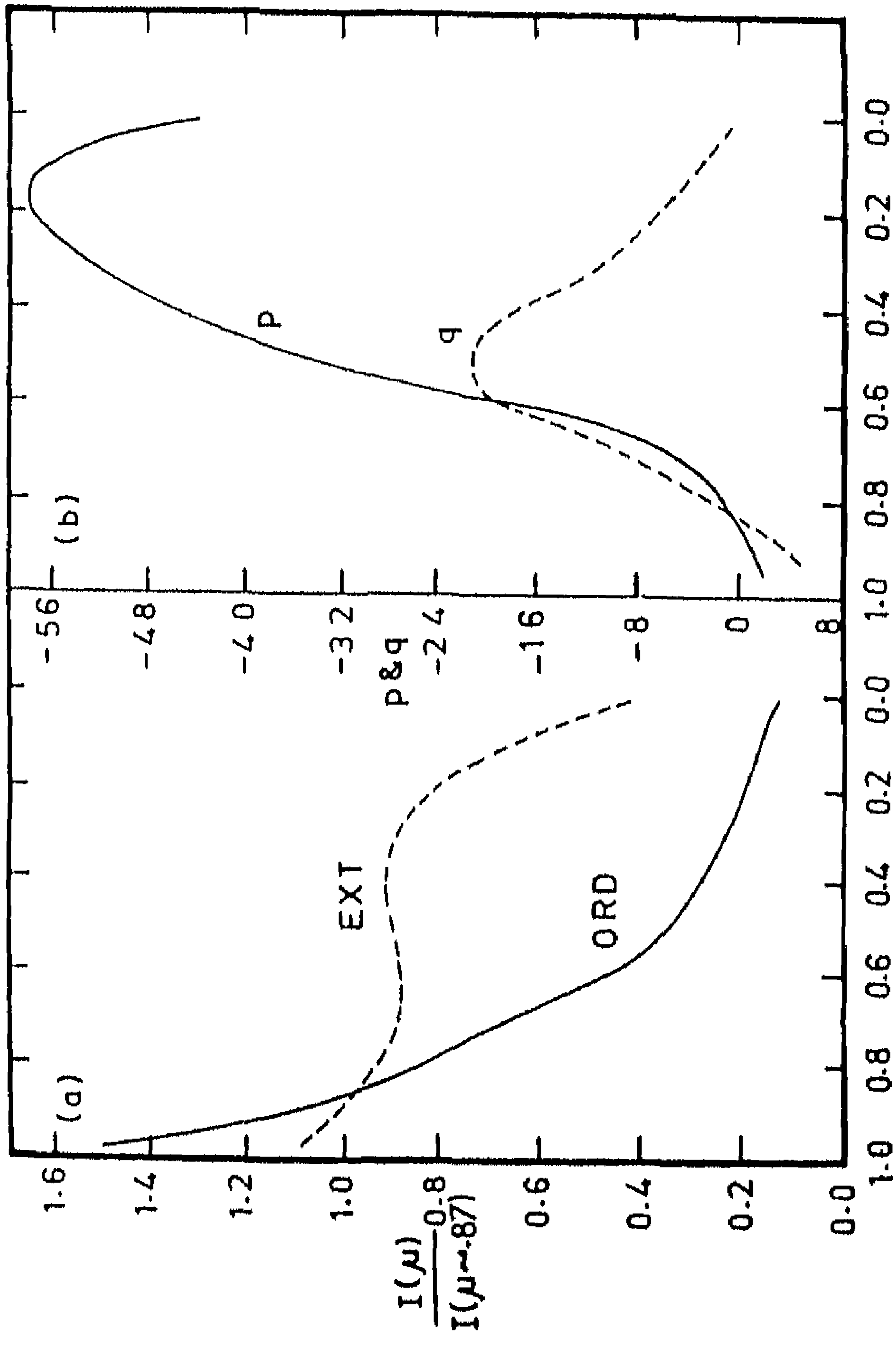
Fig.3.(a) The directionality of the normal wave emergent inten-

sities I_j/B'_ν (normalized to their values at $\mu=0.87$ in order to show

on a linear scale), and (b) their polarization for a uniform 'self

emitting' plasma slab. $B'_\nu = B_\nu(T)/2$.
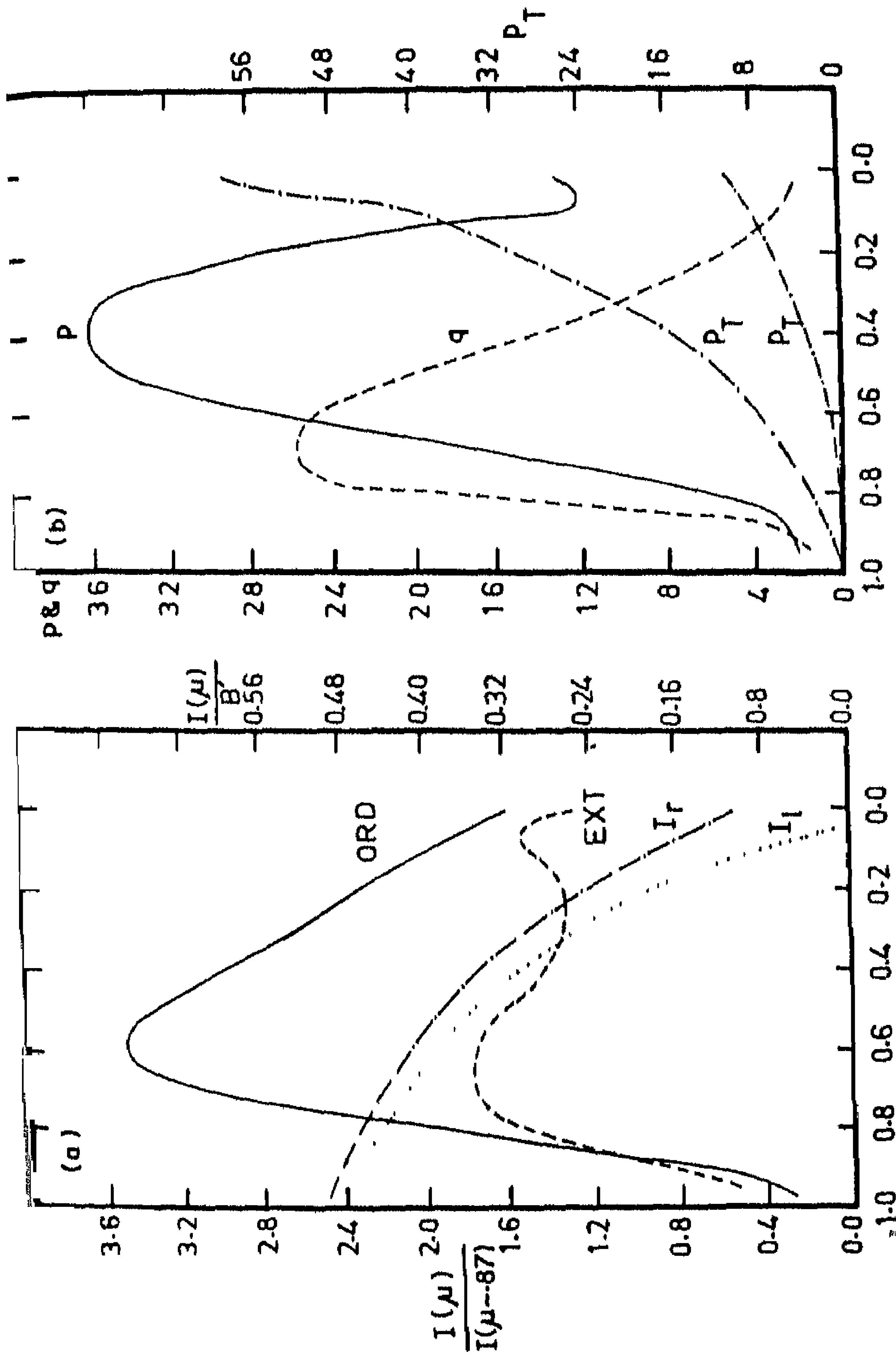
Fig.4.(a) Same as Figure 3 except the total optical depth which is taken here as 10. The non-magnetic intensities $I_{l,r}/B_\nu'$ are also shown. (b) The corresponding polarization angular distribution: The 'steeply rising' dot-dashed curve corresponds to an irradiated non-magnetic slab. $p=(I_r-I_l)/(I_r+I_l)$

to the scale on the right. The ord-wave intensity domi-
nates because large absorption ensures large emission,
and particularly because the number of scatterings is
smaller in this case. Clearly, the radiation field now
'depicts' the strong angular anisotropy of the cross-
sections, rather than the transfer effects. To obtain
maximum polarization, we have taken $\overline{\omega} \cong 1$, in the
non-magnetic case. The input given at the lower boundary
is $I_{\perp,\gamma} = B'_{\eta}$. The linear polarization P_r for this
case, see Figure 4b, reaches a maximum of around 10%
for $\mu \cong 0$. When this slab is irradiated normally on
the free surface by $I_{\ell,\gamma} (\mu \sim 1) = B'_{\eta}$ we again get large
polarizations. p and q nearly follow the same behaviour
as intensity, but the strongly linearly polarized
ord-wave dominates their general behaviour. A steep
reduction in the cross sections for photons travelling
parallel to the field (Canuto et al.,1971) is responsi-
ble for the sharp intensity maximum, the 'pencil beam'
(of half width $\sim 20°$) in Figure 3(a), as well as the
'hollow pencil beam', an intensity minimum in Figure
4(a), for very small angles of propagation. Unlike the
case of magnetic white dwarfs p is very strong in these
objects (see also Kaminker et al.,1982). For an irradi-
ated magnetized slab, the results are quantitatively
different. This polarized beaming (directionality) of
radiation is useful in constructing the pulse shapes

of X-ray pulsars, exploiting the strong dependence of

the directional diagram on ω / ω_c and ξ (see Nagel

1981; Meszaros,1982 and Silant'ev,1982).

The (conservative) scattering in a non-magnetic

slab of the same thickness gives rise to a smooth

angular dependence for the emergent intensities $I_{l,r}$

and the linear polarization p (see Figure 4). When

this slab is illuminated on the top surface (τ =0)

by a normally incident ($\mu \simeq 1$) diffuse radiation

field, a large amount of linear polarization can be

obtained with a steep increase near the limb. A

grazing incidence for example produces a negative p.

However, the detailed structure of the azimuthally

dependent radiation field is qualitatively different

from the azimuth-independent case, since in the former

case, the coupling of p and q is stronger. For

computing these later results, we have used Chandra-

sekhar's equations (1950,p.43) of Rayleigh scattering

polarization.

From the results presented above we see that

for weaker magnetic fields, the spectra and polarization

of hot white dwarf atmospheres do not differ much from

the results of simple magneto-absorption theory presented

in chapter 2. This is essentially because of the large

densities and relatively low temperatures of the atmos-

pheres of cool white dwarfs. But we have shown that the external irradiation of even such atmospheres can have dramatic effects on the polarized radiation emitted by these atmospheres. This has far reaching consequences on the modelling of the polarization of magnetic white dwarfs because, the thumb rule of large integrated linear polarization means large magnetic field in a magnetized plasma, can be misleading. And linear polarization seems to increase by large amounts in irradiated and heated atmospheres. We feel that such possibilities have to be explored in modelling the recent observations of large linear and circular polari- zation in even 'hot' white dwarfs (where we have the difficulty that we can not take strong fields to model them using magneto-absorption theory since their line data indicate low field strengths). The method of solution presented is quite simple and easily generali- zable for a wide range of situations, some of which have been demonstrated above. It is computationally economical also, since we work in normal wave representa- tion. We have calculated the radiation beaming in superstrong magnetic fields by using a small angular grid, and the results compare well with those calculated using much larger grid of angles. This useful property

arising due to the conservative nature of our differencing the transfer equation helps us in getting accurate solutions to problems where high optical depths are encountered with relatively less computing efforts, even when the highly peaked magneto-scattering cross sections are involved.

CHAPTER 4

THE SOLUTION OF THE EQUATIONS OF RADIATIVE TRANSFER

FOR SPECTRAL LINES IN ANISOTROPIC ABSORBING

MEDIA

In this chapter we shall attempt to solve the line transfer equation in a magnetized medium. First we shall clearly write down the basic line formation theory for true absorption Zeeman lines in the two parallel representations we have been using-the more general Stokes vector formulation and somewhat restrictive, normal wave formulation. A comparitive study of solutions obtained by these two formulations is already made in section 2.3. We shall first establish a link with the normal wave transfer equations written earlier for the continuum problems. Then we shall give a simple but very useful computing scheme for the practical computations quantitative in nature, where somewhat approximate but quick methods of solution are preferred. We shall demonstrate this simple procedure by applying it in some test cases. We shall also study the Zeeman line formation under general physical conditions. Finally we apply the solution scheme to quite a time consuming astrophysical computation and show that even here, with the approximations made, the accuracy is reasonably good. Also we shall show some interesting behaviour of continuum polarization in a very strong field magnetic white dwarf where cyclotron

resonance absorption phenomena is operative.

4.1 The Zeeman line transfer equations in Stokes
    vector and normal wave representation including
    the continuum polarization

(i) Stokes vector transfer equations: The LTE Zeeman
line transfer equations are described in detail for
the Zeeman multiplet line formation, in Stenflo (1971)
and Landi Degl'Innocenti (1976). For our purpose we
have chosen to work with Zeeman triplets (the normal
Zeeman effect and the Paschen Back limit), since the
conclusions drawn here are essentially independent of
this choice. Hence the relevant LTE transfer equation
is the Unno-Beckers equation, and is given by

$$\underline{M} \frac{d\underline{I}}{d\tau} = \underline{A} \, (\underline{I} - \underline{B}) \; , \qquad\qquad (4\text{-}1)$$

where

$$\underline{M} = \begin{bmatrix} \mu & & & 0 \\ & \mu & & \\ & & \mu & \\ 0 & & & \mu \end{bmatrix} \; ; \qquad \underline{A} = \begin{bmatrix} \eta_I & \eta_Q & 0 & \eta_V \\ \eta_Q & \eta_I & -\rho_R & 0 \\ 0 & \rho_R & \eta_I & -\rho_W \\ \eta_V & 0 & \rho_W & \eta_I \end{bmatrix} \qquad (4\text{-}2)$$

and

$$\underline{I} = \begin{pmatrix} I & Q & U & V \end{pmatrix}^T \; ; \quad \underline{B} = \begin{pmatrix} B & 0 & 0 & 0 \end{pmatrix}^T, \quad B = B_\eta (T) \cdot \qquad (4\text{-}3)$$

which is an 'ordinary matrix differential equation'
in plane parallel stratification with Z, the symmetry
axis of the medium being the independent variable. As
usual, μ is the angle between the Z-axis and the
direction of propagation. $\underset{\sim}{I}$, $\underset{\sim}{A}$ and $\underset{\sim}{B}$ are functions
of the optical depth τ and the angle variable μ.
For simplicity of notation, we shall not write this
dependence explicitly. The coefficients of the ab-
sorption matrix $\underset{\sim}{A}$ (also called the transfer matrix)
are given (with $\chi = 0$) by

$$\eta_{I} = \frac{1}{2} \eta_{p} \sin^{2}\psi + \frac{1}{4} (\eta_{l} + \eta_{r})(1 + \cos^{2}\psi) \; ;$$

$$\eta_{Q} = \frac{1}{2} \eta_{p} \sin^{2}\psi - \frac{1}{4} (\eta_{l} + \eta_{r}) \sin^{2}\psi \; ;$$

$$\eta_{U} = 0 ;$$

$$\eta_{V} = \frac{1}{2} (\eta_{r} - \eta_{l}) \cos\psi \; ,$$

(4-4)

where ψ = angle between the ray and the magnetic field.
If the solution for an arbitrary azimuth χ is required,
it can be obtained by rotating the solution vector using
the transformation matrix for $(Q \; U)^{T}$, namely

$$\begin{bmatrix} \cos 2\chi & -\sin 2\chi \\ \sin 2\chi & \cos 2\chi \end{bmatrix} .$$

(4-5)

For the purpose of discussion, retaining the picture of
a triplet we have,

$$\eta_l = \eta_\lambda^c + \eta_\lambda^L = \eta_\lambda^c + \eta_0 H(a, \upsilon - \upsilon_i) \,, \qquad i = p, l, r \,\cdot, \qquad (4\text{-}6)$$

where

$$\upsilon_i = \frac{\nu_i - \nu_0}{\Delta \nu_D} \quad ; \qquad \Delta \nu_D = \frac{\nu_0}{c} \sqrt{\frac{2kT}{M}} \quad ; \qquad (4\text{-}7)$$

a is the damping constant. ν_i (i=p,l,r) are the central frequencies of $\Delta M = 0, \pm 1$ transitions respectively. η_0 is the line centre absorption coefficient for zero damping (a = 0).

$$\rho_R = \rho_R^c + \rho_R^L = -\frac{\omega_0^2 \omega_c \cos \psi}{c k^4 (\omega^2 - \omega_c^2)} - \eta_0 \left[F(a, \upsilon - \upsilon_r) - F(a, \upsilon - \upsilon_l) \right] \cos \psi \,, \quad (4\text{-}8)$$

$$\rho_W = \rho_W^c + \rho_W^L = -\frac{\omega_0^2 \omega_c^2 \sin^2 \psi}{2 c \omega k^4 (\omega^2 - \omega_c^2)} - \eta_0 \Big[F(a, \upsilon - \upsilon_p) -$$

$$-\frac{1}{2} \left\{ F(a, \upsilon - \upsilon_l) + F(a, \upsilon - \upsilon_r) \right\} \Big] \sin^2 \psi \,; \qquad (4\text{-}9)$$

$\omega_0 = \sqrt{4\pi N_e e^2 / m_e}$ is the plasma frequency and $\omega_c = eB / m_e c$ the cyclotron frequency. The Voigt and the plasma dispersion function are given by

$$H(a, u) = \frac{a}{\pi} \int_{-\infty}^{+\infty} \frac{\exp[-(y+u)^2]}{y^2 + a^2} dy \quad ; \qquad F(a, u) = \frac{1}{2\pi} \int_{-\infty}^{+\infty} \frac{y \exp[-(y-u)^2]}{y^2 + a^2} dy \,, \qquad (4\text{-}10)$$

with $H(a, u) = H(a, -u)$; $F(a, u) = -F(a, -u)$. We can use the following useful relations (Heinzel, 1978)

$$F(a,u) = \frac{1}{a}\left[\frac{1}{2}\,u\,H(a,u) + \frac{1}{4}\,\frac{d}{du}\,H\,(a,u)\right] \; , \qquad (4\text{-}11)$$

or

$$F(a,u) = \frac{1}{a}\left[\frac{1}{2}\,u\,H(a,u) + \frac{1}{2}\left\{K(a,u)\,a - H(a,u)\,u\right\}\right] \qquad (4\text{-}12)$$

Therefore,

$$F(a,u) = \frac{1}{2}\,K(a,u) = \frac{1}{2}\left[\frac{1}{\pi}\int_{-\infty}^{+\infty}\frac{y\,\exp\left[-(y-u)^2\right]}{y^2 + a^2}\,dy\right] \; . \qquad (4\text{-}13)$$

The H and K functions can be computed by fast algorithms given by Matta and Reichel (1971).

The Stokes parameters profiles arising due to linear Zeeman effect and anomalous dispersion in the line, preserve symmetry (for I,Q and U) or antisymmetry (for V) about the line centre. Many authors have computed such profiles - Beckers (1969),Stenflo (1971), Landi Degl' Innocenti (1979) and Wittman (1974) to mention only few as examples. In strong magnetic fields, higher order magnetic perturbations (Stark effects which can cause large asymmetries) affect the Zeeman line profiles (Nagendra and Peraiah,1986). Apart from this, the macroscopic mass motions, stellar rotation and gravitational redshift can also produce asymmetric Stokes profiles. All such effects mentioned above can easily be included in a uni-

fied way for the computations of pure absorption lines.
If the macroscopic velocity vector $u_m(\tau)$ makes an angle
$\alpha(\tau)$ with respect to the line of sight, the Doppler
shift of the line centre frequency in the rest frame of
the star is given by

$$\nu_0(\tau) = \nu_0 + \cos \alpha(\tau) \; \frac{u_m(\tau)}{c} \; \nu_0 \quad , \tag{4-14}$$

from which we can get, for any frequency ν in the line,

$$\nu(\tau) = \nu - \cos \alpha(\tau) \; \frac{u_m(\tau)}{c} \; \frac{\nu_0}{\Delta \nu_D} \quad , \tag{4-15}$$

where

$$\nu(\tau) = \frac{\nu - \nu_0(\tau)}{\Delta \nu_D} \quad ; \quad \nu = \frac{\nu - \nu_0}{\Delta \nu_D} \quad ; \quad \Delta \nu_D = \frac{\nu_0}{c} \, u_T \tag{4-16}$$

Expressing the velocity $u_m(\tau)$ in terms of some stand-
ard mean thermal units (mtu) u_T , we have

$$\nu(\tau) = \nu - \cos \alpha(\tau) \; V_m(\tau) \quad , \tag{4-17}$$

where $V_m(\tau) = u_m(\tau) \big/ u_T$ is a dimensionless parameter.
When the continuum is taken to be polarized and magneto-
optic, the Stokes profiles are basically asymmetric since
both the absorption and dispersion coefficients do not
preserve symmetry about the line centre. The most general

and exact boundary conditions are found to be, the asymptotic boundary conditions, for both the line and continuum transfer problems. The solution calculated in the first Eddington approximation-the generalized Unno solution - is found to be a very good choice as an asymptotic boundary condition and is used by many workers in the field. However, the solutions obtained with higher order Eddington approximation also can be used as given in Landi Degl' Innocenti (1976). We use the generalised Unno solution (equations (4-18) to (4-23) at τ_{max} as the boundary condition. These equations are useful for both the continuum transfer problems of chapter 2 and the line transfer problems solved here. They are defined by the following equations:

$$I = B_\eta + \frac{\mu \, \beta \, B_\eta}{\eta_I - \eta_V^2/\eta_{IW} - \eta_{QP}^2/\eta_{IR}} \quad ; \qquad (4\text{-}18)$$

$$Q = - \frac{\eta_{QP}}{\eta_{IR}} \left(I - B_\eta\right) \quad ; \qquad (4\text{-}19)$$

$$V = \left(- \frac{\eta_V}{\eta_{IW}} - \frac{\rho\eta_{QP}}{\eta_{IR}}\right)\left(I - B_\eta\right) \quad ; \qquad (4\text{-}20)$$

$$U = \left(\rho_W V - \rho_R Q\right)/\eta_I \quad , \qquad (4\text{-}21)$$

where

$$\beta = B_{\vartheta}^{-1} \frac{dB_{\vartheta}}{d\tau} \, ,$$

(4-22)

and

$$\eta_{\mathrm{IW}} = \eta_{\mathrm{I}} + \rho_W^2 / \eta_{\mathrm{I}}$$

$$\rho = \rho_R \rho_W / (\eta_{\mathrm{I}} \eta_{\mathrm{IW}})$$

$$\eta_{\mathrm{IR}} = \eta_{\mathrm{I}} + \rho_R^2 / \eta_{\mathrm{I}} - \rho^2 \eta_{\mathrm{IW}}$$

$$\eta_{\mathrm{QP}} = \eta_{\mathrm{Q}} + \rho \eta_V$$

(4-23)

(ii) Normal wave transfer equations: The normal wave
transfer equations for the general case of Zeeman multi-
plets are given, for example in Dolginov and Pavlov
(1974). We shall give below the equations for a Zeeman
triplet. We note that these equations are also useful
in chapter 5.

First we shall show the possibility of modifying the conti-
nuum transfer equations given in chapter 2 to get the line
transfer equations. Notice that the γ factor given in
the equation (2-26) is the cold tenuous plasma ($|\eta_j - 1| << 1$)
limit of a more general expression

$$\gamma = \frac{2t_0 - t_1 - t_{-1}}{2 (t_1 - t_{-1})} \sin \psi \, \tan \psi \, ,$$

(4-24)

where $T_\alpha (\omega)$ are proportional to the diagonal components of the complex polarizability tensor in cyclic coordinates, and for the cold magneto-plasma they are given by

$$T_\alpha(\omega) = \frac{\omega_p^2}{c \left[\gamma_e - i \left(\omega - \alpha \, \omega_c \right) \right]} \, , \qquad (4\text{-}25)$$

in the usual notation. Now, for the absorption of radiation by an atomic gas in a magnetic field, with a Lorentzian profile function, these factors are given by

$$T_\alpha(\omega) = \frac{\pi c^2}{\omega^2} N_{J'} \left(2J + 1 \right) T_J^2 \, \big/ \, 4\pi \left[\gamma_J - i \left(\omega - \omega_o - \alpha \, \omega_c / 2 \right) \right] \, , \qquad (4\text{-}26)$$

where $N_{J'}$ is the number density of atoms in the lower state J'. T_J^2 is the upper level radiative width. ω_o is the line centre frequency. $\gamma_J = 2\pi \left(T_J^2 + \gamma_{coll} \right)$ is the total width of the level J. γ_{coll} is the effective collision frequency in the plasma. Since the formula (4-25) can be obtained from (4-26) by making the substitutions $\omega_c \rightarrow \omega_c/2$, $\omega_o \rightarrow \omega$, $N_{J'} \, \lambda^2 T_J^2 \rightarrow 4\pi \, \omega_p^2 \, / \, c$, all the relevant formulae of the cold plasma are still applicable to the Zeeman line formation theory after appropriate substitutions mentioned above. It is important to note that the orthogonality condition $|\alpha| \rightarrow 0$ is fulfilled only in the line wings, which forms the major

restriction on the usefulness of this approach. At the line centre,

$$|x| = \begin{cases} \omega_c \, |\sin\psi \, \tan\psi| \, / \, \mathcal{V}_J & \text{if} \quad \omega_c \, |\sin\psi \, \tan\psi| \, > \, \mathcal{V}_J \\ \\ \mathcal{V}_J \, / \, \omega_c \, |\sin\psi \, \tan\psi| & \text{if} \quad \omega_c \, |\sin\psi \, \tan\psi| \, < \, \mathcal{V}_J \end{cases} \qquad (4\text{-}27)$$

$|x| \to 1$ represents total non-orthogonality and in that case the normal wave transfer equations cannot be used. Instead of the crude procedure mentioned above, we have used the correct formulation developed by the authors mentioned above. Accordingly, the transfer equation is given by

$$\mu \frac{dI_J}{d\tau} = \frac{k_J}{k^c} \left(I_J - \frac{B\nu}{2} \right) \quad , \qquad (4\text{-}28)$$

where, as usual

$$k_J = k_J(\xi) = \frac{1}{\rho} \sum_{\alpha=-1}^{+1} t_\alpha^2 \, \zeta^{(\alpha)} \, a_\alpha^J(\xi) = \frac{1}{\rho} \sum_{\alpha=-1}^{+1} T_\alpha(\omega) \, a_\alpha^J(\xi) \qquad (4\text{-}29)$$

and k^c is the continuous absorption coefficient in (cm^2/gm) units. The other quantities appearing in equation (4-29) are given in section 2.2. As an alternative to $T_\alpha(\omega)$ given in equation (4-26), these authors give a more accurate representation of these line absorption coefficients (in cm^{-1}) as

$$T_\alpha(\omega) \simeq \frac{\pi c^2}{\omega^2} N_{J'} (2J+1) T_J \, G \left(\omega - \omega_0 - \alpha g \, \omega_c / 2 \right) \quad ; \tag{4-30}$$

$$= k^0 \, G \left(\omega - \omega_0 - \alpha g \, \omega_c / 2 \right) \, , \tag{4-31}$$

g being the Lande g-factor. The profile function $G(\omega)$ is given by

$$G(\omega) = \int_0^\infty g(t) \, exp \, (-i\omega t) \, dt \quad ; \quad \int_0^\omega G(\omega) \, d\omega = 1 \, , \tag{4-32}$$

where the time ordering function $g(t)$ is in general steeper than $exp(- T_J \, t \,)$, specific forms of which are given in Dolginov and Pavlov (1974). However, it is always assumed that the collision width is much greater than the natural width. It is shown by Pavlov (1975) that the general expression for the transfer coefficients (which are useful even in the Stokes vector formalism) are given by

$$\eta_\alpha(\omega) + i \rho_\alpha(\omega) = \frac{T_\alpha(\omega)}{\rho \, k^c} =$$
$$\frac{\eta_0}{G(0)} \left\{ G \left(\omega - \omega_0 - \alpha \omega_c / 2 \right) + i D \left(\omega - \omega_0 - \alpha \omega_c / 2 \right) \right\} \tag{4-33}$$

The line centre absorption coefficient is defined as $k^L = k^0 \, G(0) \, ,$ and $\eta_0 = k^L / k^c \, ,$ at the line centre ω_0. The real part $\eta_\alpha \, (\alpha = 0, \pm 1)$ represent the

absorption coefficients and the imaginary part ρ_α (ω) represent the anomalous dispersion coefficients for the p,l and γ Zeeman components respectively. The function D(ω) is given by

$$D(\omega) = \frac{1}{\pi} \int_{-\infty}^{+\infty} \frac{G(\omega')}{(\omega-\omega')} \, d\omega'$$

(4-34)

A comparison of equation (4-33) with the following equations

$$\eta_l = \eta_o H(\alpha, v-v_l) \; ; \; \rho_l = \eta_o F(\alpha, v-v_l), \quad l = p, l, \gamma \cdot,$$

(4-35)

with $v_l = \Delta M \, \omega_c / 4\pi \Delta v_D$ brings out clearly the connection between the two formalisms. Note that ρ_l are simply the terms appearing in the expressions for ρ_R and ρ_W the usual anomalous dispersion parameters in the Stokes vector formalism (see equations (4-8) and (4-9)).

The k_j for the continuum processes can be calculated according to the equations (2-41) through (2-53) of chapter 2, and vectorially added to the line transfer coefficients calculated above. Thus the line plus continuum polarization transfer equation can be easily solved similar to the Stokes vector formalism. The boundary conditions to be used now are

$$I_\delta(\tau_{max}) = \frac{B_\gamma(\tau_{max})}{2}\left[1 + \beta\frac{\mu}{k_\delta}\right], \quad \beta = \frac{1}{B_\gamma(\tau_{max})}\left[\frac{\partial B_\gamma(\tau)}{\partial T(\tau)} \cdot \frac{\partial T(\tau)}{\partial \tau}\right], \qquad (4\text{-}36)$$

which is a first Eddington approximation or Unno type
solution of the normal wave transfer equation, at large
optical depths. Notice that the same boundary conditions
can be used even for pure continuum problems of chapters
2 and 3.

4.2 A simplified method of solution to the polarization transfer problem - its usefulness and limitations

A simplification of the general method of solution
given earlier in section 3.3, is described for problems
which involve only absorption. This allows us to attempt
to solve under realistic conditions and with reduced com-
puting efforts, the important problem of polarization of
light emerging from magnetized stars. For true absorption
the matrix differential equation (4-1) admits an analytical
solution. The simplest is the Unno solution which is deri-
ved analytically using a Milne - Eddington approximation.
This solution is restricted and can not be used in compu-
tations involving realistic model atmospheres. Instead,
the formal solution itself can be used in realistic atmos-
pheres also. For arbitrary source function gradients,

and line formation problems the depth integrating which
occurs in the formal solution however, requires a large
number of grid points. Among the numerical solutions,
the most accurate and widely used is the Beckers' method,
which is a Runge-Kutta scheme for the vector transfer
equation. For a detailed discussion on accuracy and com-
puting times of some of the numerical solutions, see
Martin and Wickramasinghe (1979b) and Nagendra and Peraiah
(1985a) which also have been described in section 2.3.
In the computations of spectra and polarizations of mag-
netic stars (Ap stars, white dwarfs etc.), we are re-
quired to solve the transfer equation over a large number
of points on the visible disk and finally integrate these
local solutions, along the line of sight. This is a highly
time consuming but unavoidable process, particularly so
in line computations where large number of frequency points
are also involved. In view of this difficulty, one is
forced to go for faster methods though less accurate. We
have previously described a procedure based on the dis-
crete space theory (hereinafter called DSM) of radiative
transfer (see Nagendra and Peraiah (1985a) and section
3.3). Now we describe a simplification of the same, which
turns out to be faster computationally. To solve the
equation (4-1), the following boundary conditions are
given at the bottom and the top of the stellar atmosphere,

$$\underline{I}(0,\mu) = \underline{g} \quad ; \quad \underline{I}(\tau_{max}, \mu) = \underline{h} \qquad (4\text{-}37)$$

The transfer matrix $\underline{A}$ has the following characteristics

(i) It is symmetric Hermetian when $\rho_R = \rho_W = 0$ but

not so otherwise, (ii) diagonal elements are always posi-

tive, and in the special case of very weak anisotropy, $\underline{A}$

is diagonally dominant also, (iii) by a proper choice of

coordinate system, $\underline{A}$ can be diagonalized, (iv) it is irre-

ducible because, by any set of transformations, it is not

possible to reduce it to the upper triangular form. The

equation (4-1) can be written in the half space of angles

$\mu \in (0,1)$ as

$$-\underline{M}\frac{d\underline{I}^-}{d\tau} = \underline{A}^- (\underline{I}^- - \underline{B}^-) \quad ; \qquad (4\text{-}38)$$

$$\underline{M}\frac{d\underline{I}^+}{d\tau} = \underline{A}^+ (\underline{I}^+ - \underline{B}^+) \quad , \qquad (4\text{-}39)$$

with $\underline{I}^- = \underline{I}(\tau, -\mu)$ and $\underline{I}^+ = \underline{I}(\tau, \mu)$ representing the

rays emerging towards the surface of a star and entering

into the atmosphere respectively. In the integration of

the transfer equation over an elementary 'cell', $\underline{I}$, $\underline{B}$ and

$\underline{A}$ can be taken as constant, being some sort of average

of these quantities at the boundaries of the cell, bounded

by the planes τ_n and τ_{n+1} (n=1,2,3.....) (see Peraiah and Varghese, 1985; Nagendra and Peraiah 1985a). The formal solutions of the equations (4-38) and (4-39) can be written as

$$\bar{I}_n = \bar{I}_{n+1}\, exp[-\Delta\tau\, \underset{\sim}{M}^{-1}\bar{A}] + \int_{\tau_n}^{\tau_{n+1}} exp[-(t-\tau_n)\underset{\sim}{M}^{-1}\bar{A}]\underset{\sim}{M}^{-1}\{\bar{A}\,\underline{B}\}\, dt ,\tag{4-40}$$

for the outgoing ray, and

$$\overset{+}{\underset{\sim}{I}}_{n+1} = \overset{+}{\underset{\sim}{I}}_n\, exp[-\Delta\tau\, \underset{\sim}{M}^{-1}\overset{+}{A}] + \int_{\tau_n}^{\tau_{n+1}} exp[-(\tau_{n+1}-t)\underset{\sim}{M}^{-1}\overset{+}{A}]\underset{\sim}{M}^{-1}\{\overset{+}{A}\,\underline{B}\}\, dt ,\tag{4-41}$$

for the incoming ray. $\Delta\tau = \tau_{n+1} - \tau_n$, $n = 1,2......,N$, where N = number of layers. $\{\overset{\pm}{A}\ \underline{B}\}$ is the source function. For the present discussion, we shall concentrate on only the outgoing ray (4-40). now, assuming that $\{\overset{\pm}{A}\ \underline{B}\}$ is independent of optical depth - that is, it remains constant in the range τ_n to τ_{n+1}, we get an expression for $\bar{I}_n$ by performing the integration in equation (4-40), as

$$\bar{I}_n = \underline{B} + exp[-\Delta\tau\,\underset{\sim}{M}^{-1}\bar{A}] \cdot \{\bar{I}_{n+1} - \underline{B}\} ,\tag{4-42}$$

which is the usual formal solution and, again demands no restriction on $\Delta\tau$, as long as the physical properties remain constant in the range of integration.

Now, we discretize the matrix transfer equation
(4-1) by directly integrating it over an elementary
cell as before. We then obtain

$$\pm \underline{M} [\underline{I}_{n+1}^{\pm} - \underline{I}_n^{\pm}] = \tau_{n+\frac{1}{2}} \underline{A}_{n+\frac{1}{2}} [\underline{I}_{n+\frac{1}{2}}^{\pm} - \underline{B}_{n+\frac{1}{2}}] \; , \tag{4-43}$$

where the subscript (n+½) refers to the average of the
values of physical variables at τ_n and τ_{n+1}. For the
diamond difference scheme, we have

$$\underline{I}_{n+\frac{1}{2}}^{\pm} = \frac{\underline{I}_{n+1}^{\pm} + \underline{I}_n^{\pm}}{2} \; ; \quad \tau_{n+\frac{1}{2}} = \Delta \tau_n = \tau_{n+1} - \tau_n \; , \; etc., \tag{4-44}$$

which assumes that the intensity is linear in optical
depth within the cell. For further details on the
method of solution, see Peraiah (1984) and section 3.3.
Restricting ourselves to the outgoing ray, we have from
DSM, the following expressions for the outward directed
ray

$$\underline{I}_n^- = \underline{t}^- \underline{I}_{n+1}^- + \tau_{n+\frac{1}{2}} \underline{\Delta}^- \underline{A}_{n+\frac{1}{2}}^- \underline{B} = \underline{t}^- \underline{I}_{n+1}^- + \underline{\Sigma}^- \; , \tag{4-45}$$

where

$$\underline{t}^- = \underline{\Delta}^- \underline{S}^- \; , \tag{4-46}$$

$$\underline{\Delta}^- = [\underline{M} + \frac{1}{2} \tau_{n+\frac{1}{2}} \underline{A}_{n+\frac{1}{2}}^-]^{-1} \; , \tag{4-47}$$

$$\underline{\underline{S}}^{-} = [\underline{\underline{M}} - \tfrac{1}{2}\, \tau_{n+\frac{1}{2}}\, \bar{\underline{\underline{A}}}_{n+\frac{1}{2}}]\tag{4-48}$$

Now expanding the $\bar{\underline{\underline{\Delta}}}$ matrix (equation (4-47) in a matrix power series, then substituting in equation (4-45) and truncating the resulting expansion to the quadratic terms, we get

$$\bar{\underline{I}}_n \cong \bar{\underline{I}}_{n+1} - \tau_{n+\frac{1}{2}}\, \underline{\underline{M}}^{-1}\, \bar{\underline{\underline{A}}}_{n+\frac{1}{2}}\,[\bar{\underline{I}}_{n+1} - \underline{\underline{B}}_{n+\frac{1}{2}}] +$$

$$+ \tfrac{1}{2}\, \tau^{2}_{n+\frac{1}{2}}\, \Big\{ \big(\underline{\underline{M}}^{-1}\, \bar{\underline{\underline{A}}}_{n+\frac{1}{2}}\big)^{2}\, [\bar{\underline{I}}_{n+1} - \underline{\underline{B}}_{n+\frac{1}{2}}]\Big\} - \quad \cdot \quad \cdot \tag{4-49}$$

Now imposing an asymptotic boundary condition, like the Unno solution

$$\big(\bar{\underline{I}}_{N+1}\big)_U = \underline{\underline{B}}_{N+1} + \underline{\underline{M}}\,[\bar{\underline{\underline{A}}}_{N+1}]^{-1}\, \underline{\beta} \;;\; \underline{\beta} = \frac{d\underline{\underline{B}}}{d\tau}\Big|_{N+1}\,,\tag{4-50}$$

at the lower boundary (N+1) of the stellar stmosphere, we can get the emergent intensity recursively (n=N, N-1,.....1) using the equation (4-49). It is more useful when the source function is a linear or a nearly linear function of τ and the linear perturbation vector $\underline{\beta}$ is weak. In that case, we can substitute a Unno solution at each grid point n and, assuming a constancy of opacity and source function in each cell, we get a relation of the form

$$\underset{\sim}{\bar{I}}_n \cong (\underset{\sim}{\bar{I}}_n)_U - \underset{\sim}{\beta}\, \mathcal{T}_{n+\frac{1}{2}} + \tfrac{1}{2}\underset{\sim}{M}^{-1}\underset{\sim}{\bar{A}}_{n+\frac{1}{2}}\, \underset{\sim}{\beta}\, \mathcal{T}^2_{n+\frac{1}{2}} - \cdots \qquad \qquad (4\text{-}51)$$

When $\underset{\sim}{\beta} << \mathcal{T}_{n+\frac{1}{2}}\, \mathbb{1}$, this equation is stable and gives

an accurate and convergent solution even for step sizes

$\mathcal{T}'_{n+\frac{1}{2}} = \Delta\mathcal{T}_n > \mathbb{1}$. In practice, we can use the nodal

points, of the tabulated stellar atmospheric model, them-

selves as the grid points for constructing the cells, be-

cause in the deeper 'thicker' layers of the model the $\underset{\sim}{\beta}$

parameter will be very small, and in the upper layers,

where $\underset{\sim}{\beta}$ could be larger, the nodal point spacing itself

would be very small (i.e. $\mathcal{T}_{n+\frac{1}{2}} < < 1$), making the solu-

tion (4-51) still correct. Notice however, that the ori-

ginal DSM equation (4-45) is simply the implicit Crank-

Nicholson matrix approximation for $\exp\left[-\frac{\mathcal{T}_{n+\frac{1}{2}}}{2}\underset{\sim}{M}^{-1}\underset{\sim}{\bar{A}}_{n+\frac{1}{2}}\right]$

which occurs when solving the inhomogeneous parabolic

matrix differential equation (4-1). It is well known that

the Crank-Nicolson scheme is second order accurate, un-

conditionally stable, and a consistent approximation for

all step sizes, since $\mathcal{R}_e\lambda_i > 0$ (see Varga,1963,p.270),

where $\lambda_i = a_{i,n+\frac{1}{2}}/\mu$ $(i = 1, 2, 3, 4)$ are the eigenvalues of

$\underset{\sim}{M}^{-1}\underset{\sim}{\bar{A}}_{n+\frac{1}{2}}$. a_i are the eigenvalues of the transfer

matrix $\underset{\sim}{\bar{A}}$, with two of them being complex in general.

It can be clearly seen from equations (4-45)-(4-48)

that the central difference approximation to the trans-
mission matrix $\underset{\sim}{\bar{t}}$ is a matrix power series approximation
for the matrix exponential $\exp\left[-\tau_{n+\frac{1}{2}} \underset{\sim}{M}^{-1} \bar{A}_{n+\frac{1}{2}}\right]$
through quadratic terms. Similarly $\underset{\sim}{\bar{A}}$ is a backward
difference approximation to the same matrix exponential
through linear terms, again being unconditionally stable.
Thus, we can write the equation (4-45) to the lowest
order approximation as

$$\underset{\sim}{\bar{I}}_n \simeq \exp\left[-\tau_{n+\frac{1}{2}} \underset{\sim}{M}^{-1} \bar{A}_{n+\frac{1}{2}}\right]\left[\bar{I}_{n+1} + \tau_{n+\frac{1}{2}} \underset{\sim}{M}^{-1} \bar{A}_{n+\frac{1}{2}} \underset{\sim}{B}\right], \qquad (4\text{-}52)$$

and we see that the right-hand side of this equation is
convergent even for $\tau'_{n+\frac{1}{2}} \geqslant 1$. This is a conse-
quence of the approximation of linear variation of the
source function with optical depth (implied in the use
of diamond scheme). This has the important property of
causing the calculated intensities to be correct in the
'diffusion limit'. Grant (1963) has shown in this regard
that the difference equations of DSM naturally reduce to
the difference analogue of the diffusion equation (e.g.
equation (4-51)),in the limit of large $\tau'_{n+\frac{1}{2}}$. This
property is lost if one assumes a constant source function
throughout the atmosphere (see Wiscombe,1976a) or if the
source function is a highly non-linear function of opti-
cal depth. Obviously, this property of DSM equations

provides large practical advantages, particularly in the work with stellar atmospheres like those of white dwarfs. In the following section, we show the results obtained using this criterion for the problems of continuum and line polarization, using realistic model atmospheres. Since our primary interest in such computations is only the emergent (at $\tau = 0$) values of $\bar{I}$, the following simplified form, of the conventional DSM equations, namely

$$\underset{\sim}{\bar{t}}(1,N) = \underset{\sim}{\bar{t}}(1) \cdot \underset{\sim}{\bar{t}}(2) \cdot \underset{\sim}{\bar{t}}(3) \cdot \underset{\sim}{\bar{t}}(4) \cdots \cdots \underset{\sim}{\bar{t}}(N-1) \cdot \underset{\sim}{\bar{t}}(N) \; , \qquad (4\text{-}53)$$

and

$$\underset{\sim}{\bar{\Sigma}}(1,N) = \underset{\sim}{\bar{\Sigma}}(1) + \underset{\sim}{\bar{t}}(1) \cdot \underset{\sim}{\bar{\Sigma}}(2) + \underset{\sim}{\bar{t}}(1) \cdot \underset{\sim}{\bar{t}}(2) \cdot \underset{\sim}{\bar{\Sigma}}(3) + \underset{\sim}{\bar{t}}(1) \cdot \underset{\sim}{\bar{t}}(2) \cdot \underset{\sim}{\bar{t}}(3) \cdot \underset{\sim}{\bar{\Sigma}}(4) +$$

$$\cdots \cdots + \underset{\sim}{\bar{t}}(1) \cdot \underset{\sim}{\bar{t}}(2) \cdots \cdots \underset{\sim}{\bar{t}}(N-1) \cdot \underset{\sim}{\bar{\Sigma}}(N) \; , \qquad (4\text{-}54)$$

can be used. N, here is the total number of atmospheric layers considered from the model atmosphere. Though diffusion approximation places no restriction on the step size, one can use $\tau_{n+\frac{1}{2}} \simeq 2$ as a safe choice in computing the $\underset{\sim}{\bar{t}}$ and $\underset{\sim}{\bar{\Sigma}}$ matrices of the respective layers (see Kalkofen and Wehrse, 1982 a,b). These authors have made an extensive analysis of the

finite difference techniques in general. Our equation (4-45) is, for example, the polarized analogue of the equation (25) in their (1982a) paper with a half-implicit differencing weight. The thick layer operators can be generated by the usual doubling algorithm (Grant and Hunt,1969b; Peraiah,1984). We have repeated some of the test cases-the tables (1) - (5) of section 2.3, now using the diffusion approximation described in the previous section (equations (4-45),(4-50),(4-53) and (4-54)). Since the agreement is good upto the third or fourth digits, we do not repeat them here. In addition, the following two tests, namely $\psi(\tau) = (0, \pi)$ with $\psi(o)=0, \psi(\tau_{max})=\pi$ for $\chi =0$ should give $Q(o)= U(o) = 0$ and $\chi(\tau) = (0, 2\pi)$ with $\chi(o)=0$, $\chi(\tau_{max}) = 2\pi$ for $\psi = \pi/2$ should give $U(o) = V(o) = 0$, which are the checks based on symmetry requirements are satisfied exactly, confirming that no spurious sources or sinks are introduced by the diffusion approximation, even in a realistic atmosphere. We feel that, such an approach should be reasonably good in the quantitative work where accurate solutions are not needed in the initial stages of the modelling. We have got nearly 30% savings in the computing time over the earlier procedure described in section 3.3.

4.3 Zeeman line formation under general physical
     conditions: a discussion of results

In the computation of Zeeman line profiles prese-
nted in this section, we have always used the Stokes
vector representation and the equations (4-1) to (4-23).
The lines have been computed in realistic atmospheres.
But, the following assumptions are made (i) the Doppler
width $\Delta \vartheta_D$, damping constant a, and the ratio η_0 are
depth independent. All these are good approximations.
Even though both the line centre absorption coefficient
and the continuum absorption coefficient vary by large
amounts from deep in the atmosphere to the outer layers,
their ratio almost remains constant. (ii) the continuous
dichroism and anomalous dispersion are depth independent
and treated as constants with their typical values through-
out the line profile. This is also a good approximation.
We shall now proceed to discuss the results. In the
Zeeman line computations, it is generally assumed that the
field strength B, its inclination ψ with the line of
sight and its azimuth χ measured with respect to an arbi-
trary x-axix in the plane transverse to the line of sight
are always independent of the optical depth τ. In ab-
sence of any direct observational means of measuring the
depth dependence, which is definitely there, this has been

accepted as a reasonably good approximation. But it is important to know, to what extent can such depth dependence really affect the Zeeman line formation, either in a steady state atmosphere or an atmosphere having ordered velcoity fields. This will provide a basic understanding, and helps in the fine analysis of lines formed in such complicated, but realistic situations. The general conclusions remain valid for the lines formed in any magnetic atmosphere say the solar atmosphere or the white dwarf atmosphere etc.

In Figures 1 to 4 we show the changes produced by taking some of the parameters as depth dependent. A hypothetical Zeeman triplet with a line centre wavelength $\lambda_0 (\mathcal{V}=0) = 5000 \overset{o}{A}$ is used in these computations. $\mathcal{V} = \Delta \mathcal{V} / \Delta \mathcal{V}_D$ and $\mathcal{V}_p = 0 , \mathcal{V}_l = 16 , \mathcal{V}_r = -16$ correspond to the centres of the Zeeman components. $\mathcal{V}_{p,l,r} = \Delta M \left| \frac{\Delta \mathcal{V}_B}{\Delta \mathcal{V}_D} \right| , \Delta M = 0, \pm 1$ for p,l,r respectively. $a = \Gamma / 4\pi \Delta \mathcal{V}_D$ is the damping parameter, Γ being the total damping constant (in s^{-1}) of the line. We have fixed a = 0.1. The continuous dichroism is introduced by selecting $\eta_p = 1.00;$ $\eta_l = 0.94,$ $\eta_r = 1.1;$ $\rho_R^C = -10 \cos \psi$ and $\rho_W^C = -0.25 \sin^2 \psi$ μ is always taken as 0.8. η_o is taken as 10^4. All the parameters mentioned above are typical of a weak line formed in a cool, high-gravity white-dwarf atmosphere. A hydrogen rich convective equilibrium model with $T_{eff} = 9000 \overset{o}{K}$ log g = 8, from Wehrse (1976) is adopted. Figure 1 shows
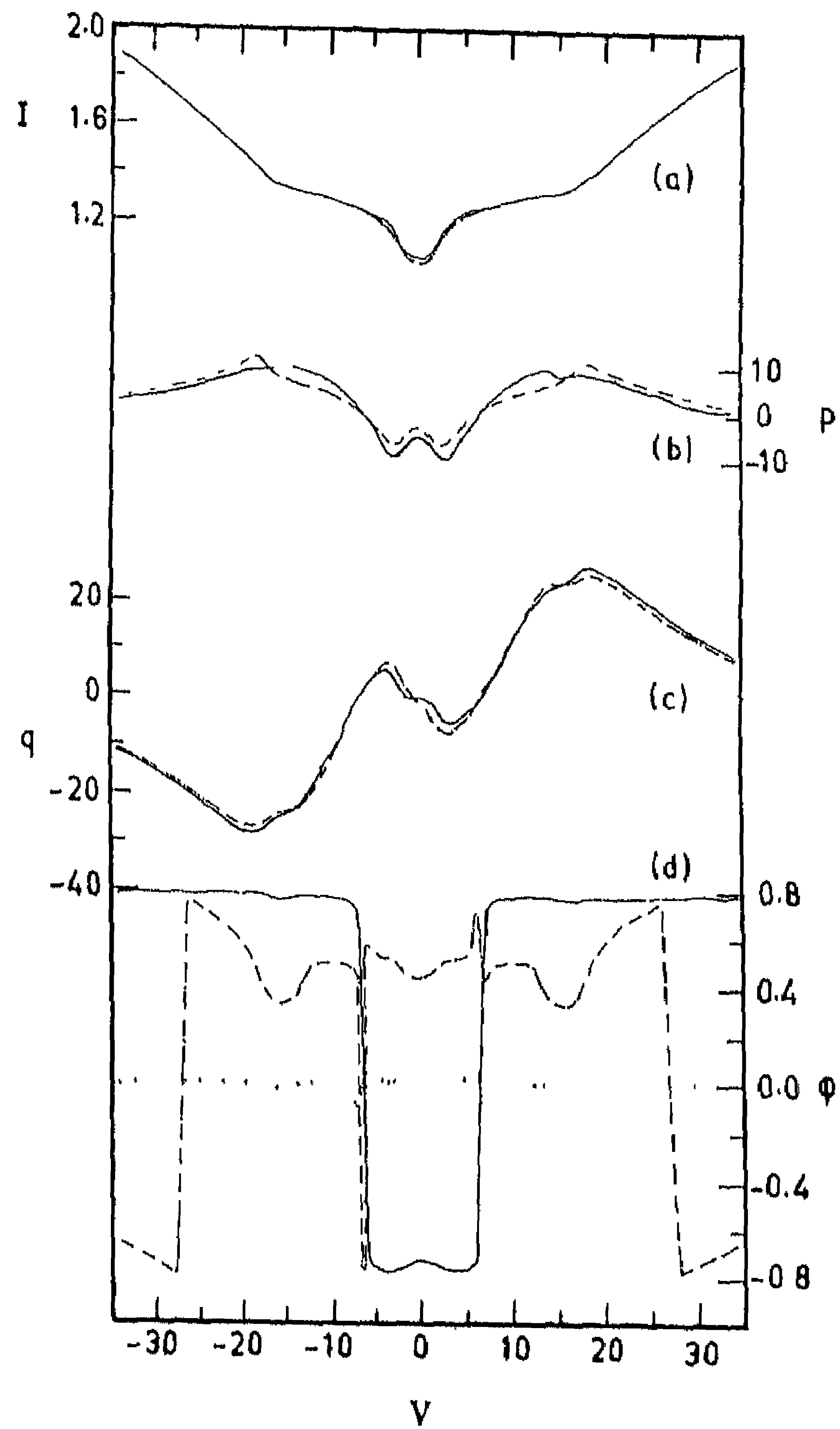
Fig.1. Intensity (a),percentage linear (b)and
circular (c) polarization,and polarization posi-
tion angle (d) for a hypothetical Zeeman triplet.
Full curves (case x):$\psi = \pi/4, \chi = \pi/4$.Dot-dashed
curves:$\psi = \pi/4, \chi = \chi(\tau)$.Dotted curve:$\psi = \pi/4$,
$\chi = 0$.

the effect of azimuth angle χ variations. The solid
curves show the Stokes profiles for a depth independent field direction ($\psi = \pi/4$; $\chi = \pi/4$) with respect to the line of sight. This case, we shall keep as
a standard and shall refer to it as case χ . The $\bar{I},p$
and q profiles for ($\psi = \frac{\pi}{4}$; $\chi = 0$) are same as for the
case χ because of the complimentary nature of the
azimuth angles $\frac{\pi}{4}$ and 0. The dotted curve in Figure
1d for this later case shows that the position angle
φ is quite small throughout the profile and arises only
because of the magneto-optical effects. Notice that
the position angle is the only parameter which distinguishes the two cases, hence the importance of its obser-
vation. We have included the depth dependence of the
azimuth angle χ in the transfer equation by replacing ρ_R
by $\rho_R - 2\mu(d\chi(\tau)/d\tau)$. A small variation represented by
$\chi(\tau) = \frac{\pi}{16} exp(-\tau)$ is used. This case is represented by
dot-dashed curves. The intensity $\bar{I}$ is not much affected
except in the core. The p profile equivalent width increases and its central depth is reduced. The q profile
is affected to a larger extent only near the π-component
of the triplet. The sharp changes in the position angle
φ near $\psi \sim 7$ are due to the fact that Q and U para-
meters simultaneously change sign in this region (see
also Staude, 1970). This is obvious because (ψ, γ /2)

are the inflection points in a symmetric Zeeman triplet.
At these points, a matching of the η_p occurs with η_ℓ
or η_r. These points are slightly shifted now, because
of the radiative transfer effects. Recently, Deguchi
and Watson (1985) have computed the Zeeman lines formed
in such a twisting magnetic field. The Stokes profiles
in Figure 1 are in good agreement with their so called
'optically thick' lines.

Figure 2 shows the changes produced by the depth
variation of ψ. For the case $\psi=0$; $\chi=0$ (indicated
by dashed lines), we can see that the σ-components are
clearly stronger and the π-component is absent; p = 0
and ϕ = 0 because it is the case of longitudinal Zeeman
effect. The q profile does not show the 'π- component
splitting' indicating that the 'coupling of the Stokes
parameters' is basically essential for such a splitting,
along with the usual magneto-optical effects (see case χ:
solid line). The variation of the angle ψ as $\psi(\tau)=\frac{\pi}{16}exp(-\tau)$,
has definite effects on the $\bar{I}$,q and ϕ profiles ($\psi=\psi(\tau)$)
$\chi=\pi/4$: dottend lines). The ϕ profile undergoes
fluctuations because of a strong coupling of the V para-
meter to Q and U through magneto-optical effects and a
changing inclination (see Beckers, 1969). p also fluc-
tuates, but it is unresolved in the figure since it is
smaller in magnitude. Notice that the ψ variation intro-
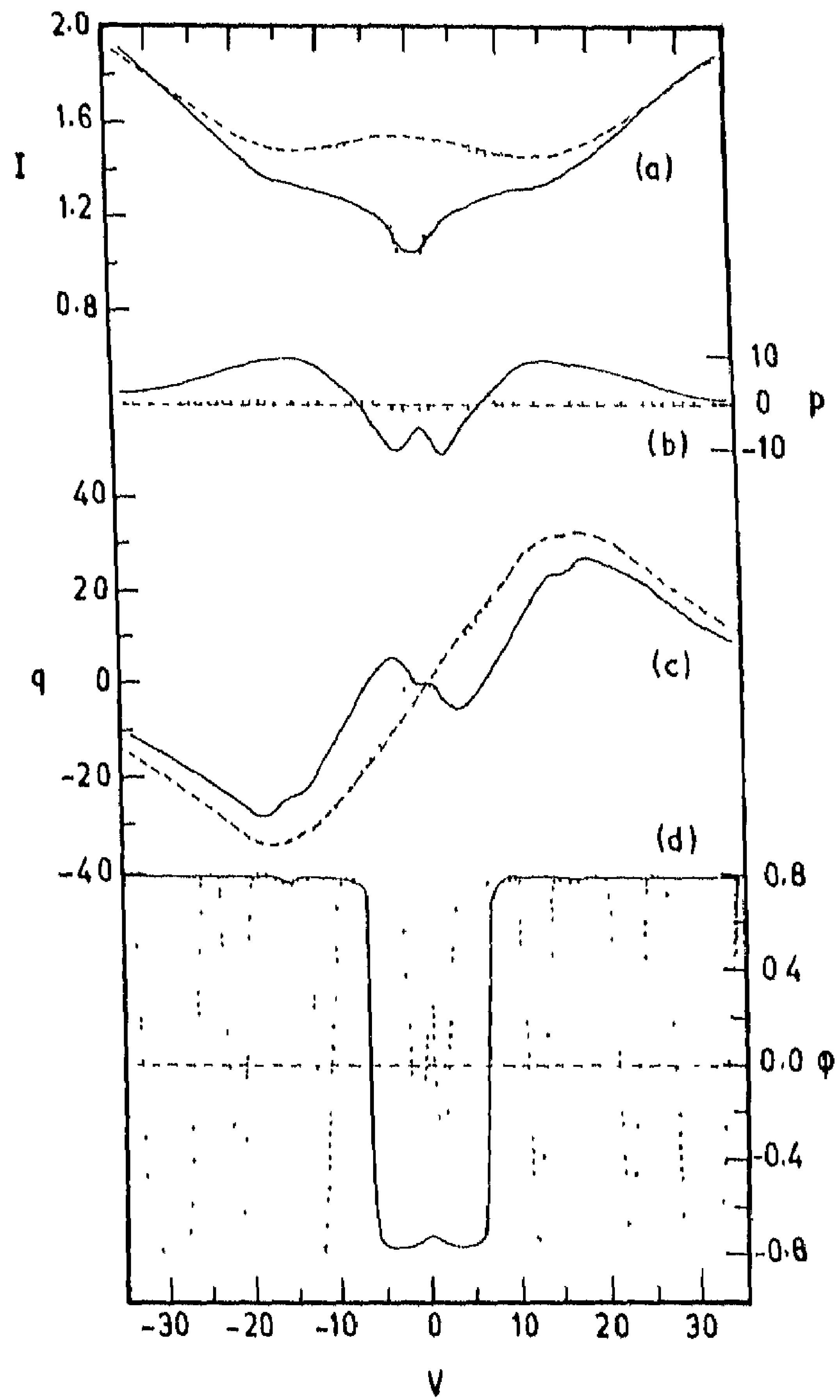
Fig.2.As Fig.1,but showing the follo-
wing cases.Full lines:case x;dashed
lines:ψ=0,χ=0;dotted lines:ψ=$\psi(\tau)$
χ = π/4,i.e. ψ variation.

duces a large deepening of the π - component in the
I profile, and a π - component splitting in the q profile.

In Figure 3 we show a combination of the simultaneous
variation as mentioned above, of ψ and χ along with a
slight variation in field strength according to the for-
mula $\vartheta_B(\tau) = 16\left\{1+0.1\left(1-exp\left(-\tau\right)\right)\right\}$, $\left(+\vartheta_l = -\vartheta_r = \vartheta_B(\tau)\right)$.
From the profiles (dashed lines), it is seen that in the
core of the line the ψ variation dominates while in the
wings $(\vartheta \sim 10)$ χ variation is important in the line for-
mation. The effect of inhomogeneous (depth dependent)
field is marginal compared to the changes produced by
angular variations. The case χ is also shown for com-
parison in this figure.

In Figure 4 we show the profiles formed in quite
general situations. The dotted lines are the profiles
formed in an arbitrarily moving atmosphere respresented
by $\vartheta(\tau) = 0.2 + 0.1(1+ exp(-\tau))$, $\alpha(\tau) = Cos^{-1}\mu + \frac{\pi}{16}exp(-\tau)$,
with the magnetic field also being taken as inhomogeneous.
The field variation is effected as mentioned before. One
can see that the field gradient enhances the asymmetry
near the line centre and reduces the same in the wings.
The full lines are the profiles when there is a change
in the angles ψ and χ only (see e.g.figure (3)). The
dashed lines represent the most general case of the pro-
files formed in arbitrarily varying angles,velocity and
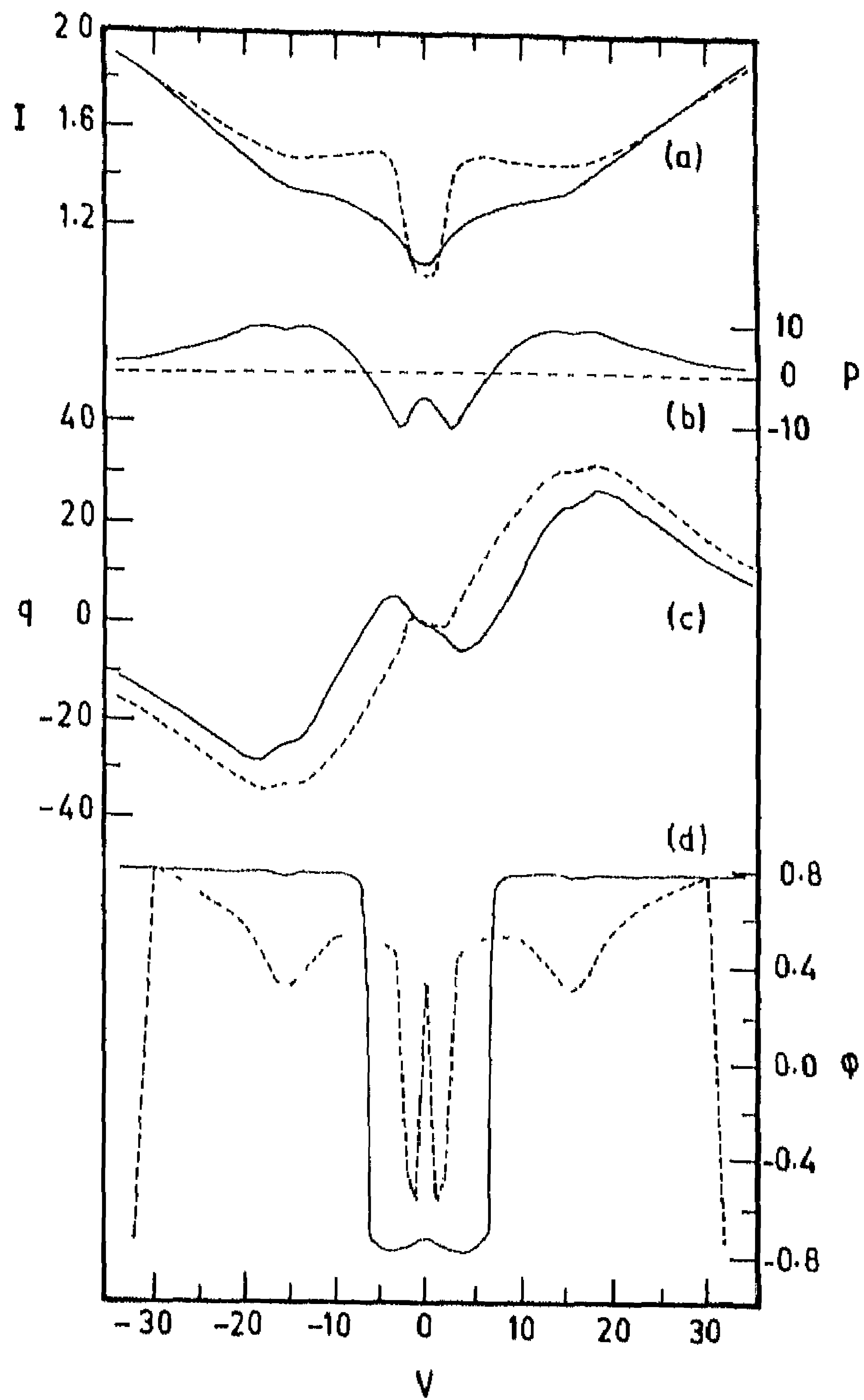
Fig.3.As Fig.1,but with the following

cases.Full lines:case x;dashed lines: ψ

= ψ(τ), $\chi = \chi$(τ) ,B=B(τ),i.e.changing ori-

entation of the field vector. The case

ψ = π/4,χ = π/4,B=B(τ))is indistinguish-

able from case x.
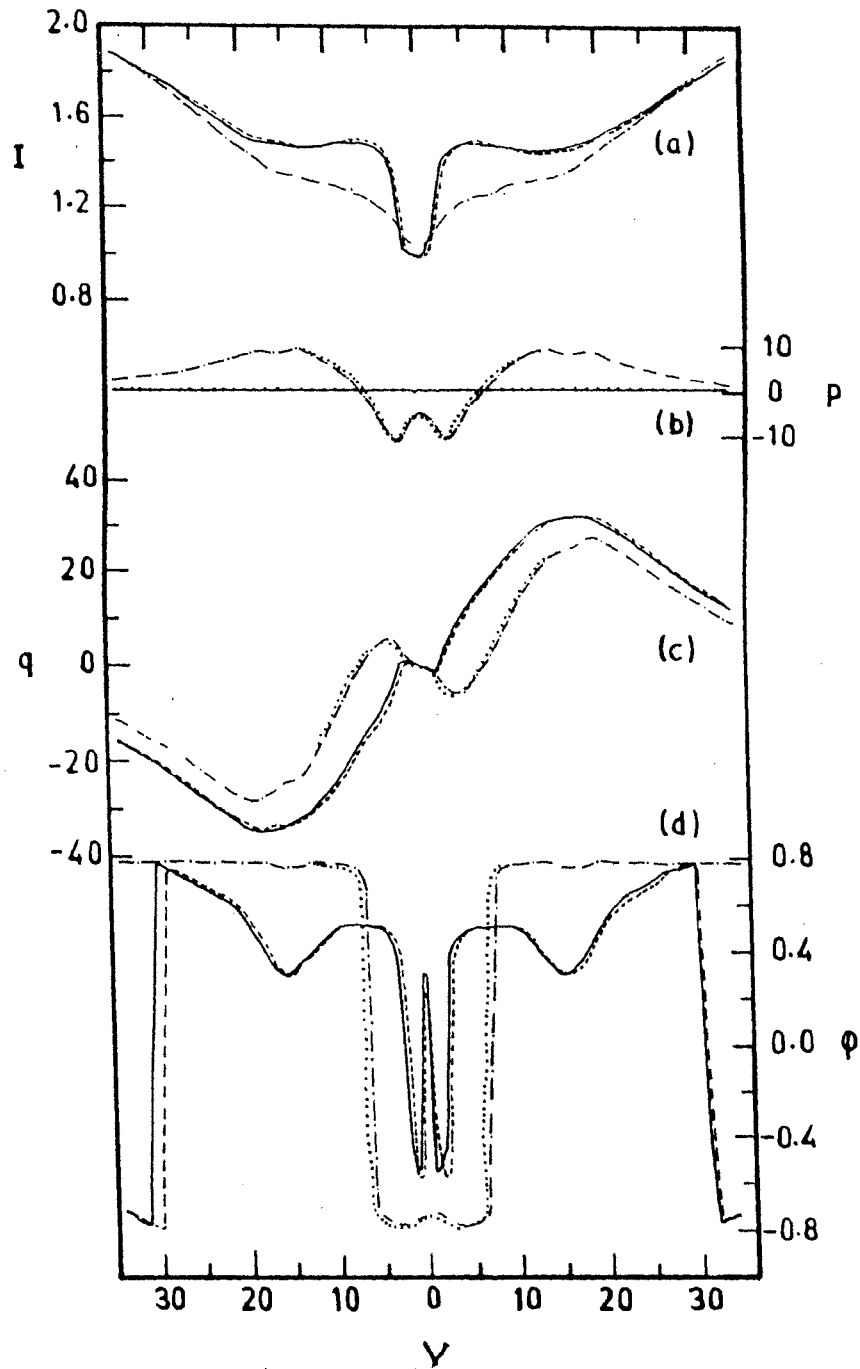
Fig.4.As Fig.1,but showing the following
cases.Dash-dot lines: case x.Dotted lines:
$\psi = \pi/4$, $\chi = \pi/4$, $V_m = V_m(\tau)$, $\alpha = \alpha(\tau)$, $B = B(\tau)$.
Full lines: $\psi = \psi(\tau)$, $\chi = \chi(\tau)$. Dashed lines:
$\psi = \psi(\tau)$, $\chi = \chi(\tau)$, $V_m = V_m(\tau)$, $\alpha = \alpha(\tau)$, $B = B(\tau)$.

magnetic fields which, excepting a small asymmetry,
are not much different from the former case (full lines).
Thus when the line shift asymmetries (dotted lines) are
weaker, the angular variation of the field vector is a
dominant mechanism which can change the shape of the
polarization profiles. It is thus clear that these
effects are quantitatively more pronounced for the solar
magnetic regions, than whitedwarf atmospheres. The spe-
cific intensity vectors are computed on 256 grid points
(16 latitudes and 16 longitudes) on the visible disk of
white dwarf for a given angle of inclination (i) of the
dipole axis to the line of sight. Equations (4-53) and
(4-54) have been used for this purpose. The disk inte-
gration, which is a double integral is performed using
a 16 point Gaussian quadrature formula. The results of
this computation are presented in table 1. We have com-
pared for few cases, our results (referred to as DA =
diffusion approximation) with the solutions obtained by
Martin and Wickramasinghe (1982) (referred to as MW).
The linear polarization is extremely small and not much
significance can be placed on it unless it is still lar-
ger in magnitude. We like to mention that the difference
is not entirely due to the approximation of our calcula-
tion of specific intensities. The coarse grid employed
for disk integration by us, also contributes to that diff-

Table 1. Disk integrated linear ($\bar{p}$) and circular ($\bar{q}$) polarization from a magnetic white dwarf for two wavelengths. i is the inclination of the dipole axis to the sight line. $\rho_R = \rho_W \equiv 0$ for all the cases.

		$\lambda = 3500\,\text{Å}$		$\lambda = 4500\,\text{Å}$	
		$\bar{p}\,(\times 10^{-5})$	$\bar{q}\,(\times 10^{-3})$	$\bar{p}\,(\times 10^{-5})$	$\bar{q}\,(\times 10^{-3})$
$i = 0°$	MW	0.00	-4.90	0.00	-5.30
	DA	0.00	-4.85	0.00	-5.27
$i = 45°$	MW	2.50	-3.50	4.20	-3.70
	DA	2.12	-3.43	3.78	-3.66
$i = 90°$	MW	5.10	0.00	8.40	0.00
	DA	4.76	0.00	7.95	0.00

erence. The above authors use a still larger number of grid points for that purpose. Thus we feel that diffusion approximation is not a bad approximation, at least for the white dwarf atmospheres.

As a further test on the usefulness of the diffusion approximation, we have computed the continuum linear and circular polarization in a magnetic white dwarf atmosphere with a central dipole field of polar field strength $B_p = 10^7$ G. A model atmosphere of a DA white dwarf with $T_{eff} = 20,000^{\circ}$ K, log g = 8, taken from Wickramasinghe (1972) is used. The continuum polarization is included according to Nagendra and Peraiah (1984), as described in section 2.2.

4.4 An astrophysical application: cyclotron resonance absorption in the magnetic atmospheres

In the review article on magnetic white dwarfs, Angel (1978) has shown some objects which show both continuum polarization indicating a high magnetic field, and absorption features which can not be identified with the Zeeman sub-components of the important lines. GD 229, G240-72, Grw + 70° 8247 are such objects. It has been suggested (Lamb and Sutherland, 1974; Angel 1977; Gnedin and Sunyaev, 1974b) that cyclotron absorption can play an important role in the optical spectrum of these objects.

Some characteristics of cyclotron absorption in real-
istic situations, as referred to magnetic white dwarfs,
has been discussed extensively by Martin and Wickrama-
singhe (1979a). An absorption coefficient for the cyclo-
tron resonance absorption has been derived quantum mecha-
nically by Lamb and Sutherland (1974). This formula
applies only to right hand circularly polarized light.
In the normal wave representation, this formula is ana-
logous to the absorption coefficient of the extraordi-
nary mode. In the cold plasma limit which we have been
using, the absorption coefficient of ordinary mode re-
mains smaller and almost constant near the cyclotron
frequency, hence its contribution being quite negligible
The collisions have been neglected in deriving this for-
mula. A classical and approximate formula has been given
by Bekefi (1966) which includes the collisional broaden-
ing of the cyclotron resonance absorption. As suggested
by Martin and Wickramasinghe (1979 a),we adopt a composite
model, in which the Lamb-Sutherland formula

$$\eta_\gamma = \frac{4\pi^{3/2}}{\omega} \left(\frac{e^2}{m_e c}\right) \left(\frac{N_e}{B}\right) \left[\frac{m_e c^2}{2kT \cos^2\psi}\right]^{1/2} \cdot \left[1 - \exp\left(-\frac{\hbar\omega}{kT}\right)\right]^{-1} \cdot \exp\left[-\frac{m_e c^2 (\omega-\omega_c)^2}{2kT\omega^2\cos^2\psi}\right] \quad (4-55)$$

is used in the Doppler core, and the larger of the
above and the collisionally damped absorption coeffi-
cient

$$\eta_\gamma = \left(\frac{e^2}{m_e c}\right)\left(\frac{N_e}{k^2}\right)\left(\frac{kT}{2\pi\hbar\omega}\right)(1+\cos^2\psi)\left[\frac{\nu_{coll}}{(\omega-\omega_c)^2 + \nu_{coll}^2}\right] \cdot$$
$$\cdot \left[\exp\left(\frac{\hbar\omega}{kT}\right)-1\right] , \qquad (4\text{-}56)$$

due to Bekefi (1966), is used in the Lorentz wings of the
Voigt like resonance absorption profile. The collisional
frequency can be calculated using

$$\nu_{coll} = \frac{\omega_o^2 e^2}{m_e V_e^3}\ln\Lambda \ ; \quad V_e = \sqrt{\frac{2kT}{m_e}} \ ; \quad \ln\Lambda \simeq 9.1 - \frac{\ln N_i}{2} + \frac{3}{2}\ln T , \qquad (4\text{-}57)$$

from Melrose (1980). The nature of the spectrum and pola-
rization depends quite strongly on the viewing angle, be-
cause of strong anisotropy of the radiation field (see
section 3.4). In Figure 5 we have shown the flux and
polarization emerging from a T_{eff} = 9000°K, log g = 8
line blanketed model in radiative equilibrium, taken
from Wehrse (1976). The resonance absorption depresses
the continuous flux spectrum in the range of wavelengths
$\lambda\lambda$ 4000-8000 $\overset{o}{A}$ (dashed line), since it operates effecti-
vely in the frequency range, approximately, $\omega_c(B_p)$ to $\omega_c(B_p)/2$,
corresponding respectively to the polar regions which con-
tribute 'strongly' in the blue, and to the equatorial re-
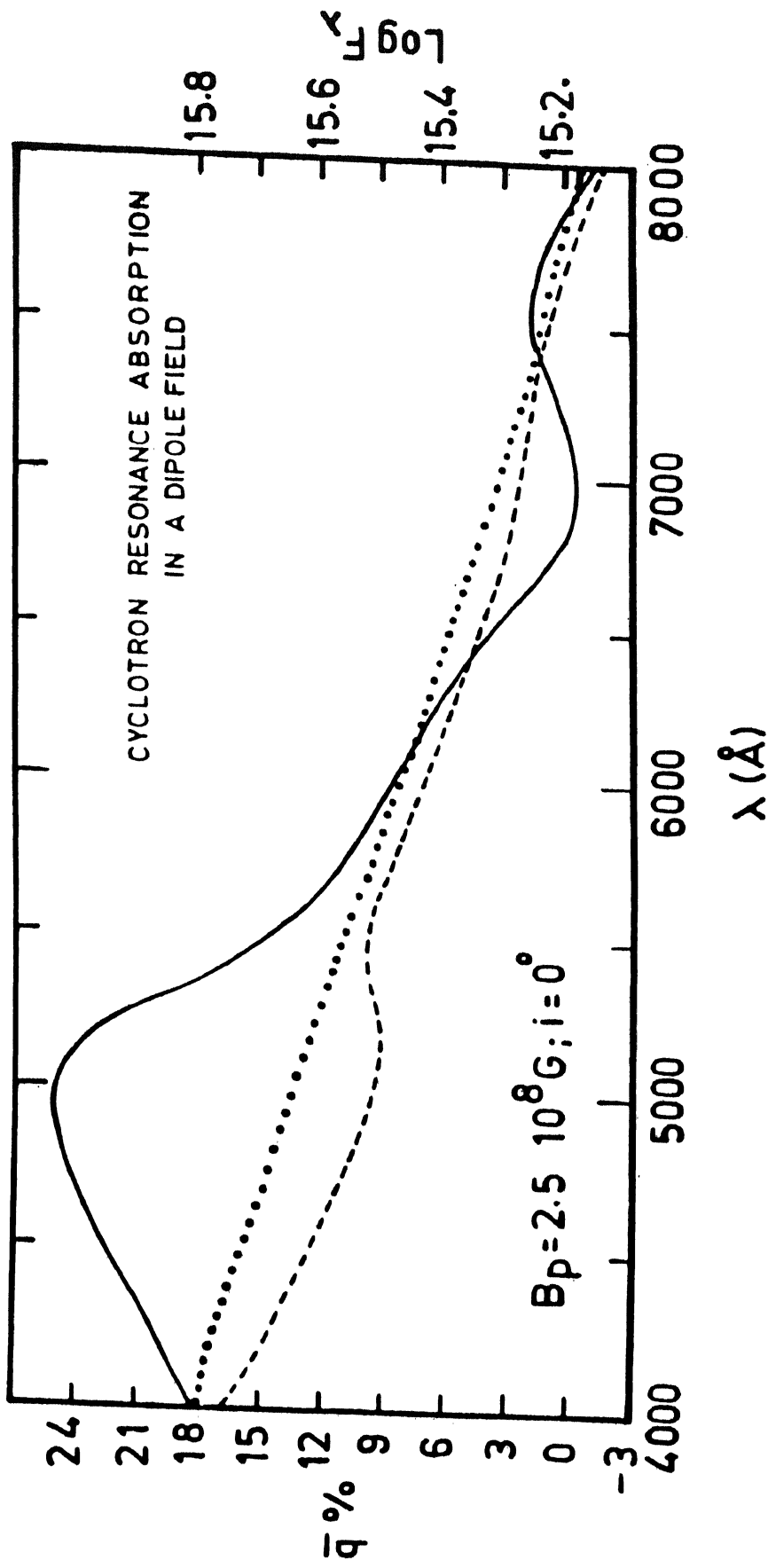
Fig.5. The disk integrated circular polarization $\bar{q}$ (full line) and spectra (dashed line) in a strong field white dwarf. The non-magnetic spectra is shown by the dotted line. The linear polarization $\bar{p} \equiv 0$, by symmetry. A $T_{eff} = 9000$ K, Log g = 8 radiative model is adopted from Wehrse (1976).

gions which contribute 'weakly' in the red—the reason

being a reduction in field strength by a factor of 2

between the pole and the equator of a dipole field.

The disk integration has to be done using a careful

selection of points. The demand for a higher order

quadrature is more in this problem. The non-magnetic

(B=0) flux spectrum is shown by the dotted line for the

sake of comparison. Since the 'collisionless plasma

approximation' absorption coefficient (equation (4-55))

has very narrow profile, its contribution is insigni-

ficant though it is very strong where as the classical

'cold plasma approximation' absorption coefficient (equa-

tion (4-56)) absorbs over large frequency band at each

point on the disk. The effective absorption band widths

are quite large because the collisional damping (equation

(4-57)) is very strong. The flux and the polarization

spectrum calculated by us differ in many respects from

those calculated by Martin and Wickramasinghe (1979a) who

use a constant value of collision frequency, which is ra-

ther high, throughout the atmosphere. We use the depth

dependent collision frequencies calculated at every depth

point using equation (4-57). This causes large variations

in the effective bandwidth of absorption throughout the

atmosphere. An extensive and systematic study of the

quantum effects in cyclotron plasma absorption has been made

by Pavlov, Shibanov and Yakovlev (1980a). The spectra
and polarization produced in a realistic atmosphere under
cyclotron mechanism are difficult to understand qualita-
tively, when the disk integration is performed. However,
certain features of the spectrum and polarization shown
in Figure 5 can be understood by comparing it with Figures
2,5 and 6 of Pavlov, Mitrofanov and Shibanov (1980b). Our
computations using other models show that the degree and
sign of polarization depend on $(\frac{d}{d\lambda}A, \underline{B})$ and $(\frac{d}{d\tau}\underline{B})$
for a given field distribution on the stellar disk. The
circular polarization $\bar{q}$ shows a strong wavelength depen-
dence, unlike the thermal continuum polarization in weak
field magnetic white dwarfs. Collisionally damped cyclo-
tron absorption is stronger than expected earlier, and the
saturation produced by it is responsible for the difficulty
in fitting thermal energy distribution to the observed
spectrum, when such a strong non-thermal phenomena is oper-
ative in the magnetic stars in general and in the white
dwarfs in particular.

CHAPTER 5

SOME NEW PHYSICAL PROCESSES WHICH AFFECT THE POLARI-
ZATION OF CONTINUUM AND LINE RADIATION

In this chapter we shall first concentrate on two
physical mechanisms which are well known in experimental
physics, namely the Stark-Zeeman effect and the plasma
polarization shift of spectral lines, and incorporate
them into the radiative transfer equation. We then solve
the transfer equations for these two problems under most
realistic situations, relaxing all the approximations
made in the chapter 4. In section 5.3 we shall discuss
the Zeeman line formation for oriented atoms. In section
5.4 we will discuss the effect of atmospheric structure,
and the line shifting mechanisms, on Zeeman line transfer.
In these two problems, we shall retain the level of appr-
oximation used in the chapter 4. The physical conditions
of the plasmas selected for these studies represent diff-
erent astrophysical situations, particularly the magnetic
stars. Finally, in section 5.5 we demonstrate the effect
of refraction of the beam of light,on the solutions obtain-
ed using the conventional polarization transfer equations
where refractive effects are not included. We solve the
pure absorption polarization transfer equation individually
taking each of these effects into account, separately.

5.1 The influence of combined Stark-Zeeman effect on line formation in a magnetic field

The Stark and Zeeman effect are equally important in computing the hydrogen line profiles in moderately strong magnetic fields, where the Zeeman or Paschen Back effects are not too dominant over the Stark effects. Such moderately strong fields (few hundreds to few thousands Gauss) are found in pre-main sequence chemically peculiar (CP) stars and Ap stars. Till now, only pure Zeeman effect is used as a basic phenomena in theoretically modelling the hydrogen line profiles in these objects. Many years ago Nguyen-Hoe et al.(1967) were the first to calculate the Stark 'profile functions' in a magnetic field using the impact approximation. R Recently, in a series of papers, Mathys (1983,1984a,b and 1985a) has developed a more accurate unified theory and computed the profile functions for a wide range of temeperatures (T_e), electron densities (N_e) and magnetic fields (B). In the unified theory, the ionic and the electronic contribution to the electric microfield distribution, is taken simultaneously into account. The unified theory approach for the non-magnetic Stark profiles is given by Smith et al.(1969); Vidal et al.(1970, 1971). The modification of the unified theory to include ion dynamical effects is presented in Cooper et al.(1974).

The hydrogen line broadening is primarily caused by
a strong linear Stark effect due to interactions between
the radiating atom or ion andlocal electric microfields
produced by perturbing ions and electrons. When an exter-
nal magnetic field is present, such as to act only as
an additional perturbation, the classical straight line
path approximation remains still valid. In a recent
work Mathys (1984b) has included the ion dynamial
effects also in the computation of Stark-Zeeman pro-
files. The Stark-Zeeman profiles can not be obtained by
simply convolving the non-magnetic Stark broadened pro-
files with pure Zeeman patterns, because the collisional
transitions between the Zeeman substates of a given level
can not be neglected (Mathys,1984b). Hence we have to
use the magnetic field modified Stark profiles, and con-
volve them with a Doppler broadening function to obtain
the required profile functions.

Since the hydrogen lines are used for deriving fund-
amental stellar parameters such as log g, a correct pro-
file function calculation, used in a realistic radiative
transfer treatment is very essential in order to fit the
observed line profiles in these magnetic stars. The
theory of polarization radiative transfer for hydrogen
line formation under the combined influence of Stark
and Zeeman effects has been formulated by Mathys (1985b).

We briefly describe the required equations and solve them to obtain the hydrogen line profiles formed in a realistic model atmosphere, for a given value of the magnetic field. The model atmosphere and the field strength represent the conditions typical of magnetic Ap stars. We use the radiative transfer formalism presented by Mathys (1985). The transfer equation in LTE, for the polarized intensity $\underline{I} = (I\ Q\ U\ V)^T$ is given by

$$\mu \frac{d\underline{I}}{d\tau} = \underline{\underline{A}}\ \underline{I} - \underline{S}$$

(5-1)

where, as usual $\mu = \cos\theta$, θ being the angle between the propagation and vertical (Z) directions. $\underline{\underline{A}}$ and $\underline{S}$ are respectively the absorption matrix (transfer matrix) and the source vector, represented as

$$\underline{\underline{A}} = \underline{\underline{I}} + \underline{\underline{A}}^L \quad ; \quad \underline{S} = \underline{J}\ B_\eta + \underline{S}^L$$

(5-2)

where $\underline{\underline{I}}$ is a (4 x 4) unit matrix and $J = (1\ 0\ 0\ 0)^T$. B_η is the Planck function. $d\tau = -k^c \rho\, dZ$, k^c being the continuous absorption coefficient (in cm^2/gm) and ρ the mass density. The line absorption matrix $\underline{\underline{A}}^L$ and the emission vector $\underline{S}^L$ are given as

$$\underline{\underline{A}}^L = N'\underline{\underline{B}}_{abs} - N\underline{\underline{B}}_{em} \quad ; \quad \underline{S}^L = N\underline{E} \quad ,$$

(5-3)

where N and N' (cm^{-3}) are respectively the populations of upper level n and the lower level n' . The stimulated emission matrix is given for a frequency ω by

$$\underline{B}_{em} = \frac{2\pi^2 \omega}{\hbar c} \left(\frac{b_{em}}{\rho k^2} \right) .$$
(5-4)

The most general form of $\underline{b}_{em}$ has been derived by Mathys (1985b). The $\underline{b}_{em}$ in a restricted (zero azimuth; $\chi \equiv 0$) coordinate system is given by

$$\left(\underline{b}_{em} \right)_0 = \begin{bmatrix} (1+\cos^2\psi)I_{xx}+\sin^2\psi I_{zz}; & \sin^2\psi(I_{zz}-I_{xx}); & 0 & ; & 2\cos\psi R_{xx} \\ \sin^2\psi(I_{zz}-I_{xx}) & ; & (1+\cos^2\psi)I_{xx}+\sin^2\psi I_{zz}; & 2\cos\psi I_{xx}; & 0 \\ 0 & ; & -2\cos\psi I_{xx} ; & (1+\cos^2\psi)I_{xx}+\sin^2\psi I_{zz}; & \sin^2\psi(R_{zz}-R_{xx}) \\ 2\cos\psi R_{xx} & ; & 0 & ; & \sin^2\psi(R_{xx}-R_{zz}); & (1+\cos^2\psi)I_{xx}+\sin^2\psi I_{zz} \end{bmatrix}$$
(5-5)

The absorption matrix, in the same choice of coordinate system is given by

$$\left(\underline{b}_{abs} \right)_0 = \begin{bmatrix} (1+\cos^2\psi)I'_{xx}+\sin^2\psi I'_{zz}; & \sin^2\psi(I'_{zz}-I'_{xx}); & 0 & ; & 2\cos\psi R'_{xx} \\ \sin^2\psi(I'_{zz}-I'_{xx}); & (1+\cos^2\psi)I'_{xx}+\sin^2\psi I'_{zz}; & -2\cos\psi I'_{xx}; & 0 \\ 0 & ; & 2\cos\psi I'_{xx} ; & (1+\cos^2\psi)I'_{xx}+\sin^2\psi I'_{zz}; & \sin^2\psi(R'_{xx}-R'_{zz}) \\ 2\cos\psi R'_{xx}; & 0 & ; & \sin^2\psi(R'_{zz}-R'_{xx}); & (1+\cos^2\psi)I'_{xx}+\sin^2\psi I'_{zz} \end{bmatrix}$$
(5-6)

where ψ is the angle between the propagation and field directions. We define

$$I_{xx} = \frac{Re}{\pi} J_{xx} \left.\vphantom{\begin{matrix}a\\b\end{matrix}}\right\} \quad ; \quad I_{zz} = \frac{Re}{\pi} J_{zz} \left.\vphantom{\begin{matrix}a\\b\end{matrix}}\right\}$$
$$R_{xx} = \frac{-I_m}{\pi} J_{xx} \qquad\qquad R_{zz} = \frac{-I_m}{\pi} J_{zz} \qquad\qquad (5\text{-}7)$$

with the emission profile functions defined as

$$J_{xx} = i \sum_{\{\ell \ell' m m'\}} < n\,\ell_a m_a \,|\,\rho_A\,|\, n\ell_a m_a > \; \times$$

$$\times \; < n\ell_a m_a \,|\,\underline{e}_x \cdot \underline{D}\,|\, n'\ell_a' m_a' > < n'\ell_b' m_b' \,|\,\underline{e}_x \cdot \underline{D}\,|\, n\ell_b m_b > \; \times \qquad (5\text{-}8)$$

$$\times \; < n'\ell_b' m_b' ;\, n\ell_b m_b \,|[\Delta\omega - \mathcal{L}(\Delta\omega_0)]^{-1}\,|\, n\ell_a m_a ;\, n'\ell_a' m_a' > \; .$$

ρ_A and $\underline{D}$ are the density operator and the dipole momentum operator of the radiator (refer to Mathys,1984b for the actual calculation of the profile functions). J_{zz} is obtained by replacing x by z in the expression above. The polarized perofiles are given (for any direction of polarization $\underline{e}$) by

$$I(\omega, \underline{e}) = \frac{-I_m}{\pi} \sum_{\{\ell,\ell',m,m'\}} < n\ell_a m_a\,|\,\underline{e}\cdot\underline{D}\,|\, n'\ell_a' m_a' > < n'\ell_b' m_b'\,|\,\underline{e}\cdot\underline{D}\,|\, n\ell_b m_b > \; \times$$

$$\times \; < n'\ell_b' m_b' ;\, n\ell_b m_b \,|[\Delta\omega - \mathcal{L}(\Delta\omega_0)]^{-1}\,|\, n\ell_a m_a ;\, n'\ell_a' m_a' > \; , \qquad (5\text{-}9)$$

where $\underline{e}$ can be $\underline{e}_x$, $\underline{e}_y$ or $\underline{e}_z$. The quantum theory required for calculating $I(\omega, \underline{e})$ is developed in the series of papers by Mathys, as already mentioned. Notice that J_{xx} and J_{zz} are closely related to $I(\omega, \underline{e}_x)$ and $I(\omega, \underline{e}_z)$ respectively. The R profiles are defined as

$$R(\omega, \underline{e}) = \frac{-Re}{\pi} \sum_{\{\ell, \ell', m, m'\}} \langle n\ell_a m_a | \underline{e} \cdot \underline{D} | n'\ell'_a m'_a \rangle \langle n'\ell'_b m'_b | \underline{e} \cdot \underline{D} | n\ell_b m_b \rangle \times$$

$$\times \langle n'\ell'_b m'_b ; n\ell_b m_b | [\Delta\omega - \mathcal{L}(\Delta\omega)]^{-1} | n\ell_a m_a ; n'\ell'_a m'_a \rangle \qquad (5\text{-}10)$$

In LTE, a further simplification is possible: the populations of various (Zeeman) sublevels are, to a very good approximation equal for a given principal quantum number n, so that onecan consider the atomic density matrix elements $\langle n\ell_a m_a | \rho_A | n\ell_a m_a \rangle$ as independent of 1 and m having a constant value given by $(\mathbf{1}/n^2)$. Thus, in LTE,

$$\left.\begin{array}{l} I_{xx} = I(\omega, \underline{e}_x)/n^2 \\[2mm] R_{xx} = R(\omega, \underline{e}_x)/n^2 \end{array}\right\} \qquad \left.\begin{array}{l} I_{zz} = I(\omega, \underline{e}_z)/n^2 \\[2mm] R_{zz} = R(\omega, \underline{e}_z)/n^2 \end{array}\right\} \qquad (5\text{-}11)$$

The absorption profile functions I' and R' can be obtained by just replacing n by n' in the above expressions. The populations of the levels n and n' can be obtained from the Saha-Boltzmann equation. The spontaneous emission vector $\underline{E}$ is given by

$$E = \frac{2\hbar \omega^3}{(2\pi c)^2} B_{em} I \qquad (5\text{-}12)$$

The profile functions mentioned above are valid for a radiator at rest. The thermal motion of the radiators can be accounted for by convolving them with a Doppler broadening function as follows (Mihalas,1978; eq.9.28)

$$\left. \begin{array}{l} \overline{I}_{xx} \cong \overline{I}_{xx}(\omega) = \int\limits_{-\infty}^{+\infty} I_{xx}\left(\omega - \frac{\varsigma}{c}\,\omega\right) W(\varsigma)\,d\varsigma \\[4mm] \overline{R}_{xx} \cong \overline{R}_{xx}(\omega) = \int\limits_{-\infty}^{+\infty} R_{xx}\left(\omega - \frac{\varsigma}{c}\,\omega\right) W(\varsigma)\,d\varsigma \end{array} \right\} \qquad (5\text{-}13)$$

with

$$I_{xx}(\omega) = \frac{10^8 \lambda^2}{2\pi c F_o} I_{xx}(\alpha) \ ; \quad \alpha = \frac{\Delta\lambda(\mathring{A})}{F_o} \ , \quad F_o = 2 \cdot 61\, e\, N_e^{2/3} \ . \qquad (5\text{-}14)$$

There are two similar expressions for $\overline{I}_{zz}$ and $\overline{R}_{zz}$. We have employed $\overline{I}$ and $\overline{R}$ profiles instead of I and R, in computing the matrix elements of ($\underline{b}_{em}$)$_o$.

$$W(\varsigma)\,d\varsigma = \frac{1}{\sqrt{\pi}}\ exp\left(-\varsigma^2/\varsigma_o^2\right)\frac{d\varsigma}{\varsigma_o} \ , \qquad (5\text{-}15)$$

is the Maxwellian velocity distribution function which is the probability of finding an atom with an observer's frame line of sight velocity ς in the range $(\varsigma,\ \varsigma + d\varsigma)$ The thermal velocity of the atoms is $\varsigma_o = \sqrt{2kT/M}$.

It is to be noted that the natural line broadening
is always negligible compared to the Stark broaden-
ing, so that the Doppler convolved Stark profiles
represent a realistic situation in a dense hydrogen
plasma.

The longitudinal ($\psi = 0$) and transverse ($\psi = \pi/2$)
Stark-Zeeman profile functions are given by

$$I_{\parallel}(\omega) = \frac{1}{2}\left[I(\omega, \underline{e}_x) + I(\omega, \underline{e}_y)\right], \tag{5-16}$$

and

$$I_{\perp}(\omega) = \frac{1}{4}\left[I(\omega, \underline{e}_x) + I(\omega, \underline{e}_y) + 2I(\omega, \underline{e}_z)\right], \tag{5-17}$$

where $\underline{e}_x$, $\underline{e}_y$ and $\underline{e}_z$ are positive unitary vectors along
ox, oy and oz respectively, with the z-axis taken along
the direction of the magnetic field. They are also called
unit polarization vectors. The factors $\frac{1}{2}$ and $\frac{1}{4}$ are in-
troduced in order to insure that the possible normali-
zation of the polarized profiles is conserved when they
are combined to get the unpolarized profiles $I_{\parallel}$ (ω) and
$I_{\perp}$ (ω). The polarized profiles, for any direction of
polarization $\underline{e}$ are given by expressions like equation
(5-9). The profile function for any arbitrary angle ψ
measured from the z-axis, can be calculated using

$$I(\psi, \omega) = I_{\parallel}(\omega) \cos^2\psi + I_{\perp}(\omega) \sin^2\psi . \qquad (5\text{-}18)$$

The normalized unpolarized profiles are given by

$$S_{\parallel,\perp}(\Delta\lambda) = C(I_{\parallel,\perp}(\Delta\lambda)/f), \quad \int_{-\infty}^{+\infty} S_{\parallel,\perp}(\Delta\lambda)\, d(\Delta\lambda) = 1, \qquad (5\text{-}19)$$

where f is the total line strength, which has to be cal-
culated by summing the squared matrix elements of the
dipole operator ($\underline{e},\underline{d}$) over the initial and final mag-
netic substates (see Mathys,1983)

$$f = C \sum_{\ell_a m_a} \sum_{\ell'_a m'_a} |\langle n\ell_a m_a | \underline{e}\cdot\underline{d} | n'\ell'_a m'_a \rangle|^2 . \qquad (5\text{-}20)$$

C is an arbitrary constant. The Doppler convolved profile
functions $\overline{S}_{\parallel,\perp}(\Delta\lambda)$ can be obtained by a convolu-
tion procedure as described above.

In Figure 1 we show the Doppler convolved H_α profile
functions calculated for an electron density $N_e = 10^{15} cm^{-3}$
temperature $T = 10^4 K$ and a magnetic field of $B = 4 \cdot 10^4 G$.
We have used the recent unified theory of Mathys (1984b)
for this purpose, which takes ion dynamics into account.
We have also marked in the figure the position of the σ^-
-component of the normal Zeeman triplet. A comparison
of this Figure with Figures 17 and 18 of Mathys (1984a)
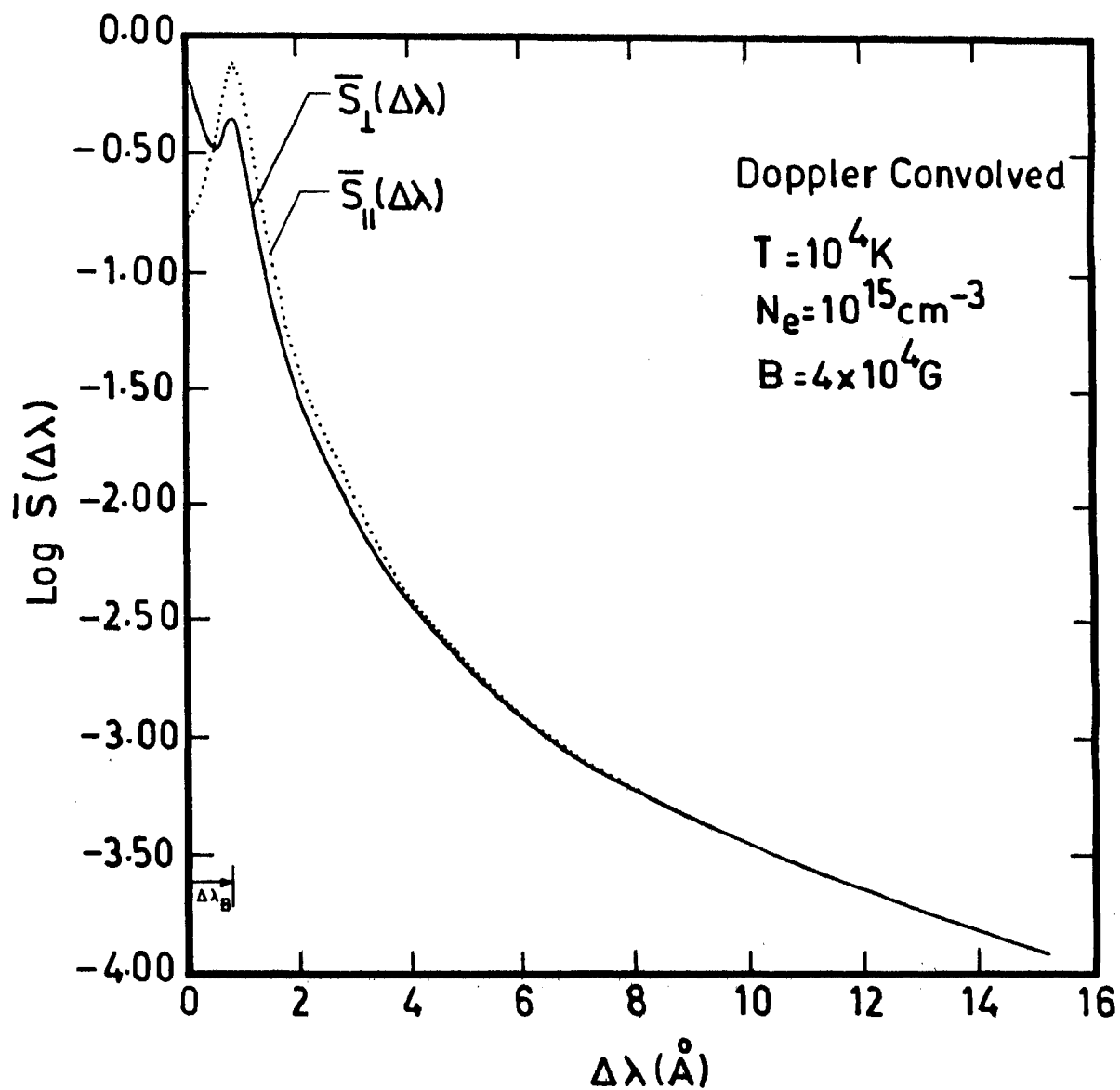
Fig.1. Combined Stark-Zeeman profile functions of H_α computed using unified dynamic theory of line broadening.

shows a close agreement. The small differences in the wings are due to the static ion theory used by Mathys (1984a) in computing those profiles. Mathys (1984a) has shown that, at high densities (such as $N_e \geqslant 10^{15} cm^{-3}$) the profile functions are flat natured, though there is a marked change near the Zeeman peaks (the positions of the σ - components). But the low density profiles show a much stronger wavelength dependence inside the line. He also has shown that the Zeeman peaks will also be narrow in low density profile functions. The Doppler convolution in general, widens the original Stark-Zeeman profile functions, and makes it deeper near the line core.

In a magnetized plasma, the atoms moving in a magnetic field 'see' an electric field (a Lorentz electric field), whose contribution to the Stark broadening is not a priori negligible, at least for the outermost layers of the stellar atmosphere, though the contribution is quite small for lower field strengths ($B < 3-4 \cdot 10^4 G$) and higher densities ($N_e > 10^{14} cm^{-3}$). Yet, the inclusion of this effect into the Stark-Zeeman profile function calculation would be rather difficult and time consuming, in view of the explicit velocity and angle dependence of this Lorentz electric field. We are grateful to Dr.G.Mathys for drawing our attention to this point through a personal communication.

For the computation of H_α line profile shown
in Figure 2b, we have chosen a model of normal stellar
atmosphere from Kurucz (1979) with T_{eff} = 20,000 K,
log g = 4.5 and log (solar abundance) = 0. The free
parameters of the calculation are: $\mu = 1$; $B = 2 \cdot 10^4 G, \Psi = \pi/2, \chi = \pi/4$
The reduced intensity $\bar{I} = I(o, \mu) / B_\gamma(o)$, where $B_\gamma(o)$
is the Planck function at the topmost layer of the trun-
cated model. $p = (\sqrt{Q^2 + U^2}/I) \cdot 100$ and $q = 0.5 \tan^{-1}(U/Q)$
represent the percentage linear polarization, and the
polarization position angle in radians respectively. The
insert shows the full drawn curve of the main figure it-
self, over a wider range of 20 $\overset{o}{A}$. The line wings reach
a continuum level at $\bar{I} \simeq 2.0$ and employed a field strength
of $B = 2.10^4$ G. The I and R profiles were computed using
the code kindly provided by Dr.Mathys, and then the con-
volution is performed to get $\bar{I}$ and $\bar{R}$. In Figure 2a we
have shown the variation of I and R profiles (in arbi-
trary units) across the line. They represent the profile
functions for the physical parameters indicated in the
figure. Notice the symmetry of the I profile functions
and the antisymmetry of R profile functions about the
line centre. We have evaluated them at the nodal points
of a (-1,+1) Gaussian quadrature which obviously has a
low resolution near the line centre. Because of this, the
positions and widths of the peaks in the I and R profiles
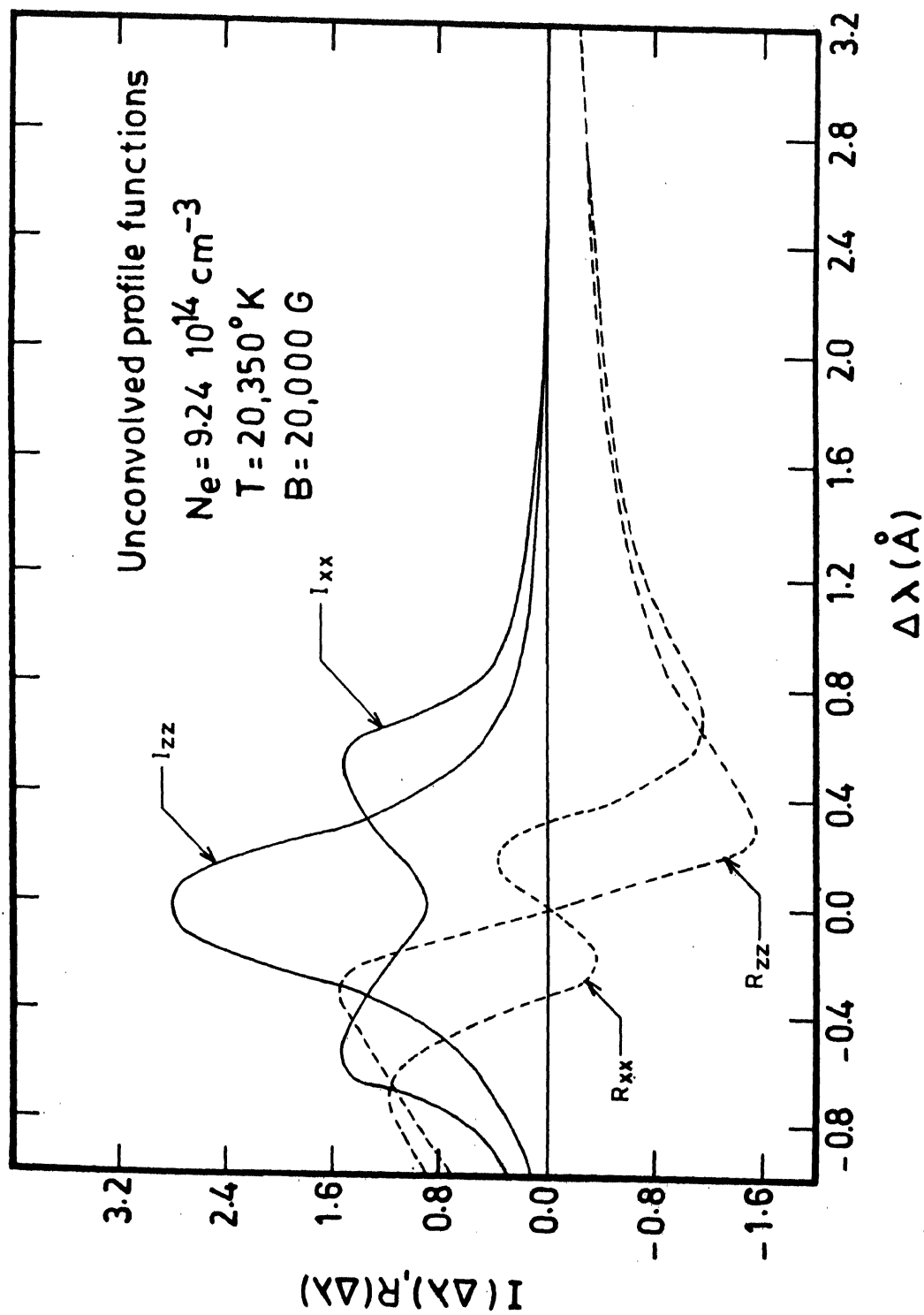
Fig. 2a The nature of I and R profiles appearing in the theory of com-
bined Stark-Zeeman effect. The profile functions correspond to H_α line.
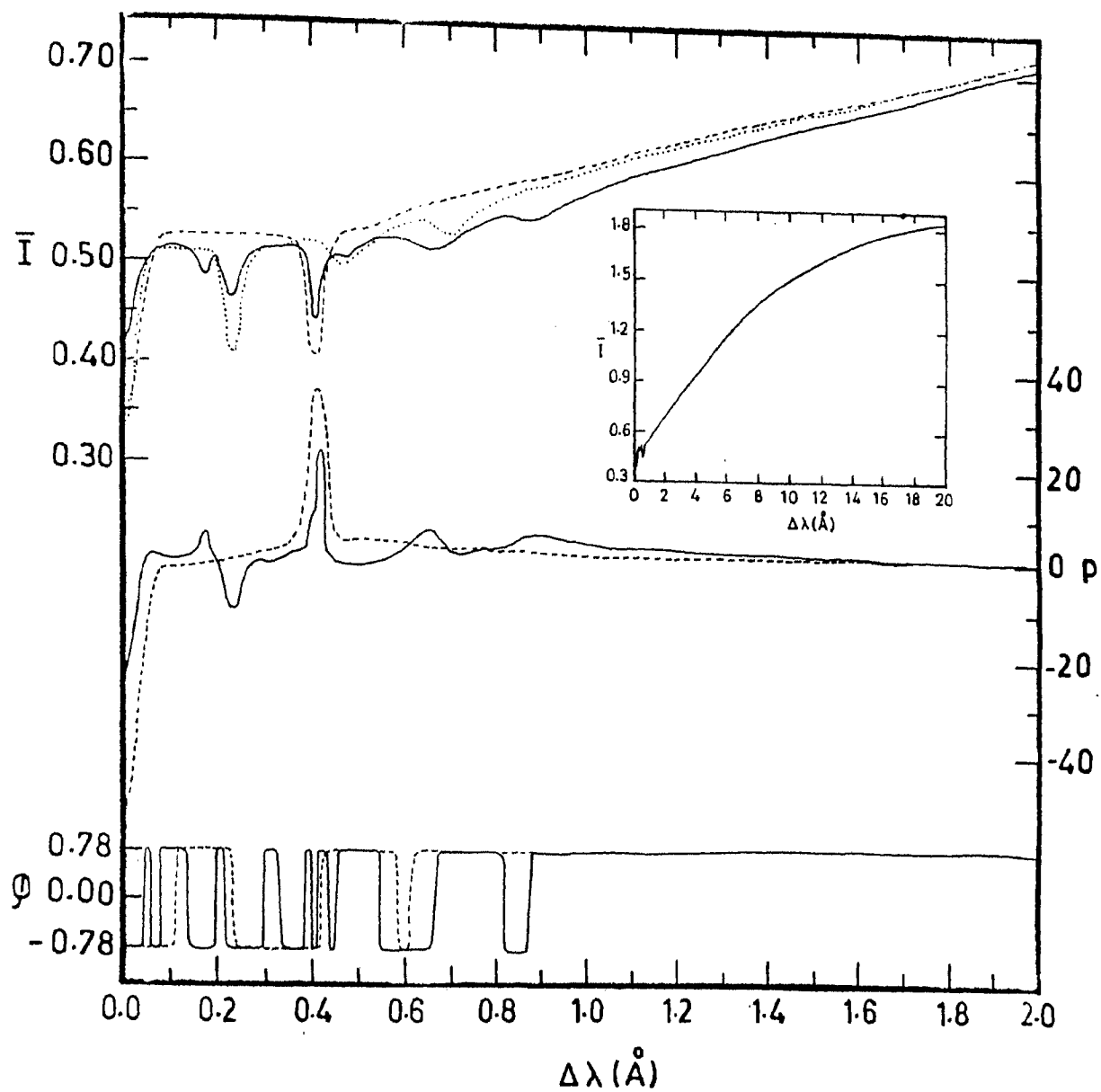
Fig.2b H$_\alpha$ line profiles (λ_o = 6563.813 Å) formed in a transverse magnetic field, under the influence of combined Stark-Zeeman effect, in a magnetic atmosphere.

are somewhat approximate. However, this Figure illustrates the behaviour of these profile functions across the line. The method of solution of the transfer equation is described in Nagendra and Peraiah '1985a) or section 3.3. The boundary condition used at $\mathcal{T} = \mathcal{T}_{max}$ is $\underline{I} = (B_1, 0, 0, 0)^T$. The depth integration of the transfer equation is stopped at $\mathcal{T}_{max} \simeq 3.2$ in order to satisfy the requirement $N_e \lesssim 10^{15} cm^{-3}$ needed to use the unified theory with ion dynamics in the profile function calculation. The lower limit of N_e is fixed by the condition $4.04 \; 10^{-3} \sqrt{N_e} \gtrsim B$. Only half of the line is shown, since it is symmetric about the line centre. The importance of treating the hydrogen lines with an exact theoretical analysis employing the theory of combined Stark-Zeeman effect has been clearly demonstrated by Mathys '1984a,1985b). We shall now see the usefulness of such a calculation when adopted into a realistic line formation problem. Since all the physical parameters are depth dependent, it is not easy to draw general conclusions using these results. However, the following qualitative remarks can be useful in the anlysis of hydrogen Zeeman lines.

The dotted line represents the H_α line computed for $B \cong 0$, which corresponds to the case of Doppler convolved pure Stark profile function. An absorption feature near $\Delta\lambda \simeq 0.2 \overset{o}{A}$ represents the region of the profile where

the Stark effect begins to be significant. The line
core is dominated by the Doppler effect. As expected
(Mathys,1985b),the central depth of this non-magnetic
line profile is larger than the corresponding magnetic
profile (the full line). Further, the line width and
the total line strength are smaller than the magnetic
profile. The important case of Doppler convolved Stark-
Zeeman line profile is shown by the full lines. For
$B = 2 \cdot 10^4 G$, $\Delta \lambda_B \simeq 0.4 \overset{\circ}{A}$ nearly equal to the Doppler width
of the line in deep layers of the atmosphere. The pro-
file functions have a prominent Zeeman peak near $\Delta \lambda = \Delta \lambda_B$
The peak is more pronounced in the case of low electron
densities. At higher densities, this peak gradually dis-
appears. This general behaviour of the profile functions
is weakly dependent on the temperature. Hence we can
say that the line shape as well as its width are mainly
determined by the electron density at different levels
in the atmosphere. The temperature dependence of the
profile function on the optical depth comes mainly through
the Doppler broadening. In other words, the Doppler con-
volution leads to wide, shallow and flat natured profile
function in the deeper layers of the atmosphere, and to
slightly narrow, centrally deep and structured profile
function in the top layers. The main characteristic of
the Satrk-Zeeman line profiles is their similarity to

the normal Zeeman pattern. This is so because, for as
strong a field strength as $B = 2.10^4 G$, the magnetic
term dominates the Stark-Zeeman profile function cal-
culation. The wings of the line profile are however
strongly damped due to ion dynamical contribution to
Stark effect, as well as due to pure Doppler broaden-
ing of the Stark-Zeeman profile functions. The dashed
lines represent the line formation by just the combined
Stark-Zeeman effect (viz.without Doppler convolution).
This intensity and polarization profiles are nearly simi-
lar to a broadened (electronic or resonance) normal
Zeeman triplet of a Lorentz line shape. The shape of the
line core region is determined by the magnetic effects
and that of wings by the Stark effect. Notice the mer-
ging of the non-magnetic Doppler broadened Stark inten-
sity profile (dotted line) with this dashed profile, in
the wings. Since these dashed lines represent the Stark-
Zeeman line formation for a radiator at rest, they are
unrealistic, and given here, only to show the effect of
Doppler convolution. These dashed profiles also serve
a purpose to show that the impact of Stark effect (as a
broadening mechanism) on the non-magnetic profiles is
more severe (see dotted lines) than on the magnetic pro-
files (see dashed lines).

The magnetic fields encountered in chemically peculiar (CP) stars or Ap stars produce a magnetic intensification of the lines, which may be nearly a factor of 2 or 3 depending on the effective field strength being longitudinal or transverse. It is well know that the abundances of these otherwise normal atmospheres have to be increased few times, to match the strength of observed line profiles. The Zeeman effect, in contrast, can much more efficiently enhance the line strength in normally saturated lines such as hydrogen lines. In the case of hydrogen lines formed in magnetic atmospheres, we have to use the Doppler convolved Stark-Zeeman profiles instead of Voigt profiles, in view of the strong linear Stark effect in hydrogen lines, which can not be depicted fully, by varying the damping constant in a Voigt profile. Also, substantial differences exist between the non-magnetic line profiles (dotted line) and the magnetic line profiles (full line), which implies that, using non-magnetic profiles for matching the observed profiles of magnetic atmospheres may lead to discrepancy.

Hence we conclude that the procedure described in this section for computing Stark-Zeeman line profiles, though time consuming for quantitative work, is useful for detailed studies on a particular line. Since these

profiles are more sensitive to the electron density, than temperature, they offer a useful tool for estimating electron density more accurately.

5.2 The plasma polarization shift of spectral lines in a strong magnetic field

The plasma polarization shift (PPS) is a line shifting mechanism which affects the lines formed in dense plasmas ($N_e \gtrsim 10^{17} \, cm^{-3}$). The examples are the atmospheres of white dwarfs and the polar cap emitting regions of accreting white dwarfs and neutron stars. The nearly linear dependence of this shift on B even for strong fields ($B > 10^{7} \, G$), and on the electron densities N_e makes it relevant in strongly magnetized dense plasmas in general. It is an effect originating in the partial screening of nuclear charge by an excess of negative space charge, mainly caused by the perturbing free electrons moving in the Coulomb field of the emitting ion. It is important only when the radiating atom is ionized, the simplest example being He II. Here the interactions. of the emitting ion with the plasma environment are responsible for an average negative space charge which partly lies 'within the bound electron orbits', and therefore partially shielding nuclear charge, thus altering the energy level structure of the emitter. The statice level

shift arises due to initial correlations and is frequency independent. Also, the shift is negligible compared to Stark effects in the case of neutral atoms. The shifts in the He-like ions is again smaller than the H-like ions. The explicit dependence of PPS on electron density (N_e) and the temperature ⁽T) leads to stronger radiative transfer effects particularly in deep layers of the stellar atmosphere. See Jaegle et al.⁽1985) for some recent experimental and theoretical work regarding PPS.

The quantum mechanical treatment of this problem is due to Griem (1974) and Volonte (1975). According to Griem's theory, the average perturber charge density due to plasma, at the (Z-1)e charged ion ⁽radiating particle) is given by

$$\rho(V) = -(eN_e) \frac{2\pi (z-1) e^2 / \hbar V}{1 - exp\left[-2\pi (z-1) e^2 / \hbar V\right]} \qquad (5\text{-}21)$$

assuming isotropic perturber distribution. V is the velocity of the perturbing electron. The shielding charge $e\Delta z_n$ within the level n (principal quantum number) is given by

$$e\Delta z_n = 2\pi \int_0^{r_n} dr \int_0^{\pi} d\theta \int_0^{\infty} dV \; r^2 \sin\theta \; \rho(V) \; P(V) \; , \qquad (5\text{-}22)$$

where $\gamma_n = (n^2/z)a_o$ is the bound orbit radius, a_o being the Bohr radius. $f(v)$ is the Maxwellian velocity distribution. The shielding by the bound electrons is negligible compared to that of the electrons in free states, because the contribution to negative space charge in the Griem's model comes mainly from free electrons in the plasma. However, in Volonte's (1975) model, the perturbing electrons move in the Coulomb field of the emitting ion considered as a point charge. In principle, these electrons can be either in bound or in free states. In the quantum mechanical treatments of both the authors, the radial integral shown above appears, and γ_n is used as a suitable cutoff radius in performing the integral. In more recent calculations, radially dependent charge density distributions in the ionic volume are also used. The shift of the level n ($n > 1$) is obtained in the hydrogenic approximation as

$$\Delta E_n \approx \Delta \left(-z^2 \frac{E_H}{n^2} \right) \approx -2z \; \Delta z_n \; \frac{E_H}{n^2} \; . \tag{5-23}$$

from which the relative wavelength shift of the level follows

$$\frac{\Delta \lambda_n}{\lambda_n} \approx -\frac{32}{3} \pi^{3/2} \left(\frac{z-1}{z^4} \right) \left(\frac{E_H}{kT} \right)^{1/2} a_o^3 \; n^2 (n^2+1) \, N_e \; , \tag{5-24}$$

where

$$a_o = \frac{h^2}{4\pi^2 m_e e^2} \quad , \quad E_H = \frac{e^2}{2a_o} \quad . \tag{5-25}$$

$\overline{\lambda}_n = \lambda_n + \Delta\lambda_n$ is the shifted position of the level.
In Griem's theory the perturbing charge density is esti-
mated 'at the nucleus' where it takes its maximum value
and is assumed to remain constant at that value, through-
out the ion volume. Such a treatment is justified for
low n values and high $\left(N_e \gtrsim 10^{17} \, cm^{-3}\right)$ density plasma en-
vironment. The ground state of an ion is not shifted in
Griem's theory. Let ν and ν' be the frequency of a point
in the unshifted and shifted profiles respectively, the
line shift being produced by PPS. Then the relative shift
can be expressed in reduced frequency units as

$$\upsilon' = \upsilon + \frac{c}{V_T} \left[\frac{\nu}{\nu_o} x_n - (x_{n'} - x_n) \frac{\nu_{n'}}{\nu_o} \right] , \tag{5-26}$$

where, as usual,

$$\upsilon = \frac{\nu - \nu_o}{\Delta\nu_D} \, , \quad \upsilon' = \frac{\nu' - \nu_o}{\Delta\nu_D} \, ; \quad \Delta\nu_D = \frac{\nu_o}{c} \sqrt{\frac{2kT}{M}} = \frac{\nu_o}{c} V_T \, , \tag{5-27}$$

and

$$x_n = \frac{32}{3} \pi^{3/2} \left(\frac{z-1}{z^4}\right) \left(\frac{E_H}{kT}\right)^{1/2} a_o^3 \, n^2 (n^2 + 1) N_e \quad . \tag{5-28}$$

$x_{n'}$ can be obtained by a replacement $\eta \to \eta'$. η' and η are the principal quantum numbers of the lower and upper energy levels. E_H is the binding energy of the ground state of hydrogen atom. We shall now estimate the effect of PPS on the spectra of He II ion in a strong magnetic field. The energy levels of this ion including linear and quadratic Zeeman effect in a strong magnetic field $(B > 10^7 G)$ have been computed by Surmelian and O'connell (1973) using the perturbation theory. We have taken those eigenvalues and included the PPS using the equations given above. It is well known that the binding energy of the ground state of hydrogen atom increases monotonically for field strengths $B > 10^8 - 10^9 G$ (Rajagopal et al.1972, Cohen et al.1970). The wavelength shift for any line in general can be computed using

$$\Delta \lambda_{nn'} \simeq -x_n \lambda_{nn'} + \frac{(x_{n'} - x_n)}{\lambda_{n'}} \lambda_{nn'}^2 , \qquad (5-29)$$

where x_n and $x_{n'}$ are as given before. The displaced wavelength is given by $\bar{\lambda}_{nn'} = \lambda_{nn'} + \Delta \lambda_{nn'}$. λ_n is the wavelength corresponding to the excitation energy of the ηth level. We have assumed in deriving the equation given above, that, $E_n > E_{n'}$. But in very strong magnetic fields, $B \gtrsim 10^9 G$ the inter-n mixing of highly excited states occurs, thus diminishing the impact of PPS, and even leading to a shift

of opposite sign compared to the corresponding transition
in a lower field strength. The ground state ionization
energy is calculated using

$$E_H = \frac{\hbar^2}{2m_e a_o^2} + \hbar\omega_L - m_e \omega_L^2 a_o^2 \quad ; \quad \omega_L = \frac{eB}{2m_e c} \tag{5-30}$$

It should be noted that the mean radius of the atom de-
creases for field strengths $B > 5 \cdot 10^8 G$. This has to be
taken into account when extending the basic formulation
of PPS theory in the presence of a strong magnetic field.
Since we are not aware of whether such a strong field
calculation exists, we have used the non-magnetic shift
formula itself as a first approximation. However, we
have consistently included the magnetic field effect on the
energy levels, by employing the magnetic field modified
eigenvalues for a given field strength. When PPS is at all
important, the linear and/or quadratic Stark effects are com-
paritively much weaker and vice versa. The asymmetry of the
resonance and subordinate lines of He II for example, are
caused mainly by PPS in a dense plasma. Hence we discuss
further, the impact of PPS on the line shift of He II lines
in a strongly magnetized plasma.

In a strong magnetic field, a large number of Zeeman
sub-components are produced (Kemic,1974) in any line. We
have selected one such subcomponent, $3d_2 - 2p_1$ which is a

very strong transition. In Figure 3a, we have shown

the wavelength displacement $\Delta\lambda$ produced by PPS and

measured with respect to the steady state wavelength

position of this transition at a given field strength.

The displacements are quite large in a low temperature

plasma, because the thermal velocity of the electrons

is smaller, leading to a larger value of time averaged

perturber charge density at the radiating ion. The dis-

placements for a transition, $2P_1 - 1S_0$ are shown in

Figure 3b. The PPS displacements curve for $\lambda = 298.26 \overset{o}{A}$,

the wavelength position corresponding to $B = 10^8$ G is

not shown, since it is unresolvable, in the adopted scale,

from the curve corresponding to $\lambda = 302.3 \overset{o}{A}$. The dis-

placements are very small because (i) they vary as the

fourth power of the principal quantum numbers of the

levels involved and (ii) they are directly proportional

to the wavelength of the transition, both of which are

smaller presently. The displacements of this resonance

transition in a non-magnetic plasma is also shown (dashed

line). In general, the displacements depend on the difference

in shifts between the upper and lower levels and are

directly proportional to the electron density N_e. While

using the PPS formulae given above, in a strongly mag-

netized plasma, it is safer to verify that the classical

straight line path approximation is satisfied. This appro-
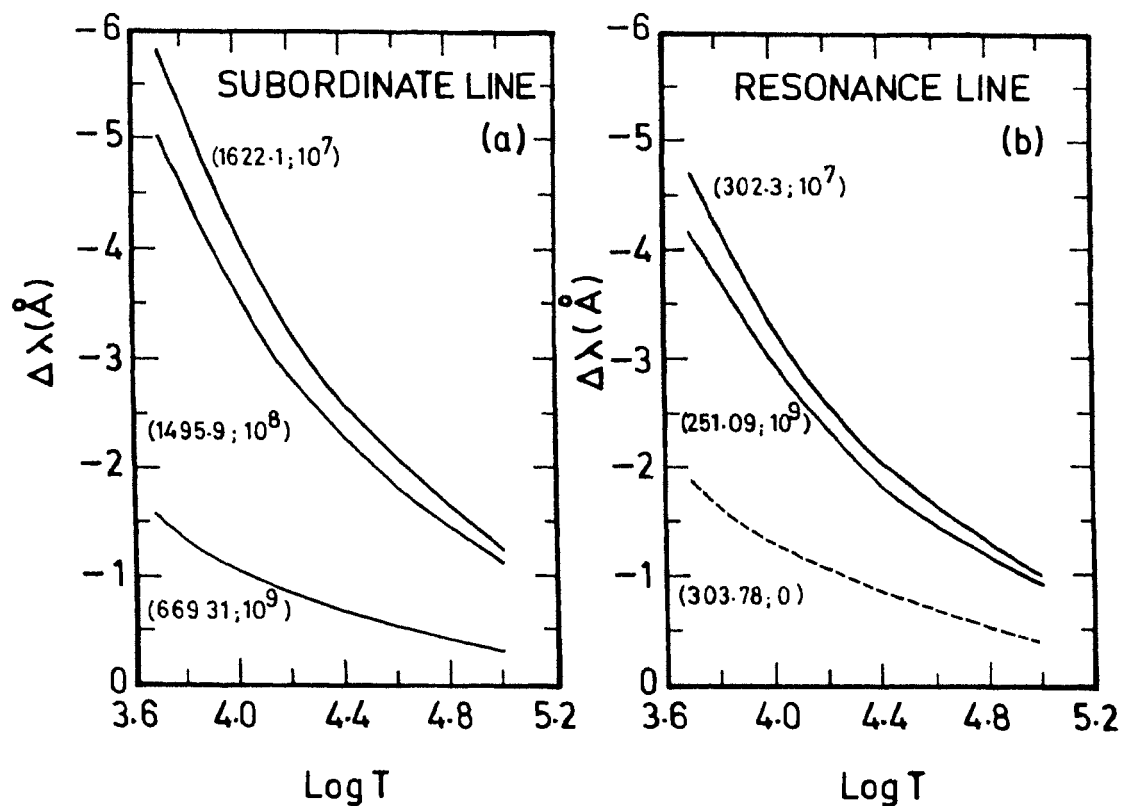
Fig.3 (a) The temperature dependence of PPS wavelength
displacements of a subordinate line Zeeman sub-compo-
nent of He II, in strong magnetic fields. The first
of the numbers in the paranthesis represents the wave-
length of the transition, corresponding to the field
strength given as second number. $N_e = 10^{18} cm^{-3}$ (b) Same
as (a), but for a strong Zeeman component of the re-
sonance line. $N_e = 10^{20} cm^{-3}$.

ximation means that $\Upsilon_{G} = \frac{m_e c}{eB} \sqrt{2kT/M} \gg \Upsilon_n = n^2 a_o/z$ namely the gyroradius is larger than the radii of the Bohr orbitals of the levels involved in the transition. It is not a stringent criterion because, the time averaged negative polarization charge overlapping the bound electron radius is actually more important than the details of the electron paths.

Now we shall compute a practically important line (He II 4685.7 $\overset{o}{A}$) which is used sometimes in the spectral line analysis as a gravity indicator. In view of this application, we have employed a realistic model atmosphere of a DB white dwarf with T_{eff} = 25,000 K and log g =9, given by Wickramasinghe (1972). The normal Zeeman pattern of this line is computed for a field strength B = 2 MG. The transfer equation and the absorption matrix elements required for the calculation, including the line plus continuum magneto-optical effects and the continuum polarization are given in Nagendra and Peraiah (1984, 1985b) and described in sections 4.1 and 2.2. We use the same notation here and mention only the changes to be made to include the PPS in the computation of a realistic line profile of He II 4685.7 $\overset{o}{A}$. Once again, as in previous section, all the physical parameters are depth dependent. The line absorption coefficients for example are now calculated using

$$\eta_i^L = \eta_o \, H(a, \upsilon - \upsilon_i) \, , \qquad i = p, l, \gamma \cdot , \tag{5-31}$$

where

$$\upsilon = \Delta\lambda / \Delta\lambda_D \quad \text{and} \quad \upsilon_i = (\Delta M \cdot \Delta\lambda_B + \Delta\lambda_{nn'}) / \Delta\lambda_D \, , \tag{5-32}$$

and $\Delta M = 0, \pm 1$ for $i = p, l, \gamma$ respectively. The wavelength shift due to PPS is given by the equation (5-29). The Zeeman shift is $\Delta\lambda_B = e B \lambda_o^2 / 4\pi m c^2$. The parameter η_o is calculated using

$$\eta_o = \frac{\pi e^2}{m_e c} \frac{N f}{\rho k^c} \frac{1}{\Delta\vartheta_D} \, . \tag{5-33}$$

The damping constant, $a = \Gamma / 4\pi \Delta\vartheta_D$, Γ being the total damping width of the line. ρ is the mass density, f is the oscillator strength of the line and N the number density of the lower level of the transition. The results of calculation are shown in Figure 4. We have computed the realistic normal Zeeman profiles of He II 4685.7 Å line adopting the model atmosphere of a helium-rich DB white dwarf (T_{eff} = 25,000 K, log g = 9) given by Wickramasinghe (1972). The model atmosphere is truncated in the electron density range ($N_e \simeq 10^{17}$ to 10^{18} cm^{-3}) to take care of validity of the simple model of PPS used in
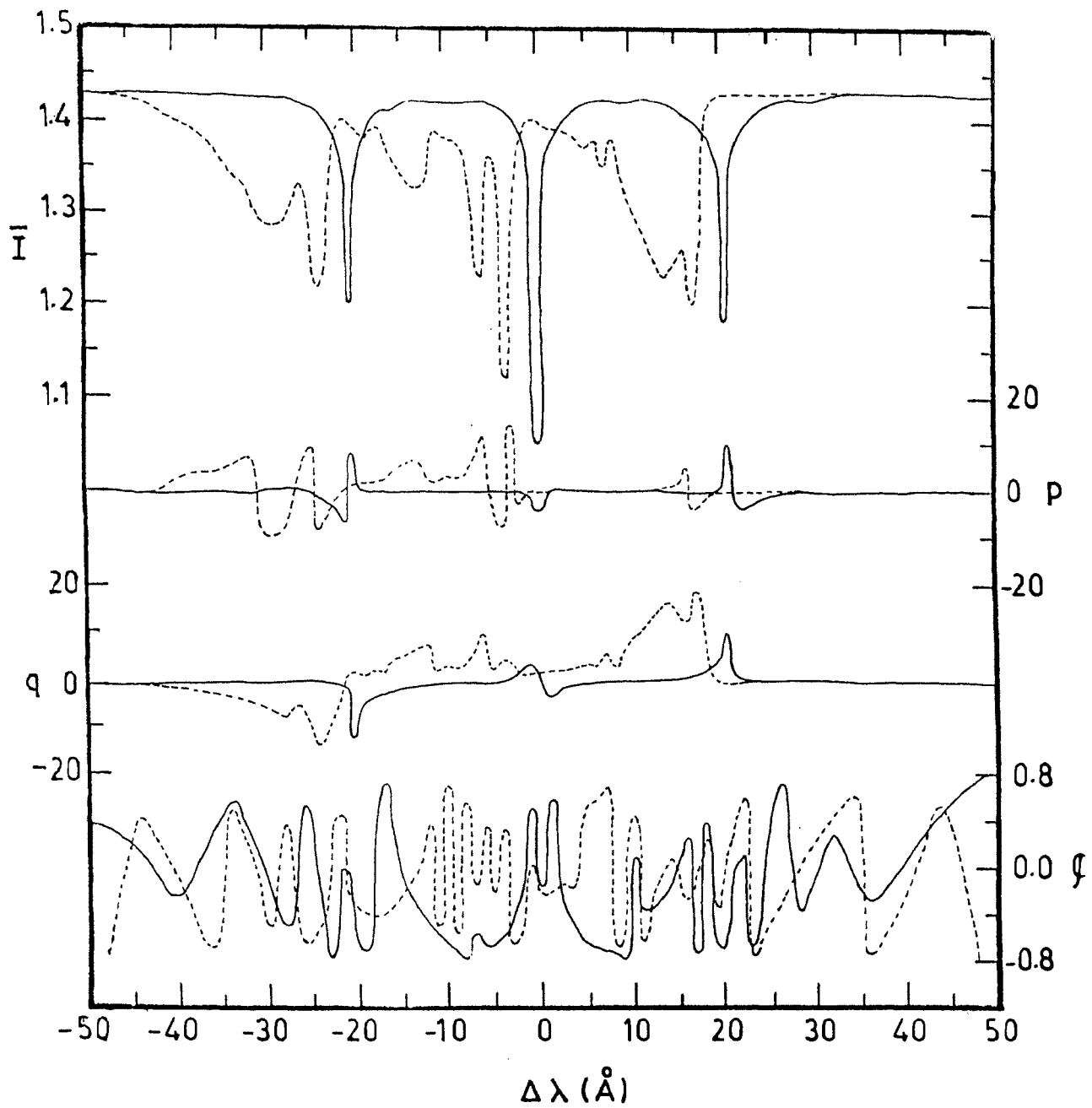
Fig.4 Impact of PPS on Zeeman line triplet of He II 4685.7
Å line. The dashed curves correspond to the case when the
PPS mechanism is included in the profile calculation.

our computations. This however, provides the optical
depth range sufficient to integrate the transfer equa-
tion accurately. The full lines correspond to the case
of normal Zeeman effect in the line, and without including
PPS. The Zeeman components are well separated since the
field strength is large, but they are narrow since the
damping constant a is quite small. The Stokes profiles
are already asymmetric because of the continuum polariza-
tion and the continuum magneto-optical effect, the later
being quite strong-in deepening the line profile and de-
polarizing it. The p and q profiles have some difference
in shape at the π and σ positions, as compared to the
Stokes profiles formed in constant opacity atmosphere
(see e.g.Figure 7). The position angle φ in particular,
is highly scrambled and less useful as a diagnostic. All
these changes occur mainly because of the depth dependence
here, of even the Doppler width and the damping constant,
which are usually kept constant (see for example section
4.3). The dashed lines show the impact of PPS on the
Zeeman intensity and polarization profiles. The profiles
clearly show a blueshift, but the shift is not uniform.
This is because the PPS strongly varies with depth. The
shift in the deepest layers of the atmosphere is nearly
20 times larger than the shift in the outermost layers.
In the deepest layers, the magnitude of PPS in fact appro-

aches the Zeeman splitting itself, for the field strength B = 2MG which we have used. This leads to an extreme overlapping of the π and σ^- -components in these layers. Such an overlapping, coupled with Doppler width variations is responsible for the appearance of additional structure in the shifted components and sharp variations in the p,q and ϕ profiles. The line strength and its polarization are also enhanced in general. Thus, an interpretation based on half width or Zeeman shift measurement becomes difficult if the PPS is not included in the calculation. Though the effect of PPS may have been overestimated here because of its approximate treatment, the qualitative features may not change in a more exact calculation. The impact of any such line shift mechanism, depends also on the degree of Zeeman splitting (strength of the magnetic field). The large asymmetries in the polarized line profiles lead to an increase in the surface averaged continuum polarization near these lines, affecting consequently, the field strength measurements which use the continuum polarization as diagnostic. The increased line blanketing due to PPS, in such high gravity white dwarf atmospheres slightly changes the original atmospheric structure which indirectly influences the spectral lines.

In the strong magnetic field white dwarfs, there
is some difficulty in understanding the differential
weakenings and shifts of the Zeeman subcomponets, be-
cause they are sometimes incompatiable with the theore-
tically calculated wavelength positions and strengths
of Zeeman subcomponents. We feel that the PPS of low
excitation resonance lines of He II in strong magnetic
fields (particularly in high gravity stars) may account
for this discrepancy in line identifications and model
fitting.

5.3 The influence of atomic orientation on Zeeman line transfer in a strong magnetic field

In a strong magnetic field the atomic magnetic
moment is preferentially oriented along the field lines,
which results in unequal populations of the Zeeman substates
of a given atomic level. This effect is important when
the magnetic fields are strong enough to produce full
Paschen-Back effect ($B >> 10^4 G$), but weak enough that
the quadratic Zeeman effect can be neglected. Hence the
high excitation lines formed in cool (T_{eff} = 6000 K)
low field ($B \lesssim 10^7 G$) magnetic white dwarfs are signi-
ficantly affected by this mechanism. Since it directly
affects strengths and depths of Stokes profiles asymmetrically,

the contribution to the broadband (continuum) polarization is quite large, when a disk integration is performed, with a given field distribution on the stellar surface.

In the present calcultions we assume that the line is affected only by normal Zeeman effect. An approximate criterion for neglecting the quadratic Zeeman effect is given as $n^4 \, B_6 << 10^4$, where B_6 is the field strength in units of M_G ($= 10^6 \, G$) and n the upper level principal quantum number. In our study we shall employ a field strength of $0.75 \, B_6$. The theory of atomic orientation is developed in Pavlov (1975) from which we have taken the relevant formulae. The normal wave transfer equations given in section 4.1 (see equations (4-28) to (4-36) are used. But, now we have employed the modified transfer coefficients which include the atomic orientation. They are given by

$$\overline{\eta}_\alpha (\omega) + i \, \overline{\rho}_\alpha (\omega) = \left(\eta_\alpha(\omega) + i \, \rho_\alpha (\omega) \right) \left[1 - \alpha W \right] + \theta \left(\hbar \omega_c / 2kT \right)^2 \qquad (5\text{-}34)$$

where

$$W = \frac{\hbar \omega_c}{8kT} \left[L(L+1) - L'(L'+1) - 2 \right] . \qquad (5\text{-}35)$$

The degree of orientation depends not only on $\left(\hbar \omega_c / 2kT \right)$,

but also on L and L$'$ of the states involved in the trans-
ition. W represents the linear perturbation to the di-
chroic opacities of the non-oriented atoms. Thus the tra-
nsitions involving high angular momentum states in a
low temperature strongly magnetized plasma are affected
by atomic orientation, to a large extent. From the equa-
tion given above it is clear that $\overline{\eta}_\alpha(\omega) + i\overline{\rho}_\alpha(\omega) \simeq \eta_\alpha(\omega) + i\rho_\alpha(\omega)$
when $\alpha = 0$ which represents the π - component of the
Zeeman triplet. Also, the σ -components are unequally
affected, leading to a symmetry breaking of the Stokes
vector profiles about the line centre.

In Figure 5 we have shown the Stokes profiles compu-
ted including this effect. A DA white dwarf model atmos-
phere with T_{eff} = 7000°K, log g = 8, taken from Wehrse
(1976) is employed. The following parameters are used:
$\eta_0 = 10^4$, $a = 0.1$, $\lambda_0 = 5000\overset{\circ}{A}$, $\mu = 1$, $\psi = \pi/4$, $\chi = \pi/4$ and a uni-
form magnetic field of B $=$ 7.5 MG. The continuum is pol-
arized and magneto-optic: $\eta^c_{p,\ell,r} = 1, 0.94, 1.1$ and $\rho^c_R = -10\cos\psi$, $\rho^c_W = -0.25\sin^2\psi$
The magnetic dichroism and anomalous dispersion are com-
puted for both the continuum and the line. The depths
of $\overline{I}$,p and q profiles at $V \simeq$ -400 are slightly smaller
than those at $V \simeq$ +400. The position angle being more
sensitive, undergoes fluctuations and distortion. We have
noticed however, that the polarized continuum in itself
contributes majorly to these type of changes in the
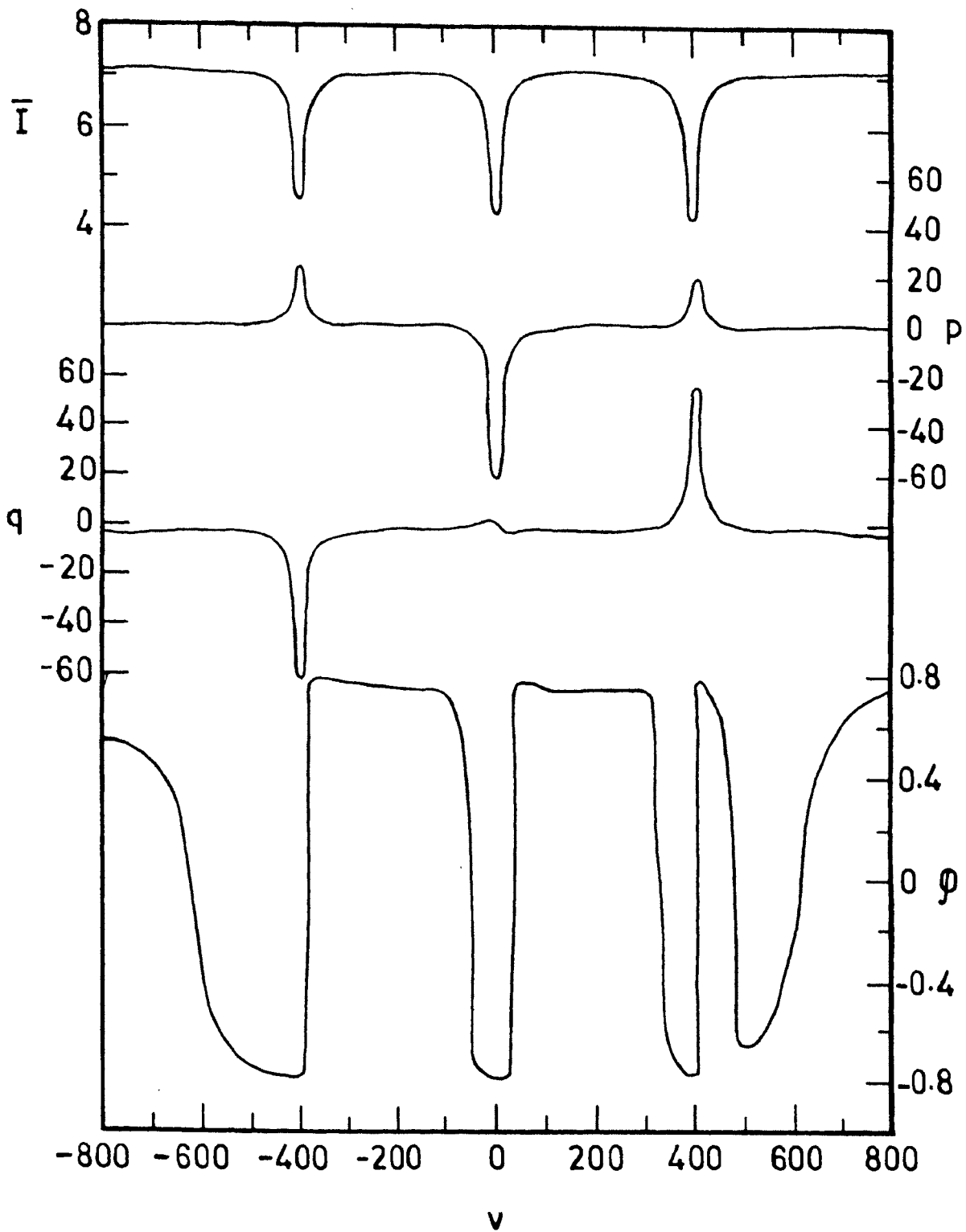
Fig.5. The variation of $\bar{I}$, p, q and the position angle φ in a Zeeman line when atomic orientation is taken into account, in the line transfer problem.

I,p,q and $\emptyset$ profiles. Hence the atomic orientation acts

as an additive perturbation along with the continuum pol-

arization, in distorting the components of Zeeman lines,

but its contribution becomes insignificant compared to

continuum polarization in the case of strong magnetic

fields ($B \gtrsim 10^2 G$). The atomic orientation effect,

for the atmospheric and line parameters we have used at

present, is quite small. Obviously, for high excitation

lines formed in cold magnetized plasma regions excited

radiatively, this effect is more significant and produces

asymmetric Zeeman profiles and contributes to broadband

polarizations.

5.4 The effect of atmospheric structure and the velocity field on the Zeeman line formation in a magnetic field

The line shape and the depth of an absorption line

largely depend on temperature structure and source func-

tion gradient in the atmosphere. In the Figure 6 we have

compared the intensity and polarization profiles formed

in model atmospheres (T_{eff} = 9000 K, log g = 8), of DA

white dwarfs which are in radiative (dashed line) and

convective (solid line) equilibrium. The model atmos-

pheres are taken from Wehrse (1976). We have used a hypo-

thetical Zeeman triplet taking representative parameters

typical of a weak line formed in a low field ($10^5 - 10^6 G$)
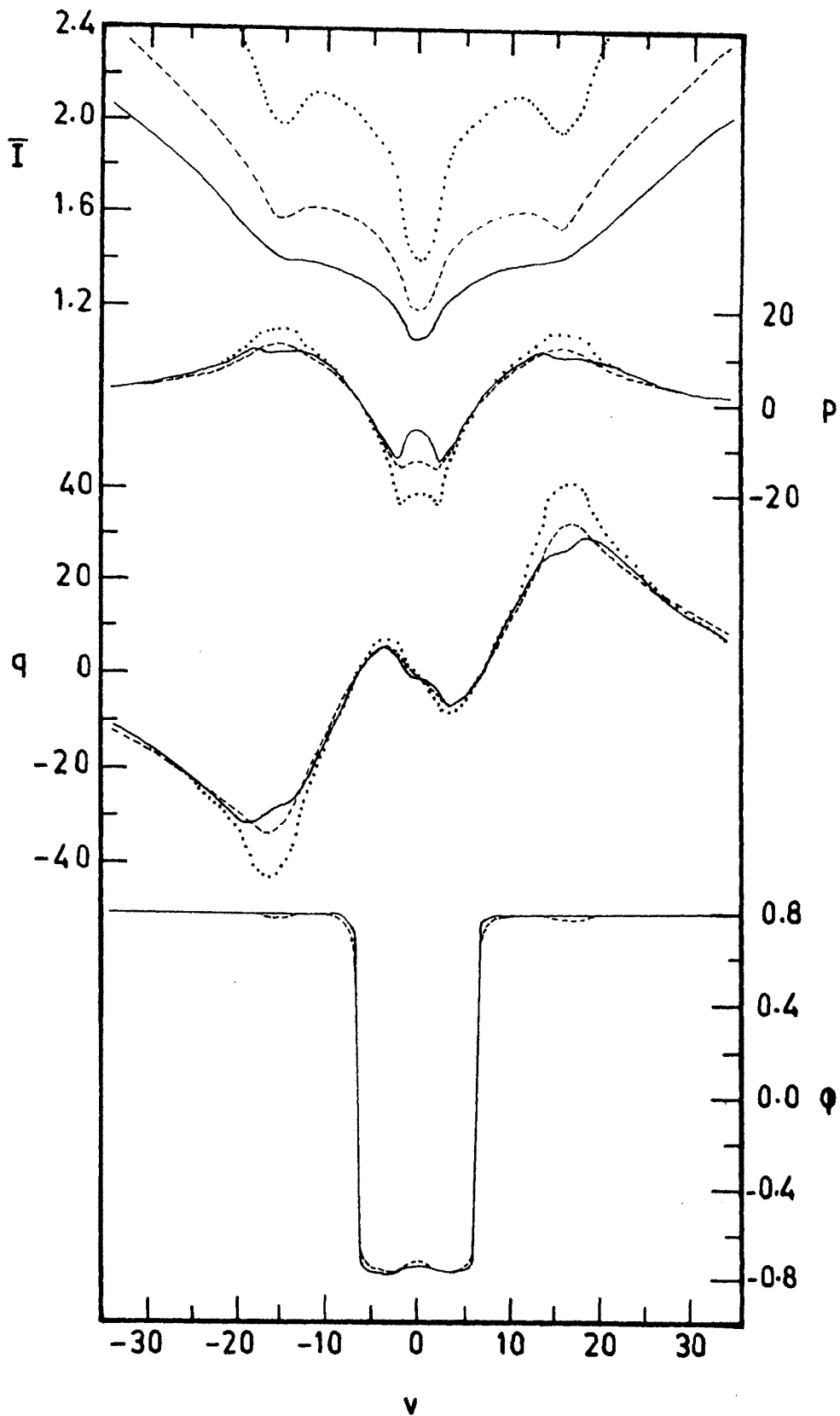
Fig.6.The variation of the Zeeman line pro-
file when different atmospheric structures
are used in the line computations.

magnetic white dwarf. The following parameters are used
in computing this hypothetical triplet: $\eta_o = 10^4$, $a = 0.1$,
$\lambda_o = 5000\,\overset{o}{A}$, $\mu = 1$, $\psi = \pi/4$, $\chi = \frac{\pi}{4}$, $\nu_{b,r} = 0, \pm 16$. The continuum is dichroic
and magneto-optic: $\eta^d_{p,\ell,r} = 1$, 0.94, 1.1 and $f^d_R =$
$-10\cos\psi$, $f^d_w = -0.25 \sin^2\psi$. The relevant equations
are described in section 4.1 (see equations (4-1) to (4-23)).
For simplicity, the transfer matrix $\underline{A}$ is taken as depth
independent; hence the constancy of Doppler width over
the depth does not introduce significant errors. The
temperature distribution is the key factor. It is clearly
seen that the lines formed in a convective model are
deeper, and wider also, than those formed in a radiative
model. In the convective model, slight distrortions are
produced in the Stokes profiles near the centre of the
π and σ -components. In the same figure we have shown
the effect of altering the source function gradient in
the outermost layers of the convective model (dotted line).
Such changes in source function gradients may be caused
for example, by an accretion of matter by the white dwarf.
Since the medium is in LTE we have introduced such a gra-
dient by simply reducing the temperature smoothly by 5%
(at $\tau = 10^{-2}$) to 10% (at $\tau = 0$) respectively. We see
that a deeper π -component is produced in this case, and
the line becomes narrow and developes triplet structure.
Marked changes in linear and circular polarization also
occur at the centres of Zeeman components. It is well

known that a similar effect occurs when one increases
the line blanketing in the model atmospheres. The posi-
tion angle φ almost remains unaffected to such changes.
In Figure 7 we show the line shifting produced by macro-
scopic steady state mass motions in the atmosphere. The
lines in a moving atmosphere can be computed by using

$$\vartheta(\tau) = \vartheta - \cos \alpha(\tau)\, V_m(\tau),$$
(5-36)

where

$$V_m(\tau) = u_m(\tau)\,/\,V_T(\tau) \; ; \quad V_T(\tau) = \sqrt{2\,kT(\tau)/M}$$
(5-37)

instead of ϑ in the calculations. $V_m(\tau)$ is the dimen-
sionless velocity parameter. $\alpha(\tau)$ is the angle between
the velocity vector $u_m(\tau)$ and line of sight. Here
we have used τ -independent velocities with $\alpha(\tau) = 0$
and τ -independent Doppler widths. The dashed lines
indicate the Stokes profiles formed in a radially inward
directed constant macroscopic velocity of 0.4 mtu($\sim 5 km/sec$);
1 mtu (mean thermal unit)= $V_T(\tau)$. The dotted lines
are computed for an outwardly expanding medium with a
velocity of 3 mtu. The Stokes profiles are blue shifted
in this case. The solid lines represent the Stokes pro-
files formed in the static atmosphere. It should be
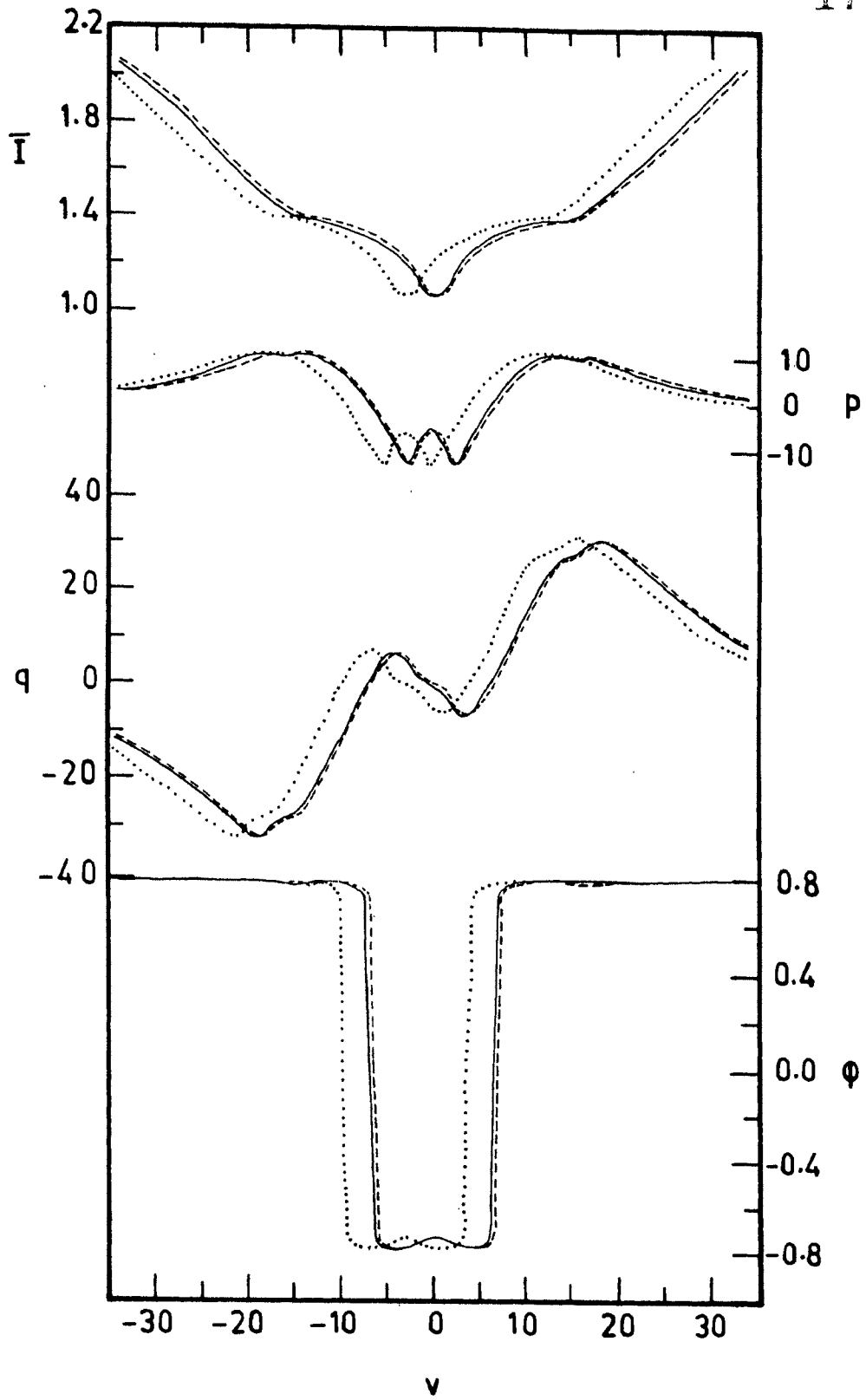
Fig.7 Zeeman line profiles formed in a
convective moving atmosphere with all the
other parameters same as Fig.6.

noticed that the gravitational redshift of spectral
lines which can be computed using

$$\upsilon\,(\tau) \;=\; \upsilon + \frac{c}{V_T}\,\left\{\left(1-\frac{2GM}{Rc^2}\right)^{-\frac{1}{2}} - 1\right\} \;,$$
(5-38)

for a white dwarf of mass M and radius R, actually gives
such a large (3-4 mtu) 'red' shift of the Stokes profiles
(Preston,1970). The gravitational redshift being isotropic
over the stellar surface, leads to a 'residual continuum
polarization' contributed by the Zeeman split lines, when
integrated over the visible disk of the star. Also, a
depth dependent velocity produces the Stokes profiles which
look wiggly, with deeper cores and increased half widths.
We feel that such processes which produce line distrotions
and line shifts in extremely overlapping Zeeman lines,
formed in strong magnetic fields, may contribute signifi-
cantly to the continuum polarization, and non-thermal like
continuum energy distribution, observed in these objects.

Thus a knowledge of the differences in line profiles
produced in different atmospheric models helps in isolating
the suitable model required for further work. We have
shown that small changes in the source function gradients
in the outer layers of the stellar atmosphere can lead
to a decrease in the equivalent width and a large increase
in the line polarization. As already pointed out, the
gravitational redshift has to be included consistently
in the line profile calculations of whit dwarfs.

5.5 <u>The ray refraction effects on the transfer of long</u>

   <u>wavelength polarized radiation</u>

The x-ray emission observed in some hot white dwarfs
indicates the presence of hot and dense plasma emitting
regions near these objects. The examples are Hz 43 and
AM Her etc. A similar situation is encountered in accre-
ting columns of weak field magnetic white dwarfs and
neutron stars in binaries. Zheleznyakov (1983) has pointed
out that a detailed anlysis of the spectra and polari-
zation of these objects in the infrared and radiowave
regions of the spectrum is needed in order to understand
the accretion mechanisms. In this section we have dis-
cussed the radiative transfer of far infra-red $(\gamma \sim 10^{12} Hz)$
'continuum radiation' as well as a frequency near the
cyclotron resonance occuring in the same spectral range.
The refraction effects are included in the calculations.
Such far infra-red observations are made for an AM Her
star by Liebert and Stockman '1983). The refractive effects
are also important in the calculation of solar radio emission.
Thus, whenever the plasma is anisotropic and the refractive
indices of normal waves differ significantly from unity,
the ray refraction effects become important.

In this section we again use cold plasma normal wave
transfer equations (see section II.1) but in a modified

form. The normal waves (polarization ellipses) remain almost orthogonal away from the cyclotron hormonics and the spectral line centres. The relevant transfer equation for the problem is (see Zheleznyakov,1970)

$$\mu \frac{du_j}{d\tau} = \frac{k_j}{k^c} \left[u_j - \frac{B_j}{2} \right] ,$$

(5-39)

where u_j are the modified specific intensities given by

$$u_j = I_j \, |\cos\alpha_j| \, / \, n_j^2 , \qquad j = 1, 2 \cdot ,$$

(5-40)

where α_j, $j = 1, 2$ is the angle between the group velocity vector $\underline{V}_g$ (direction of the energy flow in a loss free media) and the wave vector of the jth wave. n_j are the real refractive indices, and I_j are the usual normal wave specific intensities. Clearly, u_j are also (like I_j the invariants of propagation in an anisotropic refracting medium. The equation (5-39) holds only within the framework of the approximation of geometrical optics, where the ray treatment is possible. The normal wave transfer equation can be used in the place of full density transfer equation only when $\omega \, |n_1 - n_2|/c \gg (k_1 + k_2)/2$ which means that the relative phase shift between the normal waves caused as a result of propagation through unit optical depth is a large number. A simpler criterion,

which is satisfied in most of the astrophysical LTE plasmas is that $\omega \gg \gamma_{eff}$, where γ_{eff} is an effective collision frequency. This condition ensures that the normal waves are nearly orthogonal, similar and propagate independently (also see section II.1). The 'cold plasma' transfer coefficients are appliable as long as $|\omega - \delta\omega_c|$ $\gg \omega|\xi|\sqrt{2kT/m_e c^2}$, $\xi = \cos\psi$, $\delta = 1, 2, \cdots$ being the cyclotron harmonic number, is satisfied. In the case of frequencies away from the cyclotron harmonics, we use simple analytic expressions given by Zheleznyakov (1970) and Stix (1962) for the following transfer coefficients.

$$[n_j^2]_{QL} = 1 - \frac{\vartheta}{1 \mp \sqrt{u}|\xi|} \quad ; \quad [\chi_j]_{QL} = \frac{\vartheta \, \gamma_{eff}}{2\,\omega n_j \,(1 \mp \sqrt{u}\,|\xi|)^2} \quad , \qquad (5\text{-}41)$$

$$[\tan\alpha_j]_{QL} = \frac{\vartheta\sqrt{u}\,(1 - \xi^2)}{2\,[n_j^2]_{QL}\,(1 \mp \sqrt{u}\,|\xi|)^2} \quad , \qquad (5\text{-}42)$$

where QL = quasilongitudinal propagation. n_j and χ_j are the real and imaginary parts respectively, of the complex refractive indices of the normal waves. We also use

$$[n_1^2]_{QT} = 1 - \frac{\vartheta\,(1-\vartheta)}{[1-\vartheta-u\,(1-\xi^2)]} \quad ; \quad [n_2^2]_{QT} = \frac{1-\vartheta}{(1-\vartheta\,\xi^2)} \quad , \qquad (5\text{-}43)$$

$$[\chi_1]_{QT} = \frac{\vartheta\,\gamma_{eff}[(1-\vartheta)^2 + u\,(1-\xi^2)]}{2\,\omega[n_1]_{QT}\,[1-\vartheta-u\,(1-\xi^2)]^2} \quad ; \quad [\chi_2]_{QT} = \frac{\vartheta\,\gamma_{eff}}{2\,\omega\,[n_2]_{QT}} \quad , \qquad (5\text{-}44)$$

$$\left[\tan \alpha_1\right]_{QT} = \frac{u \, v \, (1-v) \, \sin 2\psi}{2 \, [n_1^2]_{QT} \, [1-v-u(1-\xi^2)]^2} \quad , \tag{5-45}$$

$$\left[\tan \alpha_2\right]_{QT} = \frac{v \, (1-v) \, \sin 2\psi}{2[n_2^2]_{QT} \, [1-v\xi^2]^2} \quad , \tag{5-46}$$

where QT = quasitransverse propagation, and

$$v = \frac{\omega_p^2}{\omega^2} \; , \quad u = \frac{\omega_c^2}{\omega^2} \; , \quad \omega_p^2 = \frac{4\pi N_e e^2}{m_e} \; , \quad \omega_c = \frac{eB}{m_e c} \; , \quad \xi = \cos \psi \; . \tag{5-47}$$

The quasilongitudinal propagation means that

$$\left[\omega_c (1-\xi^2)\right]^2 \ll \left[2\omega(1-v)\xi\right]^2 ; \quad \omega_c^2 (1-\xi^2) \ll |2\omega^2(1-v)| \; , \tag{5-48}$$

with the additional criterion for the cold plasma

$$\left[\omega(1-\sqrt{u}\,|\xi|)\right]^2 \gg v_{eff}^2 \; . \tag{5-49}$$

The quasitransverse propagation means that

$$\left[\omega_c (1-\xi^2)\right]^2 \gg \left[2\omega(1-v)\xi\right]^2 \; , \tag{5-50}$$

with the corresponding requirement for the cold plasma

$$\left[\omega\left(1-\sqrt{u(1-\xi^2)}\right)\right]^2 \gg v_{eff}^2 \; . \tag{5-51}$$

The approximations mentioned above are used to obtain simplified formulae (equations (5-41) to (5-47) from a general expression for the complex refractive index (see Zheleznyakov,1970 and Ginzburg,1964). Generally small values of ψ lead to quasilongitudinal, and large values of ψ lead to quasitransverse propagations. The effective electron ion collision frequency is given approximately, for a fully ionized plasma as

$$\nu_{eff} \approx \frac{5 \cdot 5\, N_e}{T^{3/2}}\, Ln\left[220\, T / N_e^{1/3}\right] \text{ for } T < 3 \; 10^5 \; K \; , \tag{5-52}$$

$$\nu_{eff} \approx \frac{5 \cdot 5\, N_e}{T^{3/2}}\, Ln\left[10^4\, T^{2/3} / N_e^{1/3}\right] \text{ for } T > 3 \; 10^5 \; K \; , \tag{5-53}$$

where N_e is the electron number density and T the kinetic temperature of the plasma. For a sufficiently hot medium in which the free-free absorption is the dominant mechanism, one can calculate the absorption coefficient in a simple way as

$$k_j \simeq \frac{2\omega}{c}\, \chi_j \; \cos \alpha_j \tag{5-54}$$

Near the cyclotron resonance, the absorption coefficients and the refractive indices of extraordinary and ordinary waves differ from each other by large amounts. Hence we can expect the ray refraction effect on the polarization to be stronger in this region. The cyclotron absorption

coefficients for the normal waves $(j = 1,2)$ are calculated using

$$k_1^{cyc} = \sqrt{\frac{\pi}{8}} \frac{\omega_p^2}{c\omega} \beta_T^{-1} \frac{1+\xi^2}{|\xi|} \exp\left(-\bar{Z}_1^2\right) \frac{\cos\alpha_1}{n_1^2} \quad , \tag{5-55}$$

$$k_2^{cyc} = \frac{1}{\sqrt{2\pi}} \frac{\omega_p^2}{c\omega} \beta_T^{-1} \frac{[(1-\xi^2)(2\xi^2+1)]^2}{|W|^2 |\xi| (1+\xi^2)^3} \exp\left(-\bar{Z}_2^2\right) \frac{\cos\alpha_2}{n_2^2} \quad , \tag{5-56}$$

where

$$\bar{Z}_j = \frac{\omega - \omega_c}{\sqrt{2}\, \beta_T \omega |\xi| n_j} \quad , \quad \beta_T = \sqrt{\frac{kT}{m_e c^2}} \quad , \quad \omega_c = \frac{eB}{m_e c} \quad , \tag{5-57}$$

and, the squared modulus of the probability integral is given by

$$|W|^2 = \left[\exp\left(-\bar{Z}_2^2\right)\right]^2 \left[1 + \frac{2}{\sqrt{\pi}} \int_0^{\bar{Z}_2} \exp(x^2)\, dx\right] \cdot \tag{5-58}$$

The refractive indices are calculated using (Zheleznyakov, 1980)

$$n_1 = 1 - \frac{1}{\sqrt{8}} \frac{\omega_p^2}{\omega^2} \beta_T^{-1} \frac{1+\xi^2}{|\xi|} \exp\left[-\bar{Z}_1^2 n_1^2\right] \int_0^{\bar{Z}_1 n_1} \exp(x^2)\, dx \quad , \tag{5-59}$$

$$n_2 = 1 - \frac{\omega_p^2}{\omega^2(1+\xi^2)} \cdot \tag{5-60}$$

The angles α_j are computed now, from the exact relation (Stiz, 1962)

$$\tan \alpha_j = \frac{-1}{n_j} \frac{\partial n_j}{\partial \psi} \quad , \tag{5-61}$$

since the approximations mentioned earlier are not applicable near the cyclotron resonance. The Faraday rotation of the polarization ellipse with respect to a fixed axis, in the plane, transverse to the propagation direction is given by

$$\gamma = \frac{1}{\omega^2 c} \int_L \frac{\omega_p^2 \omega_c \xi}{(n_1 + n_2)} d\ell \quad \text{radians} \; , \tag{5-62}$$

where L is the total geometrical thickness of the plasma slab.

From the table 1, it is seen that the linear (p) and circular (q) polarizations and the Faraday rotation (γ) in radians are underestimated if we neglect the ray refraction effects (by taking $n_j \cong 1$ and $\cos \alpha_j \cong 1, j=1,2$) The effect is particularly stronger for transverse propagation of the electromagnetic wave, than the longitudinal propagation, with respect to the magnetic field direction. It also tends to be stronger in a uniform magnetic field than in the non-uniform case. For calculating these results, we have used the following plasma parametrs: $T = 10^6 K$, $N_e = 1.65 \cdot 10^{14} cm^{-3}$, $\omega = 6.283 \, 10^{12} Hz$ and $\mu = 0.8$ $\psi = 10^o$ (for QL) and $\psi = 72^o$ (for QT) propagations.

	Uniform field		Non-uniform field	
$p_{QL}\%$	1.31E-4	1.09E-4	6.66E-5	5.56E-5
$q_{QL}\%$	-3.05E-1	-2.54E-1	-2.20E-1	-1.84E-1
γ_{QL}	2.33E+4	2.31E+4	1.65E+4	1.64E+4
$p_{QT}\%$	3.25E-3	8.50E-4	2.21E-3	5.32E-4
$q_{QT}\%$	-7.93E-2	-2.07E-2	-7.66E-2	-1.84E-2
γ_{QT}	7.31E+3	7.26E+3	5.17E+3	5.14E+3

Table 1. The difference between the solutions where the refractive effects are included (first column) and neglected (second column) for a uniform magnetic field $B = 10^4 G$. The last two columns show a similar comparison for a field varying as

$$B(r) = \frac{B_*}{\sqrt{2}}\left(\frac{R_*}{R_* + r}\right)^3, B_* = 10^4 G \text{ being the field}$$

ne surface ($r = 0$) of a star of radius R_* .

	Uniform field	
p%	1.70E-2	1.16E-2
q%	-1.65E+0	-1.13E+0
γ	7.65E+5	8.02E+5

Table 2. Same as table 1, but for cyclotron absorption of radiation in a uniform field $B = 3.3$ $10^5 G$ for an angle of propagation $\psi = 10^\bullet$ (quasi-longitudinal: QL). It can be noticed that the error committed in neglecting the refractive effects is now enhanced because of the transfer of radiation in optically thick medium.

Total height of the slab is 6 KM. The parameters are
representative of a dense thin corona around a white
dwarf. From the table 2 it is seen that for frequen-
cies near the cyclotron resonance ω_c the linear and
circular polarization show stronger, but qualitatively
similar behaviour as for the thermal radiation away from
the resonance (Table 1). But, the Faraday rotation de-
creases when the refractive effects are included (first
column of Table 2) because, near the resonance, η_j in
particular increase in magnitude unlike the behaviour at
a frequency far away from the resonance, where they de-
crease slightly from the values $\eta_j \simeq 1$, in the cold plasma
theory. Thus we see that in the solution of normal wave
transfer equtions, particularly for the long wavelength
radiations and near the resonances, the ray refraction
effects make significant changes in the polarization over
the conventional solutions obtained by neglecting these
effects.

The contribution of ray refraction effects to con-
tinuum polarization of low frequency radiation propagating
in a magnetoplasma is found to be significant at least
near the cyclotron resonances. Near these resonances, the
Faraday depolarization is also effectively decreased. This
later aspect may prove useful in the correct calculation
of internal Faraday rotation in transparent synchrotron
radio sources.

THE SOLUTION OF THE EQUATION OF TRANSFER FOR LINES

IN ANISOTROPIC ABSORBING-SCATTERING MEDIA IN-

CLUDING FREQUENCY REDISTRIBUTION

In this chapter we shall attempt to solve the non-
LTE (non-local thermodynamic equilibrium) equations for
the transfer of polarized radiation in spectral lines.
Our present interest is only the case of zero magnetic
field. Also, we shall use the transfer equation written
for the set of Stokes parameters I_l and I_r , thereby
restricting ourselves to the azimuthally symmetric part
of the radiation field. An extension of these restricted
Stokes vector (I_l I_r $)^T$ equation to the full Stokes
vector $(I_l\ I_r\ U\ V)^T$ equation and the inclusion of magnetic
field, naturally leads us to the transfer equation for
the well known "Hanle effect". Further, the inclusion of
frequency redistribution during the scattering process
increases the complexity of these two problems by a large
amount. Hence only few attempts have been made in solving
both of these problems in their full generality.

In the absence of magnetic fields a spectral line
may be polarized if coherent scattering plays a role in
the line formation. The coherency is caused by the in-
terference between the overlapping magnetic sublevels of
the scattering atom. This "level-crossing interference"

is modified by a magnetic field due to the change in the
degree of overlapping of the Zeeman sublevels. In the stro-
ng-field case, when the Zeeman components are well seapa-
rated, the interference effects disappear (the normal Zeeman
effect). The Zeeman effect gives rise to line polarization
in the presence of a magnetic field, regardless of whether
scattering occurs or not. The class of polarization pheno-
mena due to interference between the Zeeman sublevels in
'coherent scattering' in a magnetic field is known as the
Hanle effect. This type of polarization generally does not
disappear when the magnetic field vanishes. Collisions may
distroy the phase relations between the sublevels and make
the scattering incoherent. The interference effects then
disappear.

Polarization in coherently scattered light was dis-
covered by Rayleigh (1922). Further laboratory experi-
ments by Hanle (1924) showed how this polarization depends
on the magnetic field. The basic physical understanding
of these effects was developed by Briet (1925), Dirac (1927),
Weisskopf (1931) and Hamilton (1947) to mention only few
important references. Zanstra (1941) developed a theory to
calculate resonance line polarization in the solar atmosphere.
Chandrasekhar (1950) introduced the Stokes parameter re-
presentation of polarized light in the equation of radia-
tive transfer. This made it possible to attack much more
general problems of the transport of polarized radiation
in scattering and absorbing media. Since that time the
theory of resonance line polarization has been discussed

and developed further by a number of authors (Voigt,1951;
Warwick and Hyder, 1965; Obridko 1968; Lamb,1970;
House,1971; Stenflo,1971; Omont et al,1973; Dumont et
al.,1973; Sidlichovsky (1974). Treatments in terms of
quantum electrodynamics are found in Lamb (1970), House
(1971), Omont et.al (1973), Sidlichovsky (1974),.
Bommier and Sahal-Brechot (1978) and Landi Degl'Inno-
centi (1983). The most complete and diverse studies
in the theory and observations of resonance line pola-
rization and the Hanle effect has been conducted by
Stenflo and his collaborators (see Stenflo,1976; Stenflo
and Stenholm, 1976; Stenflo,1978; Stenflo,Baur and Elmore,
1980; Stenflo,1980; Auer,Rees and Stenflo,1980). They
have written the transfer equation in a form analogous
to the formalism normally used for the well explored
non-LTE line formation in a two level atom. This has
helped in linking these two areas of the line formation
theory. Rees and Saliba (1982), have extended this
formalism to a slightly more complicated problem of reson-
ance line polarization with partial frequency redistri-
bution, and used them in a study of Ca II K resonance line
polarization (Rees and Saliba 1983). Detailed studies on
similar lines have been carried out recently by McKenna
(1984) and the references therein). All these authors
have used the plane parallel approximation. The obser-
vations made by Brukner (1963), Stenflo (1974,1980) and

Wiehr (1975,1981) on the linear polarization in re-
sonance lines of Ca, Na and Mg have been quite success-
fully explained by these theoretical calculations. But
still, the basic theoretical approach itself needs to
be improved, since some simplifying approximations were
made in all the earlier calculations. By far the most
general solutions have been obtained by Rees and Saliba
(1982) who have compared the solutions obtained for
coherent scattering, complete redistribution and partial
redistribution (represented by $R_{\text{II}A}$) scattering mechanisms
in the line.

In this chapter we shall first describe the theory
of resonance line polarization in the form which we have
used (see Dumont et al.,1977; Rees and Saliba,1982) and
which also happens to be a most suitable form for the
parameteric study which helps develop an insight into the
physics of line formation (see Mihalas,1978). We then
describe the useful limiting forms of the general equation
and compare the solutions obtained by our method with the
solutions obtained by Rees and Saliba (1982) in these
limiting forms, by taking few test problems. We then
describe our method of solution in some detail. Finally
we present a comparison of the solutions obtained for
plane parallel and spherically symmetric media through
sample cases.

6.1 The theory of non-LTE resonance line polarization with frequency redistribution for a two-level atom

We now describe the relevant equations. The following notation is used throughout this chapter: CS= coherent scattering; CRD = complete redistribution; and PRD = partial redistribution.

Consider an atmosphere which is isotropically illuminated only at the lower boundary ($\tau = \tau_{max}$) and has isotropic distribution of scattering particles. Then the radiation field is azimuthally symmetric about the normal Z to the surface and can be described completely by two Stokes parameters, I_l and I_r as already mentioned in section 3.1. We shall use the two-level atom approach. The model atmosphres now used are finite isothermal slabs or spherical shells with (or without) a given thermal source distribution. For clarity of discussion, we shall, at present, neglect the depolarization and frequency redistribution by collisions. Our main interest is to show that accurate solutions can be obtained from the discrete space methods of solving the line transfer equation even with a modest number frequency points used for the frequency integral in the source function.

We adopt a simple vector analogue of standard non-LTE theory for a two level atom with an unpolarized background continuum. For the sake of generality, we shall write down the equations for a spherically symmetric medium.

The equation of line transfer in divergence form in spherical symmetry is given by

$$\frac{\mu}{\gamma^2} \frac{\partial}{\partial \gamma} \left\{ \gamma^2 \underline{I}(x,\mu,\gamma) \right\} + \frac{1}{\gamma} \frac{\partial}{\partial \mu} \left\{ (1-\mu^2) \underline{I}(x,\mu,\gamma) \right\} =$$

$$k_L \left[\beta + \varphi(x,\mu,\gamma) \right] \left[\underline{S}'(x,\mu,\gamma) - \underline{I}(x,\mu,\gamma) \right] \tag{6-1}$$

where $\underline{I}(x,\mu,\gamma) = [I_\ell(x,\mu,\gamma) \quad I_\gamma(x,\mu,\gamma)]^T$ is the Stokes vector specific intensity at an angle $\Theta = \cos^{-1}\mu \ (\mu \in [0,1])$ to the symmetry axis (radius) at the radial point γ in the atmosphere, and the frequency point $x = \dfrac{\gamma - \gamma_0}{\Delta \gamma_D}$ in the line. γ is the frequency of the radiation, γ_0 is the line centre frequency, and $\Delta \gamma_D$ is the Doppler width which is assumed to remain constant throughout the atmosphere. $\underline{S}'(x,\mu,\gamma)$ is the source vector. If $A(\gamma) = 4\pi\gamma^2$ is the area of the spherical shell of radius γ then writing

$$\left. \begin{aligned} \underline{u}(x,\mu,\gamma) &= A(\gamma)\,\underline{I}(x,\mu,\gamma) \\ \underline{S}(x,\mu,\gamma) &= A(\gamma)\,\underline{S}'(x,\mu,\gamma) \end{aligned} \right\}, \tag{6-2}$$

where $b(\gamma) = \dfrac{B_\gamma(\gamma)}{2}$, $B_\gamma(\gamma)$ being the local Planck function, we can write the equation (6-1) as

$$\mu \frac{\partial}{\partial \gamma} \underline{u}(x,\mu,\gamma) + \frac{1}{\gamma} \frac{\partial}{\partial \mu} \left[(1-\mu^2)\,\underline{u}(x,\mu,\gamma) \right] =$$

$$k^L \left[\beta + \varphi(x,\mu,\gamma) \right] \left[\underline{S}(x,\mu,\gamma) - \underline{u}(x,\mu,\gamma) \right], \tag{6-3}$$

for $\mu > 0$ and, for the oppositely directed beam $(\mu < 0)$ as

$$-\mu \frac{\partial}{\partial \gamma} \underline{u}(x, -\mu, \gamma) - \frac{1}{\gamma} \frac{\partial}{\partial \mu}\left[(1-\mu^2)\, \underline{u}(x, -\mu, \gamma)\right] =$$

$$k^L\left[\beta + \varphi(x, -\mu, \gamma)\right]\left[\underline{S}(x, -\mu, \gamma) - \underline{u}(x, -\mu, \gamma)\right]. \qquad (6\text{-}1)$$

The quantity β is the ratio of unpolarized continuous absorption coefficient per unit interval of x to that in the line (= integrated line opacity). The normalized line absorption profile is represented by a Voight function, written in the usual notation as

$$\varphi(x, \mu, \gamma) = \frac{H(a, x, \mu, \gamma)}{\sqrt{\pi}}; \quad \frac{1}{2}\int_{-1}^{+1}\int_{-\infty}^{+\infty}\varphi(x, \mu, \gamma)\, dx\, d\mu = 1 \qquad (6\text{-}5)$$

with constant damping to Doppler width ratio a. The source vector is given by

$$\underline{S}(x, \mu, \gamma) = \frac{\varphi(x, \mu, \gamma)\, \underline{S}^L(x, \mu, \gamma) + \beta\, \underline{S}^c(\gamma)}{\left(\beta + \varphi(x, \mu, \gamma)\right)}, \qquad (6\text{-}6)$$

where $\underline{S}^c(\gamma) = \rho(\gamma) \cdot B(\gamma)\underline{h}$; $\underline{h} = [1, 1]^T$ is the unpolarized continuum source vector. $\rho(\gamma)$ is a parameter proportional to the temperature gradient in the medium. The mean optical depth at frequency γ_0 is defined as

$$d\tau = k^L d\gamma = \frac{h\gamma_0}{4\pi\Delta\gamma_D}(N_1 B_{12} - N_2 B_{21})\, d\gamma. \qquad (6\text{-}7)$$

where B_{12} and B_{21} are the Einstein coefficients and N_1 and N_2 are the population densities of lower and upper levels respectively in a two level atom. The line source vector for a two level atom is given by

$$\underset{\sim}{S}^{L}(x,\mu,\gamma) = \begin{bmatrix} S^{L}_{\perp}(x,\mu,\gamma) \\ S^{L}_{\gamma}(x,\mu,\gamma) \end{bmatrix}$$

$$= \frac{(1-\epsilon)}{\phi(x,\mu,\gamma)} \int_{-\infty}^{+\infty}dx' \int_{-1}^{+1} \underset{\sim}{R}(x,\mu,x',\mu',\gamma)\ \underset{\sim}{u}(x',\mu',\gamma)\,d\mu' + \epsilon\,B(\gamma)\,\underset{\sim}{h}\ . \tag{6-8}$$

The scattering redistribution matrix R $(x,\mu;x',\mu',\gamma)$ accounts for the correlation in frequency, angle and polarization between the light absorbed at frequency x' in the direction μ' and emitted at frequency x in direction μ . In order to simplify the numerical solution of the transfer problem, we adopt a prescription for the redistribution matrix, suggested by Rees and Saliba (1982): a hybrid model which retains the angular correlation present in the resonance line scattering polarization via the phase matrix $\underset{\sim}{P}(\mu,\mu')$ and introduces the frequency correlation via the angle averaged scalar redistribution function $R_{IIA}(x,x')$ of Hummer (1962). It is written as

$$\underset{\sim}{R}(x,\mu,x',\mu',\gamma) = \underset{\sim}{P}(\mu,\mu')\ R_{IIA}(x,x')\ , \tag{6-9}$$

where

$$\underset{\sim}{P}(\mu,\mu') = \frac{3}{8}E_{1}\begin{bmatrix} 2(1-\mu^{2})(1-\mu'^{2})+\mu^{2}\mu'^{2} & \mu^{2} \\ \mu'^{2} & 1 \end{bmatrix} + \frac{1}{4}(1-E_{1})\cdot\begin{bmatrix} 1 & 1 \\ 1 & 1 \end{bmatrix}\ , \tag{6-10}$$

is the well-known phase matrix for resonance line
scattering (see Chandrasekhar,1950). The factor $(1-E_1)$
measures the effect of depolarization. It depends in
the j_l and j_u of the transition involved. The formulae
for E_1 are tabulated in Chandrasekhar (1950). They
correspond exactly to the quantity W_{lu} given by Omont
et al.(1972). A maximum polarization occurs for $(j_l=0) \rightarrow$
$(j_u = 1)$ type transitions (e.g. the Ca I 4227 Å resonance
line) where $E_1 = W_{lu} = 1$. In this case $\underline{P}(\mu, \mu')$ reduce
to the Rayleigh scattering phase matrix.

$$R_{II_A}(x, x') = \frac{1}{\pi^{3/2}} \int_{\frac{1}{2}|\bar{x}-\underline{x}|}^{\infty} e^{-u^2} \left[\tan^{-1}\left(\frac{\underline{x}+u}{a}\right) - \tan^{-1}\left(\frac{\bar{x}-u}{a}\right) \right] du , \qquad (6\text{-}11)$$

where

$$\bar{x} = \text{Max}(x, x') \quad \text{and} \quad \underline{x} = \text{Min}(x, x') . \qquad (6\text{-}12)$$

Thus the line source function can be rewritten as

$$\underline{S}^L(x, \mu, r) = \frac{(1-\epsilon)}{\phi(x, \mu, r)} \int_{-\infty}^{+\infty} dx' \; R_{II_A}(x, x') \int_{-1}^{+1} \underline{P}(\mu, \mu') \; \underline{u}(x', \mu') \, d\mu' + \epsilon \, \underline{S}^L(r) . \qquad (6\text{-}13)$$

The probability per scatter that the photon will be
destroyed by collisional de-excitation is given by

$$\epsilon = \frac{C_{21}}{C_{21} + A_{21} [1 - exp(-h\gamma/kT)]^{-1}} \cdot \qquad (6\text{-}14)$$

In our parametrized calcultions here, ϵ and β, are assumed in advance and are required to remain constant throughout the atmosphere.

For the calcultion of profiles under the assumption of CRD, we have used the following equation :

$$\underline{R}_{CRD}(x,\mu,x',\mu',\gamma) = \underline{P}(\mu,\mu') \; \varphi(x,\mu,\gamma) \cdot \varphi(x',\mu,\gamma). \qquad (6\text{-}15)$$

For the approximation of coherent scattering, the following equation is used:

$$\underline{R}_{cs}(x,\mu,x',\mu',\gamma) = \underline{P}(\mu,\mu') \; \delta(x-x') \; \varphi(x',\mu,\gamma) \cdot \qquad (6\text{-}16)$$

It is to be noted that the following normalization conditions

$$\frac{1}{4} \int_{-\infty}^{+\infty} dx \int_{-1}^{+1} d\mu \int_{-\infty}^{+\infty} dx' \int_{-1}^{+1} d\mu' \; \underline{R}(x,\mu;x',\mu',\gamma) = 1 \; ; \qquad (6\text{-}17)$$

and

$$\varphi(x,\mu,\gamma) = \frac{1}{2} \int_{-\infty}^{+\infty} \int_{-1}^{+1} \underline{R}(x,\mu,x',\mu',\gamma) \; dx' \; d\mu' , \qquad (6\text{-}18)$$

are always satisfied by the redistribution function. In practical computations where finite number of angle and

frequency points are employed, these normalization conditions are exploited to renormalize the redistribution functions and profile function in the selected bandwidth.

In the static medium, the following symmetry properties of redistibution matrices can be used to save the computing time:

$$\underset{\sim}{R} (x, \mu; x', \mu') = \underset{\sim}{R} (-x, \mu; -x', \mu') \; ; \tag{6-19}$$

$$\underset{\sim}{R} (x, \mu; x', \mu') = \underset{\sim}{R} (-x, -\mu; -x', -\mu') \; ; \tag{6-20}$$

$$\underset{\sim}{R} (x, \mu; x', \mu') = \underset{\sim}{R} (+x, -\mu; x', -\mu') \; ; \tag{6-21}$$

and

$$\underset{\sim}{R} (x, \mu; x', \mu') = \underset{\sim}{R} (x', \mu', x, \mu) \; . \tag{6-22}$$

When there is non-coherence in the atom's frame (e.g. $E_1 \neq 1$) the relation (6-22) is not satisfied. In a static medium one needs to calculate only half of the line profile because of the symmetry of the profile functions, redistribution functions, source functions and the specific intensity about the line centre. In all the examples studied, we solve the line transfer equation in the rest frame of the star. For a critical discussion of radiative transfer in rest frame, see Mihalas (1978).

6.2 A general numerical method of solution of the problem of resonance line polarization transfer with frequency redistribution

We shall now describe the method of solution of the polarization line transfer equations with frequency redistribution. The equations are written, again for the more general case of a spherically symmetric media. All the equations automatically go over to the special case of plane parallel medium if the curvature factor $\beta(r) \to 0$

Calculation of cell operators: In order to solve the equations (6-3) and (6-4) we use the 'discrete space theory of radiative transfer. For that purpose, we have to develop the reflection and transmission operators which embody all the physical information contained in the problem posed by us. In the discrete ordinate method where we employ a finite number of angle and frequency points (usually the nodal points of a suitable quadrature formula) to perform the respective integrations, the reflection (χ) and transmission (t) matrices are the 'matrix operators' having a matrix structure dictated by the problem at hand. The accuracy of the discrete representation for the continuous variables is determined naturally by the degree of approximation used for the discrete representation-in other words, on the number of angle and frequency points employed for

the purpose. However it should be noticed that the accuracy of the intensities and fluxes (as compared to a standard analytical solution) are generally very good even for a modest angular and frequency resolution, because the differencing schemes employed to discretize the transfer equations are essentially conservative in nature and are of second order. Hence they can be made as accurate as possible by selecting smaller and smaller step sizes. We now have to descritize the equations (6-3) and (6-4) in frequency, angle and space coordinates. For frequency discretization, we choose the discrete frequency points x_i and weights a_i so that,

$$\int_{-\infty}^{+\infty} \phi(x) f(x) dx \simeq \sum_{i=-I}^{+I} a_i f(x_i) \quad, \quad \sum_{i=-I}^{+I} a_i = 1 \quad, \tag{6-25}$$

and for the angular descritization, we choose angular points $\{\mu_j\}$ and the weights $\{c_j\}$ such that

$$\int_0^1 f(\mu) d\mu \simeq \sum_{j=1}^{m} b_j f(\mu_j) \quad, \quad \sum_{j=1}^{m} b_j = 1 \quad. \tag{6-26}$$

Following Peraiah and Grant (1973) and Grant and Peraiah (1972) we shall integrate the transfer equations (6-3) and (6-4) by using the 'cell' method. Here, we integrate the transfer equation over an interval $[r_n, r_{n+1}] \times [\mu_{j-\frac{1}{2}}, \mu_{j+\frac{1}{2}}]$ defined on a two dimensional grid. By choosing the roots μ_j and the weights c_j of Gauss-Legendre quadrature

formula of order J over $(0,1)$ we calculate the set $\mu_{j\pm\frac{1}{2}}$ as given by

$$\mu_{j+\frac{1}{2}} = \sum_{k=1}^{j} c_k \quad \text{and} \quad \mu_{j-\frac{1}{2}} = \sum_{k=1}^{j-1} c_k \quad ; \quad j = 1, 2, 3, \cdots \cdots J \cdot \tag{6-27}$$

we shall define the boundary of the angular interval as $\mu_{\frac{1}{2}} = 0$. It is obvious that $\mu_{j-\frac{1}{2}} \leq \mu_j \leq \mu_{j+\frac{1}{2}}$. Integration of equations (6-3) and (6-4) in the interval $[\mu_{j-\frac{1}{2}} , \mu_{j+\frac{1}{2}}]$ gives us, for the frequency point i in the line,

$$c_j \mu_j \frac{\partial}{\partial r} u^+_{i,j}(r) + \frac{1}{r}\left\{ (1-\mu^2_{j+\frac{1}{2}}) u^+_{i,j+\frac{1}{2}}(r) - (1-\mu^2_{j-\frac{1}{2}}) u^+_{i,j-\frac{1}{2}}(r) \right\} +$$

$$+ c_j k^L(r)\left\{ \beta + \phi^+_{i,j}(r) \right\} u^+_{i,j}(r) = c_j k^L(r)\left\{ [\rho(r)\beta + \epsilon \phi^+_{i,j}(r)]B(r)\,\underline{h} + \right.$$

$$\left. + \frac{1}{2}(1-\epsilon)\sum_{i'=-I}^{+I}a_{i'}\sum_{j'=1}^{J}[R^{++}_{i,j;i',j'}(r)\; u^+_{i',j'}(r) + R^{+-}_{i,j;i',j'}(r)\; u^-_{i',j'}(r)]c_{j'} \right\} ; \tag{6-28}$$

and

$$-c_j \mu_j \frac{\partial}{\partial r} u^-_{i,j}(r) - \frac{1}{r}\left\{ (1-\mu^2_{j+\frac{1}{2}}) u^-_{i,j+\frac{1}{2}}(r) - (1-\mu^2_{j-\frac{1}{2}}) u^-_{i,j-\frac{1}{2}}(r) + \right.$$

$$+ c_j k^L(r)\left\{ \beta + \phi^-_{i,j}(r) \right\} u^-_{i,j}(r) = c_j k^L(r)\left\{ [\rho(r)\beta + \epsilon \phi^-_{i,j}(r)]B(r)\,\underline{h} + \right.$$

$$\left. + \frac{1}{2}(1-\epsilon)\sum_{i'=-I}^{+I}a_{i'}\sum_{j'=1}^{I}[R^{-+}_{i,j;i',j'}(r)\; u^+_{i',j'}(r) + R^{--}_{i,j;i',j'}(r)\; u^-_{i,j'}(r)]c_{j'} \right\} , \tag{6-29}$$

where μ_j is taken as the mean value (or mid point) of the angle interval $[\mu_{j-\frac{1}{2}}, \mu_{j+\frac{1}{2}}]$. We have used the abbreviated notation

$$\underline{u}^{\pm}_{i,j}(r) = \underline{u}(x_i, \pm\mu_j, r) \; ;$$

$$\underline{R}^{++}_{i,j;i',j'}(r) = \underline{R}(x_i, \mu_j; x_{i'}, \mu_{j'}; r) \; ;$$

$$\underline{R}^{-+}_{i,j;i',j'}(r) = \underline{R}(x_i, -\mu_j; x_{i'}, \mu_{j'}; r) \; ;$$ (6-30)

$$\underline{\phi}^{\pm}_{i,j}(r) = \underline{\phi}(x_i, \pm\mu_j, r) \; ,$$

etc. The vector notation as of now represents 2 dimensional column vectors or (2x2) matrices. The reason for the choice (6-27) should now be obvious; it permits us to evaluate the scattering integral term with the maximum accuracy assuming that the solutions $\underline{u}^{+}_{i,j}(r)$, $\underline{u}^{-}_{i,j}(r)$ are sufficiently smooth in the angle space. Provided we consider the diffuse radiation field, we can be sure that this is indeed the case. We shall now define $\underline{u}^{\pm}_{i,j+\frac{1}{2}}(r)$ which are the intensities at the boundaries of the angular cell, as

$$\underline{u}^{\pm}_{i,j+\frac{1}{2}}(r) = \frac{(\mu_{j+1} - \mu_{j+\frac{1}{2}}) \underline{u}^{\pm}_{i,j}(r) + (\mu_{j+\frac{1}{2}} - \mu_j) \underline{u}^{\pm}_{i,j+1}(r)}{(\mu_{j+1} - \mu_j)} \; ;$$ (6-31)

$j = 1,2,3........, J-1.,$

and define $\underline{u}^{+}_{i,\frac{1}{2}}(r) = \underline{u}^{-}_{i,\frac{1}{2}}(r)$ by interpolation, as

$$\underline{u}^{+}_{i,\frac{1}{2}}(r) = \underline{u}^{-}_{i,\frac{1}{2}}(r) = \frac{1}{2}\left(\underline{u}^{+}_{i,1}(r) + \underline{u}^{-}_{i,1}(r)\right). \tag{6-32}$$

We can write a system of J equations, like the general equations (6-28) and (6-29) for the set of angles over the interval $[0,1]$. That system of equations can be written in a compact form if we use matrix representation, as shown below:

$$\underline{M}_{2J}\frac{\partial\underline{u}^{+}_{i}(r)}{\partial r} + \frac{1}{r}\left[\underline{\Lambda}^{+}_{2J}\underline{u}^{+}_{i}(r) + \underline{\Lambda}^{-}_{2J}\underline{u}^{-}_{i}(r)\right] + k(r)\left\{\beta\underline{I}_{2J} + \underline{\Phi}^{+}_{i}(r)\right\}\underline{u}^{+}_{i}(r)$$

$$= k^{L}(r)\left\{\left[\rho(r)\beta\underline{I}_{2J} + \epsilon\,\underline{\Phi}^{+}_{i}(r)\right]B(r)\underline{h}_{2J} + \right.$$

$$\left. + \frac{1}{2}(1-\epsilon)\sum_{i'=-I}^{+I}\left[\underline{a}^{++}_{i'}(r)\underline{R}^{++}_{i,i'}(r)\underline{C}_{2J}\underline{u}^{+}_{i'}(r) + \underline{a}^{+-}_{i'}(r)\underline{R}^{+-}_{i,i'}(r)\underline{C}_{2J}\underline{u}^{-}_{i'}(r)\right]\right\}; \tag{6-33}$$

and

$$-\underline{M}_{2J}\frac{\partial\underline{u}^{-}_{i}(r)}{\partial r} - \frac{1}{r}\left[\underline{\Lambda}^{+}_{2J}\underline{u}^{-}_{i}(r) + \underline{\Lambda}^{-}_{2J}\underline{u}^{+}_{i}(r)\right] + k(r)\left\{\beta\underline{I}_{2J} + \underline{\Phi}^{-}_{i}(r)\right\}\underline{u}^{-}_{i}(r)$$

$$= k^{L}(r)\left\{\left[\rho(r)\beta\underline{I}_{2J} + \epsilon\,\underline{\Phi}^{-}_{i}(r)\right]B(r)\underline{h}_{2J} + \right.$$

$$\left. + \frac{1}{2}(1-\epsilon)\sum_{i=-I}^{+I}\left[\underline{a}^{-+}_{i'}(r)\underline{R}^{-+}_{i,i'}(r)\underline{C}_{2J}\underline{u}^{+}_{i'}(r) + \underline{a}^{--}_{i'}(r)\underline{R}^{--}_{i,i'}(r)\underline{C}_{2J}\underline{u}^{-}_{i}(r)\right]\right\}, \tag{6-34}$$

where, the factor 2 in the subscripts 2J, comes because

of the two states of polarization we are considering.

In the most general $(I_\lambda \quad I_\gamma \quad U \quad V)^T$ representation of the

polarized light, 2 will be replaced by 4. As of now, the

column vectors are of dimension 2J and the matrices are

of dimension (2J x 2J). They are defined as (written here

explicitly)

$$\underline{u}_\lambda^\pm(\gamma) = \left[\underline{u}_{i,n}^\pm(L) \qquad \underline{u}_{i,n}^\pm(R)\right]^T ;$$

$$\underline{u}_{i,n}^\pm(L) = \left[u_{i,\pm1,n}(L), \quad u_{i,\pm2,n}(L), \cdots \cdots u_{i,\pm J,n}(L)\right]^T ; \tag{6-35}$$

$$\underline{u}_{i,n}^\pm(R) = \left[u_{i,\pm1,n}(R), \quad u_{i,\pm2,n}(R), \cdots \cdots u_{i,\pm J,n}(R)\right]^T ,$$

where, for example

$$u_{i,\pm j,n}(L) = 4\pi r_n^2 \, I(x_i, \pm\mu_j; r_n) , \tag{6-36}$$

with j=1,2,3........J represents the L component of the

specific intensity vector at the outer boundary of the

n^{th} shell of the stratified medium.

$$\underline{M}_{2J} = \begin{bmatrix} \underline{M}_J & \underline{o} \\ \underline{o} & \underline{M}_J \end{bmatrix} ; \quad \underline{M}_J = \left[\mu_j \, \delta_{jj'}\right] ,$$

$$\underline{c}_{2J} = \begin{bmatrix} \underline{c}_J & \underline{o} \\ \underline{o} & \underline{c}_J \end{bmatrix} ; \quad \underline{c}_J = \left[c_j \, \delta_{jj'}\right] , \tag{6-37}$$

$$\underset{\sim}{\overset{\pm}{\Phi}}_i (r) = \begin{bmatrix} \overset{\pm}{\underset{\sim}{\Phi}}_{i,n}(L) & \underset{\sim}{o} \\ \underset{\sim}{o} & \overset{\pm}{\underset{\sim}{\Phi}}_{i,n}(R) \end{bmatrix} ; \quad \overset{\pm}{\underset{\sim}{\Phi}}_{i,n}(L) = [\Phi_{i,\pm j,n}(L) \ \delta_{jj'}] ; \quad \overset{\pm}{\underset{\sim}{\Phi}}_{i,n}(R) = [\Phi_{i,\pm j,n}(R) \ \delta_{jj'}] , \tag{6-38}$$

with $j, j' = 1,2,3....J$ representing the running indices for rows and columns respectively. δ_{jk} is a Dirac delta function.

$$\underset{\sim}{h}_{2J} = [\underset{\sim}{1}_J \ \underset{\sim}{1}_J]^T ; \quad \underset{\sim}{1}_J = [1, 1, 1, \cdots 1]^T . \tag{6-39}$$

$\underset{\sim}{I}_{2J}$ is the unit matrix of dimension $(2J \times 2J)$. The curvature term $\frac{1-\mu^2}{r} \frac{\partial}{\partial \mu}$ of the original transfer equation is approximated by the $\overset{\pm}{\underset{\sim}{\Lambda}}_{2J}$ matrices which are defined according to the Peraiah-Grant method as follows:

$$\overset{\pm}{\underset{\sim}{\Lambda}}_{2J} = \begin{bmatrix} \overset{\pm}{\underset{\sim}{\Lambda}}_J & \underset{\sim}{o} \\ \underset{\sim}{o} & \overset{\pm}{\underset{\sim}{\Lambda}}_J \end{bmatrix} , \tag{6-40}$$

where the $(J \times J)$ matrices $\overset{\pm}{\underset{\sim}{\Lambda}}_J$ are defined as

$$\underset{\sim}{\overset{+}{\Lambda}}_J = [\overset{+}{\Lambda}_{jj'}] = \frac{(1-\mu^2_{j+\frac{1}{2}})(\mu_{j+\frac{1}{2}} - \mu_j)}{c_j (\mu_{j+1} - \mu_j)} ; \quad \begin{array}{l} j' = j+1 \\ j = 1,2,\cdots J-1 ; \end{array}$$

$$= \frac{(1-\mu^2_{j+\frac{1}{2}})(\mu_{j+1} - \mu_{j+\frac{1}{2}})}{c_j (\mu_{j+1} - \mu_j)} - \frac{(1-\mu^2_{j-\frac{1}{2}})(\mu^2_{j-\frac{1}{2}} - \mu_{j-1})}{c_j (\mu_j - \mu_{j-1})}$$

$$= - \frac{(1-\mu^2_{j-\frac{1}{2}})(\mu_j - \mu_{j-\frac{1}{2}})}{c_j (\mu_j - \mu_{j-1})} ; \quad \begin{array}{l} j' = j-1 \\ j = 2,3,\cdots J \end{array} \tag{6-41}$$

and

$$\underset{\sim}{\bar{\Delta}}_{J} = \left[\bar{\Lambda}_{jj'} \right] = \frac{-1}{2c_j} \, \delta_{j,1} \, \delta_{j',1} \, ,$$ (6-42)

with j and j' representing the running indices for rows and columns respectively. The matrices $\underset{\sim}{\overset{\pm}{\Lambda}}_{J}$ are called 'curvature scattering' matrices, the reason for which is explained later. Now, we define the redistribution matrices as follows:

$$\underset{\sim}{\overset{++}{R}}_{i,i'}(\gamma) = \begin{bmatrix} \underset{\sim}{\overset{++}{R}}_{i,i',n}(1,1) & \underset{\sim}{\overset{++}{R}}_{i,i',n}(1,2) \\ \underset{\sim}{\overset{++}{R}}_{i,i',n}(2,1) & \underset{\sim}{\overset{++}{R}}_{i,i',n}(2,2) \end{bmatrix} ,$$ (6-43)

where the block matrices corresponding to the components of the phase matrix are defined as

$$\underset{\sim}{\overset{++}{R}}_{i,i',n}(\alpha,\beta) = \begin{bmatrix} \overset{++}{R}_{i,1,i',1,n}(\alpha,\beta) & \overset{++}{R}_{i,1,i',2,n}(\alpha,\beta) - - - - - \overset{++}{R}_{i,1,i',J,n}(\alpha,\beta) \\ \vdots & \vdots & \vdots \\ \overset{++}{R}_{i,J,i',1,n}(\alpha,\beta) & \overset{++}{R}_{i,J,i',2,n}(\alpha,\beta) - - - - - \overset{++}{R}_{i,J,i',J,n}(\alpha,\beta) \end{bmatrix}$$ (6-44)

Here again the usual convention of $\overset{++}{R}_{i,j,i',j',n} = R(x_i \mu_j ; x'_i \mu'_j ; \gamma_n)$ is understood. The redistribution matrix (6-43) is replaced by a (4J x 4J) matrix, in the general case of complete Stokes vector $(I \, Q \, U \, V)^T$. In that case, however, it contains explicitly, all the azimuth dependent Fourier components also.

Now, to perform the discritization with respect
to the radial coordinate γ , we have to integrate the
equations (6-33) and (6-34) over spatial cell $[\gamma_n, \gamma_{n+1}]$
Such an integration from γ_n to γ_{n+1} gives us

$$\underline{M}_{2J}[\underline{u}^+_{i,n+1} - \underline{u}^+_{i,n}] + \rho_c [\underline{\Lambda}^+_{2J}\underline{u}^+_{i,n+\frac{1}{2}} + \underline{\Lambda}^-_{2J}\underline{u}^-_{i,n+\frac{1}{2}}] +$$

$$+ \tau_{n+\frac{1}{2}}[\beta\underline{I}_{2J} + \underline{\Phi}^+_i]_{n+\frac{1}{2}}\underline{u}^+_{i,n+\frac{1}{2}} = \tau_{n+\frac{1}{2}}[\rho\beta\underline{I}_{2J} + \epsilon\underline{\Phi}^+_i]_{n+\frac{1}{2}}$$

$$\mathcal{B}_{n+\frac{1}{2}}\underline{b}_{2J} + \frac{1}{2}\tau_{n+\frac{1}{2}}(1-\epsilon)\sum_{i'=-I}^{+I}[a^{++}_{i',n+\frac{1}{2}} \underline{R}^{++}_{i,i',n+\frac{1}{2}} \underline{C}_{2J} \underline{u}^+_{i',n+\frac{1}{2}}$$

$$+ a^{+-}_{i',n+\frac{1}{2}} \underline{R}^{+-}_{i,i',n+\frac{1}{2}} \underline{C}_{2J} \underline{u}^-_{i',n+\frac{1}{2}}] \; ; \tag{6-45}$$

and

$$-\underline{M}_{2J}[\underline{u}^-_{i,n+1} - \underline{u}^-_{i,n}] - \rho_c [\underline{\Lambda}^+_{2J}\underline{u}^-_{i,n+\frac{1}{2}} + \underline{\Lambda}^-_{2J}\underline{u}^+_{i,n+\frac{1}{2}}] +$$

$$+ \tau_{n+\frac{1}{2}}[\beta\underline{I}_{2J} + \underline{\Phi}^-_i]_{n+\frac{1}{2}}\underline{u}^-_{i,n+\frac{1}{2}} = \tau_{n+\frac{1}{2}}[\rho\beta\underline{I}_{2J} + \epsilon\underline{\Phi}^+_i]_{n+\frac{1}{2}}$$

$$\mathcal{B}_{n+\frac{1}{2}}\underline{b}_{2J} + \frac{1}{2}\tau_{n+\frac{1}{2}}(1-\epsilon)\sum_{i'=-I}^{+I}[a^{-+}_{i',n+\frac{1}{2}} \underline{R}^{-+}_{i,i',n+\frac{1}{2}} \underline{C}_{2J} \underline{u}^+_{i',n+\frac{1}{2}}$$

$$+ a^{--}_{i',n+\frac{1}{2}} \underline{R}^{--}_{i,i',n+\frac{1}{2}} \underline{C}_{2J} \underline{u}^-_{i',n+\frac{1}{2}}] \; . \tag{6-46}$$

Here the subscripts n, n+1 and n+½ refer to quantities at
γ_n , γ_{n+1} and $\gamma_{n+\frac{1}{2}}$ where n+½ refers to a suitable average
over the cell (or a mean value) of the parameter over the
cell bounded by γ_n and γ_{n+1}. We can take the 'shells' into
which we have stratified the medium, themselves as funda-

mental 'cells' provided certain conditions (to be
stated later) are satisfied. If not, we can subdivide
the shell into a finite number of identical subshells
where each subshell satisfies the required conditions,
and hence a subshell then represents a fundamental 'cell'.
The $\underline{r}$ and $\underline{t}$ matrices for the shell can be generated by a
doubling procedure starting from the operators of the
subshell. We have used the following definitions in
writing equations (6-45) and (6-46): $\Delta r_{n+\frac{1}{2}} = r_{n+1} - r_n$;

$\tau_{n+\frac{1}{2}} = \overset{L}{k}(r_{n+\frac{1}{2}}) \Delta r_{n+\frac{1}{2}}$; $r_{n+\frac{1}{2}} = \frac{1}{2}(r_{n+1} + r_n)$, being a mean radius.
$\rho_c = \Delta r_{n+\frac{1}{2}} / r_{n+\frac{1}{2}}$ is called the curvature factor. A convenient
definition of $\underset{\sim}{u}{}^{\pm}_{i,\, n+\frac{1}{2}}$ is

$$\underset{\sim}{u}{}^{\pm}_{i,\, n+\frac{1}{2}} = \frac{1}{2}\left(\underset{\sim}{u}{}^{\pm}_{i,\, n+1} + \underset{\sim}{u}{}^{\pm}_{i,\, n}\right) \tag{6-47}$$

which is the conventional 'diamond' difference scheme which
was used in the plane parallel case (Grant and Hunt, 1968).
Because of the scattering integral in the transfer equation,
all the frequency points in the line have to be treated
simultaneously. This means that the equations (6-45) and
(6-46) have to be written for the set $\{x_i\}$ of I frequency
points and solved. This we can do by writing the system
of equations in a matrix form. For that purpose, we need
a general index k which is defined as

$$(p, i, j) \equiv k \equiv j + (i-1)J + (p-1)IJ \; ; \quad 1 \leqslant k \leqslant pIJ \; , \qquad (6\text{-}48)$$

with p, i, and j being the running indices. J and I are the number of angle and frequency points, and p is the number of polarization parameters considered. In our present study, p = 2 and, for the general Stokes vector p = 4. Thus, now onwards our column vectors and the matrices are of dimension (2IJ) and (2IJ x 2IJ) respectively, and we do not write these subscripts explicitly, for the economy of notation. The equations (6-45) and (6-46) can now be written as

$$\underset{\sim}{M} \left[\underset{\sim}{u}^{+}_{n+1} - \underset{\sim}{u}^{+}_{n} \right] + \rho_c \left[\underset{\sim}{\Lambda}^{+} \underset{\sim}{u}^{+}_{n+\frac{1}{2}} + \underset{\sim}{\Delta}^{-} \underset{\sim}{u}^{-}_{n+\frac{1}{2}} \right] + \tau_{n+\frac{1}{2}} \underset{\sim}{\Phi}_{n+\frac{1}{2}} \underset{\sim}{u}^{+}_{n+\frac{1}{2}}$$

$$= \tau_{n+\frac{1}{2}} \underset{\sim}{s}^{+}_{n+\frac{1}{2}} + \tfrac{1}{2}(1-\epsilon)\tau_{n+\frac{1}{2}} \left[\underset{\sim}{R}^{++} \underset{\sim}{W}^{++} \underset{\sim}{u}^{+} + \underset{\sim}{R}^{+-} \underset{\sim}{W}^{+-} \underset{\sim}{u}^{-} \right]_{n+\frac{1}{2}} \; ; \; (6\text{-}49$$

and

$$\underset{\sim}{M} \left[\underset{\sim}{u}^{-}_{n} - \underset{\sim}{u}^{-}_{n+1} \right] - \rho_c \left[\underset{\sim}{\Delta}^{+} \underset{\sim}{u}^{-}_{n+\frac{1}{2}} + \underset{\sim}{\Delta}^{-} \underset{\sim}{u}^{+}_{n+\frac{1}{2}} \right] + \tau_{n+\frac{1}{2}} \underset{\sim}{\Phi}_{n+\frac{1}{2}} \underset{\sim}{u}^{-}_{n+\frac{1}{2}}$$

$$= \tau_{n+\frac{1}{2}} \underset{\sim}{s}^{-}_{n+\frac{1}{2}} + \tfrac{1}{2}(1-\epsilon)\tau_{n+\frac{1}{2}} \left[\underset{\sim}{R}^{-+} \underset{\sim}{W}^{-+} \underset{\sim}{u}^{+} + \underset{\sim}{R}^{--} \underset{\sim}{W}^{--} \underset{\sim}{u}^{-} \right]_{n+\frac{1}{2}} \; , \; (6\text{-}5$$

where, for our present studies of restricted Stokes vector we have,

$$\underset{\sim}{M} = \left[\mu \, \delta_{kk'} \right] \; ; \qquad \underline{C} \left[c_j \, \delta_{kk'} \right]$$

(6-51)

The block-diagonal curvature matrices are given by

$$\underset{\sim}{\overset{\pm}{\Lambda}} = \left[\Lambda_{kk'}^{\pm} \right] \; ; \qquad \Lambda_{kk'}^{\pm} = \Lambda_{jj'}^{\pm} = \Lambda^{\pm} \left(\mu_j , \mu_{j'} \right)$$

(6-52)

The intensity vectors are defined as

$$\underset{\sim}{\overset{\pm}{u}}_n = \left[u_{k,n}^{\pm} \right] ; \qquad u_{k,n}^{\pm} = u \left(x_i , \pm \mu_j ; \tau_n ; p \right) \; etc.$$

(6-53)

The profile function matrices are defined as

$$\underset{\sim}{\overset{\pm}{\Phi}}_{n+\frac{1}{2}} = \left[\beta + \varphi_k^{\pm} \right]_{n+\frac{1}{2}} \delta_{kk'} \; ; \qquad \varphi_{k,n+\frac{1}{2}}^{\pm} = \varphi \left(x_i , \pm \mu_j ; \tau_{n+\frac{1}{2}} ; p \right) .$$

(6-54)

The thermal source matrices are defined as

$$\underset{\sim}{\overset{\pm}{S}}_{n+\frac{1}{2}} = \left[p\beta + \epsilon \, \varphi_k^{\pm} \right]_{n+\frac{1}{2}} B_{n+\frac{1}{2}} \, \delta_{kk'} \; .$$

(6-55)

The redistribution matrices are defined as

$$\left.
\begin{aligned}
\underset{\sim}{\overset{++}{R}}_{n+\frac{1}{2}} &= \left[R_{k,k',n+\frac{1}{2}}^{++} \right] \; ; \quad R_{k,k',n+\frac{1}{2}}^{++} = R \left(x_i \, \mu_j \, p \, ; \, x_{i'} \, \mu_{j'} \, p' \, ; \, \tau_{n+\frac{1}{2}} \right) ; \\[2ex]
\underset{\sim}{\overset{-+}{R}}_{n+\frac{1}{2}} &= \left[R_{k,k',n+\frac{1}{2}}^{-+} \right] \; ; \quad R_{k,k',n+\frac{1}{2}}^{-+} = R \left(x_i \, -\mu_j \, p \, ; \, x_{i'} \, \mu_{j'} \, p' \, ; \, \tau_{n+\frac{1}{2}} \right) ;
\end{aligned}
\right\}$$

(6-56)

etc., the weights matrices are defined as

$$\underline{W}^{++}_{n+\frac{1}{2}} = \left[W^{++}_{k,n+\frac{1}{2}} \delta_{kk'} \right] \qquad \text{etc.,} \qquad (6\text{-}57)$$

with

$$\varphi^{+}_{k,n+\frac{1}{2}} W^{++}_{k,n+\frac{1}{2}} = a^{++}_{i,n+\frac{1}{2}} c_j , \qquad (6\text{-}58)$$

and the renormalized weights of integration defined by

$$a^{++}_{i,n+\frac{1}{2}} = \frac{A_i \varphi_{k,n+\frac{1}{2}}}{\sum_{k=1}^{2IJ} A_i c_j \sum_{k'=1}^{2IJ} A_{i'} c_{j'} R^{++}_{k,k',n+\frac{1}{2}}} \qquad (6\text{-}59)$$

In all the equations (6-51) - (6-59) k and k' represent
the running indices for the rows and columns of the con-
cerned matrices. They are defined as

$$k = j + (i-1)J + (p-1)IJ ; \qquad k' = j' + (i'-1)J + (p'-1)IJ ,$$
$$p = 1, 2 \qquad\qquad p' = 1, 2$$
$$i = 1, 2, 3, \cdots I \qquad\qquad i' = 1, 2, 3, \cdots I$$
$$j = 1, 2, 3, \cdots J \qquad\qquad j' = 1, 2, 3, \cdots J \qquad (6\text{-}60)$$
$$1 \leq k \leq 2IJ \qquad\qquad 1 \leq k' \leq 2IJ$$

By using the equation (6-47) we can rewrite equations
(6-49) and (6-50) in the canonical form

$$\begin{bmatrix} \underline{M} + \tfrac{1}{2}\tau\left[\underline{\phi}^+ - \tfrac{\delta}{2}\underline{R}^{++}\underline{W}^{++}\right] + \tfrac{\rho_c}{2}\underline{\Lambda}^+ & \tfrac{\tau\delta}{4}\underline{R}^{+-}\underline{W}^{+-} + \tfrac{\rho_c}{2}\underline{\Lambda}^- \\[2mm] -\tfrac{\tau\delta}{4}\underline{R}^{-+}\underline{W}^{-+} - \tfrac{\rho_c}{2}\underline{\Lambda}^- & \underline{M} + \tfrac{\tau}{2}\left[\underline{\phi}^- - \tfrac{\delta}{2}\underline{R}^{--}\underline{W}^{--}\right] - \tfrac{\rho_c}{2}\underline{\Lambda}^+ \end{bmatrix} \begin{bmatrix} \underline{u}^+_{n+1} \\[2mm] \underline{u}^-_n \end{bmatrix} =$$

$$\begin{bmatrix} \underline{M} - \tfrac{\tau}{2}\left[\underline{\phi}^+ - \tfrac{\delta}{2}\underline{R}^{++}\underline{W}^{++}\right] - \tfrac{\rho_c}{2}\underline{\Lambda}^+ & \tfrac{\tau\delta}{4}\underline{R}^{+-}\underline{W}^{+-} - \tfrac{\rho_c}{2}\underline{\Lambda}^- \\[2mm] \tfrac{\tau\delta}{4}\underline{R}^{-+}\underline{W}^{-+} + \tfrac{\rho_c}{2}\underline{\Lambda}^- & \underline{M} - \tfrac{\tau}{2}\left[\underline{\phi}^- - \tfrac{\delta}{2}\underline{R}^{--}\underline{W}^{--}\right] + \tfrac{\rho_c}{2}\underline{\Lambda}^+ \end{bmatrix} \begin{bmatrix} \underline{u}^+_n \\[2mm] \underline{u}^-_{n+1} \end{bmatrix} + \tau\begin{bmatrix} \underline{s}^+ \\[2mm] \underline{s}^- \end{bmatrix} \qquad (6\text{-}61)$$

where $\delta = (1-\epsilon)$. The subscript (n+½) is left out, for convenience. A comparison of this equation with the interaction principle

$$\begin{bmatrix} \underline{u}^+_{n+1} \\[2mm] \underline{u}^-_n \end{bmatrix} = \begin{bmatrix} \underline{t}(n+1, n) & \underline{r}(n, n+1) \\[2mm] \underline{r}(n+1, n) & \underline{t}(n, n+1) \end{bmatrix} \begin{bmatrix} \underline{u}^+_n \\[2mm] \underline{u}^-_{n+1} \end{bmatrix} \qquad (6\text{-}62)$$

(see Grant and Hunt 1969 a,b) for a fundamental layer bounded by the planes n and (n+1), gives two pairs of reflection ($\underline{r}$) and transimission ($\underline{t}$) operators (matrices). These linear operators can be expressed in terms of matrices and vectors appearing in equation (6-61). With the following auxiliary quantities

$$\underline{\varsigma}^{+-} = \left[\underline{I} - \underline{g}^{+-}\underline{g}^{-+}\right]^{-1} \; ; \qquad \underline{\varsigma}^{-+} = \left[\underline{I} - \underline{g}^{-+}\underline{g}^{+-}\right]^{-1} ,$$

$$\underline{g}^{+-} = \tfrac{\tau}{2}\underline{\Delta}^+\underline{Y}_- \qquad ; \qquad \underline{g}^{-+} = \tfrac{\tau}{2}\underline{\Delta}^-\underline{Y}_+ \qquad ,$$

$$\underline{D} = \underline{M} - \tfrac{\tau}{2}\underline{Z}_- \qquad ; \qquad \underline{A} = \underline{M} - \tfrac{\tau}{2}\underline{Z}_+ \qquad ,$$

$$\underline{\Delta}^+ = \left[\underline{M} + \tfrac{\tau}{2}\underline{Z}_+\right]^{-1} \; ; \qquad \underline{\Delta}^- = \left[\underline{M} + \tfrac{\tau}{2}\underline{Z}_-\right]^{-1} ,$$

$$Z_+ = \Phi^+ - \frac{\delta}{2} \underline{R}^{++} \underline{W}^{++} + \frac{\ell_c}{\tau} \underline{\Lambda}^+ \; ; \quad Z_- = \Phi^- - \frac{\delta}{2} \underline{R}^{--} \underline{W}^{--} - \frac{\ell_c}{\tau} \underline{\Lambda}^+ \; ,$$

$$\underline{Y}_+ = \frac{\delta}{2} \underline{R}^{-+} \underline{W}^{-+} + \frac{\ell_c}{\tau} \underline{\Lambda}^- \; ; \quad \underline{Y}_- = \frac{\delta}{2} \underline{R}^{+-} \underline{W}^{+-} - \frac{\ell_c}{\tau} \underline{\Lambda}^- \; . \qquad (6\text{-}63)$$

we can write the transmission and reflection matrices as

$$\underline{t}(n+1, n) = \underline{G}^{+-} [\underline{\Delta}^+ \underline{A} + \underline{g}^{+-} \underline{g}^{-+}]$$

$$\underline{t}(n, n+1) = \underline{G}^{-+} [\underline{\Delta}^- \underline{D} + \underline{g}^{-+} \underline{g}^{+-}] \qquad\qquad (6\text{-}64)$$

$$\underline{r}(n+1, n) = \underline{G}^{-+} \underline{g}^{-+} [\underline{I} + \underline{\Delta}^+ \underline{A}]$$

$$\underline{r}(n, n+1) = \underline{G}^{+-} \underline{g}^{+-} [\underline{I} + \underline{\Delta}^- \underline{D}]$$

and the source vectors as

$$\underline{\Sigma}^+(n+1, n) = \underline{G}^{+-} [\underline{\Delta}^+ \underline{S}^+ + \underline{g}^{+-} \underline{\Delta}^- \underline{S}^-] \tau$$

$$\underline{\Sigma}^-(n, n+1) = \underline{G}^{-+} [\underline{\Delta}^- \underline{S}^- + \underline{g}^{-+} \underline{\Delta}^+ \underline{S}^+] \tau \qquad (6\text{-}65)$$

All the cell operators given in the equation (6-64) and (6-65) correspond to a cell of optical depth of τ and curvature factor ℓ_c . The simplifications obtainable computationally in a non-polarized case, or angle average redistribution functions, or static media can be easily recognized and the computing time and memory can be saved.

We must choose τ and ℓ_c in a cell in such a way that we obtain a stable solution. The requirement for stability is the positivity of the matrices $\underline{A}, \underline{D}, \underline{\Delta}_+$ and $\underline{\Delta}_-$ $\underline{G}^{+-}$, $\underline{G}^{-+}$. For instance, consider the matrices $\underline{\Delta}_+$ and $\underline{\Delta}_-$.

To obtain non-negative $\underset{\sim}{\Delta}_+$ and $\underset{\sim}{\Delta}_-$, we must have positive diagonally dominant character, and negative off-diagonal elements in the matrices ($\underset{\sim}{M} + 1/2\,\tau\,\underset{\sim}{Z}_+$) and ($\underset{\sim}{M} + \frac{1}{2}\tau\underset{\sim}{Z}_-$) respectively. This requirement of $\underset{\sim}{\Delta}_\pm \geqslant 0$, leads to a criterion

$$\tau \leq \tau_{crit} = \min_{k} \left| \frac{\mu_k \pm \frac{\rho_c}{2}\,\Lambda^+_{kk}}{\frac{1}{2}\,(\varphi^\pm_k - \frac{\delta}{2}\,R^{++}_{kk}\,W^{++}_{kk})} \right| \; ; \tag{6-66}$$

for the diagonal elements, and

$$\left(\frac{\rho_c}{\tau}\right) < \min_{k} \left[\min_{k'=k\pm1} \left| \frac{\frac{\delta}{2}\,R_{kk'}\,W_{kk'}}{\Lambda^+_{kk'}} \right| \right] \; , \tag{6-67}$$

for the off-diagonal elements. The condition (6-66) can always be easily satisfied. However, the condition (6-67) imposes a severe restriction on the size of the curvature factor ρ_c to be used in each cell to obtain non-negative $\underset{\sim}{t}$ and $\underset{\sim}{r}$ matrices. Formally, we divide the medium into several shells of equal optical thickness. If the optical depth in each shell $\tau_{shell} > \tau_{cell}$, then we have to subdivide the shell and use the 'star algorithm' given in Grant and Hunt (1968) or Peraiah (1984), for calculting the $\underset{\sim}{r}$ and $\underset{\sim}{t}$ operators of the whole shell. If the medium is very thick, then we can use the 'doubling method' (van de Hulst,1965) which is faster. In the doubling method we choose τ and ρ_c

values satisfying the conditions (6-66) and (6-67). If very high accuracy is needed one can take small fractions of τ and ζ_c so that the truncation errors would be minimized in compounding the cell operators. It should be kept in mind that too small values of τ and ζ_c may lead to round off errors due to enhanced arithmetic operations. If we halve the shell p times, the star algorithm is repeated p times, and in this event, the curvature factor ζ_{ss} and the optical depth τ_{ss} of the subshell or 'cell' are given in terms of those of the shell (viz. ζ_s and τ_s) by

$$\zeta_{ss} \approx \zeta_s \, 2^{-p} \Big/ [1 - \zeta_s \, (2^{-1} - 2^{-p})] \; ;$$

$$\tau_{ss} = \tau_s \, 2^{-p} \, , \tag{6-68}$$

The square of the mean radius of the subshell is given by

$$\bar{r}^2 = R^2 \left\{ 1 - \zeta_s \left[K + \tfrac{1}{2} \right] + \tfrac{1}{3} \zeta_s^2 \left(K^2 + \tfrac{K}{2} + \tfrac{1}{4} \right) \right\} , \tag{6-69}$$

where ζ_{ss} corresponds to a subshell approximately midway in the shell, and ζ_s is the curvature factor for the whole shell, defined as $\zeta_s = \Delta r \big/ r_{out}$. τ_{ss} is also derived from the assumption that the absorption coefficient in the shell is uniform. R is the outer radius of the shell in terms of the inner radius of the medium, and $K = 2^{-1} - 2^{-p}$.

One of the important checks of the method is the conservation of flux. In a purely scattering medium, where energy is neither absorbed nor emitted, the input radiation energy must balance the output energy. This can be achieved only by satisfying the normalization conditions to the highest accuracy possible (say machine accuracy). The normalization condition for the redistribution function is given by

$$\frac{1}{2} \sum_{P=1}^{2IJ} \sum_{Q=1}^{2IJ} \left[W_P^{++} R_{PQ}^{++} W_Q^{++} + W_P^{-+} R_{PQ}^{-+} W_Q^{-+} \right] = 1 \quad , \tag{6-70}$$

where

$$W_{PQ} = \frac{A_i \, R_{PQ}}{\sum_{P,Q=1}^{2IJ} R_{PQ} \, A_i \, c_j} \quad , \tag{6-71}$$

and

$$[P, Q] \equiv j + (i-1) J + (p-1) I J \quad . \tag{6-72}$$

see also equation (6-60). Similarly the normalization on the curvature matrices is given by

$$\sum_{j=1}^{I} c_j \, (\Lambda_{jk}^{+} - \Lambda_{jk}^{-}) = 0 \; ; \quad k = 1, 2, \cdots \cdots J \quad . \tag{6-73}$$

The boundary conditions we have employed for the finite atmosphere of optical thickness T can be written explicitely as

$$\underset{\sim}{u}_1^+ = 0 \qquad \text{at} \quad \tau = 0$$
$$\underset{\sim}{u}_{N+1}^- = 0 \qquad \text{at} \quad \tau = T \qquad (6\text{-}74)$$

that is, no radiation is incident on either side of the medium. The continuum source function (the Planck function) is always set equal to 1. In semi-infinte atmospheres, however one has to use the conventional boundary condition

$$\underset{\sim}{u}_1^+ = 0 \quad ; \quad \text{at} \quad \tau = 0$$
$$\underset{\sim}{u}_{N+1}^- = B \quad ; \quad \text{at} \quad \tau = T \qquad (6\text{-}75)$$

Further details on the line transfer in spherical or moving media can be obtained from Peraiah (1984). We describe our parametrized study of resonance line transfer in the section 6.3.

6.3 Limiting forms of the resonance line polarization transfer problem and their solutions

In this section we shall compare the solutions obtained by our method with the accurate solutions of Rees and Saliba (1982) on some test cases, and discuss some advantages as well as difficulties of our approach in comparison with the standard Feautrier's method which

has been used by these authors and is widely used as well. We have considered only finite atmospheres with a scaled Planck function B = 100.We always use angle-averaged partial redistribution function $\mathcal{R}_{II,A}$ in the PRD calculations. We use a 3 point Gaussian angle quadrature on $0 < \mu < 1$, and a trapezoidal frequency quadrature on $0 < x < \infty$. The parameters of the study are: T, the optical thickness of the line forming region; a, the dimensionless damping parameter; ϵ, the thermalization parameter (or the probability of photon destruction during scattering); β, the parameter which represents the amount of coupling of the line to the continuum levels of atom. Other free parameter which we have now set equal to zero is the depolarization factor $d = (1-E_1)$ which represents the amount of mixing of the dipole like and isotropic radiation fields. This choice represents the case of maximum polarization attainable under a given set of conditions. The transfer problem is solved using the procedure described in the section 6.2.

Complete redistribution approximation:- The complete redistribution is quite a good approximation in the line core. It is very easy to handle in the transfer problems and economical in terms of computing efforts. Major part of the work in the theory of resonance line polarization has been done using this assumption of CRD. The definition of CRD is given in the equation (6-15).

In the following, we shall show the results of our test case with CRD, for the sake of discussion. The behaviour of CRD profiles in resonance line polarization has however been, well studied by Dumont et al.(1977) and Rees and Saliba (1982). For radiation in the normal direction ($\mu = 1$), symmetry of the problem demands that the intensity components satisfy $I_l = I_r$ and hence the linear polarization be identically zero at all the frequencies, for any redistribution function. The polarization is largest for the smallest values of μ , i.e.near the limb of the stellar atmosphere. For CRD, the line source function $\underset{\sim}{S}_L (x , \mu , r)$ (see equation (6-13)) is independent of frequency x. In Figure 1 we have shown the specific intensities and the polarizations in the line for these values of observing angles μ . It is clearly seen that the polarization is **nearly** frequency independent for the optically thin medium. However the CRD polarization profiles develop a peak at the line centre for optically thick media. The large increase of linear polarization in the line, for smaller values of μ is clearly seen in the 'line transfer calculation' also (See section 3.4,where we have shown the behaviour of intensity and polarization for the coherent scattering of the continuum radiation in a non-magnetic Thomson scattering medium). This angular behaviour of intensity and polarization has actually been observed in the
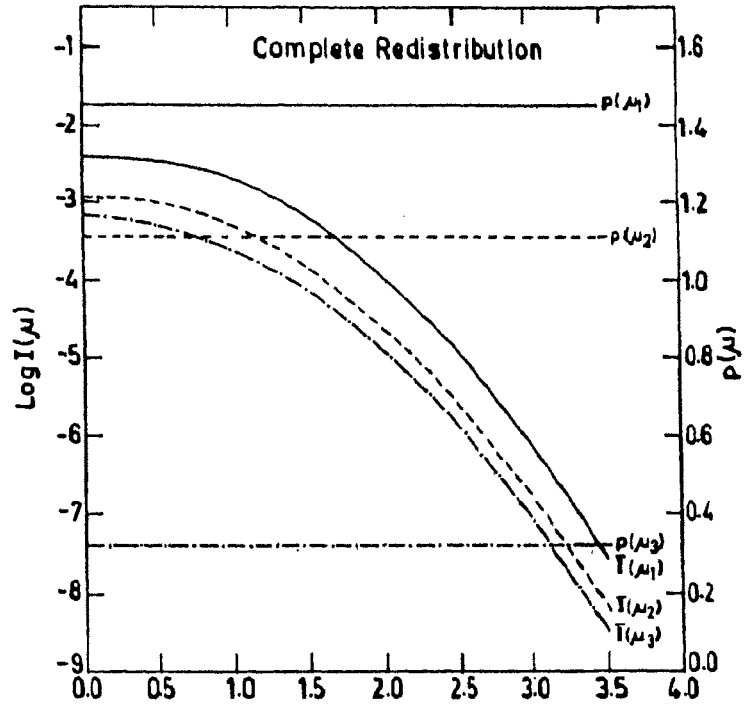
Fig.1.CRD profiles for three dire-
ctions of propagation in a plane par-
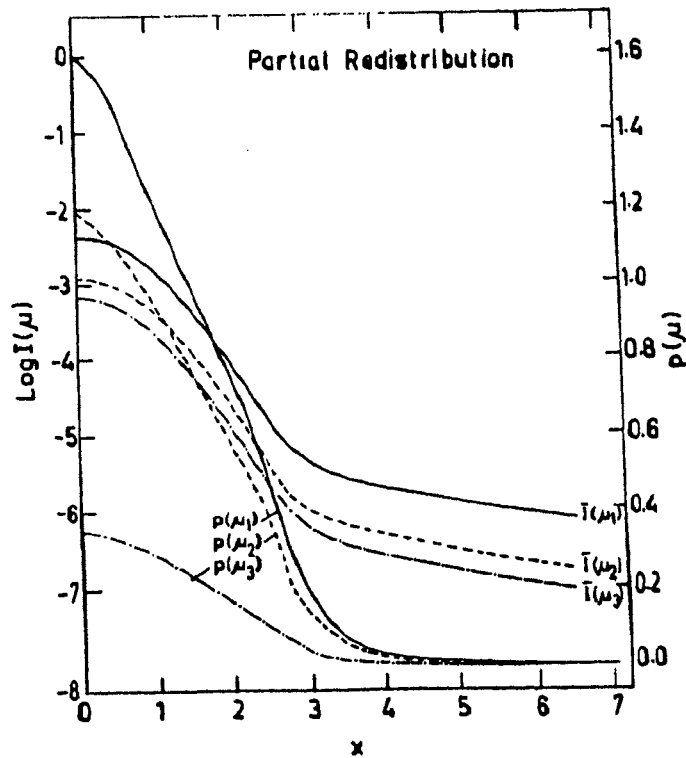allel medium, given by $\mu_1 = 0.113$, $\mu_2 = 0.5$
and $\mu_3 = 0.89$.

Fig.2.PRD profiles for the three

directions of propagation, as

mentioned in Figure 1.

solar atmosphere. In the case of stars, the integrated flux also shows a qualitatively same behaviour. This is the reason why CRD computations have been successfully used in the theoretical interpretation of observed resonance line polarizations. It has also been shown by Rees and Saliba (1982), that the difference between the line profiles and polarizations computed using CRD and PRD approximations is indeed very small in the line core region ($x < 1$). As is expected, the PRD effects are dominant in the line wings, and a careful treatment of PRD effects needs a finer frequency grid than what is normally needed for CRD computations. This point, we will also show through our model example of PRD. In table 1 we compare our solutions with those of Rees and Saliba (1982). We have computed this solution (which is the same one shown in Figure 1 also) by using a very modest frequency grid of 8 trapezoidal frequency points with a spacing of 0.5 Doppler widths. Rees and Saliba (1982) have used 20 trapezoidal frequency points, the first 15 spaced at intervals of 0.25 Doppler widths and remainder being determined logarithmically. The good agreement with their exact results is encouraging. The use of smaller number of frequency points in discrete space theory implies that the demand on the computer memory is less and a drastic reduction in the computing time because of a reduction in the size of the matrices appearing

TABLE 1a. A comparison of our CRD intensity profiles with those of Rees and Saliba (1982). Model parameters are: T = 0.1, B = 100, a = 0, ε = 10^{-4}, β = 0. An 8-point trapezoidal rule with h = 0.5 is used. The columns correspond to the specific intensity in the direction μ_j, j = 1,3. x is the reduced frequency. The first number in each row represents the results of Rees and Saliba. The second number is our result.

x	$-(\log I(\mu_1))$	$-(\log I(\mu_2))$	$-(\log I(\mu_3))$
0.0	2.37264	2.94132	3.18339
	2.37121	2.94151	3.18360
0.5	2.45894	3.04456	3.28894
	2.45814	3.04479	3.28916
1.0	2.74213	3.36032	3.60902
	2.74218	3.36061	3.60927
1.5	3.25703	3.89679	4.14628
	3.25733	3.89709	4.14852
2.0	4.00763	4.65467	4.90709
	4.00795	4.65497	4.90734
2.5	4.98301	5.63143	5.88503
	4.98334	5.63173	5.88427
3.0	6.17712	6.82570	7.07831
	6.17745	6.82600	7.07856
3.5	7.58856	8.23714	8.48975
	7.58890	8.23745	8.49001

TABLE 1b. Same as Table 1a but showing the percentage linear polarization in the profile. $p = ((I_r - I_l)/(I_r + I_l)) \times 100$.

x	$-p(\mu_1)$	$-p(\mu_2)$	$-p(\mu_3)$
0.0	1.47457	1.12443	0.32148
	1.45319	1.10778	0.31668
0.5	1.47473	1.12444	0.32148
	1.45318	1.10778	0.31668
1.0	1.47491	1.12444	0.32148
	1.45318	1.10778	0.31668
1.5	1.47497	1.12445	0.32148
	1.45318	1.10778	0.31668
2.0	1.47497	1.12445	0.32148
	1.45318	1.10778	0.31668
2.5	1.47497	1.12445	0.32148
	1.45318	1.10778	0.31668
3.0	1.47497	1.12444	0.32148
	1.45318	1.10778	0.31668
3.5	1.47496	1.12442	0.33214
	1.45318	1.10778	0.31668

TABLE 2a A comparison of our PRD intensity profiles with those of Rees and Saliba (1982). Model parameters are: T=0.1, B=100, a = 10^{-2}, ε = 10^{-4}, β= 0. An 8-point trapezoidal rule with h = 0.7 is used. a is the damping constant. The description of the tabular form, as given in Table 1.

x	$-\log(I(\mu_1))$	$-\log(I(\mu_2))$	$-\log(I(\mu_3))$
0.0	2.37388	2.94352	3.18597
	2.37178	2.94236	3.18455
0.7	2.55052	3.14928	3.39519
	2.54810	3.14711	3.39284
1.4	3.09573	3.73121	3.98189
	3.13432	3.77026	4.02005
2.1	4.11357	4.76093	5.01332
	4.13176	4.77828	5.02878
2.8	5.14654	5.79479	6.04685
	5.16388	5.81112	6.06093
3.5	5.55097	6.19886	6.44999
	5.56399	6.21107	6.46034
4.2	5.74463	6.39212	6.64230
	5.75020	6.39723	6.64638
4.9	5.89598	6.54320	6.79275
	5.89651	6.54354	6.79265

TABLE 2b. Same as Table 2a but showing the percentage linear polarization in the profile.

x	$-p(\mu_1)$	$-p(\mu_2)$	$-p(\mu_3)$
0.0	1.58358	1.20789	0.34555
	1.47667	1.12574	0.32186
0.7	1.37260	1.04623	0.29895
	1.31055	0.99870	0.28528
1.4	1.36528	1.04056	0.29732
	0.94203	0.71723	0.20446
2.1	1.44978	1.10518	0.31593
	0.65767	0.50039	0.14242
2.8	1.25158	0.95363	0.27231
	0.30473	0.23166	0.06581
3.5	0.85413	0.65018	0.18525
	0.07434	0.05648	0.01602
4.2	0.45623	0.34695	0.09864
	0.02267	0.01722	0.00488
4.9	0.18961	0.14409	0.04091
	0.00828	0.00629	0.00178

in the calculation. We feel that both these are very ad-
vantageous for detailed work in the non-LTE line transfer
computations, at least in the CRD approximation.

Partial redistribution approximation using $R_{\rm IIA}$: Through
another test case, we study the PRD line formation problem
again using a 8 point trepezoidal quadrature for frequency
integration of the transfer equation. We adopt the simpli-
fication for $R_{\rm IIA}$, suggested by Rees and Saliba (1982) in
order to simplify the transfer problem (see equations (6-8)
to (6-13)). The basic physical nature of $R_{\rm IIA}$ function is
described in Mihalas (1978). Rees and Saliba have used a
further simplification of $R_{\rm IIA}(x,x')$ redistribution function,
in treating the frequency redistribution. It is the Kneer's
(1975) approximation to $R_{\rm IIA}(x,x')$ function. This composite
formula is written conveniently as

$$R_{\rm IIA}(x,x') = <a>_{x'} \, \delta(x-x') \, \varphi(x) + (1-a_{x,x'}) \, \varphi(x) \, \varphi(x') , \qquad (6\text{-}76)$$

where

$$<a>_{x'} = \int_{-\infty}^{\infty} a_{x,x'} \, \varphi(x) \, dx , \qquad (6\text{-}77)$$

and

$$a_{x,x'} = 1 - exp\left[-(\hat{x}-2)^2/4\right] ; \qquad \hat{x} = max(|x|, |x'|) . \qquad (6\text{-}78)$$

For CRD, $a_{x,x'} \equiv 0$ and for coherent scattering (CS), $a_{x,x'} \equiv 1$.
In this formula, the line core is dominated by CRD profile,
with a gradual transition to CS in the wings.

We have used exact formula for $R_{II A}(x, x')$ given by equation (6-11), instead of the Kneer's approximation given by equation (6-76). This choice partly accounts for the difference between our results and the results of Rees and Saliba (1982) in the values of polarization, particularly in the wings. In the Figure 2 we show the intensity profile and the polarization across the line. It can be seen that in the inner line-core, $x < 0.5$, the differences between the CRD and PRD profiles are insignificant. The shape of the intensity profile is also not much different from the CRD profile. Note, however, that for the particular case of $\beta = 0$ (that is the pure line transfer without the introduction of any continuum processes), the PRD polarization tends to zero in the wings as opposed to a constant non-zero value for CRD. This special behaviour of CRD polarization profile arises because in the CRD case, photons can scatter into the wings from the core, thereby giving rise to wing polarization 'at all frequencies'. This general conclusion is true only when the optical depths are very small (say $T \lesssim 1$). But, when the optical depth T is large or an overlapping continuum radiation field is included, by setting $\beta \neq 0$, the polarization is automatically driven to zero as the radiation field merges with the unpolarized background in the far wings. This natural behaviour of polarization maxima

in the line core, and zero polarization in the far wings is correctly predicted even for as small a value of T as 0.1 which we have chosen. Hence PRD offers a better representation of resonance line polarization throughout the line profile. A good analysis of the resonance line polarization by CS, CRD and PRD as well as the effects of varying T, ϵ, β and a has been done by Rees and Saliba (1982). In the Table 2 we have compared our PRD solution with those of Rees and Saliba. It can be seen that the computation of intensities is quite exact, but the values of polarization, differ by large amount in the wings. This is not surprising because, the PRD effect is strong only in the wings. With our choice of low order quadrature, using also a rather large interval of 0.7 Doppler width, it is not possible to reproduce the sensitive polarization information correctly to a better accuracy. This situation however, can easily be improved by employing a larger number of frequency points. This in turn increases the dimensions of the matrices and consequently the computing time. We also would like to point out that our method of solution is direct unlike the iterative procedure of Rees and Saliba (1982). The method takes arbitray variation of physical variables in the medium, and can be generalized to treat the line formation under any type, of frequency redistribution mechanism or even the velocity fields in the atmosphere. Such calculations have

been described in Peraiah (1978) and Wehrse and Peraiah
(1979). The behaviour of diffuse radiation field inside
the medium can be studied as a natural outcome, without
any additional efforts,in the calculation of emergent
radiation field. Using the general equations presented
in the section 6.2,we can also solve the resonance line
polarization transfer problem with frequency redistri-
bution, in spherically symmetric media.

6.4 Resonance line polarization transfer in planar and spherical geometries - a comparison of solutions

It is well known that the plane parallel (PP) appro-
ximation is an excellent approximation when the density
scale height in the atmosphere is very small compared to
the radius of the star. It is interesting to study, as a
natural generalization of this approximation, the line
transfer problems in spherically symmetric atmospheres.
We shall attempt such a problem now, confining ourselves
to non-extended spherically symmetric atmospheres. How-
ever, the essential characteristics of the so called
'spherical radiative transfer problem' can be demonstrated
even with such a geometrically thin, shell like spherical
atmosphere. Chandrasekhar (1934) and Kosirev (1934) were
the first to examine the radiative transfer equation in

spherical symmetry. In later years, many authors have
attempted this problem both analytically and numerically.
This difficult problem has been of great importance in
the theory of radiative transfer, obviously because of
its greater generality and the immediate applications it
finds in the whole area of stellar astrophysics. The
review articles on spherical radiative transfer in the
book "Methods in radiative transfer" edited by W.Kalkofen
(1984)provide a good description, and a complete list of
references to earlier work in this field. Our main in-
terest here is to solve the radiative transfer equations
for resonance line polarization, in spherical geometry
and compare them with the plane parallel solutions. In
problems dealing with spherical symmetry, the ray conti-
nuously changes its direction with the radius vector which
amounts again to some sort of scattering, which is generally
called the curvature-scattering. This, taken together with
the scattering by free electrons or bound levels of atoms,
greatly complicates the process of emergence of radiation
from such atmospheres. There have been some attempts
towards these problems in the past (Cassinelli and Hummer,
1971; Schmidt-Burgk,1973,Shapiro and Sutherland,1982 and
others). Peraiah (1975) has developed a numerical solution
of radiative transfer equation in spherical symmetry when
the spherical medium scatters radiation in accordance with

Rayleigh phase matrix. He has studied the effects of
sphericity (curvature effects) on the angular distri-
bution of intensity and polarization in such a pure
scattering medium. The method of solution he has used
is a vector analogue of the Peraiah-Grant method (Peraiah
and Grant, 1973). We have described the method of solution
for the 'line transfer with frequency redistribution' in
spherical geometry, in section 6.2. These equations can
be used to obtain both SS and PP solutions, for any given
set of physical parameters.

We shall calculate the line profiles in isothermal
homogeneous spherical medium having the rest of the phy-
sical properties same as the PP medium, though it is natural
that the spherical atmospheres should have power-law type
radial distribution of opacities. Nevertheless, for the
non-extended atmospheres, our choice is reasonably good.
Our primary interest is just to see how curvature of the
medium affects the polarized radiation field in a medium.
We study the 'effects of sphericity' on the polarized line
transfer under all the three line scattering mechanisms
already mentioned, namely coherent scattering, complete
redistribution and partial redistribution in frequency.
We have used the same isothermal model atmosphere as mentioned
in Table 1, namely $\epsilon = 10^{-4}$, $\beta = 0$, $B = 100$; $a = 0.01$,
$T = 0.1$. The ratio (B/A) of the outer to the inner radius

of the atmosphere is a measure of sphericity of the medium. $\frac{B}{A} = 1$ represents the plane parallel atmosphere, and $\frac{B}{A} \neq 1$ a spherical atmosphere. We have used a spherical atmosphere with $\frac{B}{A} = 1.2$, a value representative of normal stellar atmospheres or thin chromospheric emission regions. We mention that, in the extended atmospheres of giant stars, this ratio can take values anywhere between few tens to few hundreds. The boundary condition employed in all the cases is that, no radiation is incident externally on either side of the PP slab or SS shell. The model actually represents high temperature emitting region with a small line optical depth.

Discussion of results: We adopt a graphical representation for our discussions. In all the Figures (3), (4) and (5), the solid line and the dashed line in each frame represent the intensity and the polarization profile respectively, in a plane parallel atmosphere . The dot-dashed curve and the dotted curve represent the corresponding intensity and polarization profiles respectively, in a spherically symmetric atmosphere. In all the computations, the specific intensity in spherical geometry is defined as $\underline{u} = r^2 \underline{I}$ where r is the radius. In the reduced radial coordinates the value of r = 1, at the inner boundary of the spherical shell, and r = (B/A) at the outer boundary. It takes intermediate values between 1 and (B/A) for other

shell boundaries in the atmosphere. For instance, in our present computations emergent vector $\underset{\sim}{I}$ can be obtained as $\underset{\sim}{I} = \underset{\sim}{U}/(B/A)^2 = \underset{\sim}{U}/1.44$, since we have selected $(B/A) = 1.2$. For the sake of comparison, we have actually plotted the U values itself to represent the spherical transfer solutions. This we have done for the sake of comparison with the PP solution vector I in the line profile. Hence, it should be remembered that the emergent specific intensity values of a SS solution are always smaller in magnitude, than the corresponding PP solutions. As expected, the intensity profiles show a limb darkening for both PP and SS situations. Also, the polarization is the largest in the tangential directions (small values of μ) in both PP and SS situations. The polarization in the SS media is smaller in magnitude than the plane parallel media. We note that this behaviour is characteristic of optically and geometrically thin emitting shells. In the photospheric type conditions, with large line optical depths, the multiple scattering effect coupled with the large sphericity can lead to the opposite of this behaviour.

We have computed the coherent scattering profiles, taking the damping parameter $a = 10^{-2}$. We have shown these profiles in Figure 3. The CS intensity profile matches with the CRD profile upto $X \simeq 3$. In the line
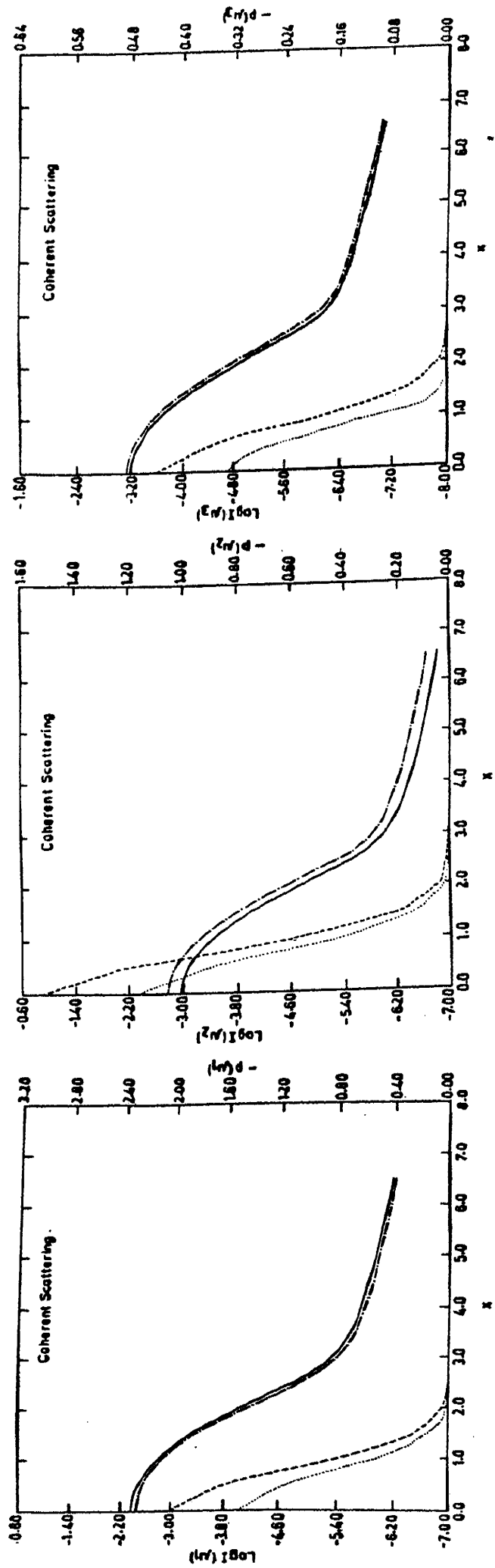
Fig.3. The lines formed under CS mechanism. The intensities $I(\mu)$ and the percentage polarizations $p(\mu)$ are shown separately for three angles of propagation μ_1, μ_2 and μ_3, in PP and SS media.

227

wings however CS produces a damped profile unlike CRD profiles. The CS profile nearly coincides with the PRD intensity profile throughout the band width of x. This is obvious because, for T = 0.1, the line wing optical depths are very small and hence the transfer effects are weak. Exactly for the same reason, the PRD effects are also weakened in the line wings. Thus the CS intensity profiles follow the shape of the absorption profile (Voigt profile currently), which is characteristic of coherent scattering in the line. The degree of polarization is however, always larger for the CS mechanism than the CRD or PRD mechanisms, because of a larger frequency coherence, which preserves the polarization during the act of scattering.

In the Figure 4 we have shown the CRD profiles. The polarization p is nearly frequency independent. The difference between the PP and SS solutions is again maximum for the large values of μ , i.e. in the radial directions in a SS medium. The difference between the PP and SS intensity profiles in the line wings, is smaller in the case of CRD mechanism of line formation than the CS mechanism. CRD profiles are similar to the PRD profiles in the line core excepting the difference in the polarization profiles.
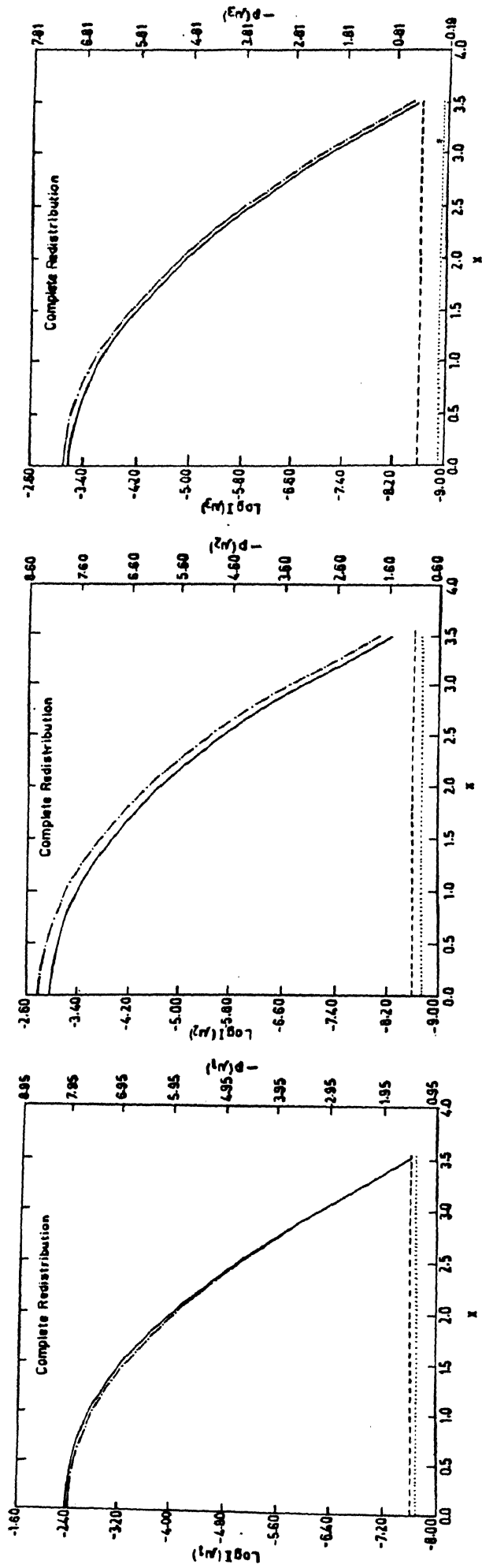
Fig. 4. Same as Fig. 3 but with the line scattering mechanism now being the CRD in frequency.
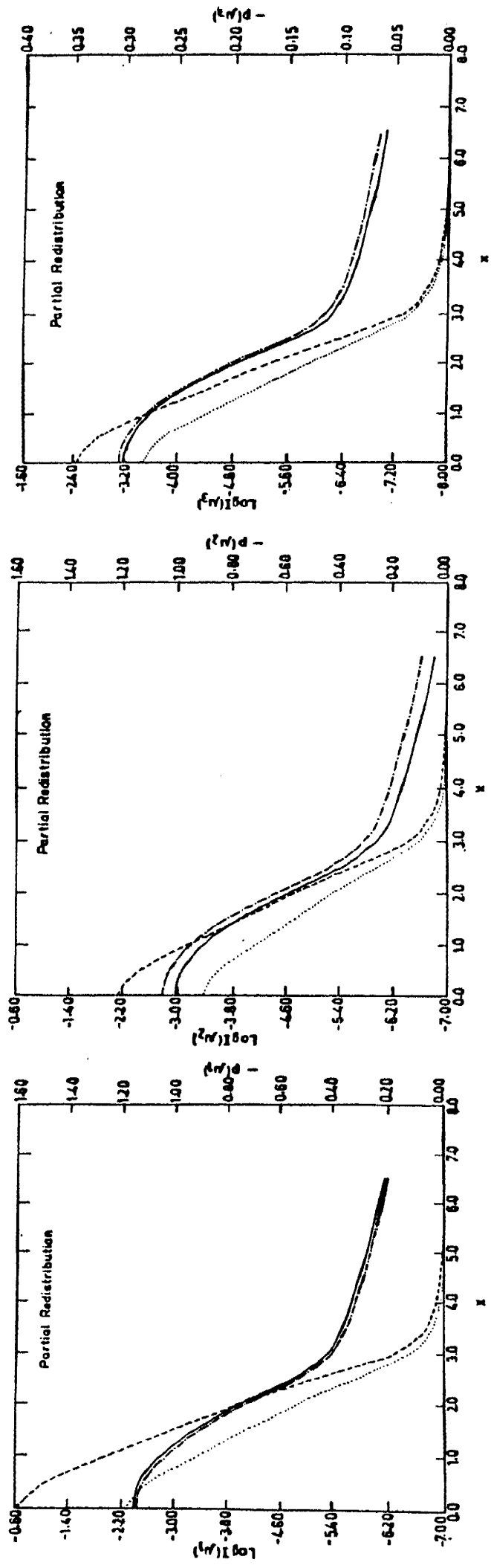
Fig.5. Same as Fig.3 except that the line scattering mechanism is now PRD in frequency.

In the Figure 5, the PRD profiles are shown. The PRD intensity profiles have CRD like behaviour in the core regions $X \lesssim 3.$, and have the CS like behaviour in the far line wings. The polarization profiles are wider ($\Delta x \simeq 3$) than the coherent scattering polarization profiles. The difference between the PP and SS polarizations is also larger in this PRD mechanism of line formation, than in either CS or CRD mechanisms. Hence we feel that, in the resonance lines which are dominated by the PRD effects, the effects of sphericity of the medium is also more severe. Hence in the calculation of such line profiles and polarizations, the spherical radiative transfer has to be used. We note that the effects of sphericity of the atmosphere on the lines, is much larger irrespective of the line scattering mechanisms, when the medium is optically thick or it is extended. We intend to study these interesting effects in detail, in our future calculations.

REFERENCES

Angel,J.R.P.: 1977,Astrophys.J.216,1

Angel,J.R.P.: 1978,Ann.Rev.Astron.Astrophys.16,487

Angel,J.R.P.,Landstreet,J.D.: 1974,Astrophys.J.191,457

Angel,J.R.P.,Borra,E.F.,Landstreet,J.D.: 1981,Astrophys.
      J.Suppl.45,457

Auer,L.H.,Rees,D.E.,Stenflo,J.O.: 1980,Astron.Astrophys.
      88,302.

Beckers,J.M.: 1969,Solar Phys.9,372

Bekefi,B.: 1966,Radiation Processes in Plasmas,Wiley,
      New York

Bommier,V.,Sahal-Brechot,S.: 1978,Astron.Astrophys.69,57

Bréit,G.: 1925,J.Opt.Soc.Am.10,439

Brukner,G.: 1963,Z.Astrophys.58,73

Canuto,V.,Lodenquai,J.,Ruderman,M.: 1971,Phys.Rev.D,3,
      2303

Cassinelli,J.P., Hummer,D.G.: 1971,Monthly Notices Roy.
      Astron.Soc.153,9

Chandrasekhar,S.: 1934,Monthly Notices Roy.Astron. Soc.
      94,522

Chandrasekhar,S.: 1950,Radiative Transfer, Clarendon Press,
      Oxford

Cohen,R.,Lodenquai,J.,Ruderman,M.: 1970,Phys.Rev.Letters
      25,L467

Cooper,J.,Smith,E.W.,Vidal,C.R.: 1974,J.Phys.B,7,L101

Deguchi,S.,Watson,W.D.: 1985,Astrophys.J.289,621

Dirac,P.A.M.: 1927.Proc.Roy.Soc.London 114,710

Dolginov,A.Z.,Gnedin,Yu.N.,Silant'ev,N.A.: 1970,J.
Quant.Spectrosc.Radiat.Transfer 10,707

Dolginov,A.Z.,Pavlov,G.G.: 1974,Sov.Astron.17,485

Dumont,S.,Omont,A.,Pecker,J.C.:1973,Solar Phys.28,271

Dumont,S.,Omont,A.,Pecker, J.C.,Rees,D.E.: 1977,Astron.
Astrophys.54,675

Gehrels,T.: 1974,Planets Stars and Nebulae Studied with
Photopolarimetry,IAU Colloq.No 23,ed. T.Gehrels,
University of Arizona Press

Ginzburg,V.L.: 1964 The Propagation of Electromagnetic
Waves in Plasmas,Pergamon Press,Oxford

Gnedin,Yu.N.,Pavlov,G.G.: 1974,Sov.Phys - JETP,38,903

Gnedin,Yu.N.,Sunyaev,R.A.:1974a,Sov.Phys - JETP,38,51

Gnedin,Yu.N.,Sunyaev,R.A.: 1974b,Astron.Astrophys.36,379

Grant,I.P.: 1963,Monthly Notices Roy.Astron.Soc.125,417

Grant,I.P.,Hunt,G.E.: 1968a,Monthly Notices Roy.Astron.
Soc.141,27

Grant,I.P.,Hunt,G.E.: 1968b,J.Quant.Spectrosc.Radiat.
Transfer 8,1817

Grant,I.P.,Hunt,G.E.: 1969a,Proc.Roy.Soc.London A313,183

Grant,I.P.,Hunt,G.E.: 1969b,Proc.Roy.Soc.London A313,199

Grant,I.P.,Peraiah,A.: 1972,Monthly Notices Roy.Astron.
Soc.160,239

Griem,H.R.: 1974,Spectral Line Broadening by Plasmas,Pure
and Applied Physics,Vol.39,Academic Press,New
York,London

Hamilton,D.R.: 1947,Astrophys.J.106,457

Hanle,W.: 1924,Z.Phys.30,93

Hardorp,J.,Shore,S.N.,Wittman,A.: 1976,in Physics of
            Ap Stars,IAU Coll.32,eds.W.W.Weiss,H.Jenkner,
            and H.J.Wood,Univ.Vienna

Heinzel,P.:1978,Bull.Astron.Inst.Czech,29,159.

House,L.L.: 1971,J.Quant.Spectrosc.Radiat.Transfer 11,367

Hummer,D.G.: 1962,Monthly Notices Roy.Astron.Soc.125,21

Jaegle,P.,Jamelot,G.,Carillon,A.: in Progress in Stellar
            Line Formation Theory,239,eds.J.E.Beckman and
            L.Crivellari,Reidel,Dordrecht

Kalkofen,W.,Wehrse,R.: 1982a,Astron.Astrophys.108,42

Kalkofen,W.,Wehrse,R.: 1982b,Astron.Astrophys.110,18

Kaminker,A.D.,Pavlov,G.G.,Shibanov,Yu.A.: 1982,Astrophys.
            Space Sci.86,249

Kemic,S.B.: 1974,Joint Institute for Laboratory Astrophysics
            Report 113

Kemp,J.C.: 1970a,Astrophys.J.162,169

Kemp,J.C.: 1970b,Astrophys.J.162,L69

Kemp,J.C.: 1977a,Astrophys.J.167,213

Kemp,J.C.: 1977b,Astrophys.J.167,794

Kneer,F.: 1975,Astrophys.J.200,367

Kosirev,N.A.: 1934,Monthly Notices Roy.Astron.Soc.94,430

Kurucz,R.L.: 1970,SAO Special Report 309

Kurucz,R.L.: 1979,Astrophys.J.Suppl.40,1

Lamb,F.K.: 1970,Solar Phys.12,186

Lamb,F.K.,ter Haar,D.: 1971,Phys.Repts.2C,1

Lamb,F.K.,Sutherland,P.G.: 1974,in Physics of Dense Matter,
           IAU Symp.53,265,ed.C.J.Hansen,D.Reidel,Dordrecht

Landi Degl'Innocenti,E.: 1976,Astron.Astrophys.Suppl.25,379

Landi Degl'Innocenti,E.: 1979,Solar Phys.63,237

Landi Degl'Innocenti,E.: 1983,Solar Phys.85,3

Landstreet,J.D.: in White dwarfs and Variable Degenerate
           Stars,IAU Coll.53,eds.H.M.Van Horn and V.Weide-
           mann,Univ.Rochester Press,Rochester

Landstreet,J.D.,Angel,J.R.P.: 1975,Astrophys.J.196,819

Liebert,J.,Angel,J.R.P.,Landstreet,J.D.: 1975,Astrophys.J.
           202,L139

Liebert,J.,Schmidt,G.D.,Green,R.F.,Stockman,H.S.,Mc-Graw
           J.T.: 1983,Astrophys.J.264,262

Liebert,J.,Stockman,H.S.: 1983,in Cataclysmic Variables
           and Low-Mass X-ray Binaries,eds.J.Patterson and
           D.Q.Lamb,D.Reidel Press

Martin,B.,Wickramasinghe,D.T.: Monthly Notices Roy.Astron.
           Soc.196,23

Martin,B.,Wickramasinghe,D.T.: 1978,183,533

Martin,B.,Wickramasinghe,D.T.: 1979a,Monthly Notices Roy.
           Astron.Soc.189,69

Martin,B.,Wickramasinghe,D.T.: 1979b,Monthly Notices Roy.
           Astron.Soc.189,883

Martin,B.,Wickramasinghe,D.T.: 1982,Monthly Notices Roy.
           Astron.Soc.200,993

Martin,B.,Wickramasinghe,D.T.: 1984 Monthly Notices
        Roy.Astron.Soc.206,407

Martin,B.,Wickramasinghe,D.T.: 1984,Astrophys.J.283,782

Mathys,G.: 1983,Astron.Astrophys.125,13

Mathys,G.: 1984a,Astron.Astrophys.139,196

Mathys,G.: 1984b,Astron.Astrophys.141,248

Mathys,G.: 1985a,Astron.Astrophys.Suppl.59,229

Mathys,G.: 1985b,in Progress in Stellar Spectral Line
        Formation Theory,381,eds.J.E.Beckman and
        L.Crivellari,Reidel,Dordrecht

Matta,F.,Reichel,A.: 1971,Math.Comp.25,339

McKenna,S.J.: 1984,Astrophys.Space Sci.108,31

Melrose,D.B.: 1980,Plasma Astrophysics,Vol.1,Gordon
        and Breach,New York.

Meszaros,P.,Bonazzola,S.: 1981,Astrophys.J.251,695

Meszaros,P.: 1982,Proc.International Workshop on Accre-
        ting Neutron Stars,eds.W.Brinkmann and J.
        Trumper,MPE Report 177,Garching,West Germany.

Meszaros,P.: 1984,Space Sci.Rev.38,325

Mihalas, D.: 1978,Stellar Atmospheres,Freeman,San
        Francisco

Nagel,W.,1981,Astrophys.J.251,278

Nagel,W.,Ventura,J.: 1983,Astron.Astrophys.118,66

Nagendra,K.N.,Peraiah,A.: 1984,Astrophys.Space Sci.104,61

Nagendra,K.N.,Peraiah,A.: 1985a,Monthly Notices Roy.Astron.
        Soc.214,203

Nagendra,K.N.,Peraiah,A.: 1985b,Astrophys.Space Sci.<u>117</u>,
121

Nagendra,K.N.,Peraiah,A.: 1986,Astron.Astrophys (to appear)

Nguyen-Hoe,,Drawin,H.W.,Herman,L.: 1967,J.Quant.Spect-
rosc.Radiat.Transfer <u>7</u>,429

Obridko,V.N.: 1968,Soln.Aktivnostj No.<u>3</u>,64

Omont,A.,Smith,E.W.,Cooper,J.: 1972,Astrophys.J.<u>175</u>,185

Omont,A.,Smith,E.W.,Cooper,J.: 1973,Astrophys.J.<u>182</u>,283

Pacholczyk,A.G.: 1977,Radio Galaxies,Pergamon Press,
Oxford

Pavlov,G.G.: 1973,Sov.Astr.<u>17</u>,209

Pavlov,G.G.: 1975,Astrofizika <u>11</u>,77

Pavlov,G.G.,Panov,A.N.: 1976,Sov.Phys-JETP,<u>44</u>,300

Pavlov,G.G. Shibanov,Yu.A.: 1978,Sov.Astr.

Pavlov,G.G.,Shibanov,Yu.A.,Yakovlev,D.G.: 1980a,Astrophys.
Space Sci.<u>73</u>,33

Pavlov,G.G.,Mitrofanov,I.G.,Shibanov,Yu.A.: 1980b,Astro-
phys.Space Sci.<u>73</u>,63

Peraiah,A.,Grant,I.P.: 1973,J.Inst.Maths.Applics.<u>12</u>,75

Peraiah,A.: 1975,Astron.Astrophys.<u>40</u>,75

Peraiah,A.: 1978,Kodaikanal Obs.Bull.Ser.A <u>2</u>,115

Peraiah,A.: 1984,in Methods in Radiative Transfer,ed.
W.Kalkofen,Cambridge University Press

Peraiah,A.,Varghese,B.A.: 1985,Astrophys.J.<u>290</u>,425

Preston,G.W.:1970,Astrophys.J.Letters <u>160</u>,L143

Rajagopal,A.K.,Chanmugam,G.,O'Connell,R.F.,Surmelian,G.L.
: 1972,Astrophys.J.177,713

Rayleigh,Lord: 1922,Proc.Roy.Soc.102,190

Rees,D.E.,Saliba,G.J.: 1982,Astron.Astrophys.115,1

Rees,D.E.,Saliba,G.J.: 1983,Proc. Astron.Soc.Australia
5 (2),186

Schmidt-Burgk,J.: 1973,Astrophys.J.181,865

Shapiro,P.R.,Sutherland,P.G.: 1982,Astrophys.J.263,902

Shipman,H.L.: 1971,Astrophys.J.167,165

Sidlichovsky,M.: 1974,Bull.Astron.Inst.Czech,25,198

Silant'ev,N.A.: 1982, Astrophys.Space Sci.82,363

Smith,E.W.,Cooper,J.,Vidal,C.R.: 1969,Phys.Rev.185,140

Staude,J.: 1970,Solar Phys.15,102

Staude,J.: 1982,HHI-STP Report 14,24

Stenflo,J.O.: 1971,in Solar Magnetic Fields,IAU Symp.43,
101,ed.R.Howard,D.Reidel,Dordrecht

Stenflo,J.O.: 1974,Solar phys.37,31

Stenflo,J.O.: 1976,Astron.Astrophys.46,61

Stenflo ,J.O.,Stenholm,L.: 1976,Astron.Astrophys.46,69

Stenflo,J.O.: 1978,Astron.Astrophys.66,241

Stenflo,J.O.: 1978,Rep.Prog.Phys.41,865

Stenflo,J.O.: 1980,Astron.Astrophys.84,68

Stenflo,J.O.,Baur,T.G.,Elmore,D.F.: 1980,Astron.Astrophys.
84,60

Stix,T.H.: 1962,The theory of Plasma Waves,McGraw-Hill,New
York

Surmelian,G.L., O'Connell,R.F.: 1973,Astrophys.space
　　　　　Sci,20,85

Unno,W.: 1956, Publ.Astron.Soc.Japan,8 108

Van de Hulst,H.C.: 1980,Multiple Light Scattering,
　　　　　Academic Press, New York

Varga, R.S.: 1963,Matrix Iterative Analysis, Englewood
　　　　　Cliffs,Prentice-Hall,NJ

Ventura,J.: 1973,Phys.Rev.A,8,3021

Ventura,J.: 1979, Phys.Rev.D,19,1684

Vidal,C.R.,Cooper,J.,Smith,E.W.: 1970,J.Quant.Spectrosc.
　　　　　Radiat.Transfer 10,1011

Vidal,C.R.,Cooper,J.,Smith,E.W.: 1971, J.Quant.Spectrosc.
　　　　　Radiat.Transfer 11,263

Voigt,H.H.: 1951,Z.Astrophys.28,176

Volonte,S.: 1975,J.Phys.B,8,1170

Warwick,J.W.,Hyder,C.L.: 1965,Astrophys.J.141,1362

Wehrse,R.: 1976,Astron.Astrophys.Suppl.24,95

Weisskopf,V.: 1931,Ann.Phys.9,23

Wehrse,R.,Peraiah,A.: 1979, Astron.Astrophys.71,289

Wesemael,F.,Auer,L.H.,van Horn,,H.M.,Savedoff,M.P.:1980,
　　　　　Astrophys.J.Suppl.43,159

Wickramasinghe,D.T.: 1972,Mem.R.astr.Soc.76,129

Wickramasinghe,D.T.,Martin,B.: 1979,Monthly Notices Roy.
　　　　　Astron.Soc.188,165

Wiehr,E.: 1975,Astron.Astrophys.38,303

Wiehr,E.: 1981,Astron.Astrophys.85,54

Wiscombe,W.J.: 1976a,J.Quant.Spectrosc.Radiat.Transfer
     16,477

Wiscombe,W.J.: 1976b,J.Quant.Spectrosc.Radiat.Transfer
     16,637

Wittmann,A.: 1974,Solar Phys.35,11

Zanstra,H.: 1941,Monthly Notices Roy.Astron.Soc.101,273

Zheleznyakov,V.V.: 1970,Radio Emission of Sun and
     Planets,Pergamon Press,New York

Zheleznyakov,V.V.: 1980,Astrofizika 16,316

Zheleznyakov,V.V.: 1983,Astrophys.Space Sci.97,229

Papers published during the course of this work

1. "Lines formed in a slowly expanding thin spherical shell": A.Peraiah,G.Raghunath and K.N.Nagendra,1980. Kodaikanal Obs.Bull.Ser.A $\underline{3}$,30

2. "Optical depth effects on the formation of spectral lines in rotating and expanding spherical atmospheres": A.Peraiah, G.Raghunath and K.N.Nagendra,1981.J.Astrophys.Astr.$\underline{2}$,277

3. "Effects of partial frequency redistribution R_{II} on the level population ratios in a resonance line": A.Peraiah and K.N.Nagendra,1983 . Astrophys. Space Sci.$\underline{90}$,237

4. "Polarization of continuum radiation in magnetic atmospheres": K.N.Nagendra and A.Peraiah, 1984. Astrophys.Space Sci.$\underline{104}$,61

5. "Some aspects of the solution of vector transfer equation in a magnetized medium": K.N.Nagendra and A.Peraiah,1985. Astrophys.Space Sci.$\underline{117}$,121

6. "Numerical solution of the radiative transfer equation in a magnetized medium": K.N.Nagendra and A.Peraiah,1985. Monthly Notices Roy.Astron. Soc.$\underline{214}$,203

7. "Some physical processes influencing the pola-
    rization of continuum and line radiation":
    K.N.Nagendra and A.Peraiah,1986. Astron.Astro-
    phys.(to appear)

Papers 4,5,6 and 7 formed the basis for chapters
2,3,4 and 5 respectively. The results of chapter 6
have not yet been published, and detailed studies
are in progress.

<u>VITA</u>

Name: K.N.Nagendra

Date of Birth: 3-7-1955

Educational Qualifications:

<u>Degree</u>	<u>Year</u>	<u>University</u>	<u>grade</u>
B.Sc.	1976	Mysore	I class
M.Sc.	1978	Mysore	I class

Academic Experience:

1. More than 6 years of research experience in Astro-physical problems. The work comprising the thesis was conducted at Indian Institute of Astrophysics, Bangalore.

2. Presently working as research associate in the Indian Institute of Astrophysics, Bangalore.

Memberships: Associate Member, Astronomical Society of India.